LA-6328-T

Thesis

UC-34a
Issued: August 1976

Theory of Low-Energy Electron-Molecule Collision Physics in the Coupled-Channel Method and Application to e-CO_2 Scattering

by

Michael A. Morrison

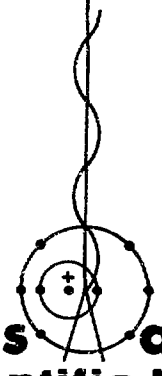

los alamos
scientific laboratory
of the University of California
LOS ALAMOS, NEW MEXICO 87545

UNITED STATES
ENERGY RESEARCH AND DEVELOPMENT ADMINISTRATION
CONTRACT W-7405-ENG. 36

This thesis was submitted to Rice University, Physics Department, Houston, Texas, in partial fulfillment of the requirements for the degree of Doctor of Philosophy. It is the independent work of the author and has not been edited by the Technical Information staff.

Printed in the United States of America. Available from
National Technical Information Service
U.S. Department of Commerce
5285 Port Royal Road
Springfield, VA 22161
Price: Printed Copy $9.75 Microfiche $2.25

TABLE OF CONTENTS

Abstract

Theory of Low-Energy Electron-Molecule Collision Physics in the Coupled-Channel Method and Application to e-CO_2 Scattering

Michael A. Morrison

A theory of electron-molecule scattering based on the fixed-nuclei approximation in a body-fixed reference frame is formulated and applied to e-CO_2 collisions in the energy range from 0.07 to 10.0 eV. The procedure used is a single-center coupled-channel method which incorporates a highly accurate static interaction potential, an approximate local exchange potential, and an induced polarization potential. Coupled equations are solved by a modification of the integral equations algorithm; several partial waves are required in the region of space near the nuclei, and a transformation procedure is developed to handle the consequent numerical problems. The potential energy is converged by separating electronic and nuclear contributions in a Legendre-polynomial expansion and including a large number of the latter. Formulas are derived for total elastic, differential, momentum transfer, and rotational excitation cross sections. The Born and Asymptotic Decoupling approximations are derived and discussed in the context of comparison with the coupled-channel cross sections. Both are found to be unsatisfactory in the energy range under consideration. An extensive discussion of the technical aspects of calculations for electron collisions with highly non-spherical targets is presented, including detailed convergence studies and a discussion of various numerical difficulties.

The application to e-CO_2 scattering produces converged results in good agreement with observed cross sections. Various aspects of

the physics of this collision are discussed, including the 3.8 eV shape resonance, which is found to possess both p and f character, and the anomalously large low-energy momentum transfer cross sections, which are found to be due to Σ_g symmetry. Comparison with static and static-exchange approximations reveal that neither predicts the correct physical properties of the collision; accurate results are obtained only in the static-exchange-with-polarization approximation.

Chapter 1. By Way of Introduction

"...Where do you want me to begin?"
"Begin at the beginning," suggested Wimsey," go on till you get to the end and then stop."

-Lord Peter Wimsey
in The Nine Tailors
(Dorothy L. Sayers)

One sometimes hears pundits declaim that atomic and molecular physics are "dead fields" in which "there are no unsolved problems." Such statements are patently fallacious, as attested by the not inconsiderable current journal and conference activity in this branch of physics. What is true is that the foundations of this field have been laid (by Schroedinger and others of the 1930 crowd of theoreists). This contrasts, for example, with elementary particle physics, where no one is quite sure how to proceed.

However, all this means for the atomic and molecular theorist is that he can proceed with confidence to tackle the wide variety of fundamental and practical problems in his field. The field is conventionally (and incorrectly) subdivided into structure problems (e.g., determination of molecular wavefunctions, calculation of atomic spectra) and dynamics problems (e.g., electron-atom collisions, heavy particle scattering). Most theorists ultimately acquire some expertise in both areas, and in point of fact a variety of current

approaches to electron scattering (e.g., pseudo-bound-state, R-matrix) blur the distinction to the extent that it becomes virtually meaningless except to suggest orientation.

One group of problems of intense recent interest involve electron-molecule collisions. Such problems are intrinsically more difficult than their counterparts in electron-atom scattering since the molecule, being multi-nuclear, is certainly not spherically symmetric (although some understandably popular targets such as H_2 and CO are atypically spherical to a certain approximation). Hence it is not currently possible to predict electron-molecule cross sections with the precision characteristic of the best electron-atom research.

We have been working in this sub-field for several years and have developed an approach to electron-molecule scattering which is in line with current research in the field. This technique, called pseudo-bound-state (PBS) has been discussed at length elsewhere[1] (together with an extensive survey of electron-molecule theory up to 1974) and published in the Physical Review[2] (see Appendix 1). We shall say a bit about this work and other related investigations we have pursued in the conclusion to this work (Chapter 9).

Partly as a consequence of our PBS studies, we became interested in the problem of electron scattering from large molecules, systems of practical interest such as CO_2, N_2O, H_2O, and so forth. Theoretical studies of such systems to date have typically employed highly approximate methods such as the Born Approximation or the Distorted-Wave Method. The reliability of such techniques for strongly anisotropic interaction potentials is dubious at best. Yet,

particularly in light of the recent interest in e-beam initiated gas lasers, such collisions are of considerable importance. At a more fundamental level, it was not clear at the time this research was initiated how one went about a theoretical study of such systems; neither the more well-established approaches (such as close-coupling) nor the new and comparatively untried L^2-variational techniques to which we alluded earlier had been applied to problems of this magnitude.

Therefore we undertook to develop a computational procedure for handling electron collisions with large molecules. We decided to base our work on the eigenfunction expansion method (c.f., close-coupling) and to try to calculate the highly important static potential energy of interaction (electron with molecular target) very accurately. The final scheme, which is discussed in Chapters 3-7, incorporates exchange (via an approximate local interaction term) and induced polarization effects. It can be (and has been) used to determine total elastic, momentum transfer, differential, and rotational excitation cross sections within the context of certain approximations to be considered below. The solution of the scattering equations is carried out by means of the standard integral equations technique. However, extensive modifications and extensions of the conventional procedure are required to treat highly anisotropic interactions.

As a test case, we selected electron-carbon dioxide scattering. The reasons for this were multiple. CO_2 in its ground electronic state is linear and has high symmetry yet is extremely large (or appears so to a theorist) being about $4a_o$ long. Thus, the potential energy of

interaction of an electron with CO_2 is sufficiently strong and non-spherical to severely test the theory. Further, this is a molecule of considerable practical interest. It is the most important constituent of the atmospheres of Mars and Venus.[3] Closer to home, CO_2 is the basis of one of the most successful continuous high-power lasers (about which we'll have more to say in Chapter 2). To add to the lure of CO_2 as a target, there existed an intriguing anomaly in the observed low-energy momentum transfer cross section for e-CO_2 scattering. Thus CO_2 was irresistible.

The present work presents the theory of low-energy electron-molecule scattering together with all the computational and numerical detail necessary to apply said theory. Throughout we use the e-CO_2 system for illustrative purposes, ultimately using our theory to try to explain the physics of this collision.

We thus commence our explorations in Chapter 2 by presenting (hopefully) sufficient background on the CO_2 molecule that the sequel will be comprehensible to readers who have not spent a couple of years with this target. This is a short chapter.

The theory proper begins in Chapter 3, where we present a detailed analysis of the static potential as required in the scattering problem. This potential characterizes the electrostatic (Coulomb) forces between the scattering electron and the otherwise isolated target molecule towards which said electron is plummeting. A second type of interaction is taken up in Chapter 4, where we turn to the elusive subject of electron exchange. After pointing out why it is all but impossible to take exchange into account rigorously, we show how to do it non-rigorously via a local (but energy-dependent) potential energy term.

Some effort is made at justifying this admittedly approximate exchange potential. In Chapter 5 we take a breather from the rather lengthy discourses of Chapters 3 and 4 to find out how to incorporate into our theory the distortion of the molecule due to the incident electron. Thus in three chapters we have dispensed with the potential.

We come then to Chapter 6, wherein the reader sees how to use the potential, a computer, and several tricks to solve the scattering equations. These (alas) coupled equations are derived, the approximations inherent in them are addressed, the numerical procedure used to solve them is discussed in detail, and a whole host of numerical problems are put to death one-by-one. Having successfully solved the scattering equations, we proceed in Chapter 7 to derive formulae for the extraction of a variety of cross sections from the asymptotic form of the scattering wave function. We also derive a couple of approximations which will be used in our study of the e-CO_2 problem.

Chapter 8 contains a very detailed discussion (well larded with examples) of the technical aspects of electron-big molecule scattering together with our results and conclusions regarding e-CO_2 scattering in the energy range from 0.07 eV to 10.0 eV. This is followed in Chapter 9 with some final remarks concerning possible future directions for research in electron-molecule physics and a few other matters.

Summarizing,[4] we have found the theory here presented to be successful in its application to the e-CO_2 problem. It leads to reliable total and momentum transfer cross sections, the latter comparing favorably with experiment, provides a theoretical explanation of the aforementioned observed anomaly, enables us to gain insight into the nature of another observed feature of e-CO_2 collisions (a

resonance at 3.8 eV), and permits some understanding of the nature of the scattering in various energy regimes. On the debit side, it is based on a number of approximations, and in particular on a rather severe approximation in the treatment of exchange, it is not purely ab-initio, having one parameter (in the definition of the induced polarization potential) which must be chosen in a somewhat ad hoc fashion, and it is not cheap. We feel, however, that these are not unreasonable considering the rather formidable nature of the system we propose to attack.

Chapter 2. A Brief Background Look at the CO_2 Molecule

The world is full of obvious things which nobody by any chance ever observes.

-Sherlock Holmes in The Hound of the Baskervilles (Arthur Conan Doyle)

§2.1 Introduction

As we mentioned in Chapter 1, the CO_2 molecule in electron collisions is the example to which we shall apply the electron-molecule scattering theory which is developed in Chapters 3-7. Thus it is appropriate to pause briefly before launching into our theoretical development to get acquainted with CO_2. Hence this chapter. In addition to pointing out important and/or interesting properties of CO_2 and its behavior in electron collisions, we here draw together and list in a hopefully systematic fashion the huge number of references on this system.

A casual overview of CO_2 in isolation is offered in section 2.2. Next, in §2.3, we survey the enormous amount of experimental (and very small amount of theoretical) work on e-CO_2 scattering which has been done to date. We close in §2.4 with a brief mention of the all-important application of CO_2 to laser physics.

§2.2 Properties of the Isolated CO_2 Molecule.[2]

Carbon dioxide is a 22-electron triatomic molecule. In its ground electronic and vibrational state it is linear with the nuclear configuration* O-C-O, the oxygen-carbon separation being about 2.19 a_o. Thus the O-O separation is 4.4 a_o. This is a very large molecule to an electron-molecule physicist, a fact that will return to haunt us in the sequel. The molecule belongs to the point group[2] $D_{\infty h}$ and has a center of symmetry. Therefore it is quite similar in its behavior under various symmetry operations to a homonuclear diatomic molecule.[3] The orbital occupancy** in this state is (see Chapter 3 and especially Table 3.1)

$$X^1\Sigma_g^+: \quad 1\sigma_u^2\ 1\sigma_g^2\ 2\sigma_g^2\ 3\sigma_g^2\ 2\sigma_u^2\ 4\sigma_g^2\ 3\sigma_u^2\ 1\pi_u^4\ 1\pi_g^4$$

For Σ_g^+ states, such as the ground state of CO_2, the odd rotational levels (i.e., odd j) do not appear in the spectrum. The moment of intertia of CO_2 is 71.1×10^{-40} gm-cm^2, which yields (via the familiar formula $I = 2m_o r_{co}^2$) a CO bond distance of 1.157×10^{-8} cm^2. The resultant rotational constant is $B_{CO_2} = 0.3937$ cm^{-1}. Using the fact that 1 cm^{-1} = 1.2398×10^{-4} eV, we find that in atomic units this constant is $B_{CO_2} = 1.795 \times 10^{-6}$ au. This, in turn, suggests that the rotational level spacing, at least for low-lying states of CO_2, is quite small. Using the fact[4] that the rotational energy in the j^{th} state is

*These conclusions are drawn from inspection of the observed Raman spectrum of CO_2.

**Also called the electronic configuration.

$$E_r = hc\, B_{CO_2}\, j(j+1), \qquad (2.1)$$

we find that for low j values, the level spacing is of the order of 10^{-4} eV. This is at least two orders of magnitude smaller than the scattering energies of interest in our application,* which range from 0.07 eV to 10.0 eV.

The vibrational level spacing, by contrast, is quite large. CO_2 has three vibrational modes:[5] the n00 symmetric stretch mode, the $0n^{\ell}0$ bending mode, and the 00n asymmetric stretch mode. These are illustrated with dumbell models in Figure 2.1. The bending mode is two-fold degenerate, i.e., there exist two normal vibrations which have the same frequency, ν_2 in the figure. (The superscript ℓ on the bending mode notation labels the particular degenerate mode under consideration.) This fact is consistent with the observation that a linear molecule has 3N-5 degrees of freedom and hence 3N-5 normal modes of vibration. (For CO_2, N = 3.) Moreover, we expect CO_2 to have degenerate as well as non-degenerate normal vibrations, since it possesses one more-than-two-fold axis of symmetry.

For completeness, we here list the symmetry elements of $D_{\infty h}$ and illustrate them for CO_2 in Figure 2.2. We have

*This happy fact will help us when we get around to making certain approximations in formulating the collision problem; see Chapter 6, especially section 6.2.

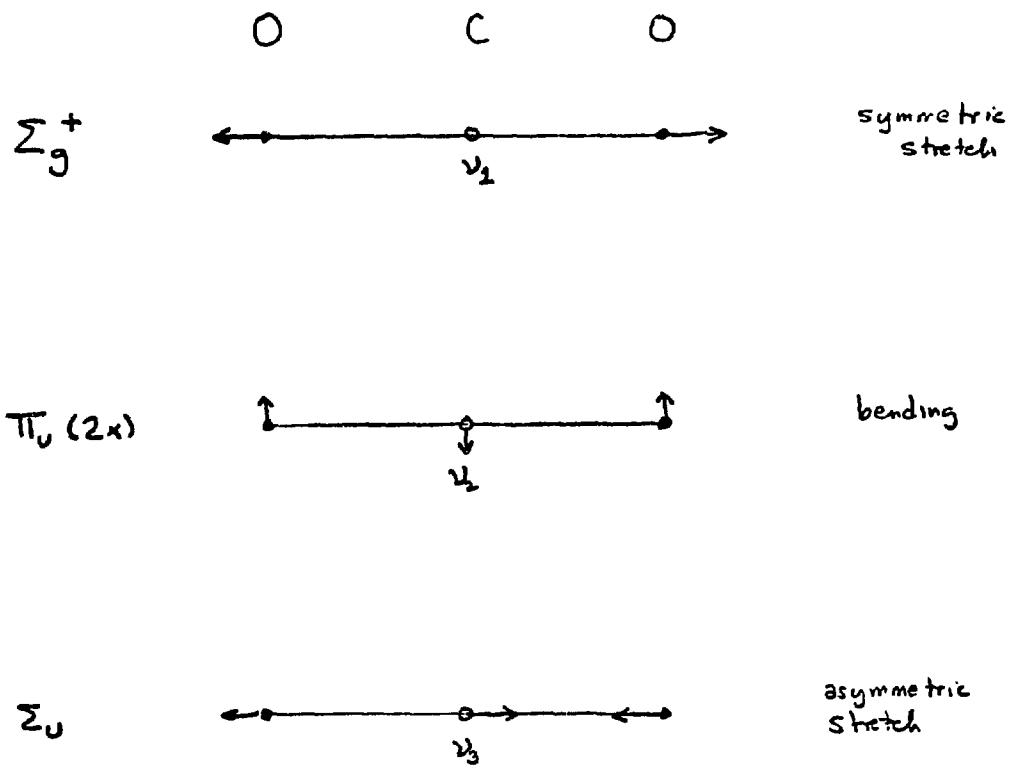

Figure 2.1

Vibrational normal modes of the CO_2 molecule together with the species corresponding to each mode. The bending mode is two-fold degenerate.

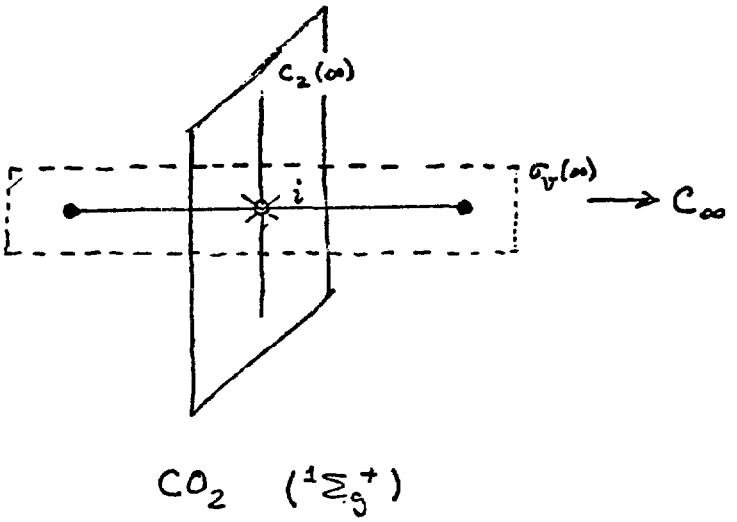

Figure 2.2

The symmetry elements of the CO_2 molecule in its linear nuclear configuration. The elements are discussed in the text.

1). an infinite-fold axis of symmetry C_∞;

2). an infinite number of C_2 symmetry axes perpendicular to C_∞;

3). an infinite number of vertical reflection planes σ_v passing through C_∞;

4). one horizontal reflection plane σ_h perpendicular to C_∞.

There are also symmetry elements which follow from these, e.g., the center of symmetry and associated inversion operator i, which defines the symmetry of a molecular state as either gerade or ungrade. Of course, the potential energy is invariant with respect to all symmetry operations permitted by the point group of the molecule.

The vibrational energy level diagram for the lowest several states is shown in Figure 2.3. The average energy spacing for the various are[1]

symmetric stretch (n00)	0.17 eV
bending ($0n^{\ell}0$)	0.08 eV
asymmetric stretch (00n)	0.29 eV

Two of the modes; the bending and asymmetric stretch, are optically active and have associated dipole moments. For example, in the bent nuclear configuration, population analysis shows[6] a polarization of the electrons toward the oxygen atoms, leading to a dipole moment directed from the oxygens toward the carbon atom. Such observations are important, for in the harmonic approximation, which has been shown to be adequate for reproducing fundamentals and lower interband transitions, the intensity of the infrared

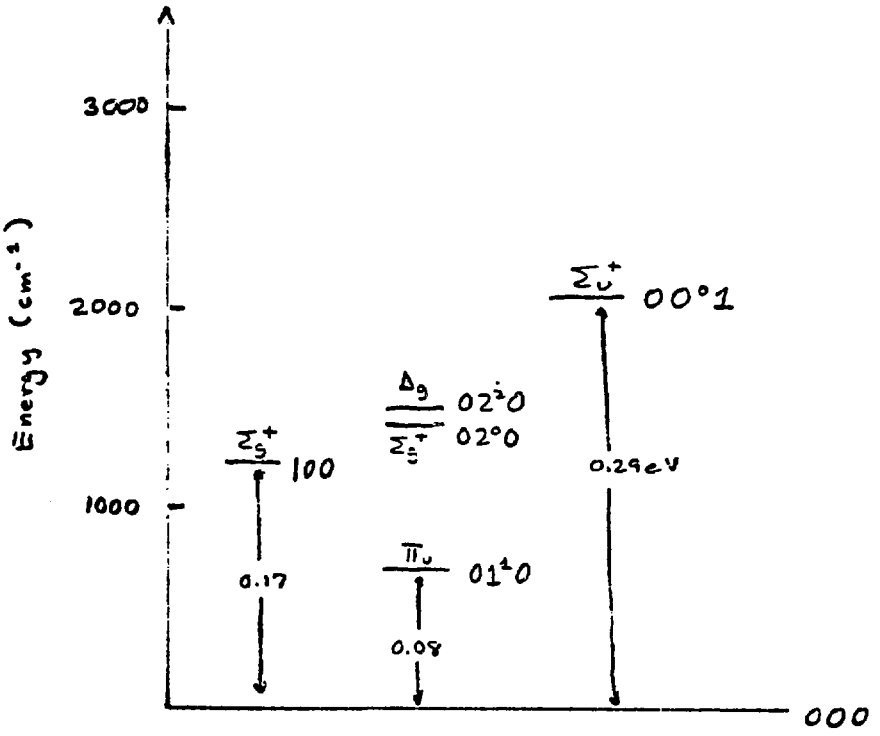

Figure 2.3

The lowest several vibrational energy levels for the CO_2 molecule.

active* bands[7] is proportional to the dipole moment derivative for the vibration under consideration.

One especially interesting feature of the vibrational structure of CO_2 is the Fermi resonance.[8] As Figure 2.3 shows, the 020 and 100 levels have nearly the same energy. This accident leads to a perturbation of the energy levels which pushes them apart.** Thus the 100 level is raised and the 02^00 lowered.

Our interest in the next several chapters is focused on the electronic states, in particular the $X^1\Sigma_g^+$ state. A great deal of work on the structure theory of CO_2 has been carried out[9-19], from the early work of Mullikan and others to the recent highly accurate computations of McLean and Yoshimine, which we discuss in considerable detail in section 3.2. In addition, there has been some important work[20-24] done on the CO_2^- ion, to which we return in section 2.3 when we look at resonances in e-CO_2 scattering.

§2.3. A Quick Survey of Electron-CO_2 Scattering

An enormous amount of experimental work on e-CO_2 scattering has been carried out to date,[29-50] beginning with the 1930

*By an infrared active vibration we mean simply[1] that a change in the dipole moment leads to emission or absorption of radiation at the fundamentals of the normal frequencies; these appear in the infrared. Symmetric molecules may have infrared inactive vibrations.

**Only the (Σ_g) 02^00 level can perturb the 100 level since it is Σ_g, and only vibrational levels of the same species (irreducible representation to group theory fans) can perturb one another.

research of Ramsauer and Kollath and continuing to recent highly accurate swarm experiments by Phelps and collaborators. Both total and momentum transfer cross sections for elastic and inelastic scattering are available, but no extensive studies of differential cross sections have been published as of this writing.

In all of this work, the results that are of especial interest to us are (a) a resonance which has been observed at 3.8 eV; (b) momentum transfer cross sections at energies below about 0.1 eV.

Boness and Schultz,[37] using a crossed-beam technique, observed resonance behavior in vibrational excitation of CO_2 by electron impact and correctly ascribed the 3.8 eV peak to a compound state of CO_2^-. This resonance has been further studied experimentally by other authors[39,40,50] and has received some theoretical attention.[20,22] As a result of the latter, it was tentatively identified as a shape resonance in Π_u symmetry. We have studied the 3.8 eV resonance in considerable detail. Our conclusions appear in Chapter 8 of the present work.

The low energy momentum transfer cross sections of Phelps et al.[49] are dear to our heart, since they initially motivated the choice of CO_2 as a target for our study. The key result and source of considerable theoretical and practical interest is shown in Figure 2.4, where we see that σ_{mom} at energies below 0.1 eV is anomalously large, larger, in fact, than σ_{mom} for some <u>polar</u> molecules!

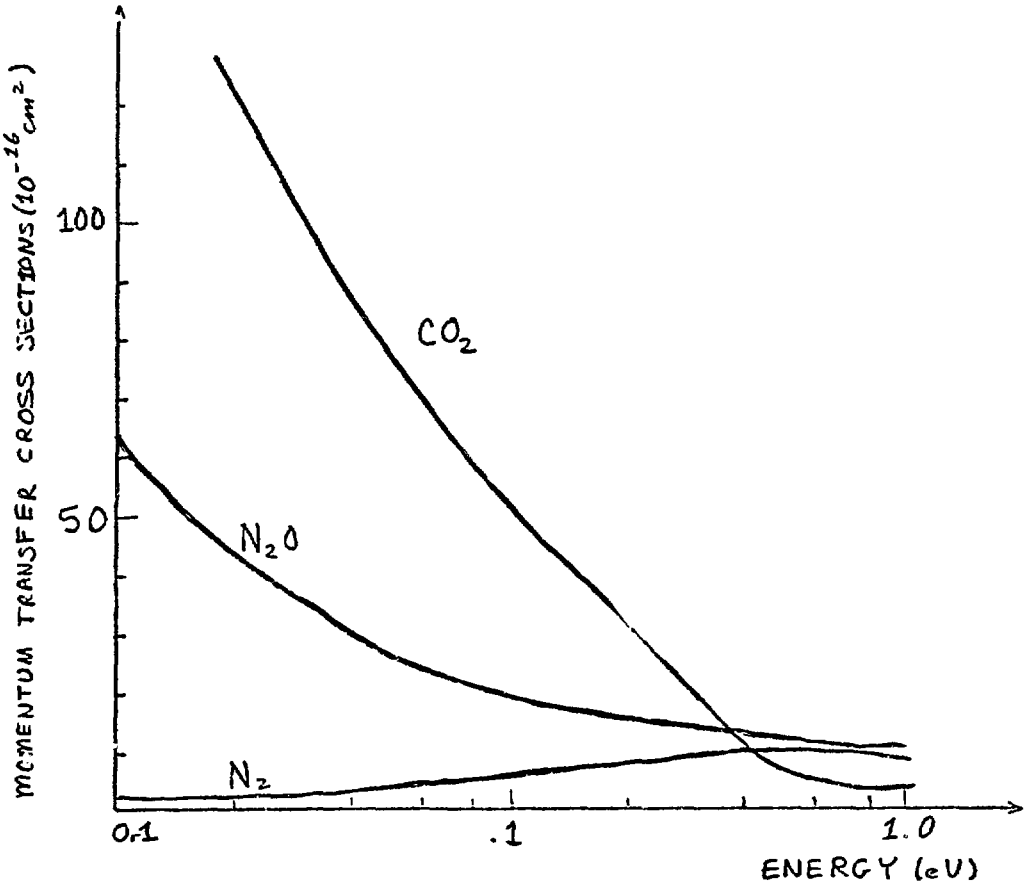

Figure 2.4

Observed momentum transfer cross sections for electron scattering from CO_2, N_2O (polar) and N_2 (non-polar). Souces: CO_2 [R. D. Hake and A. V. Phelps, Phys. Rev. 158, 70 (1967)], N_2O [J. L. Pack, R. E. Voshall, and A. V. Phelps, Phys. Rev. 127, 2084 (1962)], N_2 [A. G. Engelhardt, A. V. Phelps, and C. G. Risk, Phys. Rev. 135, A1566 (1964)].

Some early work which suggested that this was the case was carried out by Tice and Kivelson,[51] who used cyclotron resonance techniques to carry out experimental studies of low energy electron molecule scattering. These authors investigated linewidths and fit their cross sections semi-empirically to the form

$$\sigma_{CO_2} = 110\left(\frac{v}{v_0}\right)^{-1}. \tag{2.2}$$

Their momentum transfer cross sections are anomalously large at low energy, and Tice and Kivelson posit an interesting "adiabatic" model of the collision process based on the transient dipole moment which obtains when the molecule bends. Unfortunately, this model does not work at all well, predicting cross sections about 16 times too large. The present author has studied this picture of the collision in another context and found it to be unsatisfactory.[52]

The experiments of Phelps et al., which produce the data of Figure 2.4, are swarm experiments* based on drift velocity measurements. Extraction of cross sections from drift velocities and diffusion coefficients is a highly involved process entailing solution of the Boltzmann equation. To suggest the highly peculiar nature of the observed momentum transfer cross sections, we present in Table 2.1 a list of various atoms and molecules in order of

*Chapter 2 of reference (54), contains all the author considers any theoretical physics graduate student should say about swarm experments. See reference (49) for more detail.

Atoms	Molecules	Order of Magnitude
Ne		10^{-16}
O		
	O_2	
He		
Ar		
	H_2	
	CO	
	NO	
Hg		10^{-15}
Kr		
	CH_4	
	N_2O	
Xe		10^{-14}
	CO_2	
Cs		10^{-13}
	NH_3	
	N_2O	

Table 2.1

Measured momentum transfer cross sections at $\sim$ 0.1 eV in increasing order (units are cm^2). From reference (53).

increasing σ_{mom} at ~ 0.1 eV. It is also interesting to note the analogies between observed e-CO_2 scattering and observed electron-rare gas scattering. See, for example, the e-Ar cross sections[55] of Figure 2.5. We shall have much more to say on this matter in the analysis of our results (Chapter 8).

Before leaving the subject of momentum transfer cross sections, consider for a moment the definition

$$\sigma_{mom} = \int_0^{2\pi} d\phi \int_0^{\pi} \sin\theta \, d\theta \, (1-\cos\theta) \frac{d\sigma}{d\Omega} , \qquad (2.3)$$

where $d\sigma/d\Omega$ is the differential cross section. The momentum transfer cross section is finite, in general, and the factor $(1-\cos\theta)$, which goes to zero at small angles, causes forward scattering to be de-emphasized in σ_{mom}. This is in contrast to the total cross section,

$$\sigma_{tot} = \int_0^{2\pi} d\phi \int_0^{\pi} \sin\theta \, d\theta \, \frac{d\sigma}{d\Omega} , \qquad (2.4)$$

which equally weights all angles in the integrand. However, unless there is substantial scattering in either the forward or backward direction, $\sigma_{mom} \simeq \sigma_{tot}$.

The momentum transfer cross section is of practical interest, for example, because it aids in the study of the transport properties of gases, enabling one to compute, say, transport collision frequencies by appropriately averaging the momentum transport cross sections over the energy distribution of the electrons, which might be taken to be Maxwellian, e.g., the distribution function might be[56]

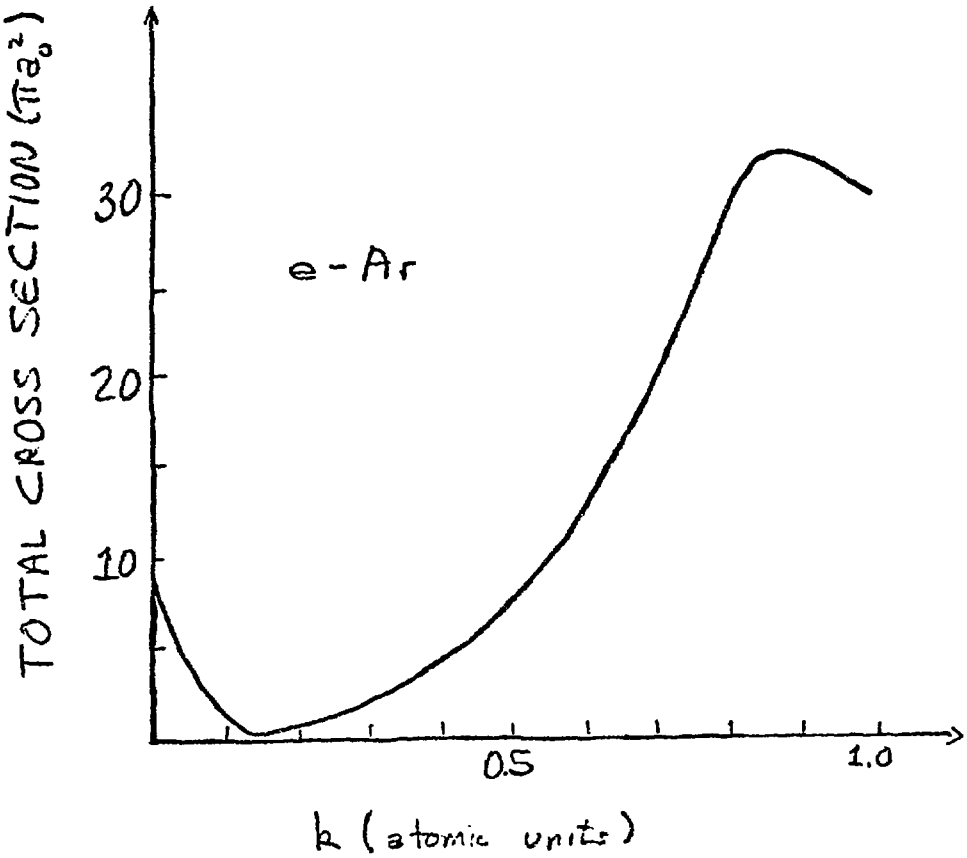

Figure 2.5

Total cross sections for e-Ar scattering in a static-exchange-with polarization model. Source: D. G. Thompson, Proc. Roy. Soc. (London) A 294, 160 (1966).

$$f(E)dE = N_e \frac{2}{\sqrt{\pi}(k_B T)^{3/2}} e^{-E/k_B T}\sqrt{E}\,dE, \qquad (2.5)$$

where k_B is Boltzmann's constant.

§2.4. Conclusion: The CO_2 Laser

We would be remiss in closing out this overview without saying a word or two about the importance of CO_2 to laser physics.[57-60] There does exist a pure CO_2 laser,[59] which is based on the fact that population inversion due to electron impact is favored at incident energies near 1 eV. The dominant energy loss mechanism is excitation of the 001 level, cross sections for decay to other levels being negligible at this energy (see Figure 2.6a).

Much more efficient is the CO_2-N_2 (and CO_2-N_2-He) laser system.[58] In this laser, N_2 acts as a "carrier of excitation," the design exploiting the near degeneracy of the v = 1 level of N_2 at 2331 cm^{-1} and the 001 level of CO_2 at 2349 cm^{-1} (see Figure 2.6b). The active laser transitions are then 001 → 02^00 at 960.8 cm^{-1} and 001 → 100 at 1063.6 cm^{-1}. The drain from 010 to the ground state is comparatively slow.

Momentum transfer cross sections as well as cross sections for vibrational excitation of, e.g., the 001 mode are thus of considerable

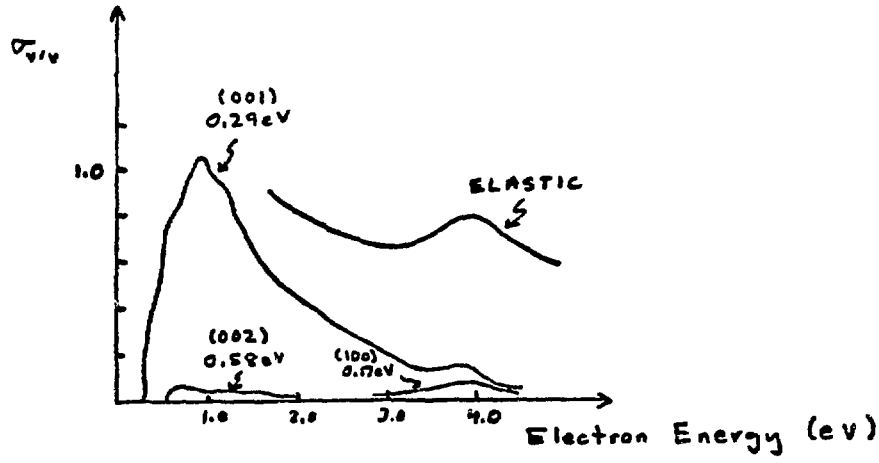

(a)

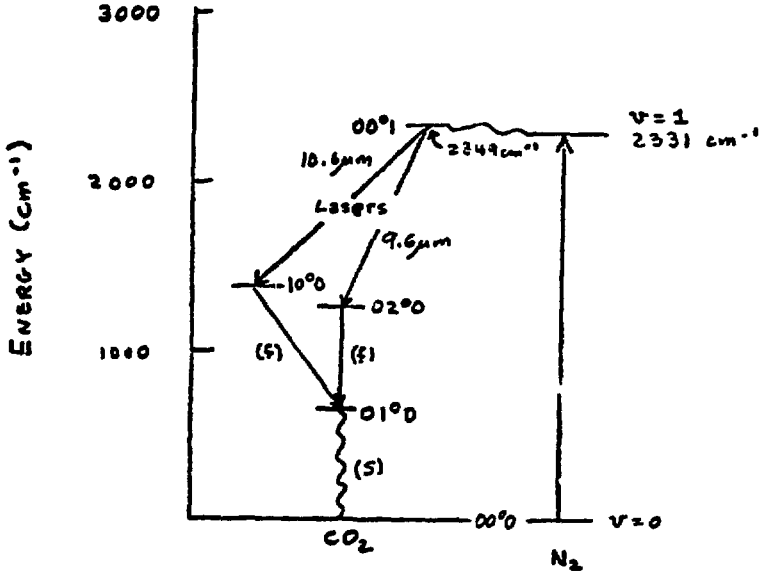

(b)

Figure 2.6

(a). Vibrational excitation cross sections observed in e-CO_2 collisions. Source: M. J. W. Boness and G. J. Schultz, Phys. Rev. Lett. 21, 1031 (1968). (b). The CO_2 - N_2 laser.

importance to experimental laser physicists.* For this reason, the application to CO_2 targets has a special appeal to us, as it addresses problems of fundamental and practical importance. In the next chapter, we begin building a theoretical structure for the analysis of such collisions, starting (where else?) with the Schroedinger equation.

*We gratefully acknowledge useful discussions with Drs. W. Leland and A. M. Lockett of the Los Alamos Scientific Laboratory on these matters.

Chapter 3. The Static e-CO_2 Interaction Potential

No, there are still difficulties, but the outline of the plot is clear and will develop itself more clearly as we proceed.

-M. Rozer to Lord Peter Wimsey in the Nine Tailors (Dorothy L. Sayers)

§3.1 Introduction: What the Static Potential is All About

In the usual time-independent formulation of quantum mechanics, we solve the omnipresent Schroedinger eigenvalue equation,

$$\mathcal{H}\psi_E = E\psi_E \,, \tag{3.1}$$

where the non-relativistic Hamiltonian describing the system is the sum of kinetic and potential energy operators $H = T + V$. For electron-target collisions, we conveniently write $H = H_{target} + T_{electron} + V_{int}$, where H_{target} describes the target system (e.g., atom, molecule, ion), $T_{electron}$ is the kinetic energy operator for the electron,* $-\frac{1}{2}\nabla^2$, and V_{int} is the electron-target interaction potential energy.

All these operators are fairly easy to write down even for a molecular target.[1] We must here focus on $V_{int} = V_{int}(\vec{r}, \vec{r}_i; \vec{R}_\alpha)$, where we let $\vec{r}$ denote the (spatial) coordinate of the scattering

*Unless otherwise indicated, atomic units are used throughout this chapter.

electron, r_i the set of coordinates of the target electrons, and $\vec{R}_\alpha$ the set of nuclear coordinates. We shall take V_{int} to describe the electrostatic interactions due to Coulomb forces between the scattering electron and the undistorted molecular target. Thus, for a molecule, we have

$$V_{int}(\vec{r}, \vec{r}_i; \vec{R}_\alpha) = -\sum_\alpha \frac{Z_\alpha}{|\vec{r} - \vec{R}_\alpha|} + \sum_i \frac{1}{|\vec{r} - \vec{r}_i|} \quad , \tag{3.2}$$

where the first summation runs over the nuclei of charge Z_α and the second over the molecular electrons. (A common origin of coordinates is assumed.) Additional interactions (exchange and induced polarization) will be addressed in Chapters 4 and 5.

In the solution of our body-frame fixed-nucleus coupled-channel equations,*

$$\left[\frac{d^2}{dr^2} - \frac{l(l+1)}{r^2} + k^2\right] u_l^{(m)}(r) = 2 \sum_{l'=0}^{\infty} V_{ll'}^{(m)}(r)\, u_{l'}^{(m)}(r), \tag{3.3}$$

we need the static potential energy averaged over the ground electronic state wavefunction** of CO_2 and "integrated over" the spherical harmonics $Y_{l'}^m(\hat{r})$ and $Y_l^m(\hat{r})$. (Recall that m, corresponding to the projection of the scattering electron's orbital angular momentum, is a good quantum

---

*A detailed derivation of these equations by the author can be found in Chapter 4 of reference (2); they will be briefly treated in Chapter 6 of this work.

**In a more general close-coupling expansion including several electronic states, we also need other matrix elements of V, such as those between the ground and excited states.

number for the problem under consideration.) Thus, if we denote the averaged static potential, which we'll call the inner molecular matrix element (IMME), by

$$V(\vec{r}) = \langle X^1\Sigma_g^+ | V_{int} | X^1\Sigma_g^+ \rangle \ , \tag{3.4}$$

then we require

$$V^{(m)}_{\ell\ell'}(r) = \langle \ell m | V(\vec{r}) | \ell' m \rangle \tag{3.5}$$

The IMME of Eq. (3.4) is also used in laboratory-frame formulations* of the close-coupling method.[3]

In this chapter, we derive and calculate $V(\vec{r})$ and $V^{(m)}_{\ell\ell'}$, and discuss their properties. The electronic wavefunction for CO_2 in the ground state is the subject of §3.2, and the expansion of the charge density is treated in §3.3. How the coefficients are used to calculate $V(\vec{r})$, the expansion of this quantity in Legendre polynomials, and derivation of an expression for $V^{(m)}_{\ell\ell'}(r)$ are topics addressed in sections 3.4 and 3.5. The calculated static expansion coefficients $v_\lambda(r)$ are presented in §3.6 and some discussion of the physics inherent in them follows. In §3.7, we chat briefly about the effective potential, and, finally, in §3.8 try to put CO_2 into some perspective by comparing its electron interaction potential energy with that of a couple of more familiar systems.

*Although this approach was abandoned rather early in this research for reasons to be discussed in Chapter 8 , a short description of it appears (for completeness sake) in Appendix 2.

§3.2 The Molecular Target Electronic Wavefunction for Ground-State CO_2

An essential first step in the calculation of the averaged potential energy $V(\vec{r})$ is selection of an electronic wavefunction for CO_2 in the ground state linear configuration;* that is, we need $\Psi_{^1\Sigma_g^+}(\vec{r}_i,\vec{R}_\alpha)$ in a form amenable to manipulation in the calculation of $V(\vec{r})$ and subsequent quantities.

Fortunately, highly accurate near-Hartree-Fock wavefunctions for CO_2 in the ground state at the equilibrium C-O separation R_{o-c} = 2.19440 a_o have been calculated by A. D. McLean and M. Yoshimine[5] and are available in tabular form.[6] As we chose to adopt these functions, we should look briefly at how they are calculated and at their quality.

The wavefunctions are obtained within the context of self-consistent-field molecular orbital theory[7] in an incarnation referred to as the expansion formulation.[8] All this really means is that the state ($X^1\Sigma_g^+$ here) is represented by a configuration** made up of SCF molecular orbitals[9] doubly-occupied with electrons of anti-parallel spins. The molecular orbitals, in turn, are constructed from an SCF atomic basis set of double-zeta quality (see below) augmented to include polarization functions. The atomic basis is built from Clementi's Hartree-Fock atomic basis[10] in a fairly complicated manner described

*A general discussion of molecular structure theory by the author appears in Chapter 5 of reference (2). See also Chapters IV and V of Schaeffer's text.(4)

**We are using the word "configuration" in the standard though perplexing quantum-chemical sense as, in general, a symmetry-adapted linear combination of Slater determinants. See reference (4), Chapter I, and try not to confuse this word with an electron configuration as discussed in Chapter 2, which quantum chemists call an orbital occupancy. The field is not noted for internal consistency.

in detail in reference (5). On top of this, the rigid-nucleus Born-Oppenheimer approximation[11] is employed i.e., the motions of the electrons and the nuclei are treated separately and R_{o-c} is frozen at some pre-determined value.

To translate, the double-zeta (DZ) basis set[10,12] contains two functions (of the same symmetry type) for each occupied atomic orbital in the separated-atoms limit. Thus, the DZ basis set is twice the size of the usual minimum basis set of molecular calculations.[4] Each atomic basis function is a symmetrized linear combination of normalized Slater-type orbitals (STO) of the form

$$\chi_p(n\,l\,m\,k\,\zeta_p) = \sqrt{\frac{(2\zeta_p)^{2n+1}}{(2n)!}}\, r_k^{n-1} e^{-\zeta_p r_k}\, Y_l^m(\hat{r}_k), \qquad (3.6)$$

where k denotes the atomic center with respect to which $\vec{r}_k$ is defined and ζ_p is a non-linear parameter which is chosen to minimize the separated-atom energies. Linear combinations of the χ_p (called symmetrized basis functions) are chosen to reflect the fact that each MO belongs to one of the irreducible representations of the point group of the target in the problem.[13] Thus for CO_2 we have σ_g, σ_u, π_g, π_u, etc. MO's which are built of basis functions of the general form $\chi_p \pm \chi_{p'}$, where χ_p and $\chi_{p'}$ are centered on symmetrically equivalent nuclei (the two oxygens, for example) and have the same quantum numbers n, ℓ, and m, and orbital exponents $\zeta_p = \zeta_{p'}$. (Obviously this problem does not arise for MO's centered on the carbon atom.) A typical wavefunction for a closed-shell system composed of N occupied orbitals

(2N electrons)* is just the usual Slater determinant[14]

$$\Psi(1,2,\ldots,N) = \left|\phi_1(1)\alpha(1)\ \ \phi_1(2)\beta(2)\ \ \phi_2(3)\alpha(3)\cdots\phi_N(2N)\beta(2N)\right|, \quad (.37)$$

where the ϕ_i are the aforementioned appropriately symmetrized orthonormal MO's.

Calculations were also carried out which supplement the DZ basis set with higher-ℓ atomic basis functions chosen to represent the polarization of the atomic electrons in the molecule and optimized to minimize the total molecular energy.[15] It is usually the case that the most important such functions are of symmetry types with angular momentum quantum number ℓ corresponding to the lowest unoccupied atomic orbital in the separated-atoms limit. Thus, for CO_2 they are d-functions ($\ell = 2$). We employ these "double-zeta plus polarization" (DZP) functions.** The resulting wavefunction has an SCF energy of -187.7037 hartrees and an electronic energy of -246.0339 hartrees. This compares to the "close-to-Hartree-Fock" SCF energy of -187.7228 hartrees.

---

*The molecular orbitals with $m > 0$ (e.g., $\pi,\Delta,\ldots$) are, of course, doubly degenerate. For example, we have π_{u_x} and π_{u_y} orbitals each of which is doubly occupied.

**McLean and Yoshimine's final basis set consists of (5s 4p 1d 1f) functions centered on each nucleus. The f functions further account for polarization but are an order of magnitude less important than are the d functions.[5]

Notice that electron correlation is not included in this calculation; such could be accomplished via a configuration interaction calculation[16] if desired (and monetarily feasible!). The SCF approximation breaks down quite stunningly for most molecules as they dissociate[17] (e.g., as $R_{O-C} \rightarrow \infty$). Thus, the SCF potential energy curves predict unreliable electronic energy separations. For some systems the situation is even more serious (e.g., SCF theory predicts[17] the wrong sign of the dipole moment for CO!). But we probably need not worry, since our work is done at the equilibrium separation and ground-state CO_2 is non-polar.

There is no point in reproducing the expansion coefficients and exponents here; however, the orbital energies, shown in Table 3.1, are of some interest. Also included in this table are the energies of the lowest unoccupied orbital of each symmetry type. Notice that $1\sigma_u$, an anti-bonding (or "nonbonding") orbital,[18] lies slightly lower in energy than does the $1\sigma_g$ bonding orbital. It is also important to note that the lowest unoccupied orbital, $5\sigma_g$, lies a whopping 0.22 au (2.99 eV) above the zero of energy. This will take on an ominous significance in the sequel.

The question remains: How "good" is the CO_2 wavefunction we have selected? One way to tell is to compare the expectation values of various operators with observed quantities. An "energy criterion" is provided by the dissociation energy, defined by McLean and Yoshimine[5] as

$$D_e = \sum_{atom} E_{atom}(DZ) - E_{mol}(DZP), \qquad (3.8)$$

where E_{atom} (DZ) is the appropriate separated-atom energy in the

Orbital	Energy (hartrees)
$1\sigma_u$	-20.64862
$1\sigma_g$	-20.64858
$2\sigma_g$	-11.46382
$3\sigma_g$	-1.53037
$2\sigma_u$	-1.47832
$4\sigma_g$	-0.80052
$3\sigma_u$	-0.74399
$1\pi_u$	-0.71315
$1\pi_g$	-0.54382
$5\sigma_g$	0.21691
$2\pi_u$	0.22606
$4\sigma_u$	0.81091
$2\pi_g$	1.34995

Table 3.1

Close-to-Hartree-Fock energies for molecular orbitals in CO_2: occupied and lowest unoccupied of each symmetry. (From reference 6.) The total electronic energy of $CO_2(X^1\Sigma_g^+)$ is -246.0339 hartrees.

double-zeta approximation. For CO_2, McLean and Yoshimine[5] report D_e = 11.12 eV compared with the observed[19] value of D_e = 16.85 eV. These authors report their molecular-orbital expansion coefficients as converged to four decimal places. Further discussion may be found in reference (6).

As one additional test, we extract the quadrupole moment* of CO_2 from our $v_2(r)$ calculated using the McLean and Yoshimine $X^1\Sigma_g^+$ wavefunction and obtain q = - 3.8598 ea_o^2. In summary, we feel that the $X^1\Sigma_g^+$ wavefunction employed in this calculation is probably at least as accurate as other approximations to be discussed below.

There do exist a few other CO_2 wavefunctions in the literature which we could have used. For example, Snyder and Basch in their extremely useful tabulation of molecular wavefunctions,[20] report Hartree-Fock wavefunctions based on a double-zeta Gaussian basis set for CO_2. However, their calculations do not include polarization orbitals, were carried out only at the equilibrium O-C separation. and yield a total energy of -187.5377 au, significantly above that of the McLean and Yoshimine wavefunction.

§3.3 Expansion of the CO_2 Charge Distribution

Given the normalized electronic wavefunction for CO_2 in the desired state, we can easily form the probability distribution in the usual way as $\Psi^*_{1\Sigma_g^+}(1,2,\ldots,N)\Psi_{1\Sigma_g^+}(1,2,\ldots N)$. A quantity which is

*Further discussion of q and its extraction appears in sections 3.5 and 3.8.

easier to think about (and look at) is the charge distribution, defined as*

$$\rho(r,\theta) \equiv N\int \psi^{*}_{^1\Sigma_g^+}(1,2,\ldots,N)\,\psi_{^1\Sigma_g^+}(1,2,\ldots,N)\,d\tau\,, \tag{3.9}$$

where we integrate over the spatial and spin coordinates of all but one of the target electrons. As its name implies, this function describes the distribution in space of the electronic charge of the molecule. It is independent of ϕ, the polar angular coordinate, because CO_2 in the linear configuration has axial symmetry. The probability of finding an electron in a volume element $dv = r^2 dr \sin\theta\, d\theta$ is simply $\rho(r,\theta)dv$.

A useful expression for $\rho(r,\theta)$ in the case at hand, where $\psi(1,\ldots,N)$ is represented as a (single configuration) Slater determinant, can be obtained by writing the charge density as an expansion in Legendre polynomials. First notice that by substituting the form of Eq. (3.7) for $\Psi_{^1\Sigma_g^+}$ in Eq. (3.9), we obtain

$$\rho(r,\theta) = \sum_{j=1}^{M} N_j \left|\phi_j(\vec{r})\right|^2, \tag{3.10}$$

where N_j is the occupation number of the j^{th} molecular orbital (e.g., $N_j = 2$ for a σ_g orbital) and the sum runs over the M occupied molecular orbitals (M = 9 for CO_2). For example, for $H_2(X^1\Sigma_g^+)$, we have $\rho(r,\theta) = 2|\phi_{1\sigma_g}(\vec{r})|^2$. Of course, the charge density must satisfy the

*This function is also variously known in chemistry circles as the "one-electron density function" and the "probability density." Care must be exercised in using the latter phrase, as different scientists sometimes have different definitions.

relation

$$\int \rho(\vec{r})\, d^3r = N, \tag{3.11}$$

where N, the number of electrons, is 22 for CO_2.

It is now no problem to expand $\rho(r,\theta)$ as

$$\rho(r,\theta) = \sum_{\lambda=0}^{\infty}{}' a_\lambda(r)\, P_\lambda(\cos\theta), \tag{3.12}$$

where $P_\lambda(\cos\theta)$ is an ordinary Legendre polynomial[21] and the prime reminds us that only even-λ coefficients are non-zero. This is true because the point group of the electronic state of CO_2 under consideration contains a horizontal reflection plane passing through the carbon nucleus (see Chapter 2).

Using the orthonormality relationship of the Legendre polynomials,

$$\int_{-1}^{+1} P_\lambda(x)\, P_{\lambda'}(x)\, dx = \frac{2}{2\lambda+1}\, \delta_{\lambda\lambda'}, \tag{3.13}$$

where $x = \cos\theta$, we find

$$a_\lambda(r) = \frac{2\lambda+1}{2}\int_0^{\pi} \rho(r,\theta)\, P_\lambda(\cos\theta)\, \sin\theta\, d\theta. \tag{3.14}$$

This is the expression we use to evaluate the necessary expansion coefficients.

In passing we should note that the McLean and Yoshimine molecular orbitals are nucleus-centered, and that therefore we must convert them to a common origin, which we handily take to be the carbon nucleus. The coordinate transformations represent a trivial application of

high school plane trigonometry. However, nothing is too trivial for a graduate student, so we herewith present the relevant formulae with reference to Figure 3.1 for the obvious definitions; to convert functions in $\vec{r}_1$ and $\vec{r}_3$ to spherical coordinates in $\vec{r}_2$, use

$$r_1^2 = r_2^2 + b^2 + 2rb\cos\theta_2 \tag{3.15a}$$

$$r_3^2 = r_2^2 + b^2 - 2rb\cos\theta_2 \tag{3.15b}$$

$$\cos\theta_3 = \frac{1}{2r_3 b}(r_2^2 - r_3^2 - b^2) \tag{3.16a}$$

$$\cos\theta_1 = \frac{1}{2r_1 b}(r_1^2 + b^2 - r_2^2). \tag{3.16b}$$

A computer program* was written to evaluate the integral in Eq. (3.14) using Gaussian quadrature.[22] For small values of λ (e.g., $\lambda \lesssim 10$), a 24-point quadrature gives results converged to <1% (compared with a 32-point quadrature) over the range of r-values required. For higher $\lambda (10 \lesssim \lambda \lesssim 30)$, a 64-point quadrature was necessary. All values of $a_\lambda(r)$ used in this work are converged to < 1%.

*Called, for no particular reason, EXPCD. Part of the logic of this code was taken from a similar code, ALAM, written by L. Collins of the Atomic and Molecular Theory group at Rice University.

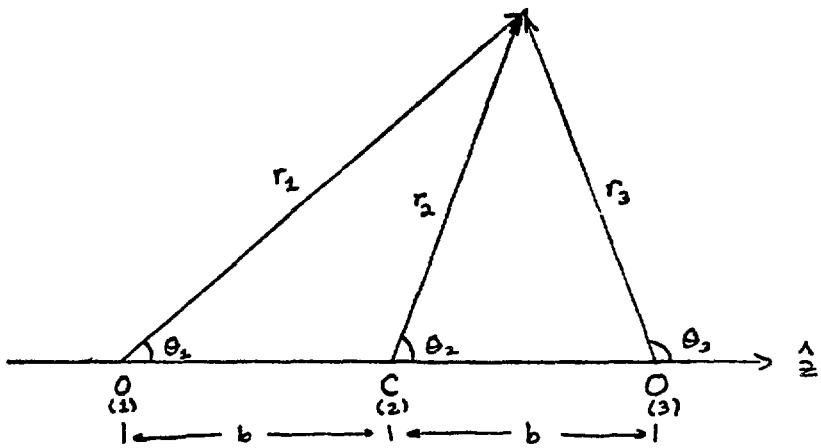

Figure 3.1

The geometry of the CO_2 molecule. The coordinates shown are related by equations in the text.

Beyond about 5.0 a_o, the $a_\lambda(r)$ can be fit to an exponential form, which obviates the need for further quadrature. Thus we fit to

$$a_\lambda(r) = A_\lambda e^{-\alpha_\lambda r} \qquad r \gtrsim 5.0 a_0 \tag{3.17}$$

using a two-point fit. We find

$$\alpha_\lambda = -\frac{\ln(y_1/y_2)}{r_1 - r_2} \tag{3.18a}$$

$$A_\lambda = y_1 e^{-\alpha_\lambda r_1} \quad , \tag{3.18b}$$

where y_1 and y_2 are the values of $a_\lambda(r)$ at adjacent points r_1 and r_2.

By far the most expensive part of the calculation of the expansion coefficients $a_\lambda(r)$ is the evaluation of $\rho(r,\theta)$ at the required θ-mesh, determined by the number of points required to accurately spline fit $a_\lambda(r)$ in calculation of $v_\lambda(r)$ [see §3.5 below]. Fortunately $\rho(r,\theta)$ need only be calculated once for a given mesh, and a code to do this* was prepared and used. A 64-point θ-mesh and 131-point r-mesh calculation of $\rho(r,\theta)$ required 273 seconds on a CDC-7600 computer.** Then each $a_\lambda(r)$ required < 15 sec.

It turned out to be necessary to compute 15 $a_\lambda(r)$ [i.e., $a_0(r)$, ...,$a_{28}(r)$] in order to converge the potential (see below). This is an unusually large number of terms even for electron-molecule scattering and is a reflection of the enormity of the target (as discussed in Chapter 2). Each $a_\lambda(r)$ typically peaks at the O-C

*CHGDIST by name.

**Once $\rho(r,\theta)$ has been determined it is used again in the calculation of the approximate exchange potential we use. See Chapter 4.

separation of 2.1994 a_o and dies off elsewhere [except $a_0(r)$, which rises near r = 0, reflecting the influence of the carbon atom at the origin]. A few typical $a_\lambda(r)$ together with $a_0(r)$ (on a logarithmic scale) are graphed in Figure 3.2.

In addition to hand checks of selected $a_\lambda(r)$, a useful verification can be carried out by means of Eq. (3.11). Substituting the expansion (3.12) in (3.11), we obtain

$$4\pi \int_o^\infty a_0(r)\, r^2\, dr = N. \tag{3.19}$$

Using our $a_0(r)$ calculated from McLean and Yoshimine's wavefunction we obtain 22.0052 for the left-hand-side of (3.19).* Since the wavefunction used is valid to no more than four decimal places, the probability distribution is expected to be good to no more than two places, suggesting that this minute amount of excess charge is no real cause for alarm.

§3.4 Calculation of the Averaged Static Potential Energy and Expansion in Legendre Polynomials

At long last we are ready to consider evaluation of the averaged static potential, $V(\vec{r}) = \langle X^1\Sigma_g^+ | V_{int} | X^1\Sigma_g^+ \rangle$ of Eq. (3.4) and of the matrix elements $V_{\ell\ell'}^{(m)}(r) = \langle \ell m | V(\vec{r}) | \ell' m \rangle$ of Eq. (3.5), which appear in the coupled equations (3.3) to be solved. Basically, this is just

*The slight excess charge of +0.0052 shows up as a Coulomb tail in $v_0(r)$, the P_0 projection of the average static potential energy. We artificially remove this from $v_0(r)$ as discussed below.

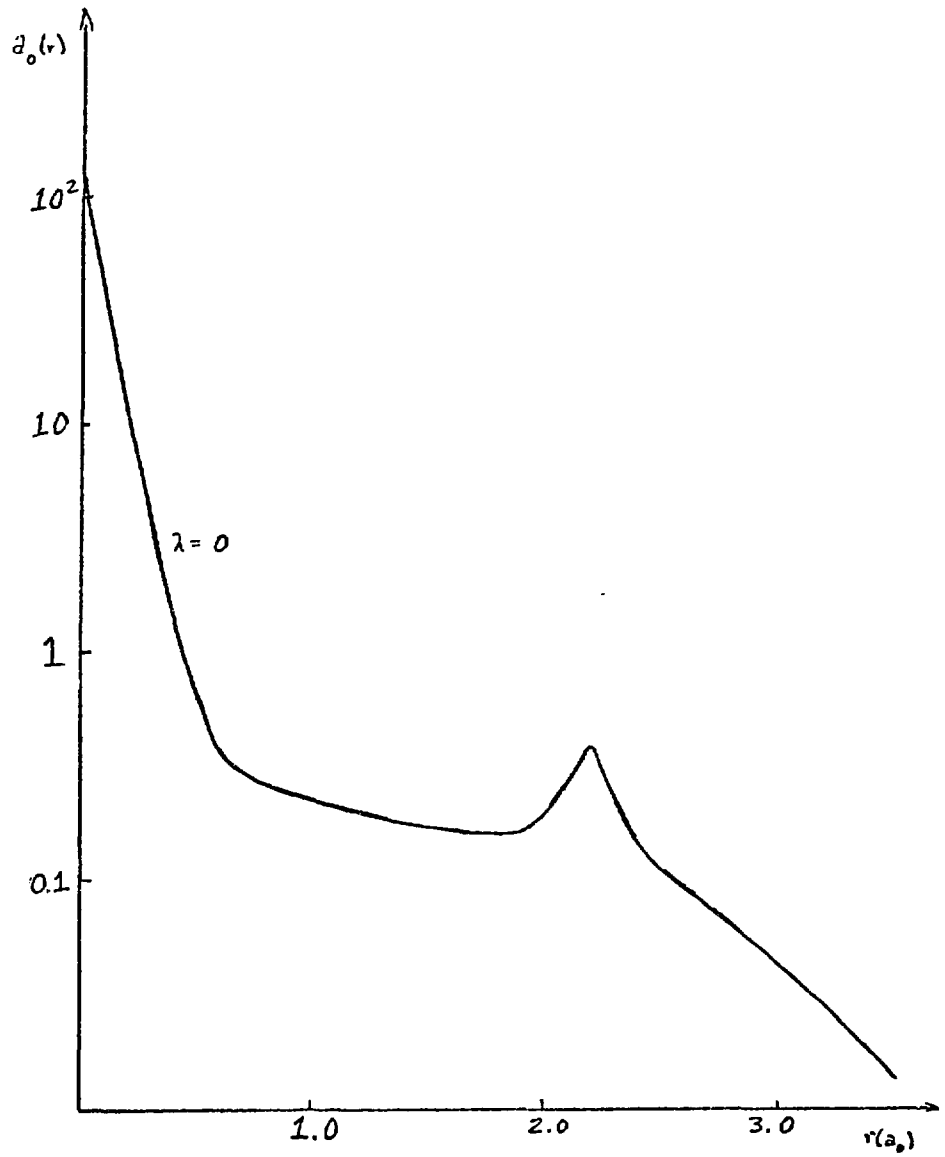

Figure 3.2

Expansion coefficients of the CO_2 charge distribution (ground electronic state) for a Legendre-polynomial expansion. (a). $\lambda = 0$; (b). $\lambda = 2$, 4, and 6. [See Eq. (3.12).]

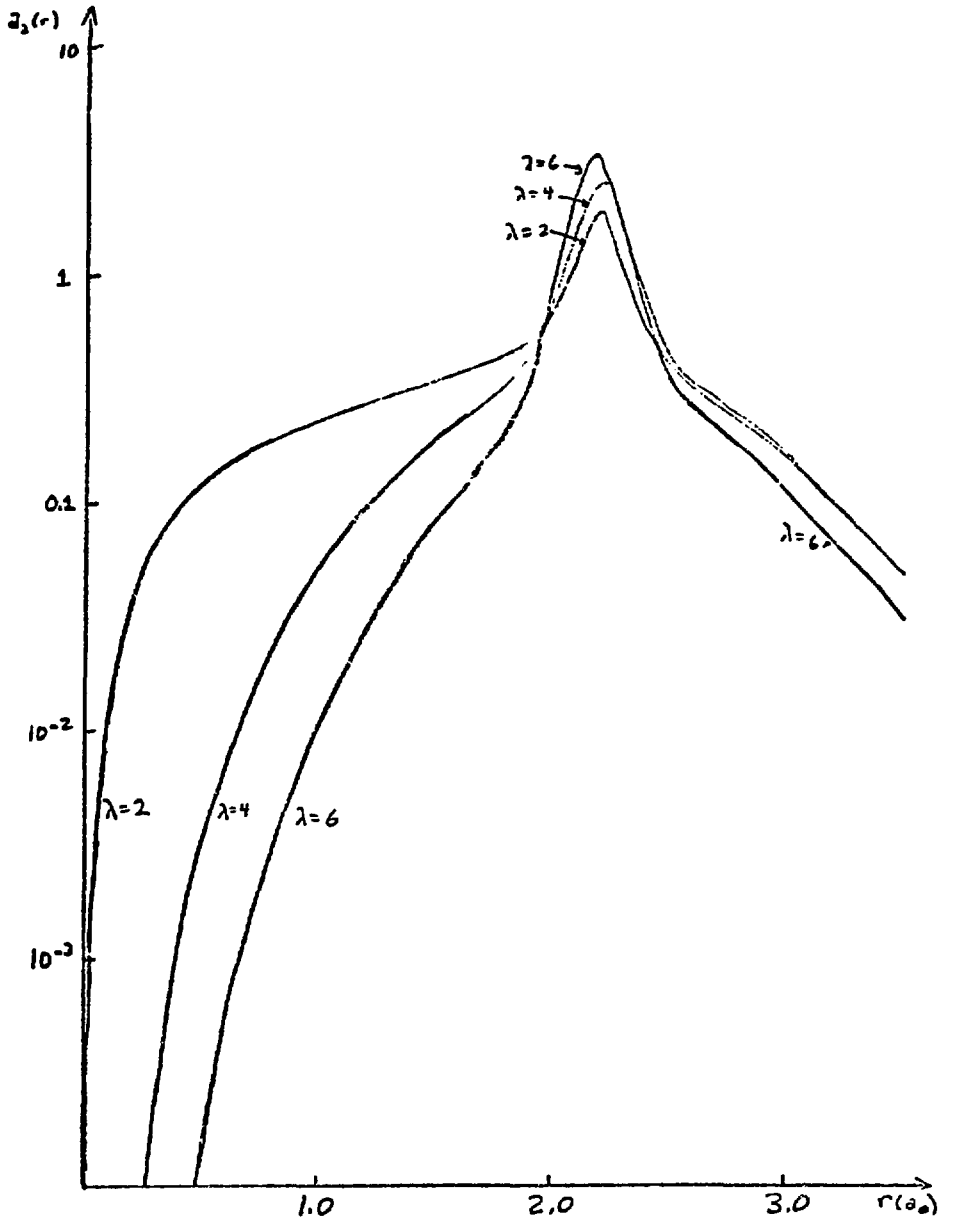

(b)

a lot of rather unexciting algebra; the key results are Eqs. (3.39) and (3.40) for V(r) and (3.43) for $V_{\ell\ell'}^{(m)}(r)$.

Onward to the algebra! We first assault the inner molecular matrix element (IMME), which, in the Born-Oppenheimer approximation, is

$$V(\vec{r}) = \int \psi^{*}_{^1\Sigma_g^+}(\vec{r}_i;\vec{R}_\alpha)\, V_{int}(\vec{r},\vec{r}_i;\vec{R}_\alpha)\, \psi_{^1\Sigma_g^+}(\vec{r}_i;\vec{R}_\alpha)\, d\tau, \tag{3.20}$$

where we integrate over all N target electronic coordinates. Sighs of relief fill the room as we realize that we can simplify this hideous integral by taking into account the known form of the electronic wavefunction. First let's introduce the interaction potential energy of Eq. (3.2) into the IMME. Assuming $\vec{R}_\alpha$ to be frozen and using orthonormality of $\Psi_{^1\Sigma_g^+}$, we obtain

$$V(\vec{r}) = -\sum_\alpha Z_\alpha \frac{1}{|\vec{r}-\vec{R}_\alpha|} + \int \psi^{*}_{^1\Sigma_g^+}(\vec{r}_i) \sum_i \frac{1}{|\vec{r}_i-\vec{r}|}\, \psi_{^1\Sigma_g^+}(\vec{r}_i)\, d\tau, \tag{3.21}$$

which we'll write as

$$V(\vec{r}) = I_1(\vec{r}) + I_2(\vec{r}), \tag{3.22}$$

separating the first (nuclear) and second (electronic) terms. For CO_2, $\alpha = 1,2,3$, and $Z_1 = Z_3 = 8$ and $Z_2 = 6$.

We can now reduce $I_2(\vec{r})$ to a sum of somewhat more congenial one-dimensional integrals. To this end, let's write the electronic wavefunction as

$$\psi_{^1\Sigma_g^+}(\vec{r}_i) = \frac{1}{\sqrt{N!}} \sum_P (-1)^P [\lambda_1(1)\ \lambda_2(2)\ \cdots\ \lambda_N(N)], \tag{3.23}$$

where we have introduced the singly-occupied spin orbitals $\lambda_i(j)$,

e.g., $\lambda_1(1) = \phi_1(\vec{r}_1)\,\alpha(1)$ and $\lambda_2(2) = \phi_1(\vec{r}_2)\,\beta(2)$ etc. The sum in Eq. (3.23) is over the N! possible permutations of the N spin-orbitals, and the factor of $(-1)^p$ enforces antisymmetry of $\Psi_{^1\Sigma_g^+}$ under pairwise electron interchange. Substituting this expression into I_2 and using the spin orthogonality of the λ_i's, we find that

$$I_2(\vec{r}_N) = \sum_{i=1}^{N} \int \lambda_i^*(1)\,\frac{1}{r_{1N}}\,\lambda_i(1)\,d1, \qquad (3.24)$$

where we've let $\vec{r}_N = \vec{r}$ to clarify* $r_{1N} \equiv |\vec{r}_1 - \vec{r}_N|$. Returning to the M spatial molecular orbitals $\phi_i(r)$, we obtain

$$I_2(\vec{r}_N) = \sum_{j=1}^{M} N_j \int \phi_j^*(\vec{r}_1)\,\frac{1}{r_{1N}}\,\phi_j(\vec{r}_1)\,d^3r_1 . \qquad (3.25)$$

Notice that this is just

$$I_2(\vec{r}_N) = \int \rho(\vec{r}_1)\,\frac{1}{r_{1N}}\,d^3r_1, \qquad (3.26)$$

where $\rho(\vec{r})$ is the charge distribution of the molecule (see §3.3). Putting it all together, we have

$$V(\vec{r}_N) = -\sum_{\alpha} Z_\alpha \frac{1}{|\vec{r}_N - \vec{R}_\alpha|} + \int \rho(\vec{r}_1)\,\frac{1}{r_{1N}}\,d^3r_1 . \qquad (3.27)$$

*We'll use $\vec{r}$ and $\vec{r}_N$ interchangeably in this chapter, preferring the former but using the latter when clarity demands it. Usually $\vec{r}_1$ is our dummy variable of integration.

This form is neither especially useful nor illuminating. However, it is valuable as an intermediary. We really want to expand $V(\vec{r})$ in Legendre polynomials and use the result to calculate $V^{(m)}_{\ell\ell'}(r)$. Let's first attack $I_1(\vec{r})$. If we let $\vec{R}$ be a vector from the carbon nucleus directed toward the oxygen along the $+\hat{z}$ direction, we have for CO_2

$$I_1(\vec{r}_1) = -\frac{6}{r} - 8\frac{1}{|\vec{r}-\vec{R}|} - 8\frac{1}{|\vec{r}+\vec{R}|} \cdot \qquad (3.28)$$

Let us expand:[23]

$$\frac{1}{|\vec{r}-\vec{R}|} = \sum_{\lambda=0}^{\infty} \frac{r_<^\lambda}{r_>^{\lambda+1}} P_\lambda(\cos\theta), \qquad (3.29)$$

where $r_< = \min(r,R)$, $r_> = \max(r,R)$ and θ is the angle between $\vec{r}$ and $\vec{R}$. Similarly,

$$\frac{1}{|\vec{r}+\vec{R}|} = \sum_{\lambda=0}^{\infty} \frac{r_<^\lambda}{r_>^{\lambda+1}} (-1)^\lambda P_\lambda(\cos\theta), \qquad (3.30)$$

where we have used $P_\lambda[\cos(\pi-\theta)] = (-1)^\lambda P_\lambda(\cos\theta)$. Therefore, we have

$$I_1(r) = -\frac{6}{r} - 16\sum_{\lambda=0}^{\infty}{}' \frac{r_<^\lambda}{r_>^{\lambda+1}} P_\lambda(\cos\theta), \qquad (3.31)$$

where only even-λ terms contribute in the second term since $1 + (-1)^\lambda = 0$ for odd values of λ.

Turning now to $I_2(\vec{r})$, we merely shove the expansion for $\rho(r,0)$ in terms of $a_\lambda(r)$, Eq. (3.12), into Eq. (3.25). We have

$$\rho(r,\theta) = \sum_{\lambda=0}^{\infty} \sqrt{\frac{4\pi}{2\lambda+1}}\, a_\lambda(r) Y_\lambda^0(\hat{r}), \tag{3.32}$$

where we have used the well-known relation[24]

$$P_\lambda(\cos\theta) = \sqrt{\frac{4\pi}{2\lambda+1}}\, Y_\lambda^0(\theta,\phi). \tag{3.33}$$

If we further expand $1/r_{1N}$ as

$$\frac{1}{r_{1N}} = \sum_{\lambda=0}^{\infty} \frac{r_<^\lambda}{r_>^{\lambda+1}}\Big)_{1N} P_\lambda(\cos\Theta), \tag{3.34}$$

where $r_< = \min(r_1, r_N)$ and Θ is the angle between $\vec{r}_1$ and $\vec{r}_N$, and convert to angular coordinates via[25]

$$P_\lambda(\cos\Theta) = \frac{4\pi}{2\lambda+1} \sum_{\mu=-\lambda}^{+\lambda} Y_\lambda^\mu(\hat{r}_1)\, Y_\lambda^\mu(\hat{r}_N)^* \tag{3.35}$$

we obtain

$$I_2(\vec{r}_N) = \sum_{\lambda=0}^{\infty} \frac{4\pi}{2\lambda+1} Y_\lambda^\mu(\hat{r}_N)^* \otimes \int \rho(\vec{r}_1) \frac{r_<^\lambda}{r_>^{\lambda+1}}\Big)_{1N} Y_\lambda^\mu(\hat{r}_1)\, d\hat{r}_1 . \tag{3.36}$$

Turning the obvious cranks, we acquire the handy form

$$I_2(\vec{r}_N) = \sum_{\lambda=0}^{\infty}{}' \left\{ \frac{4\pi}{2\lambda+1} \int_0^{\infty} a_\lambda(r_1) \frac{\xi^\lambda}{r_>^{\lambda+1}} \right)_{1N} r_1^2 \, dr_1 \Big\} P_\lambda(\cos\theta_N), \quad (3.37)$$

where we have used the orthonormality of spherical harmonics,[26]

$$\int Y_\lambda^\mu(\hat{r})^* \, Y_{\lambda'}^{\mu'}(\hat{r}) \, d\hat{r} = \delta_{\lambda\lambda'}. \quad (3.38)$$

Thus, at long last, we have the desired result; to-wit,

$$V(\vec{r}_N) = \sum_{\lambda=0}^{\infty}{}' v_\lambda(r_N) P_\lambda(\cos\theta_N), \quad (3.39)$$

where

$$v_\lambda(r_N) = -\frac{6}{r_N}\delta_{\lambda 0} - 16\frac{\rho_<^\lambda}{\rho_>^{\lambda+1}} + \left(\frac{4\pi}{2\lambda+1}\right) \int a_\lambda(r_1) \frac{r_<^\lambda}{r_>^{\lambda+1}} \Big)_{1N} r_1^2 \, dr_1, \quad (3.40)$$

with, as before, $\rho_< = \min(r_N, R)$ and $\rho_> = \max(r_N, R)$.

The final step is evaluation of

$$V_{\ell\ell'}^{(m)}(r) = \int Y_\ell^m(\hat{r}) \, V(\vec{r}) \, Y_{\ell'}^m(\hat{r}) \, d\hat{r}. \quad (3.41)$$

This is a piece of cake; we stuff Eq. (3.39) into (3.41) and let the dummy variable of integration be defined relative to the body-fixed axis, $\hat{z} = \hat{R}$. Once again wheeling in Eq. (3.33), we obtain

$$V_{\ell\ell'}^{(m)}(r) = \sum_{\lambda=0}^{\infty}{}' v_\lambda(r) \sqrt{\frac{4\pi}{2\lambda+1}} \int Y_\ell^m(\hat{r})^* \, Y_\lambda^0(\hat{r}) \, Y_{\ell'}^m(\hat{r}) \, d\hat{r}. \quad (3.42)$$

The integral of three spherical harmonics is more-or-less conveniently given[27] in terms of Clebsch-Gordan coefficients,* and we obtain

$$V_{\ell\ell'}^{(m)}(r) = \sum_{\lambda=0}^{\infty}{}' v_\lambda(r)(-1)^m \sqrt{\frac{(2\ell+1)(2\ell'+1)}{2\lambda+1}} C(\ell\ell'\lambda;00)\, C(\ell\ell'\lambda;-m,m). \qquad (3.43)$$

Notice that the matrix $\underset{\sim}{V}^{(m)}(r)$ is symmetric and that there are numerous zeros imposed by the triangle relation[29] $\Delta(\ell\ell'\lambda)$ and the restriction $\ell+\ell'+\lambda$ = even.

This matrix, though even less transparent than was the function $V(\vec{r})$, is worth a moment of Buddhistic contemplation, for it defines the partial-wave coupling in the coupled-channel differential equations to be solved in Chapter 6. For example, the fact that the symmetry of the target forces all odd-λ coefficients $v_\lambda(r)$ to be zero means that only $\Delta\ell = |\ell - \ell'|$ = even channels couple at all. Thus, the problem splits into sets within each m which are conveniently defined by the symmetry of the $e+CO_2$ system, e.g., Σ_g ($m = 0$; $\ell = 0,2,4,\ldots$), Π_u ($m = 1$, $\ell = 1,3,5,\ldots$) etc. Such a simplification is worthy of respect; without it we would have to solve more than 60 coupled equations. With this potential energy, that could turn out to be unbelievably expensive at best or numerically impossible at worst. In fact, the largest number of channels required is about 30.

*As is probably apparent by the references so far, we use the conventions of M. E. Rose, Elementary Theory of Angular Momentum[24] throughout. We have found this book, though not flawless, to be the least error-ridden of the standard texts on angular momentum. However, a Rose by any other name would be an Edmonds.[28]

§3.5 Computational Details and a Few Analytic Integrals.

This short section describes the irreducible minimum one should know about how we compute $v_\lambda(r)$; results are held for §3.6. In actual fact, we do not compute $V^{(m)}_{\ell\ell'}(r)$ at one whack. Instead we determine* $v_\lambda(r)$, store it on disc, and use it (plus additional contributions to be discussed in Chapters 4 and 5) in the integral-equation code to determine $V^{(m)}_{\ell\ell'}(r)$ as needed. For convenience in our discussion, let's write $v_\lambda(r)$ as

$$v_\lambda(r) = -\frac{6}{r}\delta_{\lambda 0} - 16\frac{p_<^\lambda}{p_>^{\lambda+1}} + \frac{4\pi}{2\lambda+1} I(r), \tag{3.44}$$

where we have introduced the integral I(r), defined as

$$I(r) \equiv \int_0^\infty a_\lambda(r_1)\left(\frac{r_<^\lambda}{r_>^{\lambda+1}}\right)_1 r_1^2\, dr_1 \ . \tag{3.45}$$

Clearly calculation of I(r) is the tricky part of the evaluation of $v_\lambda(r)$. We can rewrite this integral as

$$I(r) = \frac{1}{r^{\lambda+1}}\int_0^r a_\lambda(r_1) r_1^{\lambda+2}\, dr_1 + r^\lambda \int_r^\infty a_\lambda(r_1) r_1^{1-\lambda}\, dr_1 \ . \tag{3.46}$$

Any non-pathological integral of the form $\int_a^b f(r)dr$ can be evaluated by a Gauss-Laguerre quadrature.[30]

It is useful, though tedious, to further transform I(r). We recall from section 3.3 that beyond a certain radius, say R, $a_\lambda(r)$ is available as an analytic function given by Eq. (3.17). To avail

*The code involved and here discussed is called EXPPOT and requires as input the coefficients $a_\lambda(r)$ over a pre-determined r-mesh for all desired λ.

ourselves of this fact, let's write the second integral in Eq. (3.46) as follows:

$$r^{\lambda}\int_{r}^{\infty} a_{\lambda}(r_1)\, r_1^{1-\lambda}\, dr_1 = r^{\lambda}\int_{r}^{R} a_{\lambda}(r_1)\, r_1^{1-\lambda}\, dr_1 \;\; [\,\delta(r<R)\,] + r^{\lambda}\int_{R'}^{\infty} a_{\lambda}(r_1)\, r_1^{1-\lambda}\, dr_1, \tag{3.47}$$

where $R' = \max(R,r)$ and the first term on the right-hand side vanishes if $r > R$. We can use Gauss-Legendre quadrature to evaluate the first integral on the RHS.

We would like to put the second integral,

$$J \equiv r^{\lambda}\int_{R'}^{\infty} a_{\lambda}(r_k)\, r_k^{1-\lambda}\, dr_k, \tag{3.48}$$

into a form amenable to evaluation by Gauss-Laguerre quadrature, i.e., $\int_0^{\infty} e^{-\omega} f(\omega)\, d\omega$. A couple of transformations do the trick!

First we let $u = r_k - R'$ and use the known form for $a_{\lambda}(r)$ for $r > R$ to get

$$J = A_{\lambda} e^{-\alpha_{\lambda} R'} \int_0^{\infty} e^{-\alpha_{\lambda} u} (u + R')^{1-\lambda}\, du. \tag{3.49}$$

If we further introduce $\omega = \alpha_{\lambda} u$, then we can write

$$J = \int_0^{\infty} e^{-\omega} f(\omega)\, d\omega, \tag{3.50}$$

with

$$f(\omega) = \left(\frac{1}{\alpha_{\lambda}}\omega + R'\right)^{1-\lambda}. \tag{3.51}$$

Thus, at this stage, we have a marginally more tractable expression for I(r),

$$I(r) = \frac{1}{r^{\lambda+1}}\int_0^r a_\lambda(r_1) r_1^{\lambda+2} dr_1 + r^\lambda \int_r^R a_\lambda(r_1) r_1^{1-\lambda} dr_1 \, [\delta(r-R) + r^\lambda \frac{A_\lambda}{\alpha_\lambda} e^{-\alpha_\lambda R'} \int_0^\infty e^{-\omega} f(\omega) d\omega. \quad (3.52)$$

Now consider the case r > R, for which our integral becomes

$$I(r) = \frac{1}{r^{\lambda+1}}\int_0^R a_\lambda(r_k) r_k^{\lambda+2} dr_k + \frac{1}{r^{\lambda+1}}\int_R^r a_\lambda(r_k) r_k^{\lambda+2} dr_k + J. \quad (3.53)$$

In the second integral we know an analytic form for $a_\lambda(r)$, our old friend Eq. (3.17). We can combine this result with Eq. (3.52) by defining R'' = min (R,r) and writing, finally,

$$I(r) = I_1(r) + I_{2a}(r) + I_{2b}(r) + J, \quad (3.54)$$

where we have defined the following integrals

$$I_1(r) \equiv \frac{1}{r^{\lambda+1}} \int_0^{R''} a_\lambda(r_1) r_1^{\lambda+2} dr_1 . \quad (3.55a)$$

$$I_{2a}(r) \equiv \frac{1}{r^{\lambda+1}} \delta(r>R) \int_R^r a_\lambda(r_1) r_1^{\lambda+2} dr_1, \quad (3.55b)$$

$$I_{2b}(r) \equiv r^\lambda \, \delta(r<R) \int_r^R a_\lambda(r_1) r_1^{1-\lambda} dr_1 . \quad (3.55c)$$

The reason for this manipulation is not merely to consume space. Integrals I_1 and I_{2b} (if appropriate) simply must be done numerically. However, analytic forms for I_{2a} and J can be developed (for certain cases) and used for purposes of checking the validity of the quadrature and coding. (Such tests are useful at this stage since

we're pretty far along in the problem numerically.) Also the form (3.54) is very convenient for coding purposes and efficiency.

For J, we find that for $\lambda \leq 1$,

$$J(r) = r^{\lambda} A_{\lambda} e^{-\alpha_{\lambda} R'} \sum_{\ell=0}^{1-\lambda} \frac{(1-\lambda)!}{(1-\lambda-\ell)!} \frac{1}{\alpha_{\lambda}^{\ell+1}} (R')^{1-\lambda-\ell}. \qquad (3.56)$$

As r increases, J get progressively smaller monotonically. In the code we don't even bother to calculate it for r beyond the value at which $|J| \lesssim 10^{-8}$.

The second integral which is defined in a region where we have an analytic form for $a_{\lambda}(r)$ is I_{2a}. This can be shown to give (for r>R)

$$I_{2a}(r) = \frac{1}{r^{\lambda+1}} A_{\lambda} (\lambda+2)! \left\{ C_{\lambda} - e^{-\alpha_{\lambda} r} \sum_{\ell=0}^{\lambda+2} \frac{1}{(\lambda+2-\ell)!} \frac{1}{\alpha^{\lambda+1}} r^{\lambda+2-\ell} \right\}, \qquad (3.57)$$

where

$$C_{\lambda} = e^{-\alpha_{\lambda} R} \sum_{\ell=0}^{\lambda+2} \frac{1}{(\lambda+2-\ell)!} \frac{1}{\alpha^{\lambda+1}} R^{\lambda+2-\ell}. \qquad (3.58)$$

Both J and I_{2a} have been evaluated numerically and analytically and give identical results to eight places. The integrals I_1 and I_{2b} must be done numerically; we use Gauss-Legendre quadrature.

In order to minimize the number of points at which $a_{\lambda}(r)$ [and hence $\rho(r,\theta)$] must be evaluated, we first perform a <u>cubic spline</u> fit[31] of $a_{\lambda}(r)$ over the range $0 \leq r \leq R$, where R is the value at

which we can use the analytic form (3.17). This is a third-degree interpolation scheme which can be highly accurate for well-behaved functions. In point of fact, we found that extreme care must be exercised in regions where the function being fit is thought to change slope rapidly. As the graphs of Figure 3.2 suggest, in our case this is in the vicinity of the oxygen nucleus ($r \simeq 2.2\ a_o$). The effect here alluded to is illustrated in Figure 3.3, which shows the spline fit of $a_0(r)$ for two fits, one a 37-point fit, the other an 82-point fit. Put simply, the spline fit requires several mesh points for each order of magnitude change in the function to be fit or in regions where the curve is rapidly changing slope.

The "standard spline mesh" we finally settled on for all $a_\lambda(r)$ is 0.001 to 1.701 in steps of 0.1, 1.701 to 3.001 in steps of 0.05, and 3.001 to R in steps of 0.1.

Each $v_\lambda(r)$ required about 20 seconds of 7600 time to determine for the standard integration mesh of 453 points.*

One final computational point should be mentioned. We remove from $v_\lambda(r)$ the long-range tails for $\lambda = 0, 2, 4$. The $\lambda = 0$ tail is the spurious excess Coulomb tail alluded to in section 3.3. The $\lambda = 2$ tail defines the quadrupole moment and the $\lambda = 4$ tail the hexadecupole moment. These latter two tails are added in again at the integral-equation stage of the calculation; they are deleted

---

*See Chapter 8 for a discussion of the choice of integration mesh and a description thereof.

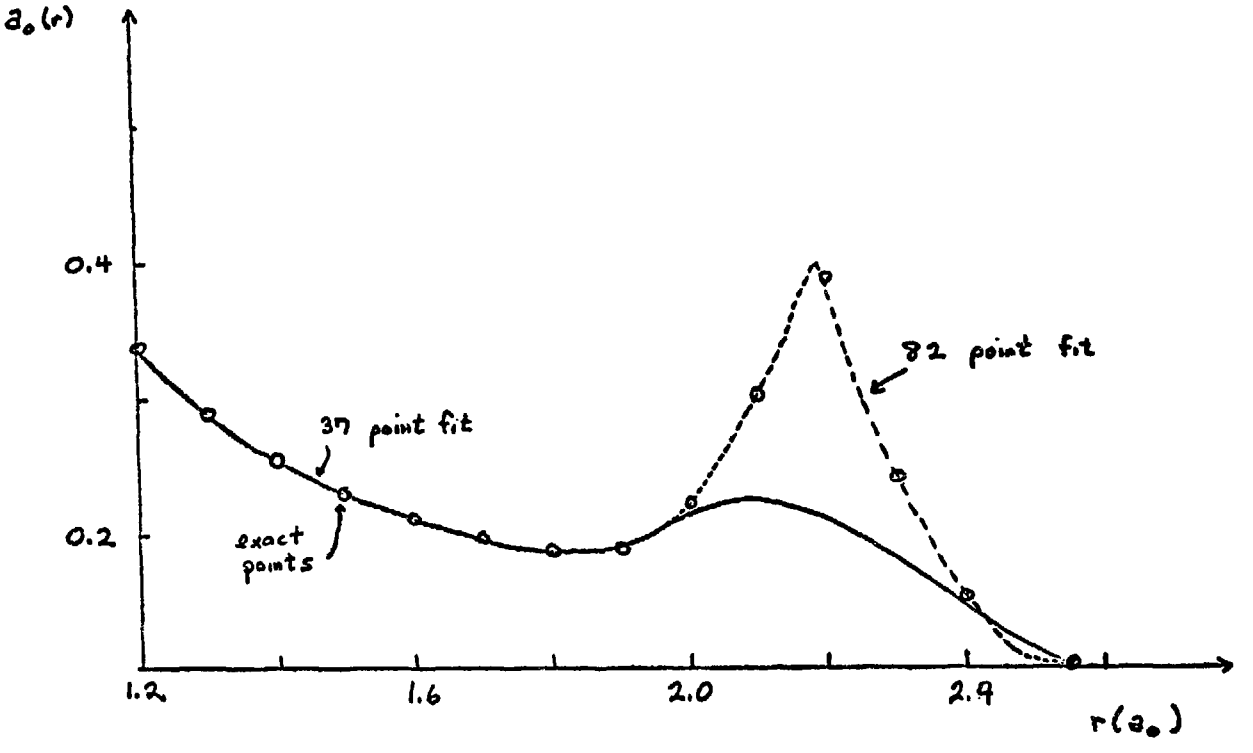

Figure 3.3

Spline fits of the $\lambda = 0$ expansion coefficients of the CO_2 charge distribution. Two fits are shown: a 37 point fit (solid line) and an 82 point fit (dashed line). Circles are points calculated by direct quadrature.

here so as to minimize the number of coefficients $v_\lambda(r)$ which must be stored. Thus we have*

$$v_0(r) \underset{r\to\infty}{\sim} \frac{q_{ex}}{r}, \tag{3.59}$$

where the excess charge was found to be $q_{ex} = 0.0052$. Similarly, we find that

$$v_2(r) \underset{r\to\infty}{\sim} -\frac{q}{r^3}, \tag{3.60a}$$

with $q = -3.85981\ ea_o^2$ and

$$v_4 \underset{r\to\infty}{\sim} -\frac{x}{r^5}, \tag{3.60b}$$

with $x = -9.38166$ au. We shall have more to say about the sign of q in section 3.8.

§3.6 Results for CO_2 and Discussion

Several typical $v_\lambda(r)$ are shown in Figure 3.4. Little need be said about these plots. However, it is useful to examine the behavior of $v_\lambda(r)$ near $r = R_{o-c}$ for high λ. We can see from an examination of Figure 3.5 and Table 3.2, which shows the value (in hartrees) of $v_\lambda(r)$ at $r = 2.19\ a_o$ (essentially the peak value), that the full static potential is exceedingly hard to converge.

The reason for this behavior and an extremely important key to the

*Cutoff functions are used rather extensively in handling the long-range terms.

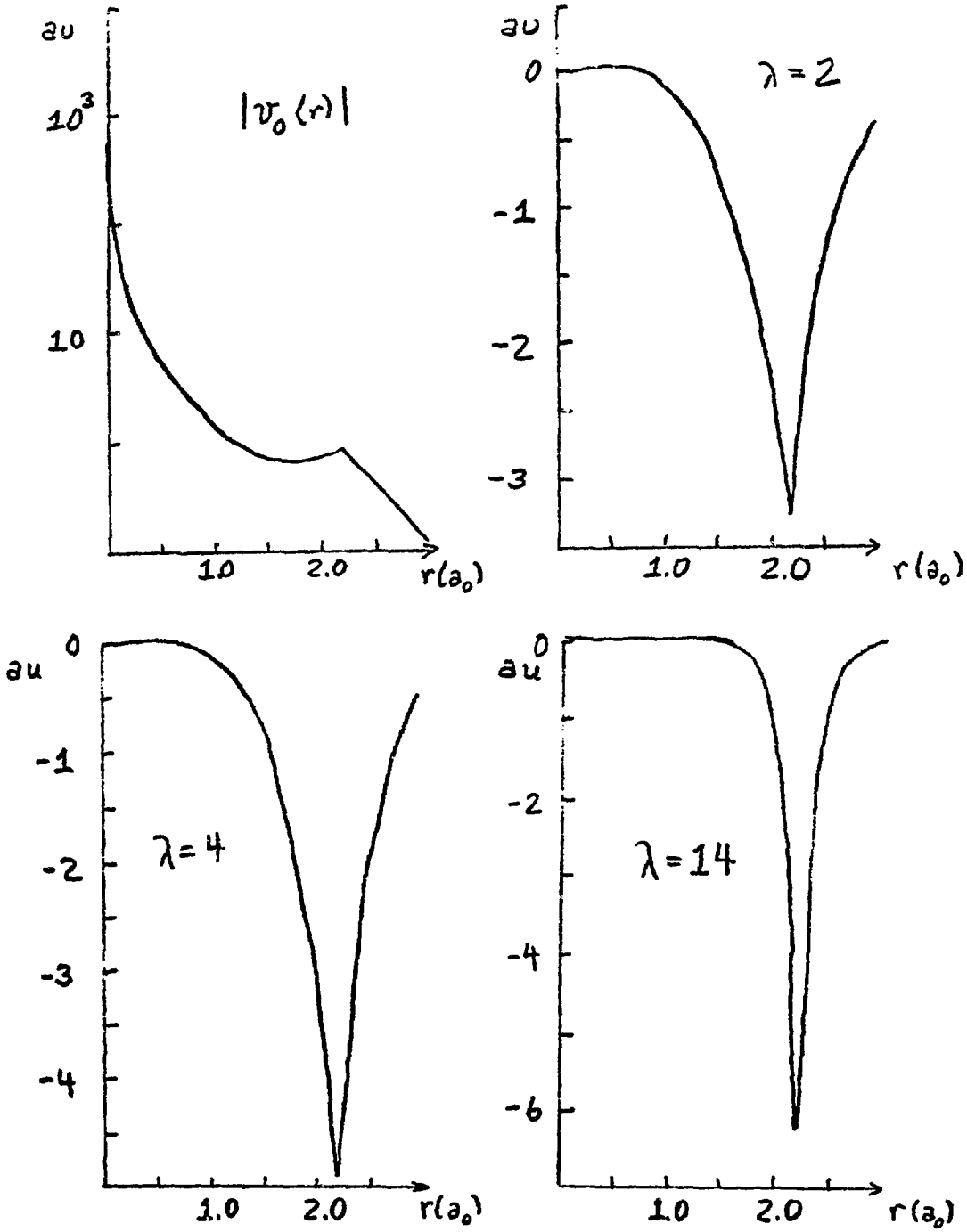

Figure 3.4

Expansion coefficients of the static e-CO_2 interaction potential energy in Legendre polynomials for λ = 0, 2, 4, and 14.

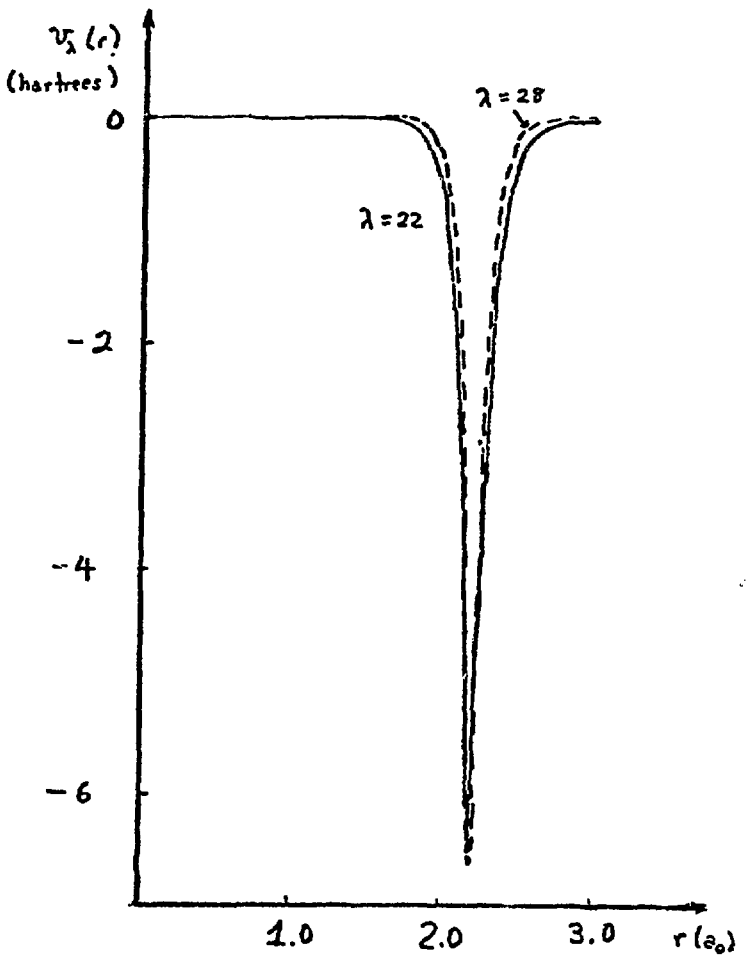

Figure 3.5

Expansion coefficients of the static e-CO_2 interaction potential energy for $\lambda = 22$ and $\lambda = 28$.

λ	$v_\lambda(r = 2.19\ a_o)$
0	-0.8805
2	-3.2900
4	-4.9437
6	-5.6341
8	-5.9516
10	-6.1181
12	-6.2237
14	-6.3028
16	-6.3680
18	-6.4230
20	-6.4700
22	-6.5083
24	-6.5392
26	-6.5631
28	-6.5807

Table 3.2

Values of the expansion coefficients of the averaged static potential $v_\lambda(r)$ in hartress at a point near the oxygen nuclei. [For this calculation, $R_{o-c} = 2.19440\ a_o$.]

computational problem at hand can be understood if we notice from Eq. (3.40) that each $v_\lambda(r)$ can be written as

$$v_\lambda(r) = v_\lambda^{nuc}(r) + v_\lambda^{el}(r), \tag{3.61}$$

where

$$v_\lambda^{nuc}(r) = -\frac{6}{r}\delta_{\lambda 0} - 16\frac{r_<^\lambda}{r_>^{\lambda+1}}, \tag{3.62a}$$

$$v_\lambda^{el}(r) = \frac{4\pi}{2\lambda+1}\int_0^\infty a_\lambda(r_1)\frac{r_<^\lambda}{r_>^{\lambda+1}}\Big]_1 r_1^2\, dr_1 . \tag{3.62b}$$

Thus we have a nuclear and an electronic contribution to each $v_\lambda(r)$. Clearly, the nuclear part is trivial (and fast) to calculate for as many λ as necessary. Au contrair, $v_\lambda^{el}(r)$ takes considerable computer time to evaluate. Moreover, once we reach fairly large values of λ, we must ask the question of just how realistic it <u>is</u> to try to extract, say, $P_{40}(\cos\theta)$ information from an electronic wavefunction, even one good as McLean and Yoshimine's.

Fortunately, this problem can be resolved. By examining the percentage contribution to $v_\lambda(r)$ of the electronic part, we find that $v_\lambda^{el}(r)$ is negligible above about $\lambda = 30$. For example, $v_\lambda^{el}(r)$ contributes 27%, 20%, and 10% to $v_\lambda(r)$ for $\lambda = 16$, 22, and 28, respectively. This behavior is also reflected in Figure 3.6, which shows the <u>electronic</u> contribution $v_\lambda^{el}(r)$ for some of the cases included in Figs. 3.4 and 3.5. (We here consider values r near R_{o-c} .)

In point of fact, the convergence trouble reflected in the graphs of $v_\lambda(r)$ we have looked at arises because $v_\lambda^{nuc}(r)$ narrows very grad-

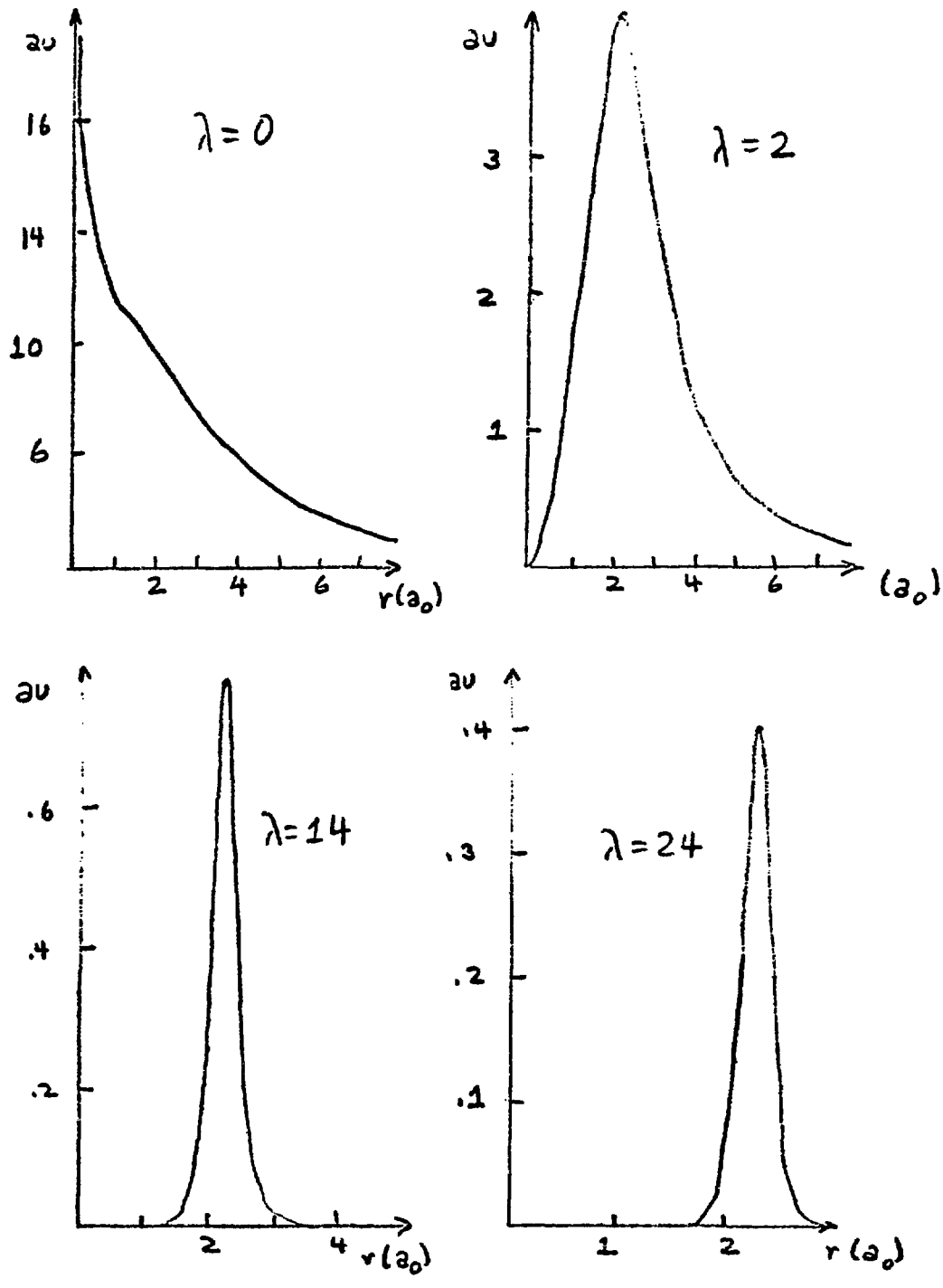

Figure 3.6

Electronic contribution to the expansion coefficients of the electron-molecule interaction potential energy for e-CO_2 for the cases λ = 0, 2, 14, and 24.

ually, the value at $r = R_{o-c}$ converging slowly to a Coulomb singularity for $V(\vec{r})$. There is an upper limit in the practical coupled-channel calculation imposed by the fact that for a fixed number of channels, N, corresponding to some ultimate partial wave, ℓ_{max}, the coupling matrix elements in $V^{(m)}_{\ell\ell'}(r)$ are zero for $\lambda > 2\ell_{max}$, as can be seen from Eq. (3.43).

Details of the convergence of the cross section in λ are more appropriately left for Chapter 8. Here let us note that in the final calculations we used 15 $v^{el}_{\lambda}(r)$ and 41 $v^{nuc}_{\lambda}(r)$, corresponding to maximum λ of $\lambda^{el}_{max} = 28$ and $\lambda^{nuc}_{max} = 80$. This is a sufficient number of terms to converge the averaged static potential $\bar{V}(\vec{r})$ to <1% and hence enough for the calculation of the cross sections. The essential point here is that one does not need $v^{el}_{\lambda}(r)$ for high λ but can't do without $v^{nuc}_{\lambda}(r)$ for high λ. Physically, this reflects the massive size of the CO_2 molecule, with an internuclear separation of 4.3888 a_o from oxygen to oxygen, and the hefty positive charges on the nuclei ($Z_c = 6$, $Z_o = 8$).

§3.7 An Introduction to the Centrifugal Barrier and its Physics

Examination of the expansion coefficients $v_{\lambda}(r)$ is helpful to the perplexed physicist trying to "visualize" the highly complex e-CO_2 interaction potential. However, it is the matrix elements $V^{(m)}_{\ell\ell'}(r)$ that appear in the coupled equations we eventually must solve and which reflect the coupling between partial waves. In the last analysis, $V^{(m)}_{\ell\ell'}(r)$ contains other contributions than the static potential (see Chapters 4 and 5). However, there is some valuable insight

to be gained by a study of the diagonal matrix element.

To get into this subject, let's write the coupled equation (3.3) as

$$\left[\frac{d^2}{dr^2} - \frac{\ell(\ell+1)}{r^2} - 2V_{\ell\ell}^{(m)}(r) + k^2\right] u_\ell^{(m)}(r) = 2\sum_{\ell' \neq \ell} V_{\ell\ell'}^{(m)}(r)\, u_{\ell'}^{(m)}(r) \tag{3.63}$$

and define the conventional effective potential as

$$V_{\ell m}^{eff}(r) = 2V_{\ell\ell}^{(m)}(r) + \frac{\ell(\ell+1)}{r^2} \quad . \tag{3.64}$$

The second term is $V_{\ell m}^{eff}(r)$ is called the centrifugal barrier. For large ℓ, it adds a repulsive part to the attractive static potential matrix element $V_{\ell\ell}^{(m)}(r)$ and therefore crudely speaking, acts to "keep the electron away from the core region" near the nuclei.

The ramifications of this fact both physically and computationally are of enormous importance, and, while some of the analysis must be deferred to Chapter 8, it is appropriate here to introduce the general ideas and look at some pictures in order to lay the foundations for discussions yet to come.*

The importance of the centrifugal force to electron-molecule scattering has been elucidated by Fano[32] and applied in an approximation called "low-ℓ spoiling."[33] Simply put, the centrifugal barrier for large-ℓ partial waves is so large that it prohibits "information transfer" between the wavefunction in the internal region (roughly inside the classical turning point) and in the external

*None of the admittedly qualitative (or intuitive) points we make in this section will be altered by the inclusion of exchange or induced polarization terms into $v_\lambda(r)$.

region (beyond the barrier). Therefore, regardless of what happens to the high-ℓ partial wavefunctions near r = 0 (they grow very rapidly as r increases from zero), they themselves will not contribute to the asymptotically-defined phase shifts except through indirect coupling. In more physical terms, to a certain approximation, ℓ can be considered a good quantum number for large enough values of ℓ, and the corresponding partial waves uncouple asymptotically. The validity of this argument is clearly system dependent as well as energy dependent. We would like to use the picture it suggests to think about the physics of the e-CO_2 collision without actually making the "low-ℓ spoiling" approximation, which would be of dubious merit for CO_2.* We thus adopt the point of view that the barrier in some sense "contains" the anisotropy of the molecular force field for partial waves with large ℓ.

We begin with the expression for the diagonal matrix element,

$$V_{\ell\ell}^{(m)}(r) = \sum_{\lambda=0}^{\lambda_{cont}} C(\ell\lambda\ell';m0)\,C(\ell\lambda\ell;00)\,v_\lambda(r), \qquad (3.65)$$

where $\lambda_{cont} = 2\ell_{max}$ is the upper limit of the λ-summation and, as usual, only even-λ terms contribute. One potential problem (sic) becomes immediately apparent: we rarely have access to $v_\lambda(r)$ for values of λ as large as $2\ell_{max}$ (which can be as large as 120). What saves the day in this case is the centrifugal barrier, which for large ℓ so overpowers $V_{\ell\ell}^{(m)}(r)$ that the effective potential is un-

*In fact, for some symmetries and energies, this approximation gives cross sections off by as much as 60% from the true answer. This is illustrated in Chapter 8.

affected by the neglect of higher-λ terms. These terms do make a difference to $V^{(m)}_{\ell\ell}(r)$, but it is $V^{eff}_{\ell m}(r)$ that "participates" in the scattering. This is illustrated in Figure 3.7, which shows two cases, $\ell = 6$ and $\ell = 12$, with two values of λ_{max} for each [λ_{max} is defined to be the maximum value of λ actually included in the summation in Eq. (3.43)].

This problem out of the way, let's look at some typical effective potentials. For $m = 0$, $V^{eff}_{\ell m}(r)$ for $\ell = 1$, 2, 3, 7, and 10 are shown in Figure 3.8. The behavior of $V^{eff}_{10,0}(r)$ is typical of other high-ℓ cases. Notice how truly enormous $V^{eff}_{\ell 0}(r)$ is for $\ell > 7$; clearly these partial waves will be of no consequence beyond 3 or 4 a_o.*

Another interesting (and very useful) effect is on display in Figure 3.9, which shows $V^{eff}_{4m}(r)$ for m = 0, 1, 2, and 3. As m increases, the effective potential is increasingly dominated by the pure $1/r^2$ barrier. This suggests that the dominant contributions to the cross section will arise from $\Sigma(m = 0)$ and $\Pi(m = 1)$ symmetries. This, in fact, turns out to be the case; higher-m symmetries do not "experience" enough of the strong short-range potential to be substantially phase shifted.

Lest we get carried away with interpretations based on these admittedly appealing physical pictures, a caveat must here be issued. These are fairly crude, essentially potential-scattering arguments. In fact, only in a very restricted "asymptotic" sense is it meaningful to even talk about an "$\ell = 3$ electron;" in fact the $\ell = 3$ partial

*This point, craftily inserted here, is the key to the truncation procedure to be discussed in Chapter 6. It is most emphatically not true that these partial waves can be neglected altogether; they strongly couple to lower waves in the region near the target.

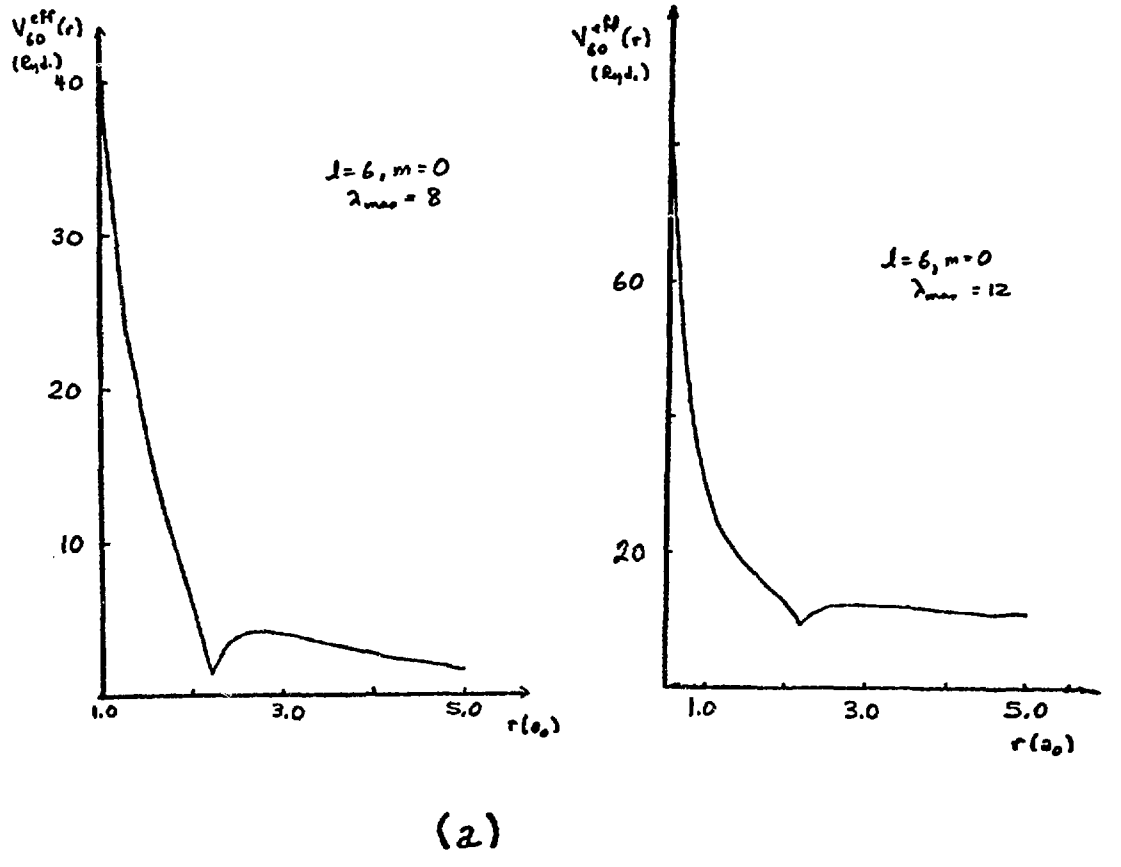

(a)

Figure 3.7

The effective potential energy for e-CO_2 scattering (a) for ℓ = 6, m = 0 and (b) for ℓ = 12, m = 0.

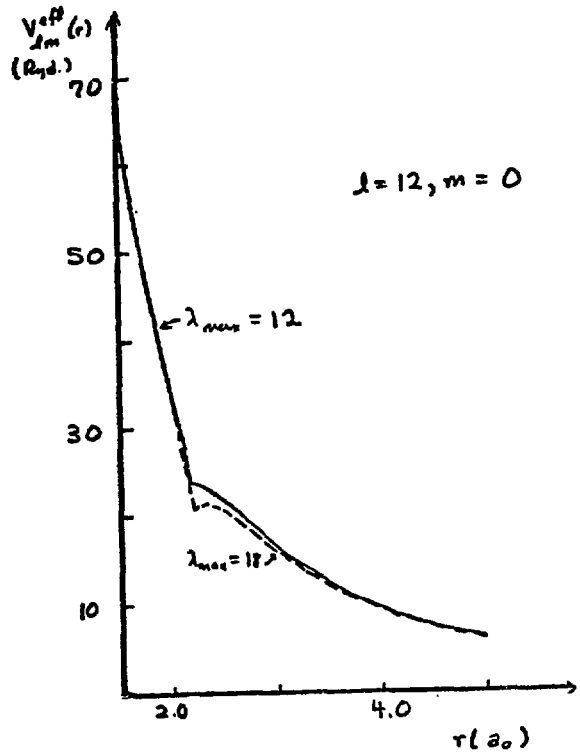
$V_{lm}^{eff}(r)$
(Ryd.)
70
50
30
10
$l = 12, m = 0$
$\lambda_{max} = 12$
$\lambda_{max} = 18$
2.0
4.0
$r(a_0)$

(b)

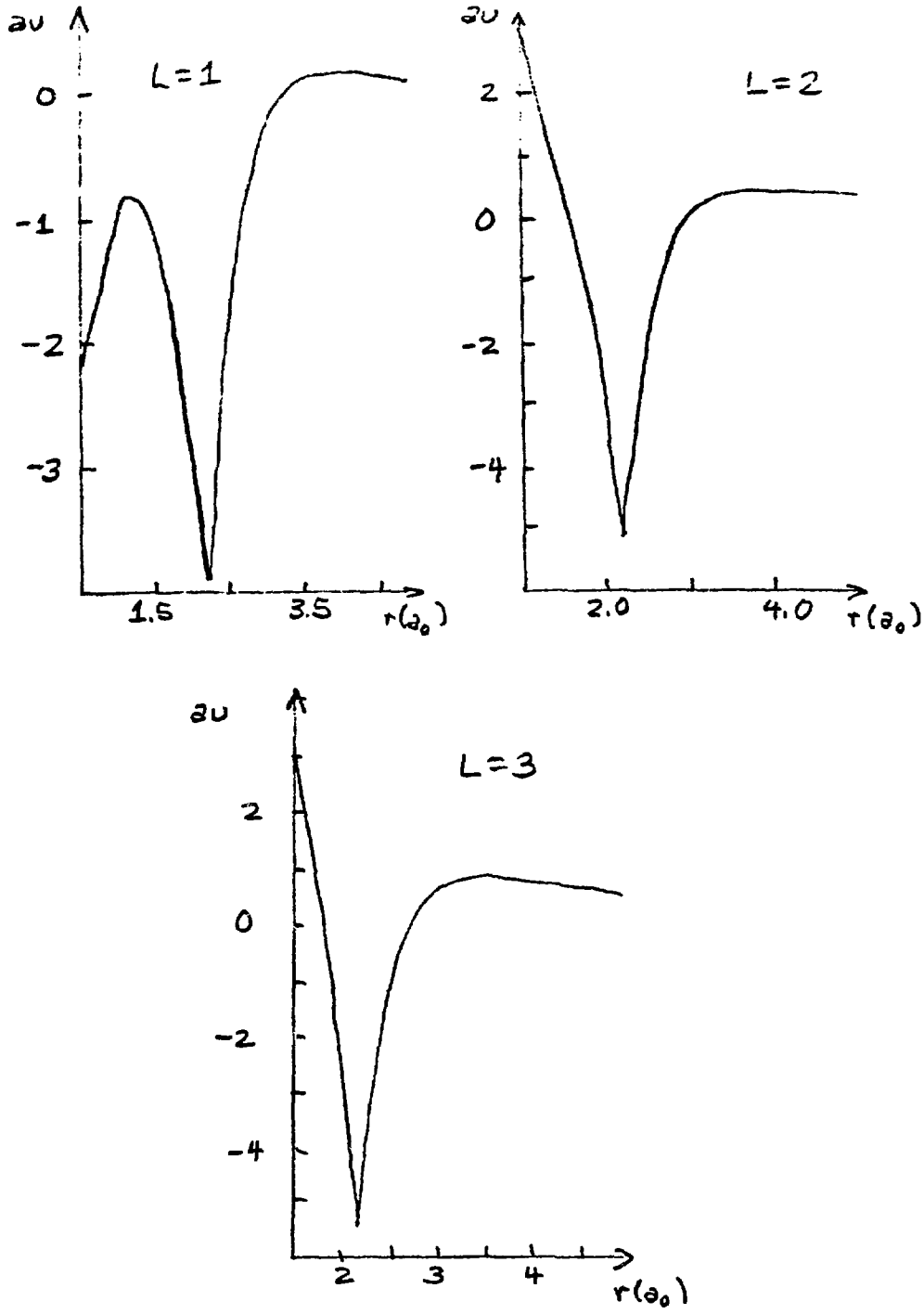

Figure 3.8

The effective potential energies for e-CO_2 scattering with m = 0 and ℓ = 1, 2, 3, 7, and 10.

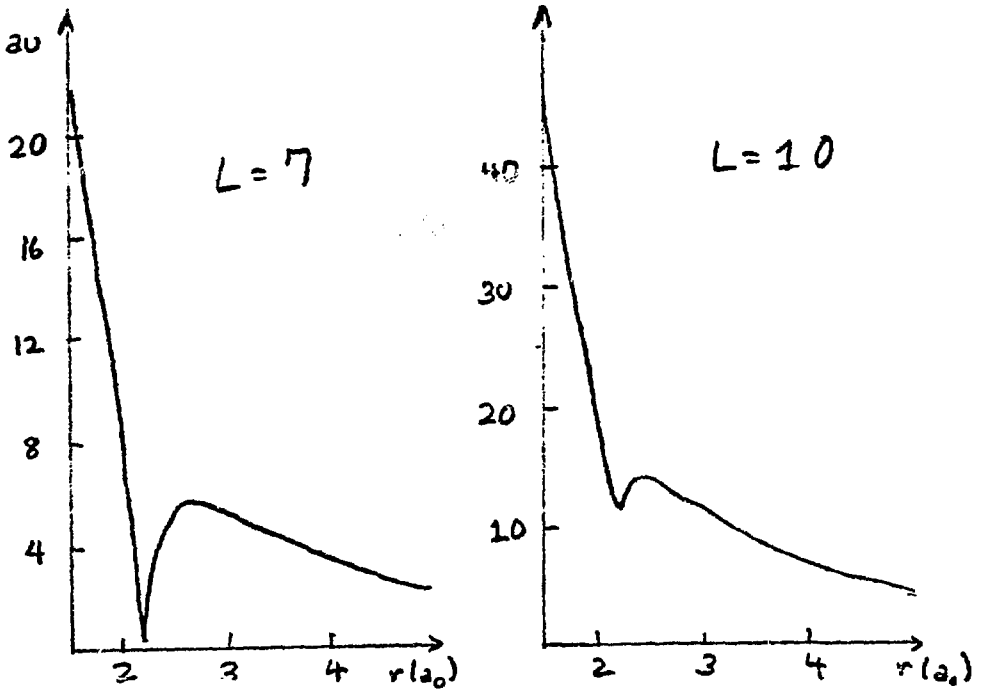
L = 7
20
16
12
8
4
2
3
4
r(a₀)
L = 10
40
30
20
10
2
3
4
r(a₀)

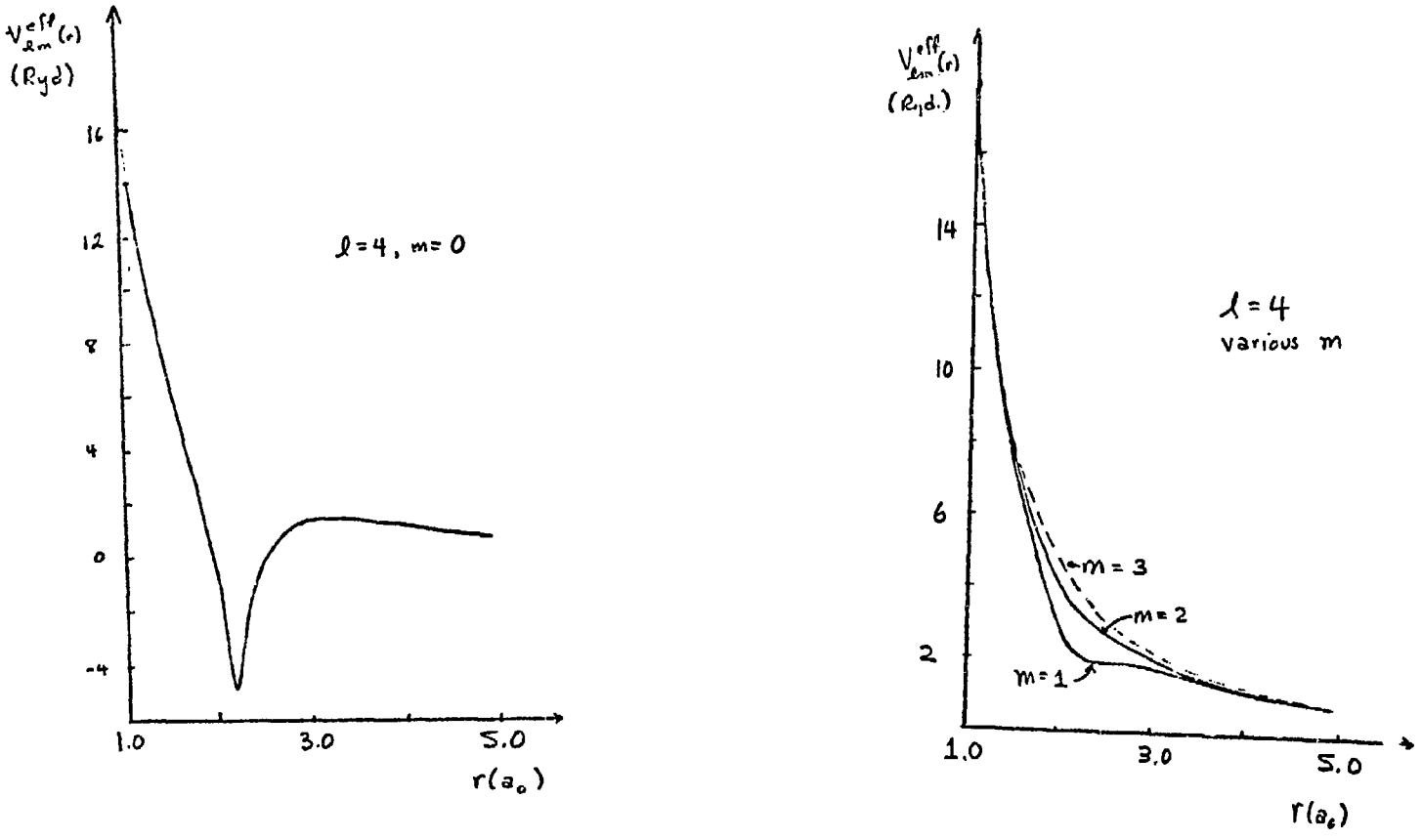

Figure 3.9

Illustration of the dependence of the e-CO_2 effective potential energy on m for $\ell = 4$.

wave is strongly coupled in the small-r region to $\lambda = 1$ and $\ell = 5$ waves, and so forth. Nevertheless, the effective potential provides a useful tool in trying to understand the physics of the collision process and, as we shall see in Chapter 8, in making certain important decisions at computation time.

§3.8 Some Terminal Remarks on the Static Potential and the Quadrupole Moment

In concluding our study of the static potential, we would like to comment briefly on the reason for the quadrupole moment of CO_2 being negative and to compare static potentials for a few other systems to that of CO_2.

The quadrupole moment tensor is defined in general as

$$\Theta_{\alpha\beta} = \frac{1}{2}\int \rho_t (3r_\alpha r_\beta - r^2 \delta_{\alpha\beta})\, d\tau, \tag{3.66}$$

where $\rho_t = \rho_t(x,y,z)$ is the total charge density (of electrons and nuclei) and $r_1 = x$, $r_2 = y$, $r_3 = z$. The integral is carried out over all space, $d\tau = dxdydz$. Since the linear (fixed-nucleus) configuration of CO_2 at equilibrium has no dipole moment, the quadrupole moment is origin-independent. Moreover, CO_2 has a two-fold axis of symmetry and $\Theta_{\alpha\beta}$ is a second-rank tensor, so the quadrupole moment can be uniquely specified by a single scalar quantity

$$q = \Theta_{zz} = -2\Theta_{xy} = -2\Theta_{yy}, \tag{3.67}$$

and the off-diagonal elements are zero.

A selection of values of q for CO_2 are given* in Table 3.3. Given the range of values that have been determined by various investigators, we do pretty well. It is the <u>sign</u> of q (negative) that is of interest here; more familiar systems (e.g., H_2, N_2) have positive quadrupole moments. In terms of the charge distribution,[38] it is generally true that negative charge distributed in a plane perpendicular to the internuclear axis $\hat{R}$ will contribute a positive amount to q while negative charge along $\hat{R}$ contributes a negative amount to q.

In fact, a (very) simple model for CO_2 can be conjured up to explain why $q < 0$. Referring to Figure 3.10a and using the drastic simplification that

$$q = \sum_{i=1}^{3} q_i z_i^2 , \qquad (3.68)$$

we argue that carbon, with Z = 6 and an atomic orbital occupancy of $1s^2 2s^2 2p^2$, has two valence electrons while oxygen, with Z = 8 and a $1s^2 2s^2 2p^4$ occupancy, has two "valence holes" and a stronger nuclear charge. We suggest that a small amount of negative charge will be pulled from the central C to each O giving the structure shown in the figure. In fact, A. D. McLean has determined[35] that this is the case; the partial charges are -0.22e on each oxygen and +0.43e on the carbon. Using Eq. (3.67) and these charges, we get $q = -2.12\ ea_o^2$, clearly negative and not really too bad a value considering the

*It may be useful to note that to convert q from CGS units for q, 10^{-26} esu-cm^2, to atomic units ea_o^2, one multiplies q times 0.7445.

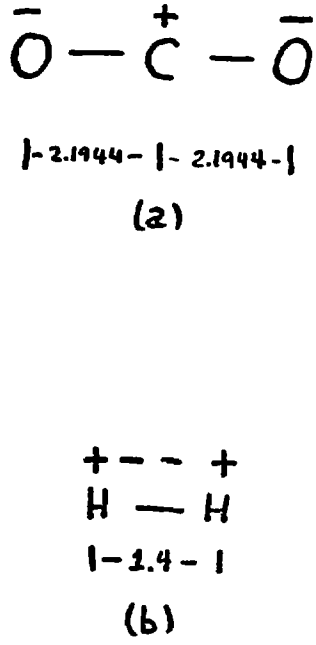

Figure 3.10

Crude models of (a) CO_2 and (b) H_2 used in the text to illustrate features of the quadrupole moment.

q (CGS units)	q (atomic units)	Source
-4.3×10^{-26}	-3.2014	34
-2.50×10^{-26}	-1.8613	35
-5.25×10^{-26}	-3.9086	36
-4.3×10^{-26}	-3.2014	37 (exp)
-5.18×10^{-26}	-3.8598	us

Table 3.3

A modest anthology of quadrupole moments for CO_2 including the present work.

appalling crudity of this model. The reverse case obtains for H_2, where the structure of the bonding is considerably different from CO_2. Here an excess negative charge builds up between the nuclei as in Figure 3.10b; this produces bonding in H_2 and leads to a positive quadrupole moment, $q = +0.49\ ea_o^2$.

As should now be apparent, CO_2 is not your average target for scattering calculations such as the ones reported here, and it is probably not a bad idea to present a couple of familiar benchmarks for comparison. We've chosen those old standbys, H_2 and N_2. In Figure 3.11 we have plots of $v_\lambda(r)$ for H_2 with $\lambda = 0,2,4,6$. The convergence in the vicinity of the nuclei $r = 0.7$, is much more rapid than in CO_2 as attested by the fact that for H_2, $v_\lambda(0.7) = -1.2027$, -2.7073, -2.8129, and -2.8149 hartrees for $\lambda = 0, 2, 4, 6$, respectively. The first three $v_\lambda(r)$ for N_2, for which $R_{N-N} = 2.068\ a_o$, are shown in Figure 3.12a.[39] Finally, $v_1(r)$, $v_3(r)$, and $v_{15}(r)$ in CO are shown in Figure 3.12b.[40] Of course, for CO, a heteronuclear molecule,* even- and odd-λ coefficients contribute to the expansion of $V(\vec{r})$. Granted that CO is not an exceedingly strong polar molecule, the contrast with CO_2 is still rather striking.

We believe our static potential for e-CO_2 collisions to be quite accurate. It is, however, the easiest part of the interaction potential to handle, because given a reasonable amount of computer time and stamina, it can be calculated ab initio and with great accuracy. Not so the far more insidious exchange interaction. Guile and craftiness are required to correctly incorporate these contributions and we turn to exchange in the next chapter.

*In Figure 3.12b, r is measured from the center-of-mass of the CO molecule. This is standard operating procedure in dealing with polar molecules.

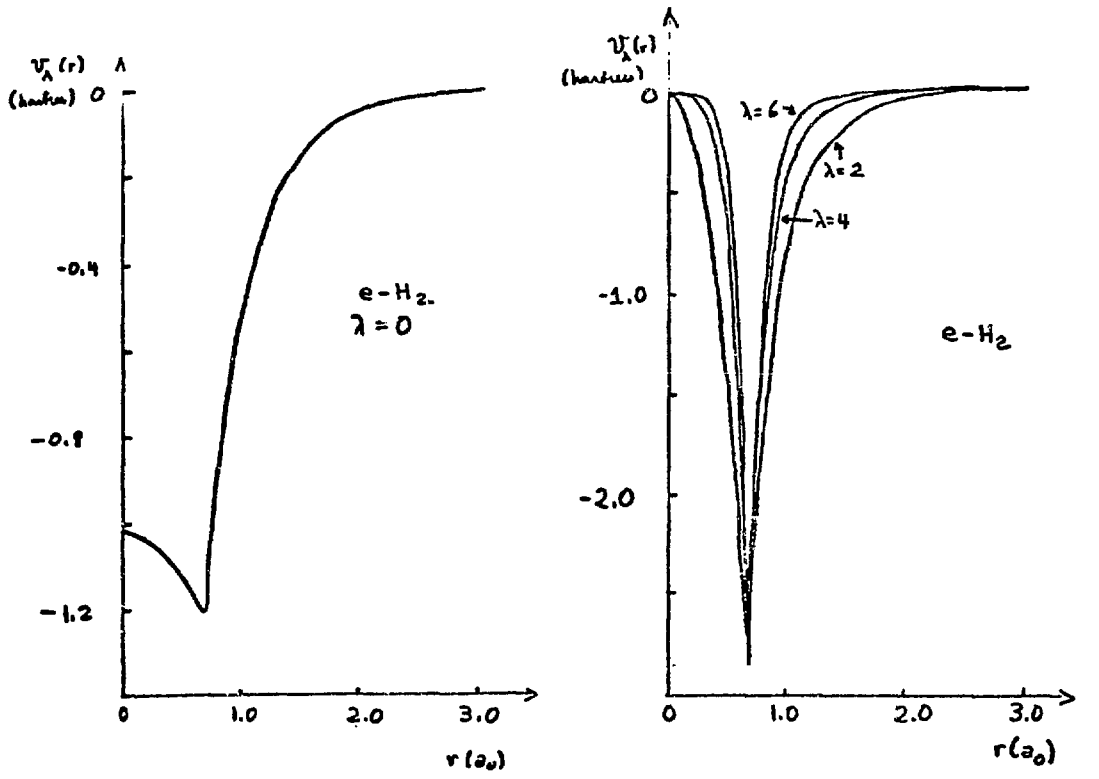

Figure 3.11

Expansion coefficients of the e-H_2 static interaction potential energy in Legendre polynomials for λ = 0, 2, 4, and 6.

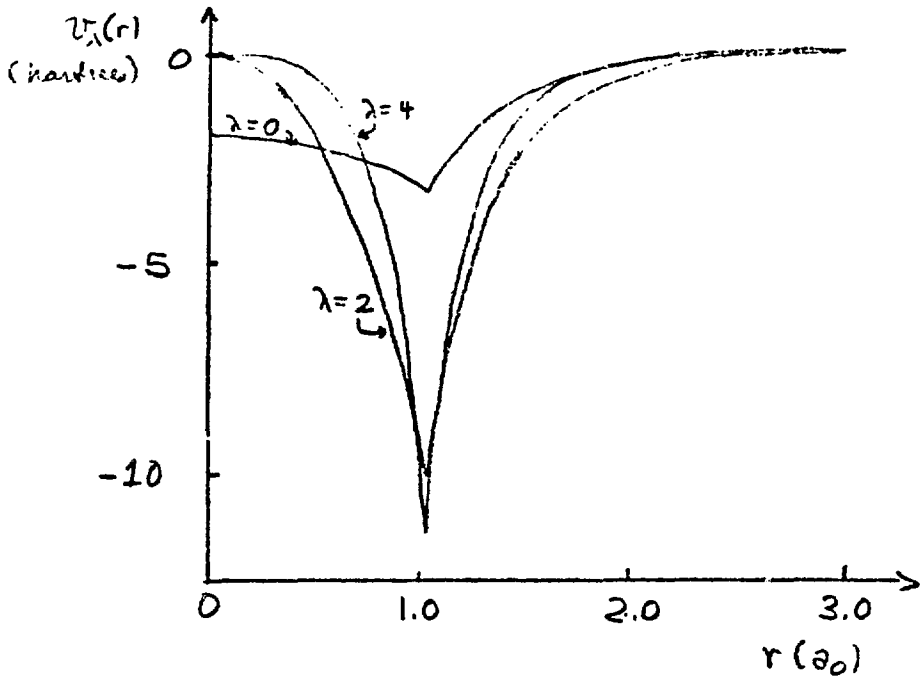

(a)

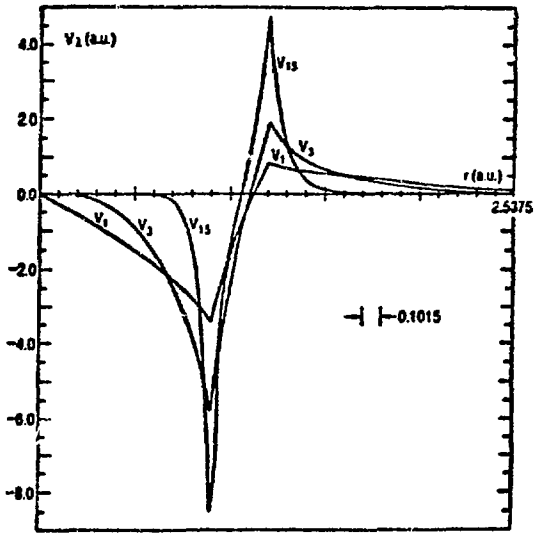

(b)

Figure 3.12

Expansion coefficients of (a) e-N_2 and (b) e-CO_2 interaction potential energies. [Source: (a). F. M. H. Faisal, J. Phys. B 3, 636.(1970); (b). N. Chandra, Phys. Rev. A 12, 2361 (1975).]

Chapter 4: Inclusion of Exchange Interactions viá an Approximate Local Exchange Potential

It is the customary fate of new truths to begin as heresies and to end up as superstitions.

-T. H. Huxley
(1825-1895)

In order to attain the impossible one must attempt the absurd.

-Miguel de Unamuno y Jugo
(1864-1936)

§4.1 Introduction: The Need for Approximate Treatments of Exchange

Exchange effects are encountered in virtually all quantum mechanical problems which involve interacting identical particles.[1] They are a consequence of conditions imposed on the wavefunctions which describe states of the system; these in turn arise from the antisymmetrization requirement, which states that the full system wavefunction $\Psi(1,2,\ldots N)$ must be antisymmetric under pairwise electron* interchange, e.g., $\Psi(1,2,\ldots,N) \xrightarrow[i \to j]{} -\Psi(1,2,\ldots N)$. In the orbital approximation, which we implicitly use throughout this work, this condition on Ψ has direct consequences through the Pauli Exclusion

*This in turn, is a consequence of the fact that electrons are fermions. See reference (1).

Principle. In fact, the double occupancy of non-degenerate molecular orbitals by electrons with anti-parallel spins is one manifestation of this principle.

The effects of electron exchange pose difficulties in both structure and scattering problems. In structure theory (and in some formulations of collision theory) one must deal with Slater determinants instead of simple product wavefunctions (as we saw in Chapter 3), with the Hartree-Fock equations rather than the vastly simpler Hartree theory,[2] and so forth. Essentially, the source of all the trouble is the fact that exchange is a non-local interaction.* This gives rise, for example, to the non-local exchange kernel of close-coupling formulations[3] and to exchange integrals in Hartree-Fock theory;[14] all of these are non-local terms in already complicated equations.

To suggest the magnitude of the problems caused by exchange in scattering calculations, it is useful to glance briefly at the coupled integro-differential equations which obtain when exchange is taken into account. We'll pick a very simple (perhaps unrepresentative) case: e-H_2 collisions in the body-frame (fixed-nuclei approximation) with no electronic excitation (H_2 in the ground $X^1\Sigma_g^+$ state). We find[3]

$$\left[\frac{d^2}{dr^2} - \frac{l(l+1)}{r^2} + k^2\right] u_l^{(m)}(r) - 2\sum_{l'} V_{ll'}^{(m)}(r)\, u_{l'}^{(m)}(r) \qquad (4.1)$$

$$= \sum_{l'} \int_0^\infty K(ll'; r_1 r)\, u_{l'}^{(m)}(r_1)\, dr_1 .$$

*That is to say, the value of the exchange potential at $\vec{r}$ depends on the value of the wavefunction over all space. See Eq. (4.2).

The exchange kernel $K(\ell\ell'; r_1 r)$ in Eq. (4.1) is defined as

$$K(\ell\ell'; r_1 r_3) = r_1 r_3 \int \Psi^{+}_{1\Sigma_g^+}(\vec{r}_1, \vec{r}_2; R) Y_{\ell}^{m}(\hat{r}_3) \left[V_{int}(\vec{r}_3, \vec{r}_2 | \vec{r}_1) - \tfrac{1}{2}\nabla_1^2 - \tfrac{1}{2}k^2 \right] \Psi_{1\Sigma_g^+}(\vec{r}_2, \vec{r}_3; R) Y_{\ell'}^{m}(\hat{r}_1) \, d\hat{r}_1 \, d^3 r_2 \, d\hat{r}_3 , \qquad (4.2)$$

where we have let $r_3 = r$ = the scattering coordinate for clarity in Eq. (4.2).

Physically, one can think of exchange as having a two-fold influence on the scattering wavefunction in electron collisions.* First, exchange behaves like a short-range attractive interaction in its effect on the wavefunction. In fact, considerable success was achieved by Lane and Geltman[5] in an early study of e-H_2 scattering in the close-coupling formulation by "mocking" exchange with a very simple, local, short-range, attractive (square well) potential energy term. In some respects, this work prefigures our own treatment of exchange.

Second, exchange, manifested through the Pauli Exclusion Principle, acts to prohibit a scattering electron of given symmetry** from occupying any of the filled target orbitals of that symmetry. Thus, a σ_g scattering-electron wavefunction in an e-H_2 collision is orthogonal to the core $1\sigma_g$ molecular orbital. This important point, used as the basis of a treatment of exchange by Burke and others,[7] was applied by N. Lane and the author in our pseudo-bound-state approach

*Mathematically speaking, in the Hartree-Fock theory exchange terms also act to cancel self-interaction terms in the HF equations.[15]

**This is a pretty loose useage. We are referring to decompositions of the scattering-electron wavefunction asymptotically into partial waves and the consequent identification of symmetries.[6]

to electron-molecule scattering. For a variety of reasons to be discussed below, we choose not to adopt this procedure.

Although methods exist for coping with the ghastly computational problems that arise when treating exchange* directly in the coupled equations,[3] these would be risky at best in the context of our particular case. The numerical problem encountered in doing just the static problem (see Chapter 6) are sufficient to make us tread warily when considering the numerical solution of more complicated equations for e-CO_2 collisions. The same argument applies to the application of Burke's orthogonalization procedure, although the nature of the possible numerical difficulties inherent in this approximation is less clear. More discussion of this alternative can be found elsewhere in this chapter.

We chose to begin with the approach which seemed computationally the easiest, namely the use of a local exchange potential. Such potentials have a long and distinguished history in structure theory and have been applied with some success to electron-atom collisions (see §4.3). Only one electron-molecule collision has been so treated.[8] In that case the molecular target chosen, H_2, was highly spherical. In light of this fact and the enormous difficulties associated with more precise treatments for collisions with big molecules, the present application has some theoretical and practical significance beyond its immediate motivation: to get the e-CO_2 problem done correctly.

*In fact, the formalism for dealing with this case in the integral equations approach has been worked out (see discussion and references in Chapter 6). However, this technique necessitates separation of the exchange kernel (an approximation) and could be numerically formidable. To date it has not been applied to real problems.

The game plan for this chapter is as follows: In §4.2 we get acquainted with local exchange potentials by reviewing and commenting on their application to structure problems. The use (and misuse) of such approximations in scattering theory is considered in §4.3, which leads us to the derivation in §4.4 of our particular choice of potential. Results for CO_2 are presented in §4.5. We conclude this chapter with a short discourse on alternate ways to include exchange, models and otherwise.

The underlying idea behind all this is to develop a physically reasonable model of the exchange interaction. The best we can hope for is a local potential which in some average approximate way mimics the true effects of exchange; we would prefer (for aesthetic reasons at least) to avoid artificial scaling or adjusted parameters at this point. That this can be achieved is the thrust of this chapter.

§4.2 Local Exchange Potentials in Bound-State Problems

In 1951, J. C. Slater introduced to molecular physicists everywhere the concept of a local exchange potential.[9] Based on the free-electron-gas model of an atom (or a molecule, for that matter), Slater's work suggested that one could take account of exchange in an approximate sense via a local potential proportional to the one-third power of the local electron density. A second important concept introduced in the same paper was that of the exchange hole (or Fermi hole). This is a region surrounding each electron in the target; it consists of a "deficiency" of electronic charge of the same spin as the

electron at the center.* Embedded in the notion of the exchange hole is the fact of the short-range nature of this interaction.

Since its introduction, the Slater Exchange Potential and related ideas have been widely applied to problems in atomic structure. In fact, it led to the SCF-Xα method, which is currently employed extensively in structure calculations in a diverse spectrum of fields.

Let's look briefly at the aspects of this theory which are relevant to our problem. At the core of the Slater exchange potential is the aforementioned free-electron gas (FEG) model[10] of the system. Let's suppose that the electrons are at T = 0°K and occupy one-electron orbitals. The energy of the uppermost filled orbital is defined to be the Fermi Energy, E_F. The picture we have of the free electron gas is of the electrons lying below the Fermi energy and floating about in accordance with Fermi-Dirac statistics.[11] In other words, the electrons are treated as non-interacting fermions. Exchange is therefore taken into account only through the Pauli Exclusion Principle; no "exchange interaction" is explicitly included in this theory.

This picture is closely allied to the free-electron approximation for solids.[12] It leads, as we shall see, to a local exchange potential V_{ex} based on the principle of translational invariance in the FEG and to the famous average exchange potential $\bar{V}_{ex}$. It is worthwhile commenting on derivation of $V_{ex}(\vec{r})$; details can be found in reference (13).

The wavefunction of an FEG electron (conventionally in a Hartree-Fock orbital) is given by a plane wave, viz.,

*Slater likes to divide the total electronic charge into two parts, one due to all the electrons with spin up and the other due to electrons with spin down.

$$u_i(\vec{r}) = \frac{1}{\sqrt{v}}\, e^{-i\vec{k}_i\cdot\vec{r}}, \tag{4.3}$$

where $\vec{k}_i$ is the electron wavevector. The distribution of these electrons in the gas is given by the Fermi-Dirac distribution function,[11]

$$N_i(E_i) = \frac{1}{\exp[(E_i - E_f)/k_B T] - 1}, \tag{4.4}$$

for an electron of energy E_i. Here k_B is Boltzmann's constant, $k_B = 1.3806 \times 10^{-16}$ erg/°K.

Very briefly, to obtain V_{ex} we begin with Slater's form of the Hartree-Fock exchange potential[14] for an electron with coordinate x_1, i.e.,

$$V_{ex}(x_1)u_i(x_1) = \sum_{k=1}^{n}\left\{\frac{1}{u_i^*(x_1)u_i(x_1)}\int u_i^*(x_1)u_k^*(x_2) \right.$$
$$\left. \otimes u_k(x_1)u_i(x_2)\frac{e^2}{r_{12}}\,dx_2\right\}u_i(x_1), \tag{4.5}$$

where x_j denotes spatial and spin coordinates and the sum is over all one-electron spin orbitals. Into this expression we substitute the plane-wave form (4.3) for the orbitals u_i and u_k and then average over the potentials acting on electrons with various wavevectors. The derivation is extremely involved and need not be repeated here since we didn't use this formulation of V_{ex}.

The result is

$$V_{ex} = -4\left(\frac{3}{8\pi}\,\frac{N}{v}\right)^{\frac{1}{3}} F(\eta), \tag{4.6}$$

where N/v is the density of electrons in volume v, η is defined by

$$\eta \equiv \frac{|\vec{k}|}{k_F}, \tag{4.7}$$

and

$$F(\eta) \equiv \frac{1}{2} + \frac{1-\eta^2}{4\eta} \ln\left(\frac{1+\eta}{1-\eta}\right), \tag{4.8}$$

with k_F the Fermi wavenumber and $\vec{k}$ the wavevector of the electron under consideration. Averaging over occupied states in the Fermi distribution, Slater obtains[15] the famous averaged exchange potential,*

$$\overline{V_{ex}} = -3\left(\frac{3}{8\pi}\frac{N}{v}\right)^{\frac{1}{3}}. \tag{4.9}$$

It is useful to rewrite Eq. (4.6) as

$$V_{ex}(\vec{r}) = -\frac{2}{\pi}\left[3\pi^2\rho\right]^{\frac{1}{3}} F(\eta), \tag{4.10}$$

where we let $\rho = N/v$.

We can now make a small but significant improvement on Eq. (4.10) by observing that usually we can determine the charge density of the system** as a function of $\vec{r}$. Let's use this fact and the FEG approximation to derive an expression for $V_{ex}(\vec{r})$ involving the Fermi wavevector as a function of $\vec{r}$. The density of states in energy (number of states/unit volume) in the FEG model is given by[16]

*This uses the fact that the average of $F(\eta)$ over the Fermi sphere is 3/4.

**See §3.2 for the appropriate definitions and notation.

$$\mathcal{D}(E) = \frac{V}{2\pi^2} 2^{\frac{3}{2}} \sqrt{E}, \tag{4.11}$$

where V is the volume under consideration.* The total number of particles in the "box" (volume V) which have energy $E \leq E_f$ is

$$N = \int_0^{E_F} \mathcal{D}(E)\, dE = \frac{V 2^{3/2}}{3\pi^2} E_F^{3/2}. \tag{4.12}$$

Therefore the Fermi energy is

$$E_F = \frac{1}{2} \left[3\pi^2 \rho \right]^{2/3}, \tag{4.12}$$

where $\rho = N/V$ is the density of electrons.

Let's now replace[1,7] the FEG constant electron density ρ by the full quantum-mechanical density $\rho(r) = \sum_{i=1}^{M} N_i |\phi_i(\vec{r})|^2$, obtaining

$$E_F(\vec{r}) = \frac{1}{2} \left[3\pi^2 \rho(\vec{r}) \right]^{2/3}. \tag{4.13}$$

Hence the Fermi wavevector, $\vec{k}_F$, is also a function of $\vec{r}$, since

$$k_F(\vec{r}) = \sqrt{2 E_F(\vec{r})}. \tag{4.14}$$

In terms of the Fermi wavevector, we have [from Eq. (4.10)]

*This expression is derived by applying periodic boundary conditions on a volume V which is small compared to the total volume of the gas but large compared to the deBroglie wavelength λ. Clearly, this breaks down at lower energies.

$$V_{ex}(\vec{r}) = -\frac{2}{\pi} k_F(\vec{r}) F(\eta). \tag{4.15}$$

We should keep in mind that the discussion is valid for bound states of the N-electron system. Thus, $V_{ex}(\vec{r})$ is an approximation to the interaction potential energy of a bound electron due to exchange with the other N-1 electrons in the system; the entire electronic system (all N electrons) is described by the charge distribution $\rho(\vec{r})$.

A word or two should be said about $\vec{k}$ in Eq. (4.3). We would like to suggest a very crude but nonetheless useful interpretation of this quantity in the context of the FEG model which we'll employ in extending the theory to collision problems. In Slater's Theory, $\vec{k}$, the wavevector associated with the electron under consideration, is not considered to be a function of $\vec{r}$; it eventually disappears when he averages to get $\overline{V}_{ex}$. If the electron energy is large enough and we are careful, we can think of $\vec{k}$ in a "classical sense" as a local momentum of the accelerating electron. Suppose the electron's total energy is E_o. A reasonable way to get an expression for $\vec{k}$ would be to use the correspondence principle and write

$$E_o = T + V \tag{4.16}$$

$$= \frac{1}{2} k^2 + V_s(\vec{r}) + V_{ex}(\vec{r}), \tag{4.17}$$

where $V_s(\vec{r})$ is the static potential of Chapter 3. This relationship yields

$$k^2(\vec{r}) = 2\left[E_0 - V_s(\vec{r}) - V_{ex}(\vec{r})\right] ; \qquad (4.18)$$

clearly $\vec{k} = \vec{k}(\vec{r})$, so $\eta = \eta(\vec{r})$ by Eq. (4.7). This interpretation of the wavevector $\vec{k}$, although good only in a very restricted sense for the case under consideration in this section will have important implications when we get to the electron scattering problem.

We should probably re-emphasize the point that this entire theoretical structure is predicated on the rather crude FEG model and is only valid provided that the local wavelength of the electron under consideration, $\lambda(\vec{r}) \propto 1/k(\vec{r})$, is small compared to the distance typical of substantial changes in the potential. Certain regions of r will not be treated correctly in this picture; e.g., very small and (or course) very large r. The range of r in which the model is applicable is often referred to[17] as the Thomas-Fermi region. For large systems, the TF region can be quite substantial in the sense that a considerable fraction of the electronic charge distribution is concentrated therein. In such cases such a local exchange approximation can be quite successful.

In closing, let us observe that the approach outlined herein differs substantially from the Thomas-Fermi theory,[18] which begins with the assumption that the averaged atomic potential in which an electron finds itself varies slowly over a deBroglie wavelength. This potential is taken to be approximately constant, and the system is treated as a FEG. It is further assumed that the gas "fills" the potential; in other words, that

$$E_F = \epsilon_F(\vec{r}) = -V(\vec{r}). \tag{4.19}$$

Using this assumption and Poisson's equation, it is possible to derive an equation relating the charge density $\rho(\vec{r})$ to $V(\vec{r})$ and to thence solve for $\rho(\vec{r})$. (In our approach, we simply pull $\rho(\vec{r})$ from the quantum mechanical structure calculation.) Thus the Thomas-Fermi theory amounts to a statistical averaging process which effectively "smears-out" the structure of the true electron distribution.[19] This approximation would seem to be doomed from the start for highly aspherical molecules.

§4.3 Local Exchange Potentials in Electron Scattering Theory.

The importance of exchange in electron-molecule collisions* is well-established.[20] Some of the procedures that have been developed over the years to introduce exchange effects into problems in these areas were mentioned in the Introduction to this chapter. The local exchange potential idea has been employed to some extent in work on electron-atom scattering, and a useful though brief discussion of this work together with a presentation of a new approximate potential appears in reference (21).

*In cases of strongly polar (heteronuclear) molecules, it is likely that the long-range interactions (especially the r^{-2} P_1 dipole interaction) so overwhelmingly dominate the total and momentum transfer cross sections that exchange effects are negligible by comparison. However, short-range effects can be important in determination of particular $j \to j'$ cross sections.[22]

Certain theoretical difficulties obtain if one tries to blindly apply the Slater effective potential of, say, Eq. (4.15) to the electron collision problem. For one thing, the scattering electron is not represented in the electronic charge density $\rho(\vec{r})$, which, in the scattering problem, is referred to the target. For low energy collisions, the scattering electron is certainly not localized in space. Depending on how you interpret the notion of a "Thomas-Fermi region," it loses significance, since the scattering electron wavefunction is in no sense contained, being itself a plane wave. It is difficult to view the electron as part of a free electron gas without really stretching the model.

A number of early investigators chose to apply Slater's averaged potential directly to problems in electron-atom scattering using the form

$$\bar{V}_{ex}(\vec{r}) = -\frac{3}{2\pi}\alpha_x\left[3\pi^2\rho(\vec{r})\right]^{1/3}, \tag{4.20}$$

where α_x is a constant. As pointed out by Hara,[8] such an approach represents a rather considerable misunderstanding, since Eq. (4.20) is obtained by averaging $F(\eta)$ over the Fermi sphere. At the center of the Fermi sphere, we have $\eta = 0$, $F(\eta) = 1$, and at the surface $\eta = 1$, $F(\eta) = \frac{1}{2}$. But for electron scattering problems $\eta > 1$! The average potential is inappropriate for the scattering electron, which has a definite energy and wavevector.

Riley and Truhlar have (correctly) applied a variety of local exchange potentials to e-He and e-Ar collisions and found some of them to be highly successful. We won't go into all the details of

these approximations: we should remark that they are all excellent approximations at high energies (> 50 eV) and that the particular approximation which we extend to the case of molecular target, the Hara Free-Electron Gas Exchange (HFEGE) approximation, is quite good at very low energies and smaller orbital angular momentum quantum numbers ℓ. At higher energies, this potential was found to give phase shifts somewhat smaller than those obtained with close-coupling calculations.

The only application to date of local approximate exchange potentials to electron-molecule collisions is that of Hara.[8] The system studied was e-H_2, and Hara's results are most encouraging. Due to the highly spherical nature of the target molecule, Hara decided (correctly) that it was appropriate to spherically average his approximate exchange potential. We certainly cannot do this for the e-CO_2 system;* this should be apparent from our discussion in Chapter 3 of the expansion coefficients of the CO_2 charge distribution.

This introductory out of the way, we proceed in the next section to a derivation of the particular local exchange potential employed in the calculations of Chapter 8 and a discussion of how this potential is incorporated into the formalism we have outlined thus far.

*In fact, a few test runs in the energy range 0.07 eV to 10.0 eV making the spherical averaging approximation produced cross sections which differed by an order of magnitude from the true result.

§4.4 Derivation of the Modified HFEGE

The derivation here presented follows closely that of Hara,[8] so we shall merely outline the steps, filling in some detail where we deviate from his analysis in order to adapt the HFEGE to the problem at hand. For simplicity of illustration, we'll consider at first a two-electron target and then make the obvious generalizations.

Our starting point is the familiar expansion of the scattering function in target states.[33] We use a properly antisymmetrized linear combination of product functions in accordance with the Pauli Exclusion Principle, viz.,

$$\Psi_E(1,2,3) = \sum_n \Big[\phi_n(1,2) F_n(3) \chi(1,2,3) + \phi_n(2,3) F_n(1) \chi_n(2,3,1) + \phi_n(3,1) F_n(2) \chi_n(3,1,2) \Big]. \tag{4.21}$$

We have denoted the target states by $\phi_n(i,j)$, the scattering function by $F_n(k)$, and the system (e + target) spin function by $\chi_n(i,j,k)$. The Schroedinger equation for this case is

$$\Big(\sum_{i=1}^{3} \mathcal{H}_i + \sum_{i>j} \frac{1}{r_{ij}} \Big) \Psi_E(1,2,3) = E \Psi_E(1,2,3), \tag{4.22}$$

where

$$\mathcal{H}_i = -\frac{1}{2} \nabla_i^2 - \frac{1}{r_{ia}} - \frac{1}{r_{ib}} \quad . \tag{4.23}$$

By definition, $\phi_n(i,j)$ satisfies the corresponding eigenvalue equation for the target, i.e.,

$$\Big(\mathcal{H}_i + \mathcal{H}_j + \frac{1}{r_{ij}} \Big) \phi_n(i,j) = E_n \phi_n(i,j). \tag{4.24}$$

For the case of the target in a singlet state, the spin function is

$$\chi_n(i,j,k) = \frac{1}{\sqrt{2}}\left[\alpha(i)\beta(j) - \alpha(j)\beta(i)\right]\alpha(k). \tag{4.25}$$

Substituting Eq. (4.21) into the Schroedinger equation (4.22) and using Eqs. (4.24) and (4.25), we obtain the usual coupled equations,

$$\left[-\tfrac{1}{2}\nabla_3^2 + V^S(\vec{r}_3) - \tfrac{1}{2}k_0^2\right]F_0(\vec{r}_3) + \sum_{n\neq 0} V_{0n}^S(\vec{r}_3)F_n(\vec{r}_3) - \sum_n V_n^{ex}(\vec{r}_3)F_n(\vec{r}_3) = 0, \tag{4.26}$$

where $V^S(\vec{r}_3)$ is the static potential energy averaged over the ground state, i.e.,

$$V^S(\vec{r}_3) = -\left(\frac{1}{r_{3a}} + \frac{1}{r_{3b}}\right) + \int \phi_0^*(1,2)\left(\frac{1}{r_{13}} + \frac{1}{r_{23}}\right)\phi_0(1,2)\,d1\,d2. \tag{4.27}$$

The static excitation potential, which gives rise to polarization terms (see Chapter 5) is

$$V_{0n}^S(\vec{r}_3) = \int \phi_0^*(1,2)\left(\frac{1}{r_{13}} + \frac{1}{r_{23}}\right)\phi_n(1,2)\,d1\,d2. \tag{4.28}$$

Finally, the exchange term in Eq. (4.26) is

$$V_n^{ex}(\vec{r}_3)F_n(\vec{r}_3) = \int \phi_0^*(1,2)\left[-\tfrac{1}{2}\nabla_1^2 - \left(\frac{1}{r_{1a}} - \frac{1}{r_{1b}}\right) + \left(\frac{1}{r_{13}} + \frac{1}{r_{23}}\right) - (E-E_n)\right]\phi_n(2,3)F_n(1)\,d1\,d2. \tag{4.29}$$

There is one such term corresponding to each target state included in the expansion of Eq. (4.21), and the full exchange potential is simply the sum of these terms; we have

$$V_{ex}(\vec{r}_3) = \sum_n V_n^{ex}(\vec{r}_3). \tag{4.30}$$

Let us now make the assumption that only the ground state (n = 0) contributes significantly to the summation and carry out the integral d2 in (4.29). Using the Schroedinger equation for $\phi_o(1,2)$, we obtain*

$$V^{ex}(\vec{r}_3)F_0(\vec{r}_3) = -\left[(\epsilon_o - \tfrac{1}{2}k_o^2)\int \chi_o^*(1)F_0(1)\,d1 + \int \chi_o^*(1)\frac{1}{r_{13}}F_0(1)\,d1\right]\chi_o(3), \tag{4.31}$$

where $\frac{1}{2}k_o^2 = E_i = E - E_o$ is the incident kinetic energy. If we now assume that $F_o(\vec{r})$ is orthogonal to $\chi_o(\vec{r})$, Eq. (4.31) reduces to

$$V_{ex}(\vec{r}_3)F_0(\vec{r}_3) \simeq -\int \chi_o^*(1)\frac{1}{r_{13}}F_0(1)\,d1\;\chi_o(3). \tag{4.32}$$

Next, we treat this expression for the exchange potential in a fashion completely analogous to Slater's treatment[13] of the Hartree-Fock exchange potential for bound states (as discussed in §4.2); we obtain

$$V^{ex}(\vec{r}) = -\frac{2}{\pi}k_F(\vec{r})F(\eta), \tag{4.33}$$

where the Fermi wavevector $\vec{k}_F(\vec{r})$ is defined by [see Eq. (4.14)]

$$k_F(\vec{r}) = \left[3\pi^2\rho(\vec{r})\right]^{1/3}, \tag{4.34}$$

with $\rho(\vec{r})$ the charge distribution of the target. The function F(η) is

*Here $\chi_o(\vec{r})$ is a core molecular orbital, one of these making up $\phi_o(i,j)$, and corresponds to energy eigenvalue ϵ_o.

of the usual form [see Eq. (4.8)]., i.e.,

$$F(\eta) = \frac{1}{2} + \frac{1-\eta^2}{4\eta} \ln\left|\frac{1+\eta}{1-\eta}\right|, \tag{4.35}$$

with

$$\eta = \frac{k(\vec{r})}{k_F(\vec{r})} \tag{4.36}$$

Finally, $k(\vec{r})$ is defined by

$$k^2(\vec{r}) = 2\left[E_i - V(\vec{r})\right], \tag{4.37}$$

$V(\vec{r})$ being the total potential energy (static + exchange) and E_i the incident kinetic energy. From the definition of the Fermi energy as the energy of the most energetic electron in the target gas (see §4.2), we can relate $k_F(\vec{r})$ to the first ionization potential of the target I (by definition, I > 0) by writing T + V = E for the "Fermi electron," viz.

$$k_F^2(\vec{r}) + 2V(\vec{r}) = -2I, \tag{4.38}$$

where we have assumed that the Fermi electron sees the same potential $V(\vec{r})$ as does the scattering electron.* Therefore we have

$$k^2(\vec{r}) = k_F^2(\vec{r}) + 2(E_i + I). \tag{4.39}$$

*This is certainly a reasonable assumption for values of $\vec{r}$ in the vicinity of the nuclei, the most important region.

The presence of I in Eq. (4.39) is extremely important; aside from this the form of the equations we have just obtained and those of §4.2 is the same. The reason for its presence is that the scattering electron is <u>not</u> part of the N-electron "fermi sea." Thus there is a negative energy gap between the zero of energy and the Fermi energy E_F as defined by Eq. (4.13). The colliding electron cannot scatter with an energy in this gap, since to do so it would have an imaginary momentum. One way of looking at what we have done by introducing I would be to say we have come up with a new Fermi energy for the entire system equal to $E_F + I$. This can be a confusing perspective, though, since in point of fact, the scattering electron is still <u>not</u> part of the Fermi sea.

An objection to this approximate potential raised by Hara himself[8] and echoed by others is that the asymptotic kinetic energy one predicts for the scattering electron based on Eq. (4.39) is $E_i + I$ rather than E_i, as it should be. At high energies this is not a problem since $E_i + I = E_i$ if E_i is large enough. At low energies, the interpretation of $\vec{k}(\vec{r})$ as some sort of classical local momentum for the acceleration (scattering) electron as discussed in §4.2 begins to run into difficulty. This interpretation, in turn, is central to the objection we are addressing. Finally, it should be noted that the short-range nature of exchange to some extent mitigates the problem. This is not to suggest that the theoretical objection is not a valid one so much as that it is not particularly significant.*

*Several such bitter pills must be swallowed in order to go along with application of a local exchange potential. For example, it is something of a leap of faith to claim that ground-state CO_2 is a free electron gas! However, the proof of the pudding is in the eating, to coin a cliche, and we refer the skeptical reader to the results of Chapter 8.

Riley and Truhlar have proposed[21] a rather simple way off the horns of this dilemma: ignore I and use instead of Eq. (4.39) the relationship

$$k^2(\vec{r}) = k_F^2(\vec{r}) + 2E_i . \tag{4.40}$$

They applied this potential (called the asymptotically adjusted free electron gas exchange or AAFEGE potential) to e-He and e-Ar collisions with some success. We believe, for the reasons suggested above, that the ionization potential should be present in the expression relating $k(\vec{r})$ to $k_F(\vec{r})$, particularly for low energy collisions such as those of interest to us. Moreover, it is perhaps a bit misleading to refer to the potential using Eq. (4.40) instead of (4.39) as asymptotically adjusted since, of course, dropping I will affect $k(\vec{r})$ for all r.

However, we did try several test calculations of e-CO_2 cross sections using the AAFEGE, the results of which will be presented in Chapter 8. Suffice it to say that in addition to exacerbating the already quite severe numerical problems with which we were trying to cope (e.g., convergence), the AAFEGE gave very poor results in the energy range 0.07 eV to 10.0 eV. For these reasons we dropped it and returned, with considerably greater success to the HFEGE.

Notice that the HFEGE potential derived above is energy dependent, i.e., the incident (scattering) kinetic energy appears in Eq. (4.39) for $k(\vec{r})$ and hence in $V_{ex}(\vec{r})$. However, once $\rho(\vec{r})$, which, of course, is not energy dependent, has been calculated, computation of $V_{ex}(\vec{r})$ at any energy requires a trivial amount of computer time. Since we have to determine $\rho(\vec{r})$ over the appropriate integration mesh anyway

in order to calculate the static potential energy of Chapter 3, it is no problem to go ahead and get $V_{ex}(\vec{r})$.

We do not spherically average $\rho(\vec{r})$ but instead use the full function $\rho(r,\theta)$ for the CO_2 target. Therefore $V_{ex} = V_{ex}(r,\theta)$. In order to incorporate this exchange potential into our formulation of the collision problem, we call upon the familiar expansion in Legendre polynomials, viz.,

$$V_{ex}(\vec{r}) = \sum_{\lambda=0}^{\infty}{}' v_\lambda^{ex}(r) P_\lambda(\cos\theta), \tag{4.41}$$

where as usual only even-λ terms contribute to the sum. It is worth pointing out that the exchange potential energy is in fact a correction to the electronic part of $v_\lambda(r)$ as derived in Chapter 3 [see Eq. (3.61) and the ensuing commentary]. Thus there is, mercifully, no need to calculate, say, $v_{80}^{ex}(r)$. We stop at $\lambda = 28$ for consistency with our limit* on $v_\lambda^{st.el.}(r)$.

Once we have determined $v_\lambda^{ex}(r)$ at the scattering energy of interest,** we simply add it to the appropriate static expansion coefficient, obtaining

$$v_\lambda(r) = v_\lambda^{st}(r) + v_\lambda^{ex}(r). \tag{4.42}$$

*In this chapter, we shall tack on a subscript "st" to the static expansion coefficients to distinguish it from the exchange terms.

**Our code to do this is called EXCHPT. It does 32-point angular Gauss-Legendre quadrature similar to that discussed in Chapter 3. The charge distribution as computed using CHGDST is input along with the usual assortment of parameters.

As a check on the code, we can do one case by hand with alacrity, namely the r → 0 limit. We have

$$V_{ex}(\vec{r}) \underset{r\to 0}{\sim} -\frac{1}{\pi}\left[3\pi^2\rho(r,\theta)\right]^{1/3} \tag{4.43}$$

since

$$\eta \underset{r\to 0}{\sim} 1 \quad \text{and} \quad F(\eta) \underset{r\to 0}{\sim} \frac{1}{2}. \tag{4.44}$$

At very small r, $\rho(\vec{r})$ reduces to [see Eq. (3.12)] the $\lambda = 0$ expansion coefficient, i.e.,

$$\rho(\vec{r}) \simeq a_0(r). \tag{4.45}$$

Thus the exchange potential in this limit can be written as

$$V_{ex}(\vec{r}) \underset{r\to 0}{\sim} -\frac{1}{\pi}\left[3\pi^2 a_0(r)\right]^{1/3}. \tag{4.46}$$

This expression was used to verify the code which calculates $V_{ex}(\vec{r})$.

As a further check, we also reproduced Hara's e-H_2 cross sections. It is interesting to observe that using the HFEGE <u>without</u> the additional approximation of spherical averaging produces only slightly better cross sections for e-H_2 scattering.

Fortunately, there are no particular numerical problems or such associated with calculation of the HFEGE. Therefore we'll move right along into a short look at the results of these computations.

§4.5 Results and Comments: Local Exchange Potential for e-CO_2 Collisions

Typically, the calculation of $v_\lambda^{ex}(r)$ for $\lambda = 0,2,\ldots,28$ over our standard integration mesh (see Chapter 8) required <16 seconds of CDC 7600 time. The largest part of this was accessing and storing the charge distribution over the predefined r- and θ-mesh discussed in Chapter 3.

Figure 4.1 shows $v_\lambda^{ex}(r)$ in the HFEGE model for r = 0.0 to 3.0 a_o at an energy E_i = 0.07 eV for two quite different cases, $\lambda = 0$ and $\lambda = 14$. The behavior of $v_{14}^{ex}(r)$ is typical of that of the exchange expansion coefficients for large values of λ. The magnitude of $v_\lambda^{ex}(r)$ decreases as λ increases and its effect on becomes significant only in the vicinity of the oxygen nuclei ($r = R_{oc} = 2.19440\ a_o$ in this application). Three intermediate cases, λ = 2, 4, and 6, are illustrated in Figure 4.2.

On the whole, the effect of $V_{ex}(\vec{r})$ is clearly attractive: it deepens the potential $V(\vec{r})$ over the static-only case, $V^{st}(\vec{r})$. At the level of the potential energy expansion coefficients, there are small regions of r for certain λ where $v_\lambda(r)$ is smaller in magnitude than $v_\lambda^{st}(r)$. [Remember that each $v_\lambda(r)$ multiplies $P_\lambda(\cos\theta)$ in the expression for the potential energy $V(\vec{r})$.] Nevertheless, the general effect is clear. Figure 4.3 shows graphs of the static $[v_\lambda^{st}(r)]$ and total $[v_\lambda(r) = v_\lambda^{st}(r) + v_\lambda^{ex}(r)]$ expansion coefficients for several values of λ.

It may appear from Figure 4.3 that, after all, the effect of the exchange potential is rather small and therefore that the multiple machinations of the chapter really amount to much ado about nothing.

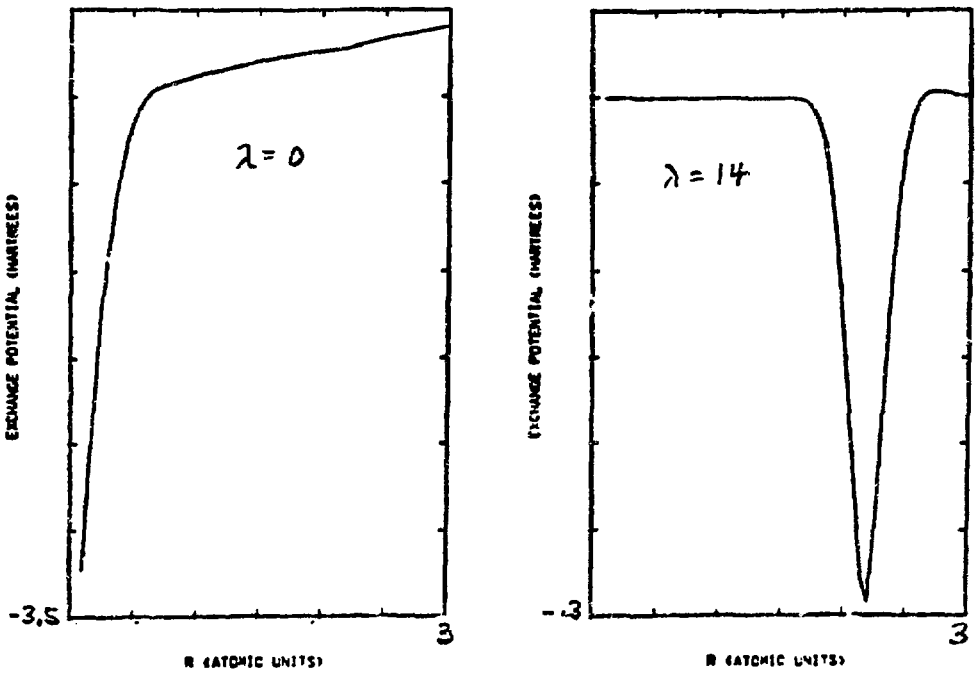

Figure 4.1

The HFEGE potential energy: expansion coefficients for $\lambda = 0$ and $\lambda = 14$ at 0.07 eV for e-CO_2 scattering.

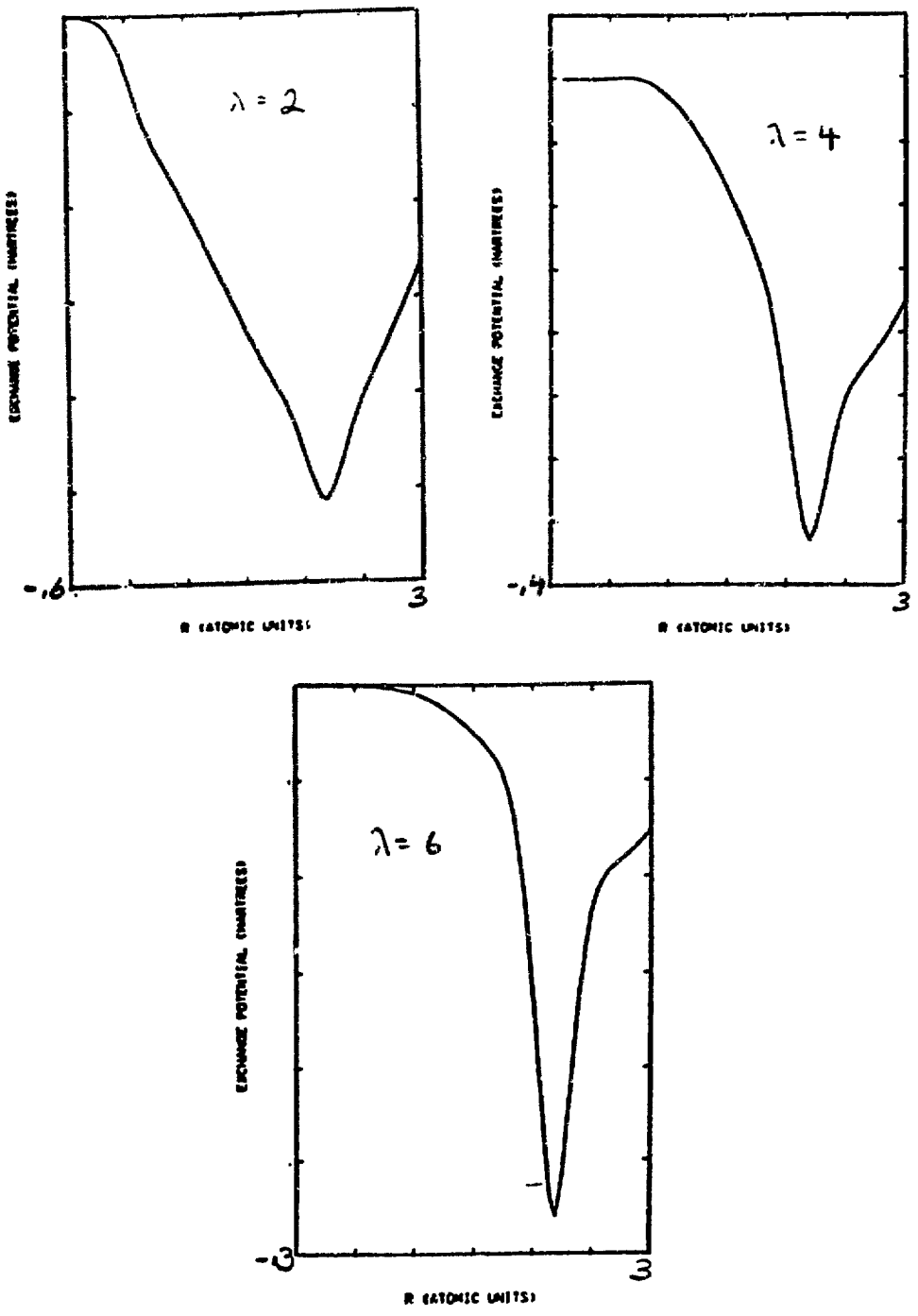

Figure 4.2

The HFEGE potential energy: expansion coefficients for λ = 2, 4, and 6 at 0.07 eV for e-CO_2 collisions.

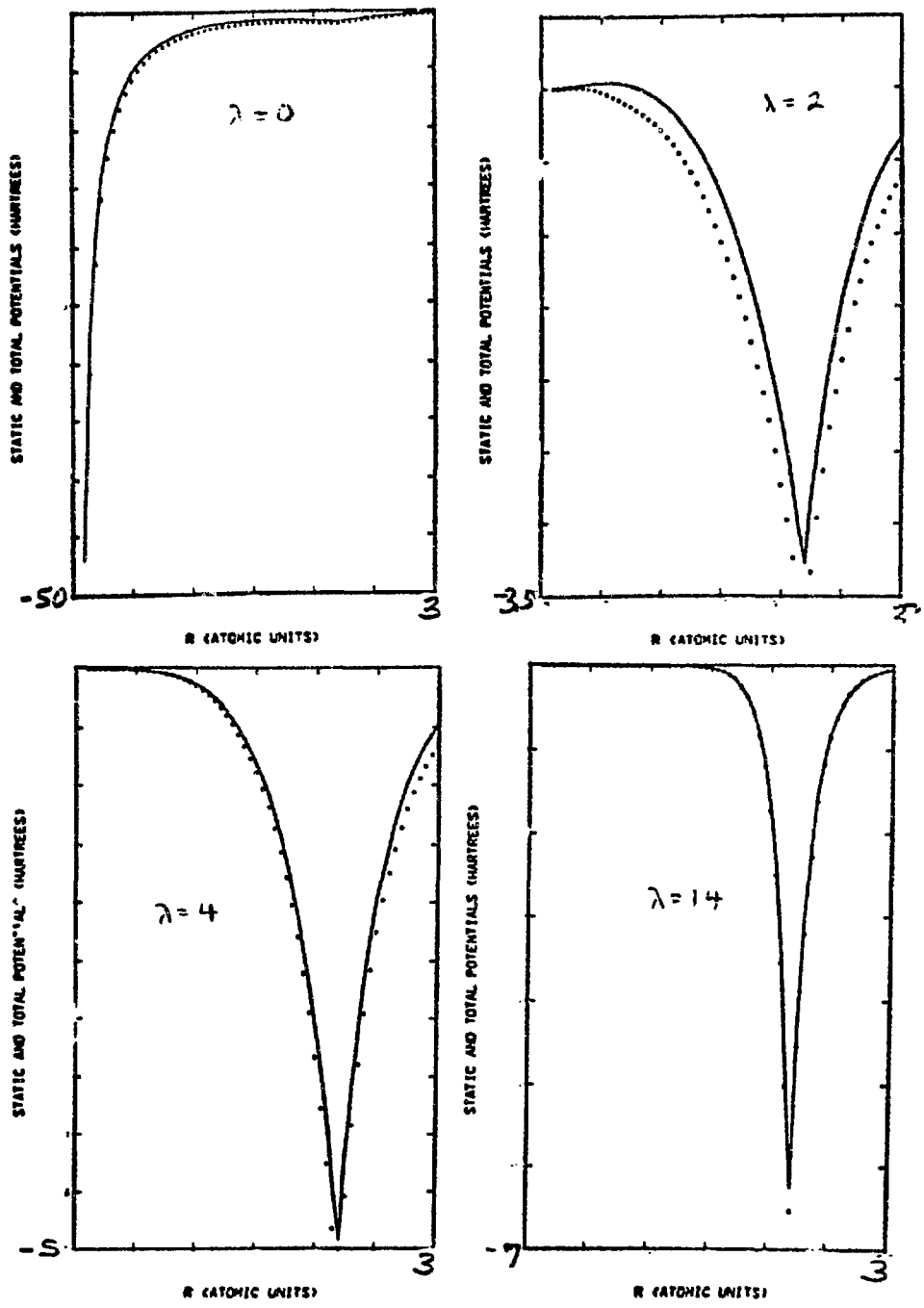

Figure 4.3

Static (solid) and total (dotted) potential energy coefficients for e-CO_2 for λ = 0, 2, 4, and 14 using the HFEGE potential energy at 0.07 eV.

Wrong! For as we shall discover when we actually study cross sections (still a couple of chapters away in 8), the addition of the exchange potential has a huge influence on the results obtained from the coupled-channel calculations. The same is true of the induced polarization terms, which we'll get to in Chapter 5.

The energy dependence of $V_{ex}(\vec{r})$, to which we alluded in the preceeding section and which appears in Eq. (4.40) for $k(\vec{r})$, makes so small a change in $v_\lambda^{ex}(r)$ that it doesn't even show up well on a graph. The two extremes of the cases we considered, 0.07 eV and 10.0 eV, are compared for $\lambda = 0$ and $\lambda = 4$ from $r = 0.0\ a_o$ to $r = 3.0\ a_o$ in Figure 4.4. Even this small difference affects the cross sections, though.

The AAFEGE, mentioned briefly in §4.4 and used by Riley and Truhlar in e-atom problems, is more attractive than is the HFEGE. The two potentials are compared for $\lambda = 0$ and $\lambda = 2$ at an energy of 0.07 eV in Figure 4.5. We did carry out a couple of calculations using the AAFEGE, so this figure is presented for completeness.

§4.6 An Alternate Approach to the Exchange Question

In a sense, we have focused so far on one of the two effects of exchange which were mentioned in §4.1, namely, the short-range attractive character of the interaction. In fact, it is entirely possible (though not clear) that some of the orthogonalization aspects of exchange are incorporated in the potential we employ. In any event, an alternate approach to the problem of the inclusion of exchange exists due to Burke and co-workers. The philosophy behind Burke's approach is quite different from ours; it is predicated on enforcing orthogonality

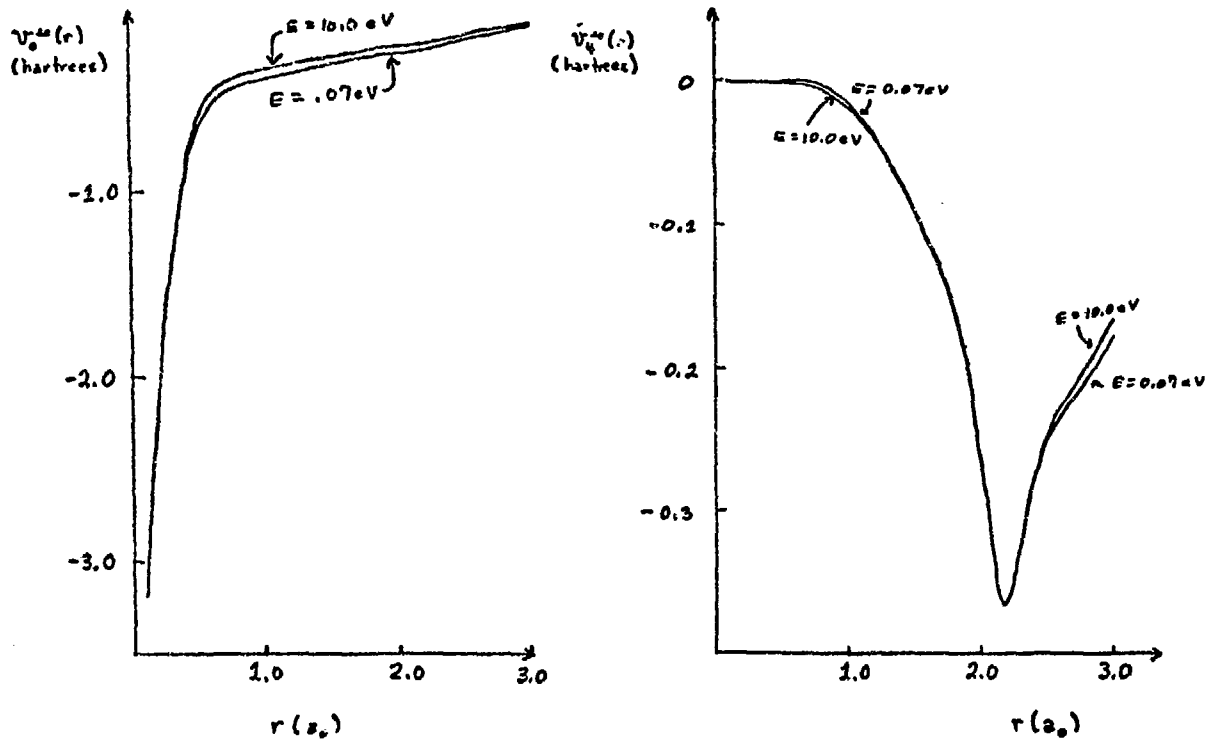

Figure 4.4

Energy dependence of the HFEGE potential energy: Expansion coefficients for $\lambda = 0$ and $\lambda = 4$ at an energy of 0.07 eV and at 10.0 eV.

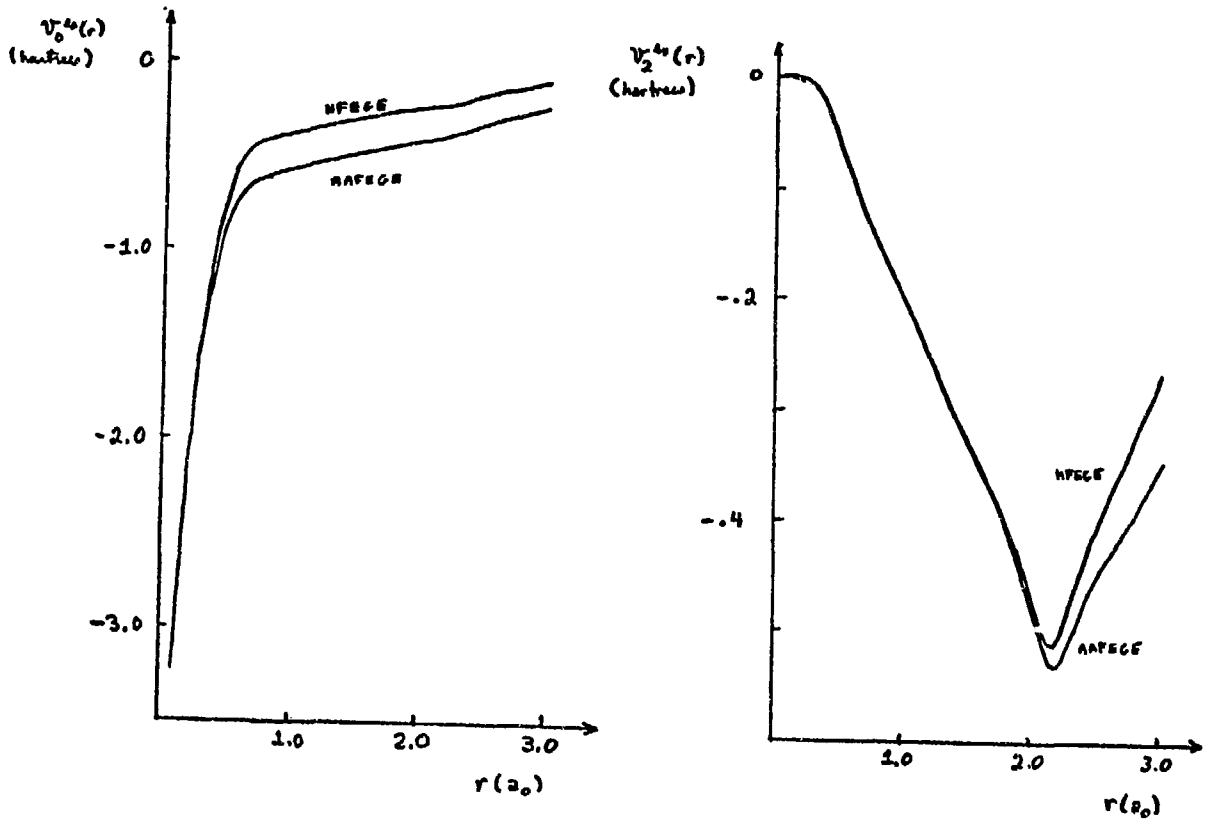

Figure 4.5

Comparison of the expansion coefficients foe $\lambda = 0$ and $\lambda = 2$ for the HFEGE and AAFEGE potential energies.

of the scattering function to the core orbitals which have the same symmetry.

We chose not to adopt this technique for reasons to be presented below. However, it is an important contribution, and so we should consider it briefly here.

The first in a series of papers developing this approach was written by Burke and Sinfailam[24] and is important to the present discussion mainly as a precursor. These authors use the Kohn variational principle[25] to derive coupled equations for electron-molecule scattering in a body-fixed reference frame. They take into account exchange, obviously; otherwise we would not here be considering their work. They do not include polarization effects. Single-center coordinates are employed, and a single-configuration fully antisymmetrized molecular-orbital wavefunction for the system (e + molecule) based on SCF target orbitals is incorporated into the theory. In deriving the coupled equations [using the tiresome but apparently inevitable expansion of $V(\vec{r})$ in Legendre Polynomials a la Eq. (3.39)], Burke and Sinfailam explicitly use the orthogonality constraint in the exchange term. Having obtained the resultant coupled equations, cross sections in the lab frame are derived from the body-frame S-matrix by a transformation which neglects the rotational spacing of the target.*

A significant advance in this work, which is really rather traditional, was subsequently made by Burke and Chandra,[26] who developed a

*We have performed a somewhat similar analysis in our derivation of the rotational excitation cross section from body-frame T-matrix elements. See Chapter 7 for details.

new way to treat exchange which is conceptually based on the notion of a pseudopotential.[27] This procedure entails replacing the exchange terms in the usual coupled equations by Lagrange multipliers[28] which are determined so as to force orthogonality of the scattering orbital to bound orbitals of the same symmetry. The resulting coupled differential equations take on the form

$$\left[\frac{d^2}{dr^2} - \frac{\ell(\ell+1)}{r^2} + k^2\right] u_\ell^{(m)}(r) - 2\sum_{\ell'} V_{\ell\ell'}^{(m)}(r)\, u_{\ell'}^{(m)}(r) = \sum_{\alpha=1}^{M'} \lambda_\alpha \phi_\alpha^{(\ell m)}(r), \tag{4.47}$$

where the summation on the right-hand-side runs over all bound orbitals, $\phi_\alpha^{(\ell m)}(r)$ which have the same symmetry as $u_\ell^{(m)}(r)$, assumed to be M' in number. Techniques for solution of these equations are discussed in reference (26). These authors believe that the resultant terms have the effect of diminishing the influence of the nuclear singularities by keeping the electron out of the vicinity of the nuclei. However, the effect as seen in their convergence studies on e-N_2 collisions is none too striking and suggests a consequent "saving" of only a couple of terms, e.g., $v_{12}(r)$ and $v_{14}(r)$, over the more conventional treatment.

The same authors[29] have presented an outline of how to carry out a similar calculation on the extremely challenging problem of e-H_2O collisions. However, to date no calculations using this method on this problem have been reported.

A couple of further less significant but nonetheless interesting applications and extensions of this approach have appeared. These include a calculation of rotational excitation cross sections in e-N_2

collisions,[30] documentation of a computer code based on this work,[31] and application of the method[32] to a heteropolar target, CO.

Why, then, did we choose not to adopt this procedure at the outset? First, there are certain problems with the theoretical underpinnings of the method. For example, it in no way adjusts scattering wavefunctions corresponding to symmetries for which there are no core orbitals to orthogonalize to. This could be a serious complication. For example, let's consider e-N_2 scattering. This is precisely the system which Burke and Chandra[26] choose for their initial study. Now, there is a fairly well-known $^2\Pi_g$ resonance at an incident energy of about 0.2 Ryd. This resonance is thought to be almost purely d-wave. The problem is that the orbital occupancy of ground state N_2 is

$$X\,^1\Sigma_g^+: \quad 1\sigma_g^2\, 2\sigma_g^2\, 1\sigma_u^2\, 2\sigma_u^2\, 3\sigma_g^2\, 1\pi_u^4 \,. \tag{4.48}$$

There is no core π_g orbital. The aforementioned resonance does not appear in the correct energy range in the static-exchange calculations of Burke and Chandra.[26] They <u>do</u> ultimately produce the resonance by introducing a polarization potential and appropriately adjusting the cutoff parameter (see Chapter 5). This is an entirely appropriate way to proceed, but it does make the polarization potential entirely responsible for the resonance. This may present an unrealistic physical picture of the scattering. Moreover, the deficiency here illustrated could conceivably be more serious in other cases. For example, in e-H_2 scattering, where the target has only $1\sigma_g$ orbitals, how do you produce the 3.4 eV $^2\Sigma_g$ resonance,[33] which arises in part from σ_u scattering functions?[34]

In contrast, the local exchange potential, however inelegant the assumptions on which it is based, at least corrects all symmetries. The problem suggested above with the orthogonalization procedure can be viewed as a partial consequence of the fact that it simply neglects one rather important aspect of the effect of exchange.

A second probable problem caused us to shy away from Burke's method as a first crack at the exchange question. As should become apparent in Chapters 6 and 8, the solution of the coupled-channel equations for $e\text{-}CO_2$ by the integral equations technique is by no stretch of the imagination straightforward or easy numerically. Indeed, in some ways, our problem pushes this approach to the scattering far beyond previous applications. Given this fact, it was not clear that the further numerics associated with the orthogonalization would not make these computational complications even worse.

Finally, taking a ruthlessly pragmatic point of view, it seemed clear that introduction of a local exchange potential, which was theoretically somewhat more appealing for the reasons suggested above, would be much easier than the orthogonalization procedure.

Had the modified HFEGE not performed so spectacularly, we would probably have gone ahead and tried a combination of the two ideas. In fact, such a scheme seems to us to be the most interesting and reasonable way to approach the problem of exchange, which will continue to haunt us so long as we seek to solve electron scattering problems involving many-electron targets. In the simple case of, say, an H_2 target, it is possible to make clever simplifications[35] of the exchange kernel appearing in the coupled equations for the scattering and thence to solve said equations to a relatively high degree of accuracy. However, when confronted with a 22-electron,

inordinately anisotropic target, it is less clear how to proceed. "Electron-big molecule" problems are not likely to go away and will remain of fundamental and practical importance in the forseeable future. At present, it seems that these problems, which would put considerable strain on even the newer less-well-established L^2-variational approaches to electron-molecule collisions (see Chapter 9), could be profitably attacked along the lines suggested here. Clearly, all one's intuition and skill at "model building" will have to be brought to bear on such systems.

However, returning to earth, CO_2 is not the place to start such an admittedly fascinating study. One should begin with simply atomic targets, say He and Ar, then go to simple homonuclear diatomics such as H_2 and N_2, and perhaps a mildly polar molecule, say CO. Then perhaps it would be reasonable (if numerically feasible) to try CO_2. Our goal at present is to get reliable cross sections for e-CO_2 scattering, and we find that the modified HFEGE presented in §4.4 works quite well. We shall see this once we plow through a short discussion of polarization potentials (Chapter 5) and a not-so-short presentation of coupled-channel equations and their solution by integral equation methods (Chapter 6).

Chapter 5. Long-Range Terms and the Induced Polarization Potential

> Solomon saith, there is no new thing upon the earth. So that as Plato had an imagination, that all knowledge was but rememberance, so Solomon giveth his sentence, that all novelty is but oblivion.
>
> -Francis Bacon
> Essays (LVIII)

§5.1. Introduction: Why We Need a Polarization Potential.

And now for something completely different. In the last two chapters we studied various kinds of interactions between the scattering electron and the undistorted target molecule. The derivation of the static contribution to the electron-molecule potential energy was more or less straightforward, but in the last chapter we plunged headfirst into the world of exchange, a universe of eerie approximations, weird models, and strange assumptions. Throughout these discussions, furtive reference has been made to additional potential energy terms; it is to these induced long-range terms that we turn in this brief chapter.

The static and static-exchange approximations neglect all perturbations of the target by the scattering particle. This assumption is not, in general, particularly reliable. The incident electron, being a charged particle, will act to distort the target

if its kinetic energy is not too large. This effect can be incorporated into the theory by means of the inclusion of a simple analytic term $V_p(\vec{r})$ in the potential energy, yielding for the final potential energy

$$V(\vec{r}) = V_{st}(\vec{r}) + V_{ex}(\vec{r}) + V_p(\vec{r}). \tag{5.1}$$

In section 5.2 we will examine the physical origin of this additional term and the theoretical justification for the particular analytic form we employ, Eq. (5.16). We do this initially in the context of electron-atom collisions because most of the pioneering work in this area focused on such problems. We then turn in section 5.3 to the particular case of CO_2, examine its polarizability, and close by summarizing the results we have obtained for the total potential energy.

§ 5.2. Adiabatic Polarization Potentials in Electron Scattering

The static and static-exchange approximations could be quite useful for scattering by electrons with large incident kinetic energies, k^2, since the target electrons will not have sufficient time to adjust to the perturbing influence of the electron zipping by. In point of fact, the response of the target in this case is highly non-adiabatic and is manifested by electronic excitation of the target.

The hitch is that we are concerned here with slow collisions.

In such cases, it is appropriate[1] to view the response of the target as occurring adiabatically*. This concept sets up an appealing physical picture of the electron, when viewed from the perspective of one of the target electrons (to anthropomorphize) as frozen at position $\vec{r}$. This electron will thereby set up a static external electric field which will polarize the target. In fact, we shall see that a dipole moment is induced in the target. It is therefore proper to ascribe the effect to an induced polarization interaction and to call the resulting potential an adiabatic polarization potential.[2]

This theory was first introduced in the study of e-H collisions where[1] the potential energy has the long-range form

$$V_p(r) \underset{r\to\infty}{\sim} -\frac{\alpha}{2r^4} P_0(\cos\theta), \tag{5.2}$$

α being the static polarizability[3] of hydrogen (in atomic units, 4.5 au). In order to understand the origin and nature of the forces reflected in polarization potentials, let's take a look at this comparatively simple problem.

The logical if obvious way to obtain a potential energy within the picture suggested above is via time-independent perturbation theory.[4] The first relevant quantity is the

*The proliferation of the word "adiabatic" and its cohorts (e.g., "impulse") in electron scattering theory is a source of nearly limitless confusion. Care must be taken to understand what is responding adiabatically. Contrast, for example, the adiabatic fixed-nuclei approximation to the approximation here discussed.

first-order perturbed wavefunction for the target:[1]

$$\phi'(\vec{r}_1,\vec{r}) = \phi_0(\vec{r}_1) - \sum_{\gamma\neq 1} \frac{V_{0\gamma}(\vec{r})\,\phi_\gamma(\vec{r}_1)}{E_\gamma - E_0} \quad , \tag{5.3}$$

where $\phi_0(\vec{r}_1)$ is the unperturbed ground-state target wavefunction, the sum in the second term runs over all target states, and the excitation potential matrix element is defined by

$$V_{\gamma\gamma'}(\vec{r}) \equiv \int \phi_\gamma^*(\vec{r}_1)\frac{1}{|\vec{r}-\vec{r}_1|}\phi_{\gamma'}(\vec{r}_1)\,d^3r_1 \, . \tag{5.4}$$

The wavefunction in Eq. (5.3) goes to zero asymptotically as r^{-2}.

Of even greater significance is the second order correction to the potential;[5] this is the induced polarization potential. We have

$$V_p(\vec{r}) = \sum_{\gamma\neq 0} \frac{|V_{\gamma 0}(\vec{r})|^2}{E_0 - E_n} \, . \tag{5.5}$$

One can show[6] by direct evaluation of the potential for e-H scattering that $V_p(\vec{r})$ in Eq. (5.5) satisfies the requisite asymptotic condition (5.2) with α equal to the static polarizability. Alternately, Martin et. al. demonstrate[1] that

$$V_p(\vec{r}) \underset{r\to\infty}{\sim} -\frac{1}{3}\sum_{\gamma\neq 0} \frac{|\langle\gamma|\vec{r}|0\rangle|^2}{E_\gamma - E_a} r^{-4} \, . \tag{5.6}$$

Since the polarizability is given by

$$\alpha = \frac{2}{3} \sum_{\gamma \neq 0} \frac{|\langle \gamma | \vec{r} | 0 \rangle|^2}{E_\gamma - E_0} \quad . \tag{5.7}$$

Eq. (5.6) reduces to (5.2) as required. Clearly, as asserted earlier, an induced dipole moment has appeared!

Important light was shed on this subject by Castillejo, Percival, and Seaton[8], who showed that if the incident energy k^2 is so small that inelastic collisions are energetically forbidden*, then the adiabatic theory is valid as $r \to \infty$. The asymptotic form of the full system wavefunction for the ℓ^{th} partial wave becomes (to first order in the distortion)

$$\psi_\ell^{\pm}(\vec{r}_1;\vec{r}) \underset{r\to\infty}{\sim} \phi'(\vec{r}_1;\vec{r})\, \chi_\ell^{\pm}(\vec{r}), \tag{5.8}$$

where ϕ' is given by Eq. (5.3) and $\chi_\ell^{\pm}(\vec{r})$ is the scattering function. Castillejo et. al. further show that if we introduce a radial scattering function $u_\ell^{\pm}(r)$ in the usual way, then the equation this function satisfies can be written asymptotically as

$$\left[\frac{d^2}{dr^2} - \frac{\ell(\ell+1)}{r^2} + \frac{\alpha}{r^4} + k^2\right] u_\ell^{\pm}(r) = 0 \quad . \tag{5.9}$$

*For electron-hydrogen scattering, this amounts to $k^2 < 0.75$.

This last point is particularly interesting. Expounding a bit on it, what Castillejo and colleagues did was to write the usual coupled equations for the ground-state case,*

$$\left[\nabla^2 + k_0^2\right]\chi_0(\vec{r}) = \sum_{\gamma} U_{0\gamma}(\vec{r})\chi_\gamma(\vec{r}), \qquad (5.10)$$

and proceed to prove that the coupling terms on the right-hand-side could be replaced by a diagonal potential energy, which for large r varies as $-\alpha/2r^4$, with α given by Eq. (5.7). The reasonableness of this idea is suggested by the observation that as r grows to infinity, the matrix element $U_{\gamma\gamma'}(\vec{r})$ for $\gamma \neq \gamma'$ goes to zero as fast as r^{-2}.

In slightly more physical terms, this result means that the effect of closed channels in the eigenfunction expansion method is to take into account induced polarization effects. One of the most interesting conclusions reached by these authors is that for e-H collisions, including <u>all</u> of the closed bound (discrete) hydrogen atom states only gives 81% of the polarizability; the rest comes from continuum states of the target. One is saved from having to include all these states in an actual calculation by the fact that it is valid to take the experimentally (or ab-initio theoretically) determined polarizability, incorporate the long-range form into the potential energy, and just ignore closed channels insofar as induced interactions are concerned.

*Their matrix element includes the nuclear repulsion term as well as electron-electron interactions.

In fact, life is not quite that simple. We suggested above that this picture breaks down as the scattering energy increases. Well, it also ceases to be valid for small r. Thinking intuitively, we find that this makes sense, for as the scattering electron "speeds up" as it approaches the target, the adiabaticity of the response of the target becomes unrealistic. Martin et. al. showed[1] that if one uses the perturbation theory expression for $V_p(\vec{r})$ directly for all r, the effect of the perturbations is over-estimated at small r, the error being particularly serious for s-waves in electron-hydrogen scattering.

This difficulty is easily circumvented by the use of a cutoff function, which effectively removes the r^{-4} polarization potential at small r values.[10]

Such an approach is usually taken in electron-molecule collision problems.[11] Much of the analysis described above and the validity of the adiabatic polarization potential generalize readily to molecular targets. There is one huge difference, though: the polarizability of a molecule is not spherically symmetric.[7] This results in a $P_2(\cos\theta)$ term in the long-range analytic form along with the usual $P_0(\cos\theta)$ contribution.

Another interesting situation obtains in the case of molecular targets. Here we have electronic excitation plus two additional kinds of motion and corresponding excitations: rotational and vibrational. These require so little energy that one can study the related inelastic processes within the context

of the adiabatic approximation presented in this section.[13]

The standard analysis of the polarizability of a molecule proceeds to generate two constants, $\alpha_{\parallel}$ and $\alpha_{\perp}$, the components of the polarizability parallel and perpendicular to the internuclear axis. (These quantities are often denoted α_z for the parallel component and α_x for the perpendicular component.) Usually, these are combined to yield the spherical and non-spherical polarizabilities,

$$\alpha_0 = \frac{1}{3}(\alpha_{\parallel} + 2\alpha_{\perp}) \tag{5.11a}$$

$$\alpha_2 = \frac{2}{3}(\alpha_{\parallel} - \alpha_{\perp}), \tag{5.11b}$$

respectively. The resultant long-range polarization potential is given by[12]

$$V_p(\vec{r}) \underset{r\to\infty}{\sim} -\frac{\alpha_0}{2r^4} P_0(\cos\theta) - \frac{\alpha_2}{2r^4} P_2(\cos\theta), \tag{5.12}$$

where we have left in $P_0(\cos\theta) = 1$ for clarity.

The usual application of Eq. (5.12) to electron-molecule problems is to incorporate the aforementioned cutoff function. A typical such function might have the form

$$C(r) = 1 - e^{-(r/r_c)^p}, \tag{5.13}$$

where r_c is the cutoff radius and p is the cutoff exponent.

Other more complicated forms have been investigated for particular targets with considerable success.[13]

Before we examine our particular application of all this theory, we should point out that intuitively one expects polarization forces to be quite important at low energies for angular momenta $\ell > 0$. Thinking classically, we recall that the impact parameter is $b \sim \ell/k$, so for slow collisions (small k) and finite angular momentum, the "distance of closest approach" isn't really very close, keeping the electron in the far region, where polarization forces will dominate. Granted that this argument is crude, it is true that in electron-atom scattering, polarization forces are found[1] to be the dominant influence for sufficiently small k. The analysis is complicated enormously for electron collisions with molecular targets because of the hated partial wave coupling, without which this report would be substially shorter.

§5.3. Application to CO_2 Targets.

For CO_2, the parallel and perpendicular components of the polarizability are determined to be[14]

$$\alpha_{\parallel} = 40.1 \times 10^{-25} \ cm^3 \tag{5.14a}$$

$$\alpha_{\perp} = 19.7 \times 10^{-25} \ cm^3 . \tag{5.14b}$$

From Eq. (5.11) we obtain the spherical and non-spherical polarizabilities, viz.,

$$\alpha_0 = 26.5 \times 10^{-25}\ \text{cm}^3 = 17.90\ \text{au} \tag{5.15a}$$

$$\alpha_2 = 13.6 \times 10^{-25}\ \text{cm}^3 = 9.19\ \text{au}, \tag{5.15b}$$

where we have used the fact that 1 $a_o^3 = 1.4804 \times 10^{-25}$ cm^3 and 1 au = ea_o^3 for polarizabilities to convert to atomic units. To put this quantity in perspective, we present polarizabilities for several other familiar molecules in Table 5.1. Clearly, there is nothing particularly striking about the values for CO_2.

We choose to employ a cutoff function for the induced polarization terms of the form (5.13) with $r_c^p = 2.59\ a_o$ and $p = 6$. The value of p was selected to give a fairly sharp cutoff; this choice is quite standard for electron-molecule problems. The choice of 2.59 a_o for the cutoff radius is somewhat less obvious. Since it involved values for particular cross sections, we shall defer the explanation of this selection to Chapter 8.

There is one further long-range interaction which should be kept in mind: the r^{-3} quadrupole term discussed in Chapter 3. This is a $P_2(\cos\theta)$ contribution. It differs markedly from the non-spherical polarizability term in that it is <u>not</u> induced; rather it is an intrinsic property of the target charge distribution (see §3.8). Since we choose to remove this interaction from the determination of the $v_2(r)$ static term for convenience,

Molecule	$\alpha_{\parallel}$	α_1	α_0	α_2
H_2	9.3	7.1	7.83	1.47
N_2	23.5	14.5	17.60	6.20
O_2	23.5	12.1	15.90	7.60
N_2O	48.6	20.7	30.0	18.6
CO	26.0	16.25	19.50	6.50
CO_2	40.1	19.7	26.50	13.60

Table 5.1

A selection of polarizabilities [from reference (14)] for several molecules. Shown are various $a \cdot 10^{25}$ cm^3. Equation (5.11) was used to determine a_0 and a_2.

we must define a quadrupole cutoff function for use when we add the interaction term back in at the time of solving the scattering equation (see Chapter 6). We again use the form (5.13) with $r_c^q = 4.0\ a_o$ and $p = 6$.

Putting all this together, the full long-range part of the electron-CO_2 interaction potential energy is

$$V_{LR}(\vec{r}) = \left[-\frac{\alpha_0}{2r^4} - \frac{\alpha_2}{2r^4} P_2(\cos\theta)\right] C^0(r) - \frac{Q}{r^3} P_2(\cos\theta)\, C^2(r). \quad (5.16)$$

To this we add $V_{ex}(\vec{r})$ as given in Chapter 4 and $V_{st}(\vec{r})$ with the quadrupole removed as described in Chapter 3. The final penultimate potential energy is then

$$V(\vec{r}) = V_{st}(\vec{r}) + V_{ex}(\vec{r}) + V_{LR}(\vec{r}). \quad (5.17)$$

After all the work of the last three chapters, what do we do with this potential energy now that we have it? The answer will be found in the next chapter, where we look at the scattering equation.

Chapter 6. The Scattering Problem: Solution of Coupled Equations by Integral Equations Techniques

I dare say that's an idea which has already occurred to you, but with the weight of my great mind behind it, no doubt it strikes the imagination more forcibly.

-Lord Peter Wimsey
in Strong Poison
(Dorothy L. Sayers)

§6.1. Introduction

In this chapter we at long last confront scattering theory. Our goal is to get from the potential $V(\vec{r})$ of Eq. (5.17) to the T-matrix from which we can extract cross sections. We shall defer discussion of the calculation of actual cross sections to Chapter 7, preferring to keep our attention here focused on the coupled radial equations and their solution.

We shall briefly outline the derivation of the radial coupled equations in the body-frozen reference frame in §6.2; a very detailed presentation of this material by the author is available elsewhere.(1) The next two sections show how to solve these equations in general via the integral equations algorithm: the method is explicated in the context of single-channel scattering in §6.3, and extensions to

multi-channel coupled equations are considered in §6.4. The calculation of the T-matrix is taken up in §6.5. A couple of important modifications to the standard integral equations formulation are discussed in §6.6, and various numerical problems which must be addressed in solving our particular problem form the substance of §6.7.

The integral equations method, which forms the main topic of this chapter, has been applied to a number of problems with some success[2-8]. If it is possible to treat exchange in an approximate yet physically reasonable way*, e.g., as a local interaction along lines outlined in Chapter 4, this method provides an accurate and efficient means for solving radial coupled equations. However, application of the algorithm to realistic systems such as the one under consideration here necessitates considerable care and a number of extensions of the standard methodology. We shall examine these modifications in the sequel. The actual calculations we performed for e-CO_2 scattering are the subject of Chapter 8.

§6.2. Obtaining the Coupled Radial Equations

For completeness, we here survey the derivation of the radial coupled equations in a body-fixed reference frame.[1] We make the fixed-nuclei approximation, allowing for no rotation or vibration

*If one actually includes the exchange kernel in the algorithm, as conventionally formulated, one in effect must solve twice as many equations as really necessary. See reference (3).

of the target*. The CO_2 molecule is assumed in our application to be frozen in its symmetric linear nuclear configuration in the ground electronic state (see Chapter 3). This picture is reasonable on physical grounds[10] provided that the incident electron kinetic energy is not less than $\sim 10^{-4}$ eV. We thus choose the internuclear axis to lie along the polar axis of our single-center coordinate system. We make the further approximation that the full interaction potential energy can be represented by a local function of the scattering coordinate. This assumption has been discussed at length in Chapter 4, and in Chapter 5 we presented detailed expressions for the total potential energy.

Now, we begin with the non-relativisitic Schroedinger equation for the electron-molecule system, i.e.,

$$(\mathcal{H}-E)\Psi_E(\vec{r}_i,\vec{r};R)=0, \tag{6.1}$$

where R appears parametrically and $\hat{R}$ not at all, since we are working in body-fixed coordinates. The Hamiltonian in Eq. (6.1) is conveniently written as

$$\mathcal{H}=\mathcal{H}_{target}-\frac{1}{2}\nabla^2+V_{int}(\vec{r},\vec{r}_i;R). \tag{6.2}$$

*This does not mean that we cannot calculate these excitation cross sections eventually (See Chapter 7). For example, if certain conditions are satisfied we can use the adiabatic nuclei approximation to determine them. This theory was discussed by the author in reference (1).

The interaction potential energy was discussed in section 3.1. The target functions are eigenfunctions of the molecular Hamiltonian, i.e.,

$$\mathcal{H}_{target}\,\phi_n(\vec{r}_i;R) = \epsilon_n\,\phi_n(\vec{r}_i;R), \tag{6.3}$$

where ϵ_n are the SCF energies in the model employed in this work and the functions $\phi_n(\vec{r}_i;R)$ are the wavefunctions determined by McLean and Yoshimine and discussed in Chapter 3.

We now expand the system wavefunction in the complete set of target states defined by Eq. (6.3), obtaining

$$\Psi_E(\vec{r},\vec{r}_i;R) = \sum_{n'} F_{n'}(\vec{r})\,\phi_{n'}(\vec{r}_i;R). \tag{6.4}$$

We further expand each scattering function $F_{n'}(\vec{r})$ in spherical harmonics, viz.,

$$F^{(n)}_{n'}(\vec{r}) = \frac{1}{r}\sum_{\ell' m'} u^{(\ell n)}_{n'\ell' m'}(r)\,Y^{m'}_{\ell'}(\hat{r}), \tag{6.5}$$

where we denote the incident channel by (ℓ n). [Notice that we work in the formalism of "asymptotic" partial waves[1]. Thus the set of functions used will have to be appropriately combined in order to produce the true scattering function, which must behave asymptotically like an incident plane wave plus an outgoing spherical scattered wave.] The summation in Eq. (6.5) is restricted by the

symmetry of the $e\text{-}CO_2$ system. Thus if the state under consideration is gerade[11], only even-ℓ terms contribute to the sum, while if it is ungerade, only odd-ℓ terms contribute. For this reason, we might label the wavefunction with an additional subscript, call it η, to denote the symmetry of the total system. However, in our formulation this is not really necessary, since the projection of the electron's orbital angular momentum along the internuclear axis is a good quantum number. Thus, the potential matrix element which couples various partial waves within the ground electronic state is diagonal in m [see Eq. (3.43)].

Dropping all but the ground electronic state in the summation of Eq. (6.4), taking the above facts into account, and using the matrix elements determined in Chapter 3, we obtain the coupled radial differential equations

$$\left[\frac{d^2}{dr^2} - \frac{\ell(\ell+1)}{r^2} - 2V_{\ell\ell}^{(m)}(r) + k^2\right] u_\ell^{(m)}(r) = 2\sum_{\ell' \neq \ell} V_{\ell\ell'}^{(m)}(r)\, u_{\ell'}^{(m)}(r). \tag{6.6}$$

In this set of equations, k^2 is the incident electron kinetic energy (in Rydbergs), $V_{\ell\ell'}^{(m)}$ is given by Eq. (3.43), and we have suppressed the label $n = 0$ for the ground state on the scattering wavefunction.

The various symmetries are defined by m and the allowed values of ℓ according to the inversion symmetry of the state. We have

$$\Sigma_g: \quad m = 0, \quad \ell = 0, 2, 4, \ldots \tag{6.7a}$$

$$\Sigma_u : \quad m = 0 , \quad \ell = 1, 3, 5, \ldots \tag{6.7b}$$

$$\Pi_g : \quad m = 1, \quad \ell = 2, 4, 6, \ldots \tag{6.7c}$$

$$\Pi_u : \quad m = 1, \quad \ell = 1, 3, 5, \ldots \tag{6.7d}$$

and so forth.

The radial wavefunctions $u_\ell^{(m)}(r)$ obey the usual partial wave scattering boundary conditions[12],

$$u_\ell^{(m)}(0) = 0 \tag{6.8a}$$

$$u_\ell^{(m)}(r) \underset{r\to\infty}{\sim} \hat{j}_\ell(kr)\delta_{\ell\ell_o} - \hat{n}_\ell(kr)\, K_{\ell\ell_o}^{(m)} , \tag{6.8b}$$

where $K_{\ell\ell_o}^{(m)}$ is an element of the K-matrix and ℓ_o denotes the initial channel. For the S-matrix, we use $\underset{\sim}{K}$ and the familiar result

$$\underset{\sim}{S} = (\underset{\sim}{1} + i\underset{\sim}{K})\cdot(\underset{\sim}{1} - i\underset{\sim}{K})^{-1} , \tag{6.9}$$

where $\underset{\sim}{1}$ is the unit matrix, and the T-matrix is related by

$$\underset{\sim}{T} = \underset{\sim}{1} - \underset{\sim}{S} \tag{6.10}$$

We obtain cross sections from the T-matrix as described in the next

chapter.

It is worth remarking that the coupling of partial waves in Eqs. (6.6) is governed by restrictions on the matrix elements parading through these equations. These "selection rules" were discussed in Chapter 3; many of them are consequences of particular Clebsch-Gordan coefficients which appear in Eq. (3.43).

A more "physical" factor influencing the relative importance of various partial waves with finite angular momentum is the centrifugal barrier, $-\ell(\ell+1)/r^2$, as manifested through the effective potential, which appears on the left-hand-side of Eq. (6.6), i.e.,

$$V^{\rm eff}_{\ell m}(r) = -\frac{\ell(\ell+1)}{r^2} - 2V^{(m)}_{\ell\ell}(r). \tag{6.11}$$

We discussed the physics of the effective potential in §3.7 and will return to it later in this chapter. In terms of this quantity, Eqs. (6.6) take on the slightly more illuminating form

$$\left[\frac{d^2}{dr^2} + V^{\rm eff}_{\ell m}(r) + k^2\right] u^{(m)}_{\ell}(r) = 2\sum_{\ell'\neq\ell} V^{(m)}_{\ell\ell'}(r)\, u^{(m)}_{\ell'}(r). \tag{6.12}$$

In closing, we should say a word about matrices. Although we initially present the integral equations procedure (in the next section) in the context of a single-channel problem for purposes of clarity, the multi-channel matrix generalization is of immediate importance.

The point to be made is that each of Eqs. (6.6) is a second-

order linear ordinary differential equation. Therefore[13], there are 2N linearly independent solutions to the set (where each solution, of course, has N components, one for each partial wave coupled into the problem). Of these solutions, N are regular at the origin and N are irregular. Physics, as manifested in the boundary condition of Eq. (6.8a), immediately demands that we dump the N irregular solutions, but this still leaves us with a total of N linearly independent solutions to Eq. (6.6). Thus it is appropriate to tack an additional subscript, a "solution index", onto the scattering function, writing, say, $u_{\ell\nu}(r)$. Thus, each set of N solutions to Eqs. (6.6), each element of which has N components, is quite appropriately represented by a matrix $\underset{\sim}{u}^{(m)}(r)$. In fact, the solution index corresponds to the initial channel, which we called ℓ_o in Eq. (6.8b). Thus, using an alternate form of the boundary conditions, we have

$$u^{(m)}_{\ell\nu}(r) \underset{r\to\infty}{\sim} e^{-i(kr-\ell\frac{\pi}{2})}\delta_{\ell\nu} - S^{(m)}_{\ell\nu}\, e^{i(kr-\ell\frac{\pi}{2})}. \tag{6.13}$$

In the partial wave analysis, the solutions evidently do not satisfy the required scattering boundary conditions[12],

$$\psi_k(\vec{r}) \underset{r\to\infty}{\sim} e^{i\vec{k}\cdot\vec{r}} + \frac{e^{ikr}}{r} f_k(\hat{r}), \tag{6.14}$$

where $f_k(\hat{r})$ is the scattering amplitude from which one obtains

total cross sections and other sundries. There is no cause for panic, though, since we can always form a linear combination of the solutions, viz.,[1]

$$\mathcal{Y}_k(\vec{r}) = \sum_{\substack{\ell\nu \\ m}} a_{\ell\nu}\, u_{\ell\nu}^{(m)}(r)\, Y_\ell^m(\hat{r}) \tag{6.15}$$

and determine the expansion coefficients so that Eq. (6.14) is satisfied.

One further point should be made and then we shall begin. The method to be outlined below is quite general in the sense that it is well applied to body-frame equations such as (6.6) or to the set of coupled equations which obtains in the laboratory (or space fixed) reference frame. This approach to the electron-molecule problem is outlined in Appendix 2. It is usually formulated by coupling the electron's orbital angular momentum to the molecular rotational angular momentum to form a total angular momentum. The resultant coupled equations look like

$$\left[\frac{d^2}{dr^2} - \frac{\ell'(\ell'+1)}{r^2} + k_{j'}^2\right] u_{j'\ell'}^{Jj\ell}(r) = \sum_{j''\ell''} W_{j'\ell'j''\ell''}^{(J)}(r)\, u_{j''\ell''}^{Jj\ell}(r), \tag{6.16}$$

where $(j\ell)$ denote the initial channel. These equations separate into sets according to J. The matrix elements in Eqs. (6.16) are quite different from our old friends of Eq. (3.43). The feature to be noted here is that the mathematical form of Eqs. (6.16) and its attendant

boundary conditions,

$$u^{J_j \ell}_{j'\ell'}(0) = 0 \tag{6.17a}$$

$$u^{J_j \ell}_{j'\ell'}(r) \underset{r\to\infty}{\sim} e^{-i(k_j r - \ell\frac{\pi}{2})}\delta_{\ell\ell'}\delta_{jj'} - \left(\frac{k_j}{k_{j'}}\right)^{\frac{1}{2}} S^{J}_{j\ell,j'\ell'}\, e^{i(k_{j'} r - \ell'\frac{\pi}{2})}, \tag{6.17b}$$

is the same as that of the body-frame equations (6.6) and (6.8). [In fact, this is a key point in the frame transformation theory of electron-molecule scattering. See reference (15).] Provided one is very careful to keep his indices straight, precisely the same numerics can be used to solve both sets of equations. In point of fact, we began our study of the e-CO_2 problem in the lab frame, shifting over to a body-fixed frame only when it became apparent that such a frame was more appropriate owing to the enormous number of partial waves required for convergence. Nevertheless, the numerical aspects of the problem were the same in both cases, and we have codes to treat both frames.

§6.3. The Integral Equations Algorithm: the Single-Channel Case

There exist a wide variety of approaches to the problem of solving a set of coupled, second-order linear ordinary differential equations. One of the most widely used of these is the Numerov algorithm[16], which takes the equations on their own terms and solves

them as differential equations. An alternate plan of attack is to convert the set of coupled differential equations into a set of coupled integral equations and solve these using quadrature[2-9]. This is the scheme we have adopted and modified to tackle e-CO_2 scattering.

In words, we shall take our set of coupled differential equations with appropriate boundary conditions and write a general solution matrix as the sum of a homogeneous solution which is regular at the origin and an inhomogeneous (or particular) solution. We then obtain an integral equation for the particular solution in terms of a Green's function which has built into it the aforementioned boundary conditions. (We also determine the homogeneous solution with ease.)

To solve the remaining integral equation, we write it so that it separates into a homogeneous equation, which turns out to be a Volterra equation of the second kind, and an inhomogeneous equation, the solution of which turns out to be equal to a constant times the homogeneous solution. Thus the solution of the whole problem is reduced to solving a Volterra equation, which is accomplished by quadrature.

An excellent presentation of the standard method in the case of coupled equations is available in reference (17). Believing that new numerical methods are best introduced in a simple context, we here present a fairly detailed derivation for a potential scattering

problem. The multi-channel equations appear in the next section.

The familiar partial-wave scattering equation for a spherical potential[18] is

$$\left[\frac{d^2}{dr^2} - \frac{\ell(\ell+1)}{r^2} - U(r) + k^2\right] u_{k\ell}(r) = 0, \tag{6.18}$$

where $\ell = 0,1,2,\ldots$ correspond to s-, p-, d-wave scattering, etc. and where U(r) is the potential energy in Rydbergs. [Notice that a set of N such equations obtains if we set the off-diagonal matrix elements in our coupled equations equal to zero.] As usual, we require

$$u_{k\ell}(0) = 0. \tag{6.19a}$$

The asymptotic boundary condition can be written as

$$u_{k\ell}(r) \underset{r\to\infty}{\sim} e^{-i(kr-\ell\frac{\pi}{2})} - S_{k\ell}\, e^{i(kr-\ell\frac{\pi}{2})}, \tag{6.19b}$$

where we have assumed that $r^2U(r)$ goes to zero as r approaches infinity. An equivalent boundary condition is

$$u_{k\ell}(r) \underset{r\to\infty}{\sim} \sin(kr-\ell\tfrac{\pi}{2}) + K_{k\ell}\cos(kr-\ell\tfrac{\pi}{2}), \tag{6.19c}$$

where the (now) scalar K-"matrix" is related to the phase shift by

$$K_{k\ell} = \tan \eta_\ell (k). \tag{6.20}$$

For convenience, let us define the differential operator

$$\mathcal{D}_\ell = \frac{d^2}{dr^2} - \frac{\ell(\ell+1)}{r^2} + k^2 \tag{6.21}$$

so that Eq. (6.18) becomes simply

$$\mathcal{D}_\ell \, u_{k\ell}(r) = U(r) \, u_{k\ell}(r). \tag{6.22}$$

Any solution of Eq. (6.22) can be written[19] as the sum of a homogeneous solution $u^h_{k\ell}(r)$, which is the general solution of the homogeneous equation

$$\mathcal{D}_\ell \, u^h_{k\ell}(r) = 0 , \tag{6.23}$$

and a particular solution $u^p_{k\ell}(r)$, which is one solution of Eq. (6.22). (Sometimes, the homogeneous solution is called the "complimentary function" and the particular solution the "particular integral".) Thus we have

$$u_{k\ell}(r) = u^h_{k\ell}(r) + u^p_{k\ell}(r). \tag{6.24}$$

The solutions of the homogeneous equation (6.23) are the familiar

Ricatti-Bessel and Ricatti-Neumann functions[20], which we shall write $\hat{j}_\ell(kr)$ and $\hat{n}_\ell(kr)$, respectively. Equivalently, we could use the Riccati-Hankel functions of the first and second kind, defined as

$$\hat{h}_\ell^{(1)}(kr) = \hat{j}_\ell(kr) + i\,\hat{n}_\ell(kr) \tag{6.25a}$$

$$\hat{h}_\ell^{(2)}(kr) = \hat{j}_\ell(kr) - i\,\hat{n}_\ell(kr). \tag{6.25b}$$

These various functions all satisfy the spherical Bessel equation; they differ in their asymptotic behavior as

$$\hat{j}_\ell(kr) \underset{r\to\infty}{\sim} \sin\left(kr - \ell\tfrac{\pi}{2}\right) \tag{6.26a}$$

$$\hat{n}_\ell(kr) \underset{r\to\infty}{\sim} -\cos\left(kr - \ell\tfrac{\pi}{2}\right) \tag{6.26b}$$

$$\hat{h}_\ell^{(1)}(kr) \underset{r\to\infty}{\sim} -i\,e^{i\left(kr - \ell\frac{\pi}{2}\right)} \tag{6.26c}$$

$$\hat{h}_\ell^{(2)}(kr) \underset{r\to\infty}{\sim} i\,e^{-i\left(kr - \ell\frac{\pi}{2}\right)}. \tag{6.26d}$$

They are all related to the corresponding spherical functions as, for example, $\hat{j}_\ell(kr) = kr\,j_\ell(kr)$, etc. Clearly, only the Ricatti-Bessel function satisfies the boundary condition at r = 0, viz., Eq. (6.19a). Therefore the homogeneous solution is

$$u^h_{k\ell}(r) = \hat{j}_\ell(kr). \tag{6.27}$$

We solve for the particular solution by using Green's function methods[22]. We seek the solution of the equation

$$\mathcal{D}_\ell G_\ell(r,r') = \delta(r-r'), \tag{6.28}$$

where $\delta(r - r')$ is the Dirac delta function, with the usual property that

$$\int_{-\infty}^{+\infty} F(x)\,\delta(x-x')\,dx = F(x') . \tag{6.29}$$

Then the particular solution to Eq. (6.22) is simply

$$u^p_{k\ell}(r) = \int_0^\infty G_\ell(r,r')\,U(r')\,u^p_{k\ell}(r')\,dr'. \tag{6.30}$$

For $r \neq r'$, Eq. (6.28) becomes

$$\mathcal{D}_\ell G_\ell(r,r') = 0 \qquad (r \neq r') \tag{6.31}$$

It follows that the Green's function is given by

$$G_\ell(r,r') = \begin{cases} a\,\hat{j}_\ell(kr) & r<r' \\ b\,\hat{h}^{(1)}_\ell(kr) & r>r' \end{cases} . \tag{6.32}$$

where we have chosen the particular Ricatti function for r>r' to match the desired boundary conditions (see below). To determine a and b, we match across the boundary at r = r'. Integrating between r' - ε and r' + ε, we obtain[23]

$$\lim_{\varepsilon \to 0} \frac{d}{dr} G_\ell(r,r') \Big|_{r'-\varepsilon}^{r'+\varepsilon} = 1 \tag{6.33}$$

Integrating again, we find

$$\lim_{\varepsilon \to 0} G_\ell(r,r') \Big|_{r'-\varepsilon}^{r'+\varepsilon} = 0 \tag{6.34}$$

If we substitute Eq. (6.32) into (6.33) and (6.34), let $\varepsilon \to 0$, and carry out some rather lengthy and boring algebra using the relationship

$$\frac{d}{dr} f_\ell(r) = f_{\ell-1}(r) - \frac{1}{r} f_\ell(r)(\ell+1),$$

which is satisfied by any of the four Ricatti functions, and lots of scratch paper, we obtain the full desired Green's function, viz.,

$$G_\ell(r,r') = \begin{cases} kr r' h_\ell^{(1)}(kr') j_\ell(kr) & r < r' \\ kr r' h_\ell^{(1)}(kr) j_\ell(kr') & r > r' \end{cases} \tag{6.35}$$

where we have also used the fact that

$$j_{\ell-1}(kr)\,h_{\ell}^{(1)}(kr) - j_{\ell}(kr)\,h_{\ell-1}^{(1)}(kr) = -\frac{1}{(kr)^2}\,. \tag{6.36}$$

Now, where are we? We set out to solve the Schroedinger Equation (6.18) for the ℓ^{th} partial wave subject to the boundary conditions of Eq. (6.19). The solution $u_{k\ell}(r)$ is given by

$$u_{k\ell}(r) = \hat{j}_{\ell}(kr) + \int_0^{\infty} G_{\ell}(r,r')\,U(r')\,u_{k\ell}(r')\,dr', \tag{6.37}$$

where $G_{\ell}(r,r')$ is given by Eq. (6.35). The asymptotic and r = 0 boundary conditions are contained implicitly in this equation with the Green's function we are using. Equation (6.37) is an integral equation for $u_{k\ell}(r)$; by solving it and examining the solution in the limit $r \to \infty$, we can determine phase shifts and cross sections for the ℓ^{th} partial wave.

Perhaps a word or two about integral equations in general is in order. The general form for such an equation is[25]

$$\lambda \int_a^b K(x,y)\,f(y)\,dy + g(x) = h(x)\,f(x),$$

where f(x) is the unknown function, λ is a constant parameter, and h(x) and g(x) are known functions. K(x,y) is called the kernel of the equation. Several special cases have been the subject of intensive study[26], e.g.,

h(x) = 0 Fredholm Equation of the First Kind

$h(x) = 1$ Fredholm Equation of the Second Kind

$K(x,y) = 0$ $y > x$ Volterra Equation

We seek to use this knowledge to solve our equation, (6.31). To do so, we reluctantly introduce some new notation[2]. Let

$$g_\ell^{(1)}(r) \equiv j_\ell(kr) \tag{6.38a}$$

$$g_\ell^{(2)}(r) = h_\ell^{(1)}(kr) \tag{6.38b}$$

and define $r_< = \min(r,r')$ and $r_> = \max(r,r')$. Then the Green's function becomes

$$G_\ell(r,r') = krr' g_\ell^{(1)}(r_<) g_\ell^{(2)}(r_>), \tag{6.39}$$

and the integral equation (6.37) can be written as

$$u_{k\ell}(r) = krg_\ell^{(1)}(r) + \int_0^\infty krr' g_\ell^{(1)}(r_<) g_\ell^{(2)}(r_>) U(r') u_{k\ell}(r') dr'$$

or, equivalently if less clearly, as

$$u_{k\ell}(r) = krg_\ell^{(1)}(r) + krg_\ell^{(2)}(kr)\int_0^r r' g_\ell^{(1)}(r') U(r') u_{k\ell}(r') dr'$$

$$+ krg_\ell^{(2)}(r)\int_r^\infty r' g_\ell^{(2)}(r') U(r') u_{k\ell}(r') dr'.$$

The problem is that this equation is not obviously in a convenient form such as those alluded to above. However, by biting the bullet and rewriting this equation one last time we can convert it into a special type of Volterra equation[25]. We begin with

$$u_{k\ell}(r) = kr g_\ell^{(1)}(r) + kr g_\ell^{(2)}(kr)\int_0^r g_\ell^{(1)}(r') U(r') u_{k\ell}(r')\, dr'$$

$$- kr g_\ell^{(1)}(r)\int_0^r r' g_\ell^{(2)}(r') U(r') u_{k\ell}(r')\, dr'$$

$$+ kr g_\ell^{(1)}(r)\int_0^\infty r' g_\ell^{(2)}(r') U(r') u_{k\ell}(r')\, dr'.$$

If we now make the identifications in the general form:

$$f(x) = u_{k\ell}(r) \tag{6.40a}$$

$$g(x) = kr g_\ell^{(1)}(r)\left[\int_0^\infty r' g_\ell^{(2)}(r') U(r') u_{k\ell}(r')\, dr' + 1\right] \tag{6.40b}$$

$$K(x,y) = kr\left[g_\ell^{(1)}(r) g_\ell^{(2)}(r') - g_\ell^{(2)}(r) g_\ell^{(1)}(r')\right] U(r') \tag{6.40c}$$

$$h(x) = 1 \tag{6.40d}$$

$$x = r,\ y = r' \tag{6.40e}$$

we see that we have a Volterra equation of the second kind,[22] with the inhomogeneous term, g(x), given by Eq. (6.40b).

Introducing homogeneous and particular solutions to this

equation, say $u^0_{k\ell}(r)$ and $u^1_{k\ell}(r)$, respectively, we find that the homogeneous solution satisfies a Volterra equation of the first kind,

$$u^0_{k\ell}(r) = krg^{(1)}_\ell(r) + krg^{(2)}_\ell(r)\int_0^r g^{(1)}_\ell(r')U(r')\,u^0_{k\ell}(r')\,dr' - krg^{(1)}_\ell(r)\int_0^r r'g^{(2)}_\ell(r')U(r')\,u^0_{k\ell}(r')\,dr'. \tag{6.41}$$

while the particular solution satisfies the aforementioned equation of the second kind.

To solve for the particular solution, we shall introduce a normalization constant C defined as

$$u^1_{k\ell}(r) = C\,\chi_{k\ell}(r). \tag{6.42}$$

Because the particular solution satisfies an inhomogeneous Volterra equation, the normalization is not arbitrary, and we cannot just define C = 1, for example. If we substitute this definition into the particular equation and choose C such that

$$\int r'g^{(2)}_\ell(r')U(r')\left[u^0_{k\ell}(r') + C\,\chi_{k\ell}(r')\right]dr' = C \tag{6.43}$$

then the particular equation reduces to

$$\chi_{k\ell}(r) = krg^{(1)}_\ell(r) + krg^{(2)}_\ell(r)\int_0^r r'g^{(1)}_\ell(r')\,U(r')\,\chi_{k\ell}(r')dr' - krg^{(1)}_\ell(r)\int_0^r r'g^{(2)}_\ell(r')U(r')\,\chi_{k\ell}(r')\,dr',$$

which is identical to Eq. (6.41)! Therefore we have

$$\chi_{k\ell}(r) = u^{0}_{k\ell}(r)$$

and the inhomogeneous solution is related to the homogeneous solution via

$$u^{1}_{k\ell}(r) = C\, u^{0}_{k\ell}(r) \tag{6.44}$$

Finally, the full solution for the ℓ^{th} partial wave is simply

$$u_{k\ell}(r) = (1+C)\, u^{0}_{k\ell}(r). \tag{6.45}$$

This means that all we have to do to treat the problem at hand is to solve for the homogeneous solution. Solving for C in Eq. (6.42) we find

$$C = \left[\int_0^\infty g_\ell^{(2)}(r')U(r')\,u^{0}_{k\ell}(r')\,dr'\right]\left[1-\int_0^\infty g_\ell^{(2)}(r')\,U(r')\,u^{0}_{k\ell}(r')\,dr'\right]^{-1}, \tag{6.46}$$

so that the full solution can be written as

$$u_{k\ell}(r) = u^{0}_{k\ell}(r)\left[1-\int_0^\infty r' g_\ell^{(2)}(r')U(r')\,u^{0}_{k\ell}(r')\,dr'\right]^{-1}. \tag{6.47}$$

It is important to keep in mind that we solve (by quadrature) for the homogeneous solution $u^o_{k\ell}(r)$, not for the physical solution $u_{k\ell}(r)$. We determine the latter once we reach the asymptotic region (i.e., values of r such that the potential is effectively zero) via Eq. (6.47) and extract the phase shift by boundary matching to a linear combination of Ricatti-Bessel and Ricatti-Neumann functions,

$$\tan\eta_\ell(k) = \frac{\hat{j}_\ell(kr) - u_{k\ell}(r)}{\hat{n}_\ell(kr)} \quad . \tag{6.48}$$

So, how then do we solve for $u^o_{k\ell}(r)$? The equation under consideration is (6.41). Although a variety of useful techniques for developing analytic solutions to integral equations have been developed,[26] it is not in general possible to so attack our equation. For example, we found in Chapter 3 that over a certain range of values of r, we only know the potential energy appearing in the equation as a table of numbers. Thus, we replace the integrals in Eq. (6.41) by quadrature sums, obtaining

$$\begin{aligned} u^o_{k\ell}(r_i) = {} & kr_i\, g^{(1)}_\ell(r_i) + kr_i\, g^{(1)}_\ell(r_i) \sum_{j=1}^{i} g^{(1)}_\ell(r_j)\, U(r_j) \\ & \otimes u^o_{k\ell}(r_j)\, w_j - kr_i\, g^{(1)}_\ell(r_i) \sum_{j=1}^{i} g^{(1)}_\ell(r_j)\, U(r_j)\, u^o_{k\ell}(r_j)\, w_j \,, \end{aligned} \tag{6.49}$$

where the set of numbers r_i defines a mesh of r values over which we propose to calculate the solution and where w_j are the quadrature

weights. These depend on the particular quadrature scheme to be used. Tables of the quadrature points and weights are available; see, for example, reference (27).

If we plough right into the solution of (6.49), we would have to do so iteratively, a ghastly prospect. However, a moment's thought reveals that the i^{th} terms in the summations cancel, and the equation reduces to

$$u^{o}_{k\ell}(r_i) = kr_i g_\ell^{(1)}(r_i) + kr_i g_\ell^{(2)}(r_i) \sum_{j=1}^{i-1} g_\ell^{(1)}(r_j) U(r_j)\, u^{o}_{k\ell}(r_j) w_j$$

$$- kr_i g_\ell^{(1)}(r_i) \sum_{j=1}^{i-1} g_\ell^{(2)}(r_j) U(r_j)\, u^{o}_{k\ell}(r_j) w_j . \qquad (6.50)$$

This equation enables us to simply step our way out into the large-r region, since we know the initial condition on the wavefunction at r_0. Moreover, the value of the homogeneous solution at r_i depends only on its values at $r_0, r_1, \ldots, r_{i-1}$.

Before turning to the multi-channel generalization of these results, let us take advantage of all this work to extend the formalism to the case where the equation to be solved possess an inhomogeneous term g(r), e.g., suppose we are confronted with

$$\mathcal{D}_\ell\, u_{k\ell}(r) = U(r)\, u_{k\ell}(r) + g(r) . \qquad (6.51)$$

We go after this equation just as we did (6.22) with the homogeneous solution given by (6.27) and the particular solution being the

solution of the integral equation

$$u^{p}_{k\ell}(r) = \int_0^\infty G_\ell(r,r')\left[U(r')\,u^{p}_{k\ell}(r') + g(r')\right]dr'. \qquad (6.52)$$

The Green's function is unchanged; it is given by (6.35). Notice that we must require that $r^2 g(r) \to 0$ as $r \to \infty$ for the derivation to carry through. The solution of Eq. (6.52) proceeds as before with $U(r)u^{p}_{k\ell}(r)$ replaced by $U(r)u^{p}_{k\ell}(r) + g(r)$.

§6.4. The Integral Equations Algorithm: The Multi-Channel Case

In the coupled-channel case we seek to solve Eq. (6.6). Here we focus on the situation which obtains when all the channels of interest are open (the case of closed channels is treated in reference 17). The analysis proceeds exactly as in the previous sections except that we introduce several matrices. If we have N coupled channels, then we shall define an N × N potential energy matrix, $\underset{\sim}{V}^{(m)}(r)$, the $\ell\ell'$ element of which is $V^{(m)}_{\ell\ell'}(r)$, an N × N diagonal matrix for the centrifugal barrier contribution, $\underset{\sim}{L}(r)$, the $\ell\ell'$ element of which is $[\ell(\ell+1)/r^2]\,\delta_{\ell\ell'}$ and a diagonal k^2 matrix. If we further let each solution (corresponding to a particular ν) be denoted by an N-component column vector, then the full solution is represented by an N × N matrix, $\underset{\sim}{u}^{(m)}(r)$. With all these definitions, the coupled equations are written as

$$\frac{d^2}{dr^2}\,\underset{\sim}{u}^{(m)}(r) = \left[\underset{\sim}{V}^{(m)}(r) + \underset{\sim}{L}(r) - \underset{\sim}{k}^2\right] \cdot \underset{\sim}{u}^{(m)}(r). \tag{6.53}$$

Let us define the diagonal matrix $\underset{\sim}{G}^{j}(r)$, where*

$$\left[\underset{\sim}{G}^{j}(r)\right]_{\ell\ell'} = G_{\ell}^{j}(r)\,\delta_{\ell\ell'}, \tag{6.54}$$

with

$$G_{\ell}^{1}(r) = \hat{j}_{\ell}(kr) \tag{6.55a}$$

$$G_{\ell}^{2}(r) = -\frac{1}{k}\,\hat{n}_{\ell}(kr). \tag{6.55b}$$

Further, let us introduce yet another matrix,

$$\underset{\sim}{G}^{ij}(r|r') = \underset{\sim}{G}^{i}(r) \cdot \underset{\sim}{G}^{j}(r'). \tag{6.56}$$

Then the matrix counterpart of Eq. (6.37) can be written as

$$\begin{aligned}\underset{\sim}{u}^{(m)}(r) = \underset{\sim}{G}^{1}(r) &+ \int_0^r \underset{\sim}{G}^{12}(r'|r) \cdot \underset{\sim}{V}^{(m)}(r') \cdot \underset{\sim}{u}^{(m)}(r')\,dr' \\ &+ \int_r^{\infty} \underset{\sim}{G}^{21}(r'|r) \cdot \underset{\sim}{V}^{(m)}(r') \cdot \underset{\sim}{u}^{(m)}(r')\,dr'.\end{aligned} \tag{6.57}$$

*We have chosen slightly different notation in this section in order to conform to other published discussions of this algorithm such as those of references (3) and (17).

We now introduce homogeneous and particular solutions, which we shall denote $\underset{\sim}{u}^{0}(r)$ and $\underset{\sim}{u}^{1}(r)$ in order to avoid confusion with the true solution $\underset{\sim}{u}^{(m)}(r)$. The homogeneous solution turns out to satisfy

$$\underset{\sim}{u}^{0}(r) = \underset{\sim}{G}^{1}(r) + \int_{0}^{r} \underset{\sim}{G}^{21}(r|r') \cdot \underset{\sim}{V}^{(m)}(r') \cdot \underset{\sim}{u}^{0}(r')\, dr' - \int_{0}^{r} \underset{\sim}{G}^{12}(r|r') \cdot \underset{\sim}{V}^{(m)}(r') \cdot \underset{\sim}{u}^{0}(r')\, dr' \tag{6.58}$$

and the particular solution is given by

$$\underset{\sim}{u}^{1}(r) = \underset{\sim}{y}^{0}(r) \cdot \underset{\sim}{C} \tag{6.59}$$

where the constant matrix $\underset{\sim}{C}$ is

$$\underset{\sim}{C} = \left[\underset{\sim}{1} - \int_{0}^{\infty} \underset{\sim}{G}^{2}(r') \cdot \underset{\sim}{V}^{(m)}(r') \cdot \underset{\sim}{u}^{0}(r')\, dr' \right]^{-1} \cdot \left[\int_{0}^{\infty} \underset{\sim}{G}^{2}(r') \cdot \underset{\sim}{V}^{(m)}(r') \cdot \underset{\sim}{u}^{0}(r')\, dr' \right]. \tag{6.60}$$

The full solution is simply

$$\underset{\sim}{u}^{(m)}(r) = \underset{\sim}{u}^{0}(r) \cdot \left[1 - \int_{0}^{\infty} \underset{\sim}{G}^{2}(r') \cdot \underset{\sim}{V}^{(m)}(r') \cdot \underset{\sim}{u}^{0}(r')\, dr' \right]^{-1}. \tag{6.61}$$

We should point out that the integrand in Eq. (6.61) must be calculated anyway in the process of developing the homogeneous solution and hence

may conveniently be stored, making it a trivial matter to extract the T-matrix.

It is conventional to introduce a little more notation. This will aid us when we examine the quadrature formulas used to compute the homogeneous solution. Thus, we shall define

$$\underset{\sim}{I}^1(r) = \int_0^r \underset{\sim}{G}^1(r') \cdot \underset{\sim}{V}^{(m)}(r') \cdot \underset{\sim}{u}^0(r')\, dr' \tag{6.62a}$$

$$\underset{\sim}{I}^2(r) = \underset{\sim}{1} + \int_0^r \underset{\sim}{G}^2(r') \cdot \underset{\sim}{V}^{(m)}(r') \cdot \underset{\sim}{u}^0(r')\, dr' . \tag{6.62b}$$

In terms of these integrals, Eq. (6.58) takes on the more elegant form

$$\underset{\sim}{u}^0(r) = \underset{\sim}{G}^1(r) \cdot \underset{\sim}{I}^2(r) - \underset{\sim}{G}^2(r) \cdot \underset{\sim}{I}^1(r) . \tag{6.63}$$

The physical wavefunction is related to the homogeneous solution by

$$\underset{\sim}{u}^{(m)}(r) = \underset{\sim}{u}^0(r) \cdot (\underset{\sim}{1} + \underset{\sim}{C}) . \tag{6.64}$$

In these equations, we have explicitly introduced the minus sign in the definition of $G_\ell^2(r)$ so that $G_\ell^2(r) = (1/k)\, \hat{n}_\ell(kr)$ henceforth.

It follows from these definitions that

$$\underset{\sim}{1} + \underset{\sim}{C} = [\, \underset{\sim}{I}^2(\infty)\,]^{-1}$$

since

$$\underset{\sim}{C} = [\underset{\sim}{I}^2(\infty)]^{-1} \cdot [\underset{\sim}{1} - \underset{\sim}{I}^2(\infty)] \quad . \tag{6.65}$$

The computational details of the solution for $\underset{\sim}{u}^0(r)$ represent trivial modifications of these equations along lines suggested in §6.4. Defining

$$\underset{\sim}{I}^1(r_{i-1}) = \sum_{j=1}^{i-1} \underset{\sim}{G}^1(r_j) \cdot \underset{\sim}{V}^{(m)}(r_j) \cdot \underset{\sim}{u}^0(r_j)\, w_j \tag{6.66a}$$

$$\underset{\sim}{I}^2(r_{i-1}) = \underset{\sim}{1} + \sum_{j=1}^{i-1} \underset{\sim}{G}^2(r_j) \cdot \underset{\sim}{V}^{(m)}(r_j) \cdot \underset{\sim}{u}^0(r_j)\, w_j \,, \tag{6.66b}$$

we have

$$\underset{\sim}{u}^0(r_i) = \underset{\sim}{G}^1(r_i) \cdot \underset{\sim}{I}^2(r_{i-1}) - \underset{\sim}{G}^2(r_i) \cdot \underset{\sim}{I}^1(r_{i-1}). \tag{6.67}$$

The constant matrix $\underset{\sim}{C}$ is simply

$$\underset{\sim}{C} = [\underset{\sim}{I}^2(r_{max})]^{-1} \cdot [\underset{\sim}{1} - \underset{\sim}{I}^2(r_{max})] \tag{6.68}$$

where r_{max} is the largest value of r used in the step integration defined by Eq. (6.67).

Notice that the I-matrices of Eqs. (6.66) can be generated from the convenient formula

$$\underset{\sim}{I}^{j}(r_{i-1}) - \underset{\sim}{I}^{j}(r_{i-2}) + \underset{\sim}{G}^{j}(r_{i-1}) \cdot \underset{\sim}{V}^{(m)}(r_{i-1}) \cdot \underset{\sim}{u}^{o}(r_{i-1})\, w_{i-1} . \tag{6.69}$$

The relevant initial conditions on these quadratures for starting the integration at r = 0 are

$$\underset{\sim}{I}^{1}(0) = \underset{\sim}{0} \tag{6.70a}$$

$$\underset{\sim}{I}^{2}(0) = \underset{\sim}{1} \tag{6.70b}$$

$$\underset{\sim}{u}^{o}(0) = \underset{\sim}{0} . \tag{6.70c}$$

[In some applications of this method it is appropriate to start the solution or certain channels of the solution at some non-zero value of r. See reference (17).]

Hand calculation verification of the computer code which implements these equations is facilitated by noticing that if r_0 is zero, then

$$\underset{\sim}{u}^{o}(r_i) = \underset{\sim}{G}^{1}(r_1) \tag{6.71}$$

$$\underset{\sim}{I}^{1}(r_1) = \underset{\sim}{G}^{1}(r_1) \cdot \underset{\sim}{V}^{(m)}(r_1) \cdot \underset{\sim}{G}^{1}(r_1)\, w_1 \tag{6.72a}$$

$$\underset{\sim}{I}^{2}(r_1) = \underset{\sim}{1} + \underset{\sim}{G}^{2}(r_1) \cdot \underset{\sim}{V}^{(m)}(r_1) \cdot \underset{\sim}{G}^{1}(r_1) w_1 . \tag{6.72b}$$

These results further tell us the useful fact that $\underset{\sim}{I}^1(r) \simeq 0$ for small values of r.

§6.5. Extraction of the T-matrix.

We carefully chose the Green's function in Eq. (6.55) to correspond to the asymptotic boundary condition

$$u_\ell^{(m)}(r) \sim \sin\left(kr - \ell\tfrac{\pi}{2}\right)\delta_{\ell\ell_0} + K^m_{\ell\ell_0}\cos\left(kr - \ell\tfrac{\pi}{2}\right). \tag{6.73}$$

The K-matrix so defined is real and symmetric, while the S-matrix, related by Eq. (6.9) or equivalently

$$\underset{\sim}{S} = \left[\left(1 - \underset{\sim}{K}^2\right) + 2i\,\underset{\sim}{K}\right]\cdot\left(\underset{\sim}{1} + \underset{\sim}{K}^2\right)^{-1} \tag{6.74}$$

is unitary and symmetric.[21]

Letting r become large in Eq. (6.64), we obtain

$$\underset{\sim}{u}^{(m)}(r) \underset{r\to\infty}{\sim} \left[\lim_{r\to\infty}\ \underset{\sim}{u}^0(r)\right]\cdot\left(\underset{\sim}{1} + \underset{\sim}{C}\right), \tag{6.75}$$

The behavior of the homogeneous solution in this limit is given by

$$\lim_{r\to\infty}\ \underset{\sim}{u}^0(r) = \underset{\sim}{s}(r)\cdot\underset{\sim}{I}^2(\infty) + \underset{\sim}{k}^{-1}\cdot\underset{\sim}{c}(r)\cdot\underset{\sim}{I}^1(\infty), \tag{6.76}$$

where we have used Eq. (6.58) and introduced two new sin and cos matrices,

$$[\underset{\sim}{s}(r)]_{ll'} = \sin\left(kr - l\tfrac{\pi}{2}\right)\delta_{ll'} \tag{6.77a}$$

$$[\underset{\sim}{c}(r)]_{ll'} = \cos\left(kr - l\tfrac{\pi}{2}\right)\delta_{ll'} \tag{6.77b}$$

and the diagonal constant matrix $\underset{\sim}{k}$. A little manipulation yields

$$\underset{\sim}{u}^{(+)}(r) \underset{r\to\infty}{\sim} \underset{\sim}{s}(r) + \underset{\sim}{c}(r)\cdot\underset{\sim}{k}^{-1}\cdot\underset{\sim}{I}^{1}(\infty)\cdot[\underset{\sim}{I}^{2}(\infty)]^{-1}.$$

But the K-matrix in the multi-channel case is obtained from[18]

$$\underset{\sim}{u}^{(+)}(r) \underset{r\to\infty}{\sim} \underset{\sim}{s}(r) + \underset{\sim}{c}(r)\cdot\underset{\sim}{k}^{-\frac{1}{2}}\cdot\underset{\sim}{K}\cdot\underset{\sim}{k}^{1/2}.$$

Making the obvious identifications, we have

$$\underset{\sim}{K} = \underset{\sim}{k}^{-1/2}\cdot\underset{\sim}{I}^{1}(\infty)\cdot[\underset{\sim}{I}^{2}(\infty)]^{-1}\cdot\underset{\sim}{k}^{1/2}. \tag{6.77c}$$

Of course, we do not actually use $\underset{\sim}{I}^{2}(\infty)^{-1}$ but rather $[\underset{\sim}{I}^{2}(r_{max})]^{-1}$, where r_{max} must be in the asymptotic region as defined above.

We shall ultimately obtain cross sections in terms of the T-matrix, which is complex and hence can be written as

$$\underset{\sim}{T} = \underset{\sim}{R} + i\,\underset{\sim}{I}.$$

A little algebra using Eq. (6.74) and $\underset{\sim}{T} = \underset{\sim}{1} - \underset{\sim}{S}$ leads to

$$\underset{\sim}{I} = -2\underset{\sim}{K}\cdot(\underset{\sim}{1}+\underset{\sim}{K}\cdot\underset{\sim}{K})^{-1} \tag{6.78a}$$

$$\underset{\sim}{R} = -\underset{\sim}{K}\cdot\underset{\sim}{I}. \tag{6.78b}$$

The calculation of cross sections from $\underset{\sim}{R}$ and $\underset{\sim}{I}$ will be detailed in Chapter 7.

This concludes the discussion of the standard integral equations formulation. In the next section we take a look at the machinations required if one is to use this technique on any but the simplest systems.

§6.6. The Transformation-Truncation Procedure*

In this section, we shall introduce a fairly substantial modification of the integral equations algorithm discussed above. The primary motivation for use of this procedure rests in severe numerical difficulties which were encountered in our early efforts. It turned out that in addition to resolving the most serious of these difficulties, the transformation-truncation procedure has some theoretical interest in so far as it addresses the physical wave-

*We are most grateful to Dr. Lee A. Collins for his invaluable assistance in the development of this procedure.

function and the question of the relative importance of large-ℓ partial waves to the final cross section. In this last regard, we shall harken back to the discussion of the effective potential in Chapter 3.

By way of introductory, let us recall from Eq. (6.64) that the physical wavefunction $\underset{\sim}{u}^{(m)}(r)$, from which we obtain physically meaningful scattering data, differs from the homogeneous solution $\underset{\sim}{u}^{o}(r)$ for which we solve in Eq. (6.63) by a constant matrix. In the physical wavefunction we can identify channels (elements) with particular partial waves; these channels couple, in some cases quite strongly, in the region of small and intermediate r, but asymptotically we can (for some systems and some symmetries in the e-CO_2 problem) actually identify particular distinct ℓ-channels. The point is that these "physically meaningful" channel solutions are mixed in the homogeneous solution. [In the standard formulation of the last section, we return to the physical wavefunction once we get to the asymptotic region by multiplying by $[\underset{\sim}{I}_2(\infty)]^{-1}$.]

For nice nearly spherical targets, these features of the algorithm pose no serious problems, although it is usually necessary to "stabilize" the wavefunction. [See reference (7) and section 6.6C below for discussions of this proceedure.] However, for the highly anisotropic case of e-CO_2 scattering, we have a very strong static potential energy and must retain a huge number of channels to achieve convergence. What, precisely, is the problem? Well, in the region

of high anisotropy (i.e., the vicinity of the nuclei), the mixing of physical channels to which we alluded above does no real harm, since the high-ℓ solutions are pretty large in this region. (This is negated somewhat by the centrifugal barrier considerations for very large partial waves; see below.) These functions die away beyond the centrifugal barrier. Problems arise because some of the solutions are too large to be treated computationally by conventional means. The end result is a loss of significance and a singular (or nearly singular) I^2-matrix. In fact, this phenomenon was first noticed when we observed that in calculations where a large number of channels were retained, the product $\underset{\sim}{I}^2(\infty)^{-1} \cdot \underset{\sim}{I}^2(\infty)$ was not equal to the unit matrix, but had huge off-diagonal elements.

Intuitively, one would think that beyond some value of r considerably smaller than r_{max}, the offending high-ℓ solutions components would be superfluous; the reasons for this were explicated in Chapter 3 in our comments on the effective potential. Beyond this value of r, these channels carry no flux themselves and so do not contribute to the cross sections. Moreover, it is ridiculous to expect them to "back-couple" significantly to the small-ℓ components, which do make significant contributions. These arguments are most emphatically not valid in the region of highest anisotropy, and this is what makes the calculations rather forbidding.

It is therefore reasonable to truncate a large number

of these "superfluous" channels, say, all $\ell \geq \ell_{trunc}$ beyond a certain radius, say r_{trunc}. But to do this in a meaningful manner, one must first transform the homogeneous solution being calculated into the physical solution, for one cannot just mindlessly lop off rows and columns from the homogeneous solution without also tossing out flux (i.e., contributions to the cross section) along the way.

In point of fact, merely truncating as suggested above is not sufficient to resolve all the numerical glitches in the problem. One must transform the homogeneous solution to the physical solution at values of r smaller than r_{trunc}. To understand why this is true, it is necessary to look at the procedure being proposed in some detail. So enough words; on with the equations!

What, if anything, is the effect on the integral equations algorithm as presented in section 6.4, of applying a constant transformation, say $\underset{\sim}{D}$ to $\underset{\sim}{u}^o(r)$ at some r along the way of the integration? In other words, consider the transformed wave-function

$$\underset{\sim}{\bar{u}}(r) = \underset{\sim}{u}^o(r) \cdot \underset{\sim}{D} \tag{6.79}$$

where $\underset{\sim}{u}^o(r)$ satisfies Eq. (6.63). What equation does $\underset{\sim}{\bar{u}}(r)$ satisfy? To answer, we multiply Eq. (6.63) on the right by the transformation, obtaining

$$\underset{\sim}{\bar{u}}(r) = \underset{\sim}{G}^1(r) \cdot \underset{\sim}{\bar{I}}^2(r) - \underset{\sim}{G}^2(r) \cdot \underset{\sim}{\bar{I}}^1(r) \tag{6.80}$$

where the transformed I^i-matrices are simply

$$\underset{\sim}{\bar{I}}^i(r) = \underset{\sim}{I}^i(r) \cdot \underset{\sim}{D} \qquad [i = 1, 2]. \tag{6.80b}$$

For purposes of calculation, the quadrature formulas of section 6.4 are easily generalized to

$$\underset{\sim}{\bar{u}}(r_i) = \underset{\sim}{G}^1(r_i) \cdot \underset{\sim}{\bar{I}}^2(r_{i-1}) - \underset{\sim}{G}^2(r_i) \cdot \underset{\sim}{\bar{I}}^1(r_{i-1}) \tag{6.81}$$

and

$$\underset{\sim}{\bar{I}}^i(r_{i-1}) = \underset{\sim}{\bar{I}}^i(r_{i-2}) + \underset{\sim}{G}^i(r_{i-1}) \cdot \underset{\sim}{V}^{(m)}(r_{i-1}) \cdot \underset{\sim}{\bar{u}}(r_{i-1}) w_{i-1} \tag{6.82}$$

The numerical procedure for transforming at r_{trans} is clear. We have $\underset{\sim}{u}^o(r_{trans})$ and $\underset{\sim}{I}^i(r_{trans})$. Hence we can generate transformed wavefunctions and I^i-matrices at r_{trans} via Eq. (6.78) and (6.80). We then proceed with the algorithm exactly as before: the computational form of (6.81) and (6.82) is the same as that of their untransformed counterparts (6.67) and (6.69). This important observation has happy consequences for the frustrated programmer trying to modify an already complicated computer code!

We are all set except for one thing: the K-matrix. The obvious way to proceed is to calculate

$$\bar{\underset{\sim}{K}} = \underset{\sim}{k}^{-\frac{1}{2}} \cdot \bar{\underset{\sim}{I}}^{1}(\infty) \cdot \left[\bar{\underset{\sim}{I}}^{2}(\infty)\right]^{-1} \cdot \underset{\sim}{k}^{\frac{1}{2}} \tag{6.83}$$

But is this identically equal to $\underset{\sim}{K}$ as determined by Eq. (6.77c)? If not, we cannot extract useful cross sections from the matrix in Eq. (6.83) and are in a lot of trouble. Well, the answer is yes. To see this, we just shove Eq. (6.80) for i = 1 and i = 2 into Eq. (6.83), recalling from some distant course in matrix algebra, that

$$\left[\underset{\sim}{I}^{2}(\infty) \cdot \underset{\sim}{D}\right]^{-1} = \underset{\sim}{D}^{-1} \cdot \left[\underset{\sim}{I}^{2}(\infty)\right]^{-1} \tag{6.84}$$

In no time at all, we see that the two matrices are identical.

The truncation procedure is comparatively trivial to carry out. Once we have stepped out to r_{trunc}, we merely transform one more time, returning to the physical wavefunction, identify the offending unwanted channels, and dump them from the wavefunction matrix in the calculation.

There is one further point that should be addressed. In the actual calculation, we found rather abruptly that one transformation is not sufficient. The potential is simply so strong that no sooner do you undo (by transforming) the numerical damage the potential has done than it is in there again, messing up your developing transformed wavefunction. Thus frequent transformations are usually required, especially for symmetries requiring a large

number of channels (e.g., Σ_g, which, as we shall see in Chapter 8, is a virtually endless source of difficulty).

Are multiple transformations a problem? Certainly not; otherwise we'd never have raised the question. The reason is that when we reach a second transformation radius, say r_2, we hit the transformed wavefunction not the homogeneous solution with, say, D_2. Thus

$$\underset{\sim}{\bar{\bar{u}}}(r_2) = \underset{\sim}{\bar{u}}(r_2) \cdot \underset{\sim}{D}_2 \tag{6.85}$$

$$= \underset{\sim}{u}^{\circ}(r_2) \cdot \underset{\sim}{D} \cdot \underset{\sim}{D}_2 \tag{6.86}$$

The produce of the two constant transformations is equivalent to a single transformation, say $\underset{\sim}{E} = \underset{\sim}{D} \cdot \underset{\sim}{D}_2$.

The next logical question is: what do we use for the constant transformation matrix, $\underset{\sim}{D}$? In line with our earlier comments, the most desirable choice would be

$$\underset{\sim}{D} = \left[\underset{\sim}{I}^2(\infty) \right]^{-1}, \tag{6.87}$$

for then the transformed wavefunction would in fact be the physical wavefunction. This would be grossly inefficient, though, since we calculate $\underset{\sim}{I}^2(r)$ via Eq. (6.67) and hence would have to do the problem twice, for we can't get $[\underset{\sim}{I}^2(\infty)]^{-1}$ without transforming, which we can't do without $\underset{\sim}{I}^2(\infty)$.

A way out of this problem is provided by defining

$$\underset{\sim}{D} = \left[\underset{\sim}{I}^2(r_{trans})\right]^{-1} \tag{6.88}$$

so that

$$\underset{\sim}{\bar{u}}(r_{trans}) = \underset{\sim}{u}^{o}(r_{trans}) \cdot \left[\underset{\sim}{I}^2(r_{trans})\right]^{-1}. \tag{6.89}$$

Once we have transformed in this manner, we can truncate the unwanted channels provided that we are at large enough r that $\underset{\sim}{I}^2(r_{max}) \simeq \underset{\sim}{I}^2(\infty)$. In our application, to be illustrated in Chapter 8, we found by direct examination of $\underset{\sim}{I}^2$ and by convergence tests in r_{trunc} that our choice for this quantity was adequate to satisfy this criterion even though it was <u>much</u> closer to r = 0 than to $r = r_{max}$.

The truncation procedure therefore saves computer time as well as helping get around the numerical difficulties which originally motivated it. Beyond the truncation radius, we propogate a much smaller wavefunction matrix (e.g., 5 channels rather than 32 channels) and need to calculate consequently fewer matrix elements and Green's functions. The major saving, however, comes in the reduced matrix manipulations.

One final word must be said about multiple transformations. Suppose we have transformed at $r = r_1$ and are happily propogating, viz.,

$$\bar{\underset{\sim}{u}}(r) = \underset{\sim}{u}^{0}(r) \cdot \left[\underset{\sim}{I}^{2}(r_1) \right]^{-1} \tag{6.90a}$$

$$\bar{\underset{\sim}{I}}^{i}(r) = \underset{\sim}{I}^{i}(r) \cdot \left[\underset{\sim}{I}^{2}(r_1) \right]^{-1}. \tag{6.90b}$$

We then reach r_2, where we decide we must transform a second time. We use

$$\underset{\sim}{D}_2 = \left[\bar{\underset{\sim}{I}}^{2}(r_2) \right]^{-1}, \tag{6.91}$$

rather than $\underset{\sim}{I}^{2}(r_2)^{-1}$ so that the transformation on $\bar{\underset{\sim}{u}}(r)$ effectively "undoes" the first transfirmation, i.e.,

$$\begin{aligned} \bar{\bar{\underset{\sim}{u}}}(r_2) &= \bar{\underset{\sim}{u}}(r_2) \cdot \left[\bar{\underset{\sim}{I}}^{2}(r_2) \right]^{-1} \\ &= \underset{\sim}{u}^{0}(r_2) \cdot \left[\underset{\sim}{I}^{2}(r_1) \right]^{-1} \cdot \left[\underset{\sim}{I}^{2}(r_2) \right] \cdot \left[\underset{\sim}{I}^{2}(r_2) \right]^{-1} \end{aligned}$$

$$\Longrightarrow \qquad \bar{\bar{\underset{\sim}{u}}}(r_2) = \underset{\sim}{u}^{0}(r_2) \cdot \left[\underset{\sim}{I}^{2}(r_2) \right]^{-1} \tag{6.92}$$

This is done so that as we move along, the multiply-transformed wavefunction will resemble the physical solution as closely as possible. (It is also more convenient computationally.)

In the final analysis, we found that by using the transformation procedure and exercising extreme care in certain other numerical

aspects of the calculation (see below) it was possible to properly converge the cross sections for e-CO_2 scattering. In effect, the transformation tries to "segregate" the very small wavefunction components from the important not-so-small low-ℓ components in the developing u-matrix. It is not an approximation. The second step of the procedure, elimination of superfluous channels at the truncation radius, is an approximation but, as we reason and shall see in the sequel, it is a very good one.

Lastly, let us say a word about our choice of the parameters r_{trunc} and ℓ_{trunc}. In general, one can use the graphs of the effective potential energy (e.g., Figure 3.7) to predict these quantities, although the caveats issued in section 3.7 regarding care in using such arguments must be kept in mind. It is true, for example, that beyond $r = 4.0\ a_o$, the $\ell = 12$ partial wave does not contribute at all to the scattering for, say, Σ_g symmetry, and can be summarily dropped from the calculation. Nevertheless, the acid test of any such procedure is convergence; we try a couple of values for each parameter and ensure that the cross sections are unchanged. The number of partial waves which must be retained does depend on the symmetry under consideration. For example, for Σ_g we could use $\ell_{trunc} = 10$ with $r_{trunc} = 4.0\ a_o$, while for Π_g we require $\ell_{trunc}=16$ with the same truncation radius. More computational details can be found in section 8.2.

§6.7. Still More Numerical Difficulties

We now must address the undeniably boring subject of little, picky, numerical problems which we encountered along the way in our studies. However tedious all this appears, these matters must not be skipped over, for if one blindly uses standard computer codes to calculate standard quantities in a problem as extreme (in some ways) as is ours, one is guaranteed no end of trouble (and incorrect answers).

A. The Trouble With Bessel Functions.

One might think that something as innocuous as calculations of the various Ricatti functions appearing in the equations of section 6.5 would be quite straightforward; there are hundreds of codes floating around the physics community to perform just such a task[28]. Alas, we find that very many channels being required in our problem for r values near the origin lead to problems. The calculation of the required functions is a little tricky and (potentially) expensive.

The spherical Bessel and Neumann functions obey the recurrence relation[20]

$$\mathcal{J}_{\ell-1}(x) + \mathcal{J}_{\ell+1}(x) = \frac{2\ell+1}{x}\,\mathcal{J}_{\ell}(x), \tag{6.93}$$

which is at the heart of most standard techniques for evaluation of these functions. The obvious (and usual) thing to do is to take into account the known and easily evaluated analytic forms for these functions at small orders, e.g.,

$$j_0(x) = \frac{1}{x}\sin x \quad , \qquad n_0(x) = -\frac{1}{x}\cos x \tag{6.94}$$

$$j_1(x) = \frac{1}{x^2}\sin x - \frac{1}{x}\cos x \quad , \quad n_1(x) = -\frac{1}{x^2}\cos x - \frac{1}{x}\sin x ,$$

and recurr upwards to obtain the corresponding function of the desired order.

However, it is preferable for especially large orders in the calculation of the spherical Bessel functions, to use a downward recurrence scheme;[29] more accurate values of $f_\ell(r)$ are obtained in this manner, the problem arising because the spherical Bessel function gets very small for large orders and small arguments. The idea is to introduce a new function proportional to the desired one. If we are interested in, say, $j_m(x_o)$, we write

$$F_\ell(x) = p\, j_\ell(x) . \tag{6.95}$$

Next, we select some $N > m$, say $N = 2m$, and set

$$F_N(x_o) = 1 \tag{6.96a}$$

$$F_{N+1}(x_o) = 0 \tag{6.96b}$$

where Eq. (6.96b) is arbitrary. The larger N we choose, the better

will be our answer. However, machine limitations (see section D below) can throw a monkey wrench into the works.

Now, using the recurrence relation (6.93), we step DOWN to $F_0(x_0)$, saving $F_m(x_0)$ along the way. We can then determine the proportionality constant p from

$$F_0(x_0) = p\, j_0(x_0) = p\, \frac{1}{x_0} \sin x_0 \tag{6.97}$$

Then we find the desired quantity via

$$j_m(x_0) = \frac{1}{p} F_m(x_0).$$

As a general rule of thumb, we recommend

upward recurrence for $x^2 > \ell(\ell + 1)$

downward recurrence for $x^2 < \ell(\ell + 1)$

However, this still does not resolve all the problems. At small values of the argument for large orders, the factor $(2\ell + 1)/x$ can become quite small. An additional factor of this magnitude is accumulated for each step down. The end result is usually a number so small that most computers underflow.

The way around THIS problem is to use the series representation for the Bessel function[30], i.e.,

$$J_\nu(x) = \left(\frac{x}{2}\right)^\nu \sum_{k=0}^{\infty} \frac{(-1)^k}{k!\,\Gamma(\nu+k+1)} \left(\frac{x}{2}\right)^{2k}. \tag{6.98}$$

This result is valid for all real arguments. It is easy to derive from this an expression for the spherical Bessel function, to wit:

$$j_\ell(x) = \frac{1}{2}\left(\frac{x}{2}\right)^\ell \sum_{k=0}^{\infty} \frac{(-1)^k\, 2^{2(\ell+k+1)}(\ell+k+1)!}{k!\,[2(\ell+k+1)]!} \left(\frac{x}{2}\right)^{2k}. \qquad (6.99)$$

We find the series to be convergent by k = 2 for x < 0.01 and ℓ up to 58.

A handy recurrence algorithm can be developed based on Eq. (6.99). We find

$$j_\ell(x) = \frac{1}{2}\left(\frac{x}{2}\right)^\ell \sum_{k=0}^{\infty} C_k(\ell, x), \qquad (6.100)$$

with the coefficients generated by means of

$$C_{k+1}(\ell, x) = -\frac{(m+1)\,x^2}{(k+1)(2m+2)(2m+1)}\, C_k(\ell, x), \qquad (6.101)$$

where

$$m = \ell + k + 1 \qquad (6.102)$$

and

$$C_0 = \frac{4 \cdot 2^{2\ell} \cdot (\ell+1)!}{(2\ell+2)!}\,. \qquad (6.103)$$

All the techniques in this subsection were coded in a subroutine in the electron-molecule code and extensively checked using a hand calculator, other codes, and various published tables.[31]

B. The Trouble With Clebsch-Gordan Coefficients

The usual procedure for calculating Clebsch-Gordan coefficients is to use a combination of the analytic forms and recurrence relations for these coefficients; these formulas can be found in reference (31). Initially, such was our procedure. However, as we increased the number of channels and hence the value of the maximum argument, we found that these nice convenient formulae give incorrect answers due to a loss of significance in the calculation. In particular, one cannot trust the result for $C(j_1\ j_2\ j_3;\ m_1\ m_2\ m_3)$ for j_1, j_2, or j_3 greater than about 10 if standard formulas in single precision are used.

Fortunately, a code exists due to Caswell and Maximon[33] which gets around the problem and will calculate Clebsch-Gordan coefficients for values of j_i up to about 80. This program uses a combination of logarithm arithmetic and double precision to perform the calculation and is highly recommended to anyone faced with the prospect of calculating large numbers of coefficients in this range. As an indication of the efficient nature of this code, we found that it took less time to re-evaluate the coefficients needed to calculate matrix elements each time the integral equations code was executed

than it did to calculate them once and read them in for each execution. (Of course, this conclusion is highly machine dependent and should be taken with the usual grain of salt.)

One thing should be noted. The code in question calculates Wigner 3j coefficients rather than Clebsch-Gordan coefficients. However, the convergence is easily made[32] via

$$C(j_1 j_2 j_3; m_1 m_2 m_3) = (-1)^{j_1 - j_2 + m_3} \sqrt{(2j_3+1)} \begin{pmatrix} j_1 & j_2 & j_3 \\ m_1 & m_2 & -m_3 \end{pmatrix}. \quad (6.104)$$

Having once been burned, we performed very extensive tests of the validity of this code using the invaluable though difficult to use tables of Rotenberg et. al. for comparison. For all values of j_i of interest, the code performs without error.

For even larger values of j_i, which we mercifully need not concern ourselves with, there exist recently developed[34] formulae which are very efficient. These are here mentioned for completeness.

C. Stabilization

As has been noted by other authors, in the generation of the homogeneous solution via the integral equations algorithm, it is possible for linear dependence to creep into the solutions due to numerical loss of significance in certain channels. This situation is particularly egregious when lots of channels are involved.

A procedure called stabilization has been developed[4-9]

to address this particular computational problem, and a clear and detailed discussion of it is available in reference (35). Essentially, the method entails decomposing the homogeneous solution at the stabilization radius, where we intend to stabilize, into the product of upper- and lower-triangular matrices and replacing the homogeneous solution matrix with the resultant upper-triangular matrix.[36] This forces linear independence of the N solutions being developed at the stabilization radius.

Frequent stabilizations can be required, because creeping linear dependence can re-infect the stabilized solution. Moreover, one must apply the stabilization step before the solution matrix becomes singular; once this has happened, you can't save the situation.

D. The Ad Hoc Neumann Cutoff Procedure

Unfortunately, we are not quite out of the jungle of numerical complications yet. Fortunately, we do not run into the problems discussed in A when calculating Neumann functions, for these are not small at small r. The problem is that they are large at small r. In fact, the computer overflows in trying to calculate them for small argument and large order. For example, the spherical Neumann function for $\ell = 56$, which is required for Σ_g symmetry, at $k^2 = 0.005$ and $r = 0.001$ is larger than 10^{312}, the machine upper limit for a CDC 7600. On less impressive machines, the limit is much lower and the problem consequently encountered for small orders.

There are a variety of ways to treat the problem. The most elegant and exact is to scale the I^i-matrices and thereby avoid

either the overflow at small r of the spherical Neumann function or the underflow of the spherical Bessel function. The latter occurrence effectively starts certain high-order solution channels "late", i.e., at some $r \neq 0$. We have tested the importance of this for the T matrix elements by artificially inducing the same effect in our computer program. The answers are unchanged until the starting radius becomes much larger than the values of r for which the machine can calculate the spherical functions.

A simple though approximate way to tackle the overflowing Neumann functions is to simply cut them off. In other words, when in the recurrence $n_\ell(kr)$ grows to some predetermined upper cutoff, we just replace all larger values of the function with a (large) constant. This procedure is founded in the expectation that a number of such huge magnitude is so large compared to other elements of the matrix, that it can reasonably be replaced by another large number without significantly affecting the wavefunction being developed.

Because of the admittadly ad hoc and approximate nature of this trick, very thorough tests of its effect on wavefunctions, I^i-matrices, and T-matrix elements were carried out. To our astonishment, we found that not only did the procedure resolve the problem here presented but it enabled us to converge the Σ_g cross sections, which had begun to show characteristics of divergence owing to numerical instabilities in the calculation. This problem, how this procedure resolved it, and other ways around it, will be discussed in Chapter 8, where we look at some numbers.

§6.8. Conclusion

Chapters 3 - 6 completely describe the collion problem theoretically up to but not including the actual calculation of cross sections. The theory we have described if used with care can probably be used to treat electron collisions with any molecule smaller than or about the same size as CO_2. The application to heteronuclear targets is quite straightforward, requiring allowance for even- and odd-λ terms in the expansion of the potential energy in Legendre polynomials. In fact, the author (in collaboration with Dr. L. Collins) has carried out some calculations in the lab frame using our codes to study e-CsF scattering. The modifications required were straightforward. The further extension to non-linear molecules (say, water) remains a challenge and might involve rather extensive code revision. The theory should apply, however.

At the risk of redundancy, let us stress in conclusion that without the procedures of sections 6.6 and 6.7 or their equivalents the integral equations method cannot be applied to problems such as e-CO_2 scattering. But what of the Numerov algorithm? Might we adopt it?

We decided against this approach for several reasons. First the integral equations algoritha used in conjunction with the stabilization procedure discussed above is a more stable method than Numerov, which encounters similar numerical problems sooner in the integration. Second, the integral equations method is faster, since inward-outward integration is not required.

These arguments are less compelling if exchange must be inclu-

ded via a kernel in the integral equations procedure. See reference (3) for a discussion of this case.

Chapter 7. Diverse Cross Sections for Electron-Molecule Scattering

Little Jack Horner
Sits in a corner
Extracting cube roots to infinity,
An assignment for boys
That will minimize noise
And produce a more peaceful vicinity.

-Frederick Winsor
The Space Child's Mother Goose

§7.1. Introduction: The Point of it All

In this, the final phase of our theoretical analysis of the electron-molecule collision problem, we shall present formulae for the calculation of actual cross sections. It is these quantities which permit us to compare with the experimental results discussed in Chapter 2 and that permit ultimate insight into the physics of the scattering event. They are of paramount importance.

Our starting point is the T-matrix. As we showed in Chapter 6, we first calculate the real symmetric K-matrix via Eq. (6.77c) and then extract from it the real and imaginary parts of the T matrix using Eqs. (6.78). We shall assume here that we have obtained these quantities and seek to use them.

With one exception, all the numerical quantities we shall discuss in the "results chapter", which follows this one, are extracted by formulae to be revealed here, from the T-matrix. We do use the eigenphases, though, and they are derived from the

K-matrix[1]. We simply diagonalize the K-matrix and take the arctangent of the resulting eigenvalues; these are the eigenphases (or eigenphase shifts). If used with care, the eigenphases and associated eigenvectors which emerge from the diagonalization, can be a useful tool in the study of electron-molecule physics[2]. We shall have considerably more to say about eigenphases in Chapter 8.

We present formulas for the total cross sections in §7.2, for differential and momentum transfer cross sections in §7.3, and for rotational excitation cross sections in §7.4. This section also discusses briefly the transformation from body-fixed to space-fixed (or laboratory) reference frame. The last two sections of this chapter present two approximations which will be used in the sequel: the Born Approximation (in a partial wave analysis) and the Asymptotic Decoupling Approximation.

§7.2. Total Cross Sections for Elastic Scattering

As the author has shown in detail elsewhere[3], the total cross section for elastic scattering is given in terms of the body-fixed T-matrix elements by the simple formula

$$\sigma_{tot} = \frac{\pi}{k^2} \sum_{\ell\ell' m} |T^{(m)}_{\ell\ell'}|^2, \qquad (7.1)$$

where k^2 is the scattering energy in Rydbergs. The formula is obtained by first deriving an expression for the cross section in

the body-fixed reference frame and then averaging said expression over all molecular orientations.*

Notice that in Eq. (7.1) we sum over m, the quantum number corresponding to the projection of the orbital angular momentum of the scattering electron along the z axis. This is a good quantum number, since the system has axial symmetry [i.e., $V(r,\theta)$ is independent of the polar angle ϕ], so there do exist solutions of the scattering equations the ϕ-dependence of which is given by $e^{im\phi}$ and can be factored out. However, to obtain a scattering function which satisfies the plane-wave scattering boundary conditions [C.f., Eq. (6.14) and accompanying discussion] we must sum over m, including the factor of $e^{im\phi}$, of course. This is reflected in Eq. (7.1).

In practice, we shall take advantage of the fact that our problem separates by symmetries of the full e-CO_2 system (see section 6.2) and treat each symmetry separately, summing at the end of obtain the total cross sections.

§7.3. Differential Elastic and Momentum Transfer Cross Sections

An equation for the differential cross section can be obtained by deriving[3] a fixed-nuclei expression for this quantity, transforming to a space-fixed reference frame via the ever-popular

*For convenience, the average is actually performed by integrating over the directions of the incident wavevector. See reference (3).

D-matrices[4], and then averaging over the Euler angles which define the orientation of the target with respect to the space-fixed axes. The rather formidable algebraic contortions necessary to derive the formula can be found in reference (4). The result, presented here to correct an error in the earlier document[3], is

$$\frac{d\sigma}{d\theta} = \frac{1}{4k^2} \sum_{\ell\ell' m} \sum_{\bar{\ell}\bar{\ell}'\bar{m}} \sum_{L} \frac{1}{(2L+1)} \left[(2\ell+1)(2\ell'+1)(2\bar{\ell}+1)\right.$$
$$\left.(2\bar{\ell}'+1)\right]^{\frac{1}{2}} C(\ell'\bar{\ell}'L;00)\, C(\ell'\bar{\ell}'L;-m,\bar{m}) \qquad (7.2)$$
$$C(\ell\bar{\ell}L;00)\, C(\ell\bar{\ell}L;-m,\bar{m})\, i^{(\ell-\ell')}\, (-i)^{(\bar{\ell}-\bar{\ell}')}$$
$$T^{m}_{\ell\ell'}\, T^{\bar{m}}_{\bar{\ell}\bar{\ell}'}{}^{*}\, P_L(\cos\theta).$$

In trying to cope with such a hideous expression, it is useful to introduce the notion of a "channel index" i, defined as $i = (\ell_i, \ell_i', m_i)$. In terms of this index, Eq. (7.2) can be slightly more conveniently written as

$$\frac{d\sigma}{d\theta} = \frac{1}{4k^2} \sum_{ij} \sum_{L} \frac{1}{(2L+1)} \left[(2\ell_i+1)(2\ell_i'+1)(2\ell_j+1)(2\ell_j'+1)\right]^{\frac{1}{2}}$$
$$C(\ell_i'\ell_j'L;00)\, C(\ell_i\ell_j L;00)\, C(\ell_i'\ell_j' L;-m_i,m_j) \qquad (7.3)$$
$$C(\ell_i\ell_j L;-m_i,m_j)\, i^{(\ell_i-\ell_i')}\, (-i)^{(\ell_j-\ell_j')}\, T^{m_i}_{\ell_i\ell_i'}\, T^{m_j}{}^{*}_{\ell_j\ell_j'}$$
$$P_L(\cos\theta).$$

There is a whole series of restrictions on the summations in Eq. (7.3). A Clebsch-Gordan coefficient $C(j_1j_2j_3,m_1m_2m_3)$ is zero[3] unless $m_3 = m_1 + m_2$, $\Delta(j_1j_2j_3)$, $|m_1| \leq j_1$, $|m_2| \leq j_2$, and $|m_3| \leq j_3$. Moreover, $C(j_1j_2j_3,000) = 0$ unless $j_1 + j_2 + j_3$ is even. Applying these to Eq. (7.3), we see that for any set of channel indices (ij), the correponding terms in the summation

are zero unless

$$|m_i| \leq \min(\ell_i, \ell_i') \tag{7.4a}$$

$$|m_j| \leq \min(\ell_j, \ell_j') \tag{7.4b}$$

$$|M| \leq L, \tag{7.4c}$$

where we define $M = m_j - m_i$. Also we must satisfy

$$\ell_i + \ell_j + L = \text{even} \tag{7.5a}$$

$$\ell_i' + \ell_j' + L = \text{even} \tag{7.5b}$$

$$\Delta(\ell_i \ell_j L) \text{ and } \Delta(\ell_i' \ell_j' L), \tag{7.6}$$

or, equivalently,

$$\max(|\ell_i - \ell_j|, |\ell_i' - \ell_j'|) \leq L \leq \min(\ell_i + \ell_j, \ell_i' + \ell_j'). \tag{7.7}$$

In the actual calculation, we only determine T-matrix elements for partial waves up to some ℓ_{max}, chosen by effective potential considerations such as those discussed in Chapters 3 and 6 and by experience. For example, for Σ_g symmetry, we have $m = 0$ and typically $\ell = 0,2,\ldots,8$, while for Σ_u we have $m = 0$ and $\ell = 1,3,\ldots,9$.

Notice, however, that the sum over m_i and m_j in Eq. (7.3) runs over positive and negative values, i.e., for each term corresponding to m_i or m_j non-zero, we have contributions due to $\pm m_i$ and/or $\pm m_j$ as appropriate.

For practical reasons, it is desirable to develop an efficient computational scheme for determining the differential cross section from this formula. Equation (7.1), with its seven summations, won't do. Because of its fairly wide potential applicability, we here present a sketch of a procedure which we developed to perform these computations.

Let us introduce the real and imaginary components of the T-matrix as in Eq. (6.78), and write Eq. (7.3) in terms of them as

$$\frac{d\sigma}{d\theta} = \frac{1}{4k^2} \sum_L \frac{1}{(2L+1)} P_L(\cos\theta) \sum_{ij} C_{ij}^L (R_i R_j + I_i I_j), \qquad (7.8)$$

where N is the number of channels* as defined by the channel index introduced above, and where $R_i = R^{m_i}_{\ell_i \ell_i'}$, etc. The coefficients c_{ij}^L are developed as

$$C_{ij}^L = \left[(2\ell_i+1)(2\ell_i'+1)(2\ell_j+1)(2\ell_j'+1)\right]^{\frac{1}{2}} i^{\ell_i - \ell_i'} (-i)^{\ell_j - \ell_j'} C(\ell_i \ell_j L; 00) C(\ell_i' \ell_j' L; 00) C(\ell_i \ell_j L; -m_i, m_j) C(\ell_i' \ell_j' L; -m_i, m_j). \qquad (7.9)$$

*These are assigned based on the particular symmetries and partial waves retained in the integral equations calculation as the first step in our code (DCSMOM) which evaluates these cross sections.

In deriving Eq. (7.8) we have used the fact that $c_{ij}^{L} = c_{ji}^{L}$ so that when summed the imaginary part of $T_{\ell_i \ell_i'}^{m_i} T_{\ell_j \ell_j'}^{m_j *}$ is zero. Defining a new matrix, call if J_L, as

$$J_{ij} = R_i R_j + I_i I_j \tag{7.10}$$

and using $J_{ij} = J_{ji}$, we can write Eq. (7.8) as

$$\frac{d\sigma}{d\theta} = \frac{1}{4k^2} \sum_{L=0}^{L_{max}} \left(\frac{1}{2L+1}\right) P_L(\cos\theta) \left[\sum_{i=1}^{N} c_{ii}^{L} J_{ii} + 2 \sum_{i=1}^{N-1} \sum_{j>i}^{N} c_{ij}^{L} J_{ij}\right], \tag{7.11}$$

where $L_{max} = 2\,\ell_{max}$, ℓ_{max} corresponding to the largest ℓ partial wave included (for any symmetry). Finally, let us define one more coefficient, viz.,

$$d_L = \left(\frac{1}{2L+1}\right)\left[\sum_{i=1}^{N} c_{ii}^{L} J_{ii} + 2 \sum_{i=1}^{N-1} \sum_{j>i} c_{ij}^{L} J_{ij}\right], \tag{7.12}$$

so that the differential cross section assumes the convenient form

$$\frac{d\sigma}{d\theta} = \frac{1}{4k^2} \sum_{L=0}^{L_{max}} d_L P_L(\cos\theta). \tag{7.13}$$

We can use Eq. (7.13) to derive a handy formula for the momentum transfer cross section. The latter is defined as[5]

$$\sigma_{mom} = \int_0^{2\pi} d\phi \int_0^{\pi} \sin\theta \, d\theta \, (1-\cos\theta) \frac{d\sigma}{d\theta} , \tag{7.14}$$

which can be written as

$$\sigma_{mom} = \sigma_{tot} - 2\pi \int_0^{\pi} \sin\theta \, d\theta \cos\theta \frac{d\sigma}{d\theta} , \tag{7.15}$$

where, of course, the total cross section is (by definition)

$$\sigma_{tot} = \int_0^{2\pi} d\phi \int_0^{\pi} \sin\theta \, d\theta \frac{d\sigma}{d\theta} . \tag{7.16}$$

We now substitute Eq. (7.13) into (7.15) and use the orthogonality relation[6] of the Legendre polynomials on the interval [-1,+1], obtaining

$$\sigma_{mom} = \sigma_{tot} - \frac{\pi}{3k^2} d_1 \tag{7.17}$$

and

$$\sigma_{tot} = \frac{\pi}{k^2} d_0 . \tag{7.18}$$

Thus we see that the total and σ_{mom} cross sections emerge as happy byproducts of our calculation of the differential cross section.

For the application to electron collisions with CO_2, the phase factors in the differential cross section vanish, since it

is always true that $|\ell_i - \ell_i'|$ and $|\ell_j - \ell_j'|$ are even (this, in turn, is a consequence of the fact that the target possesses inversion symmetry).

Finally, we should point out that it is efficacious not to have to explicitly include positive and negative values of m_i and m_j in the channel index table. This can be avoided by the simple expedient of replacing c_{ij}^{L} in the definition of d_L, Eq. (7.12), by a new coefficient, call it b_{ij}^{L}, and summing over channel indices i and j defined to incorporate only non-negative values of m_i and m_j. We thus define

$$b_{ij}^{L} = C^{L}(\ell_i \ell_j \ell_i' \ell_j'; m_i m_j) + C^{L}(\ell_i \ell_j \ell_i' \ell_j'; -m_i, m_j)\ (1-\delta_{m_i 0})$$

$$+ C^{L}(\ell_i \ell_j \ell_i' \ell_j'; m_i, -m_j)\ (1-\delta_{m_j 0}) \qquad (7.19)$$

$$+ C^{L}(\ell_i \ell_j \ell_i' \ell_j'; -m_i, -m_j)\ (1-\delta_{m_i 0})\ (1-\delta_{m_j 0}).$$

where we have explicitly indicated the quantum numbers on each c_{ij}^{L} of Eq. (7.9) and where the delta function kills off unnecessary terms.

The above algorithm was coded and very carefully tested. We incorporated several internal consistency checks, such as independently calculating the total cross section by Eq. (7.18) and then by Eq. (7.16) using our differential cross sections and numerical quadrature.

We then compared the results with the total cross section determined by summing the cross sections for individual symmetries in the integral equations calculation. In all cases, we found agreement.

The "acid" test of the code was performed by taking T-matrix elements for e-H_2 scattering at several energies and reproducing published differential cross sections[7] to three significant figures. Such extensive testing was deemed necessary when our calculated differential cross sections for e-CO_2 scattering began displaying some rather peculiar behavior; see Chapter 8 for a discussion.

§7.4. Determination of Rotational Excitation Cross Sections from the Body Frame T-Matrix

In this section we seek to determine rotational excitation cross sections for electron-molecule scattering making the fixed-nuclei approximation. We have the fixed-nuclei T-matrix elements in the body frame. The first step is the transformation of this matrix into the laboratory frame. In order to determine this transformation, we must first obtain the unitary transformation which relates the body and laboratory frames. We shall use unprimed coordinates to refer to the body frame and primed coordinates to refer to the lab frame.

The two frames are defined by the angular (rotational) functions, and the T-matrices in the two frames are just matrix representations of the T-operator in the two bases:

$$T^{J}_{j\ell,j'\ell'} = \langle j\ell JM \mid T \mid j'\ell' JM \rangle \tag{7.20a}$$

$$T^{m}_{\ell\ell'} = \langle \ell\lambda m \mid T \mid \ell'\lambda m \rangle. \tag{7.20b}$$

where $|j\ell JM\rangle$ refers to the coupled angular momentum rotational functions in the lab, i.e.,

$$\mathcal{Y}^{JM}_{j\ell}(\hat{r},\hat{R}) = \sum_{m_j m_\ell} C(j\ell J; m_j m_\ell M) Y_j^{m_j}(\hat{R}) Y_\ell^{m_\ell}(\hat{r}) \tag{7.21}$$

or, in general (for states with $m \neq 0$)

$$\mathcal{Y}^{JM\lambda}_{j\ell}(\hat{r},\alpha\beta\gamma) = \sum_{m_j m_\ell} C(j\ell J; m_j m_\ell M) Y_\ell^{m_\ell}(\hat{r}) \, \psi_{j m_j \lambda}(\alpha\beta\gamma). \tag{7.22}$$

In this expression, m_j is the projection of the rotational angular momentum of the target along the space-fixed axis z', while λ is the projection of same along the internuclear axis. Further, $\psi_{jm_j\lambda}(\alpha\beta\gamma)$ is the symmetric top wavefunction for Euler angles $\alpha\beta\gamma$, which define the orientation of the body frame with respect to the lab frame. Thus we have

$$\psi_{jm_j\lambda}(\alpha\beta\gamma) = \sqrt{\frac{2j+1}{8\pi^2}} \, \mathcal{D}^{j}_{m_j\lambda}(\alpha\beta\gamma)^{*}. \tag{7.23}$$

In the fixed-nuclei approximation, the body-frame basis functions are the spherical harmonics

$$|\ell \lambda m\rangle = Y_\ell^{m-\lambda}(\hat{r}), \tag{7.24}$$

where we have used the convention that m is the projection of the system (electron + molecule) angular momentum along the body frame z axis (i.e., the internuclear axis). These functions were used to define the T-matrix in the body frame. (If we do <u>not</u> make the fixed-nuclei approximation in the body frame, the rotational hamiltonian will couple different values of $m-\lambda$ and the problem will not separate so nicely.)

Now, let's determine the unitary transformation $\underset{\sim}{C}$ that converts the lab basis set into the body basis set, i.e., we seek c_{ij} such that

$$\phi_i^{(b)} = \sum_j c_{ij}\, \psi_j^{(\ell)}, \tag{7.25}$$

where the lab basis functions are defined by Eq. (7.22) and the body functions by Eq. (7.24). The expansion coefficients are therefore

$$c_{ij} = \langle \psi_j^{(\ell)} | \phi_i^{(b)} \rangle = \langle j \ell \lambda J M | \ell' \lambda m \rangle . \tag{7.26}$$

To determine these coefficients, we shall transform the j^{th} lab frame function into the body frame and carry out the coordinate-space angular integration in Eq. (7.26) in body coordinates. Using the well-known relation (see reference (4), Eq. (4.29a))

$$Y_\ell^m(\hat{r}') = \sum_{m'} \mathcal{D}^{\ell\,*}_{mm'}(\alpha\beta\gamma)\, Y_\ell^{m'}(r), \tag{7.27}$$

we obtain

$$\psi_j^{(e)} = \sum_{m_j m_\ell} C(j\ell J; m_j m_\ell M)\sqrt{\frac{2j+1}{8\pi^2}}\,\mathcal{D}^{j\,*}_{m_j\lambda} \sum_{m_\ell'} \mathcal{D}^{\ell}_{m_\ell m_\ell'}\, Y_\ell^{m_\ell'}(\hat{r}), \tag{7.28}$$

where we have used the form of the rotational wavefunction for the internuclear orientation. We now combine the two D-matrices appearing in this result using the series

$$\mathcal{D}^{j_1}_{\mu_1 m_1}\mathcal{D}^{j_2}_{\mu_2 m_2} = C(j_1 j_2 j; m_1 m_2)\,C(j_1 j_2 j; \mu_1\mu_2)\,\mathcal{D}^{j}_{m_1+m_2,\,\mu_1+\mu_2} \tag{7.29}$$

and substitute the result into our expression for c_{ij}. Carrying out the easy integration we obtain

$$c_{ij} = \sum_{m_j m_\ell}\sum_{\lambda} C(j\ell J; m_j m_\ell)\,C(j\ell L; -m_j, -m_\ell)$$
$$C(j\ell L; -\lambda, -m+\lambda)\sqrt{\frac{2j+1}{8\pi^2}}\,\mathcal{D}^{L}_{m_j+m_\ell,\,m}(\alpha\beta\gamma)\,\delta_{\ell\ell'} \tag{7.30}$$

We can further simplify this result by noting the delta function implied by the presence of the Clebsch-Gordan coefficient in Eq. (7.30), obtaining, finally,

$$c_{ij} = \sqrt{\frac{2j+1}{8\pi^2}}\,C(j\ell J; \lambda, m-\lambda)\,\mathcal{D}^{J}_{M,m}(\alpha\beta\gamma)\,\delta_{\ell\ell'}. \tag{7.31}$$

Notice that for sigma target states ($\lambda = 0$) this reduces to

$$c_{ij} = \sqrt{\frac{2j+1}{8\pi^2}}\, C(j\ell J; 0\, m)\, \mathcal{D}^{J}_{M,m}(\alpha\beta\gamma). \tag{7.32}$$

Our next task is to transform the matrix representation of the T-operator in the body frame into the lab frame. We have

$$T^{J}_{j\ell,j'\ell'} = \int \sum_{\substack{\ell''\ell''' \\ m}} \langle j\ell\lambda J M | \ell''\lambda m\rangle \; \bar{T}^{m}_{\ell''\ell'''} \otimes \langle \ell'''\lambda m | j'\ell'\lambda J M\rangle \; d(\alpha\beta\gamma), \tag{7.33}$$

where we also integrate (average) over the Euler angles defining the molecular orientation. In matrix notation, this result can be written

$$T^{(L)}_{kn} = \int \sum_{\rho\sigma} c_{k\rho}\, T^{(S)}_{\rho\sigma}\, c^{\dagger}_{\sigma n}\; d(\alpha\beta\gamma) \tag{7.34}$$

where

$$c^{\dagger}_{\sigma n} = c^{*}_{n\sigma}\,. \tag{7.35}$$

Substituting our result for c_{ij} into the above equation, we find

$$T^{J}_{j\ell,j'\ell'} = (-1)^{\ell+\ell'} \sum_{m} C(J\ell j; -m, m-\lambda)\, C(J\ell' j'; -m, m-\lambda)\, T^{m}_{\ell\ell'}, \tag{7.36}$$

where we have used the orthogonality of the D-matrices[4] to carry out the Euler-angle integration. Again it is worth noting that for Σ states this expression reduces to

$$T^{J}_{j\ell,j'\ell'} = (-1)^{\ell+\ell'} \sum_{m} C(J\ell j; -m, m) C(J\ell' j'; -m, m)\, T^{m}_{\ell\ell'} \qquad (7.37)$$

Now (at last) we can calculate rotational excitation cross sections. In the lab frame, they are derived from the formula[11]

$$\sigma_{jj'} = \frac{\pi}{k_j^2 (2j+1)} \sum_{J} (2J+1) \sum_{\ell\ell'} |T^{J}_{j\ell,j'\ell'}|^2 . \qquad (7.38)$$

Since we make the fixed-nuclei approximation, we ignore the spacing of the rotational energy levels and set

$$k_j^2 = k^2 \qquad (\text{all } j), \qquad (7.39)$$

where k^2 is the scattering energy in Rydbergs. It is useful to introduce notation for the real and imaginary parts of the T matrix, to wit:

$$T^{m}_{\ell\ell'} = R^{m}_{\ell\ell'} + i\, I^{m}_{\ell\ell'} , \qquad (7.40)$$

whence the formula for excitation from j to j' becomes

$$\sigma_{jj'} = \frac{\pi}{k^2 (2j+1)} \sum_{J} (2J+1) \sum_{\ell\ell'} \left[R^{J}_{j\ell,j'\ell'}{}^2 + I^{J}_{j\ell,j'\ell'}{}^2 \right] . \qquad (7.41)$$

Using the above derived transformation, our final result for the desired cross section is

$$\sigma_{jj'} = \frac{\pi}{k^2(2j+1)} \sum_J (2J+1) \sum_{\substack{\ell\ell' \\ m\bar{m}}} P^{J\lambda}_{jj'}(\ell\ell' m\bar{m}) \left[R^{m}_{\ell\ell'} R^{\bar{m}}_{j'j'} + I^{m}_{\ell\ell'} I^{\bar{m}}_{j'j'} \right], \quad (7.42)$$

where we have defined a coefficient

$$P^{J\lambda}_{jj'}(\ell\ell' m\bar{m}) = C(J\ell j; -m, m-\lambda)\, C(J\ell' j'; -m, m-\lambda) \cdot C(J\ell j; -\bar{m}, \bar{m}-\lambda)\, C(J\ell' j'; -\bar{m}, \bar{m}-\lambda) \quad (7.43)$$

for convenience. We should note in closing that formally the sum over J runs J = 0,1,2,... and the ℓ summations are then defined by the value of J, j, and j' subject to the usual triangle restrictions. For a given value of J, m can take on values (integral) consistent with the restrictions

$$|m| \leq J, \quad \text{and} \quad |\bar{m}| \leq J, \quad (7.44)$$

where we must keep in mind that for non-zero values of m the summation includes both positive and negative values.

The total cross section is invariant under the unitary transformation we have obtained and can be calculated in the body frame from the familiar formula

$$\sigma_{tot} = \frac{\pi}{k^2} \sum_m \sum_{\ell\ell'} |T^{m}_{\ell\ell'}|^2 \quad (7.45)$$

or in the lab frame from the rotational excitation cross sections via

$$\sigma_{tot} = \sum_{j'} \sigma_{jj'}, \qquad (\text{all } j'). \tag{7.46}$$

§7.5. Electron-molecule Scattering in the Born Approximation

The familiar Born Approximation (BA) is a highly appealing way to study collisions because it is simple conceptually and cheap computationally. If it works well, one might suggest, all the above labor is somewhat analogous to using a sledgehammer to kill a gnat. Thus in Chapter 8 we shall examine the validity of this approach, and hence it is necessary for us to derive a couple of equations here.

The essential idea[13] of the BA is the neglect of the distortion of the incident plane wave by the scatterer. Gerjuoy and Stein[14] demonstrated the validity of this approximation for electron molecule collisions at very low energies. This result may appear contradictory, since the BA is usually thought to be[13] a high energy approximation. The point is that for electron-molecule collisions at low energies, long-range multipole and induced interactions dominate the scattering. We discussed this point in Chapter 5.

Our objective here is to apply the BA to elastic scattering of electrons from homonuclear molecules in a single-center partial wave expansion. The undistorted ℓ^{th} partial wave is just the

Ricatti-Bessel function $\hat{j}_\ell(kr)$, which solves the usual equation

$$\left[\frac{d^2}{dr^2} - \frac{\ell(\ell+1)}{r^2} + k^2\right] \hat{j}_\ell(kr) = 0. \tag{7.47}$$

Thus the wavefunction matrix $\underset{\sim}{u}^{(m)}(r)$ which is in general non-diagonal is given in the Born Approximation by

$$u^B_{ij}(r) = \delta_{\ell_i \ell_j} \hat{j}_{\ell_i}(kr) . \tag{7.48}$$

Now, the K-matrix can be calculated in general from[5]

$$\underset{\sim}{K} = -\frac{1}{k} \int_0^\infty \underset{\sim}{u}^B(r)^* \cdot \underset{\sim}{U}(r) \cdot \underset{\sim}{u}^{(m)}(r)\, dr, \tag{7.49}$$

where

$$[\underset{\sim}{V}(r)]_{ij} = \langle \ell_i\, m \,|\, V(\vec{r}) \,|\, \ell_j\, m \rangle \tag{7.50}$$

and $\underset{\sim}{U}(r) = 2\underset{\sim}{V}(r)$ in atomic units. Of course, V(r) is the electron-molecule interaction potential energy averaged over the ground state of the target. We shall consider only long-range terms, as discussed in Chapter 5. Hence the potential of interest is

$$V(\vec{r}) = -\frac{\alpha_0}{2r^4} - \left(\frac{\alpha_2}{2r^4} + \frac{Q}{r^3}\right) P_2(\cos\theta). \tag{7.51}$$

In the Born Approximation, Eq. (7.49) becomes

$$\underset{\sim}{K} = -\frac{1}{k}\int_0^\infty \underset{\sim}{u}^{\alpha}(r)\cdot\underset{\sim}{U}(r)\cdot\underset{\sim}{u}^{\beta}(r)\,dr. \tag{7.52}$$

Writing the usual expansion of $V(\vec{r})$, Eq. (3.39), in terms of spherical harmonics, we find

$$V(\vec{r}) = \sum_{\lambda=0}^{\infty}{}' v_\lambda(r)\sqrt{\frac{4\pi}{2\lambda+1}}\; Y_\lambda^0(\hat{r}). \tag{7.53}$$

If we now define the quantities

$$I_\lambda(l_i m_i\, l_j m_j) = \int\int Y_{l_i}^{m_i}(\hat{r})^* Y_\lambda^0(\hat{r})\, Y_{l_j}^{m_j}(\hat{r})\,d\hat{r} \tag{7.54a}$$

$$J_\lambda(l_i m_i\, l_j m_j) = \sqrt{\frac{4\pi}{2\lambda+1}}\; I_\lambda(l_i m_i\, l_j m_j) \tag{7.54b}$$

then the matrix $\underset{\sim}{V}(r)$ becomes

$$\left[\underset{\sim}{V}(r)\right]_{ij} = \sum_{\lambda=0}^{\infty}{}' v_\lambda(r)\, J_\lambda(l_i m_i\, l_j m_j), \tag{7.55}$$

where we acknowledge that for our system (in the fixed-nuclei approximation) m is a good quantum number. The integral I_λ is easily evaluated as shown in reference (4).

We now substitute Eq. (7.55) into (7.52) to obtain an expression for K_{ij} in the Born Approximation, viz.,

$$K^m_{ij} = -2k \sum_{\lambda=0}^{\infty}{}' J_\lambda(l_i m\, l_j m)\, R_\lambda(l_i l_j), \tag{7.56}$$

where we have defined the radial integral

$$R_\lambda(l_i l_j) = \int_0^\infty j_{l_i}(kr)\, v_\lambda(r)\, j_{l_j}(kr)\, r^2\, dr. \tag{7.57}$$

For the potential energy of Eq. (7.51) we have the integrals

$$R_0(l_i l_j) = -\frac{\alpha_0}{2} \int_0^\infty j_{l_i}(kr)\, r^{-2}\, j_{l_j}(kr)\, dr \tag{7.58a}$$

$$R_2(l_i l_j) = -\frac{\alpha_2}{2} \int_0^\infty j_{l_i}(kr) r^{-2} j_{l_j}(kr)\, dr - Q \int_0^\infty j_{l_i}(kr) r^{-4} j_{l_j}(kr)\, dr, \tag{7.58b}$$

which suggests the convenient notation

$$R^{(n)}(l_i l_j) \equiv \int_0^\infty j_{l_i}(kr)\, r^{-n}\, j_{l_j}(kr)\, dr. \tag{7.59}$$

Now, from Eq. (7.56), we have for the Born K-matrix

$$K^m_{ij} = -2k\left[J_0(l_i m l_j m)\, R_0(l_i l_j) + J_2(l_i m l_j m)\, R_2(l_i l_j)\right]. \tag{7.60}$$

But $C(l_j\ 0\ l_i; 0\ 0\ 0) = \delta_{l_i l_j}$ so we have

$$J_0(l_i m\, l_j m) = \delta_{l_i l_j}. \tag{7.61}$$

Using this fact and Eq. (7.54), we can rewrite Eq. (7.60) as

$$K^{m}_{\ell\ell'} = k\alpha_0 R^{(2)}(\ell\ell')\delta_{\ell\ell'} + k\sqrt{\frac{4\pi}{5}}\, I_2(\ell m \ell' m)\left[\alpha R^{(1)}(\ell\ell') + 2Q\, R^{(1)}(\ell\ell')\right]. \tag{7.62}$$

To evaluate the radial integrals $R^{(n)}(\ell_i \ell_j)$, we introduce Bessel functions of the first kind via

$$j_\ell(kr) = \sqrt{\frac{\pi}{2kr}}\, J_{\ell+\frac{1}{2}}(kr) \tag{7.63}$$

and use the integral[15]

$$\int_0^\infty J_\mu(at)\, J_\nu(at)\, t^{-\lambda}\, dt = \frac{a^{\lambda-1}}{2^\lambda}\,\Gamma(\lambda) \cdot \frac{\Gamma\left(\frac{\nu+\mu-\lambda+1}{2}\right)}{\Gamma\left(\frac{\mu-\nu+\lambda+1}{2}\right)\Gamma\left(\frac{\nu-\mu+\lambda+1}{2}\right)\Gamma\left(\frac{\mu+\nu+\lambda+1}{2}\right)}, \tag{7.64}$$

which is finite and exists provided that

$$\mu + \nu + 1 > \lambda > 0 \quad \text{and} \quad a > 0. \tag{7.65}$$

In our case, this excludes the possibility $\ell_i = \ell_j = 0$. Using the well-known properties of the gamma function, e.g., $\Gamma(n+1) = n!$ for non-negative integers n, we find

$$R^{(1)}(\ell_i \ell_j) = \frac{\pi}{8}\, \frac{\Gamma\left(\frac{\ell_i+\ell_j}{2}\right)}{\Gamma\left(\frac{\ell_i-\ell_j+3}{2}\right)\Gamma\left(\frac{\ell_j-\ell_i+3}{2}\right)\Gamma\left(\frac{\ell_i+\ell_j+4}{2}\right)} \tag{7.66a}$$

$$R^{(2)}(l_i l_j) = \frac{\pi k}{8} \frac{\Gamma\left(\frac{l_i+l_j-1}{2}\right)}{\Gamma\left(\frac{l_i-l_j+4}{2}\right)\Gamma\left(\frac{l_j-l_i+4}{2}\right)\Gamma\left(\frac{l_i+l_j+5}{2}\right)} \quad . \tag{7.66b}$$

These can be simplified as

$$R^{(1)}(l_i l_j) = \frac{\pi}{8} \frac{1}{n(n-1)\Gamma\left(\frac{l_i-l_j+3}{2}\right)\Gamma\left(\frac{l_j-l_i+3}{2}\right)} \tag{7.67a}$$

$$R^{(2)}(l_i l_j) = \frac{\pi k}{4(2n-1)} \frac{\Gamma(n+\frac{1}{2})}{\Gamma(n+2+\frac{1}{2})\Gamma\left(\frac{l_i-l_j+4}{2}\right)\Gamma\left(\frac{l_j-l_i+4}{2}\right)} \quad , \tag{7.67b}$$

where we have defined an integer

$$n = \frac{1}{2}(l_i + l_j) \tag{7.68}$$

and used various other properties of the gamma function.

Equations (7.67) in conjunction with (7.62) enable us to evaluate $\underset{\sim}{K}$ in the Born Approximation at any desired energy and for any symmetry except Σ_g [recall the limitation imposed by Eq. (7.65)]. Given the K-matrix we can obtain the T-matrix using the formulas of section 6.5 and the total cross section using the results of section 7.2.

Alternatively, we can diagonalize the K-matrix, take the arctangent of the eigenvalues, and thereby obtain the eigenphases η_i. Then the cross sections for each symmetry can be obtained from[17]

$$\sigma^{(m)} = \sum_j \frac{4\pi}{k^2} \sin^2 \eta_j \,. \tag{7.69}$$

Notice that for $m \neq 0$, $\sigma^{(m)}$ must be multiplied by 2 in computing σ_{tot} in order to take account of the two-fold degeneracy of molecular orbitals with $|m| > 0$.

In closing, let us note that a simple analytic form for the diagonal elements of the K-matrix in the Born Approximation obtains in the special case where we take account only of the quadrupole interaction term in Eq. (7.51), viz.,

$$K_{\ell\ell}^{(m)} = k \frac{Q}{5} (-1)^m \frac{2\ell+1}{\ell(\ell+1)} C(\ell\ell 2; 00)\, C(\ell\ell 2; m, -m). \tag{7.70}$$

The expression given above is useful for hand-checking the code which carries out BA calculations (called BORN01).

§7.6. Conclusion: The Asymptotic Decoupling Approximation

We mentioned in Chapter 6 that the so-called low-ℓ spoiling approximation, which assumes the asymptotic partial wave to be uncoupled and approaches the collision problem in this framework, is not expected to be valid in general for highly anisotropic targets such as CO_2. We shall look at calculations in an equivalent to this approximation in the next chapter. This is the asymptotic decoupling approximation (ADA).

In the ADA we go ahead and determine the full aymptotic T-matrix as in Chapter 6, taking into account all relevant interactions, but when calculating cross sections we uncouple the partial waves in the asymptotic region. There are two ways to effect this: we can introduce the eigenphases, replacing $T_{\ell\ell'}^{m}$ with

$$T_{\ell\ell'}^{m} = \delta_{\ell\ell'}\left(1 - e^{2i\eta_{\ell m}}\right) \tag{7.71}$$

or, equivalently,

$$T_{\ell\ell'}^{m} = \delta_{\ell\ell'}\left(1 - \cos 2\eta_{\ell m} - i \sin \delta_{\ell m}\right). \tag{7.72}$$

An alternate procedure is to simply set $T_{\ell\ell'}^{m} = 0$ for $\ell \neq \ell'$ in Eqs.(7.11) etc. This is preferable in general since we cannot always uniquely associate each eigenphase shift with a single partial wave for e-CO_2. (This is, in general, possible for less anisotropic cases such as H_2 or, perhaps, N_2.)

This concludes the theoretical edifice in which we choose to study electron-molecule collisions. We now turn to the results obtained from the calculations outlined in Chapters 3 through 7.

Chapter 8. Electron-CO_2 Collisions: Results and Discussion of the Calculation

> Our sum machines never drop a figure, nor our looms a stitch; the machine is brisk and active, when man is weary; it is clearheaded and collected, when man is stupid and dull; it needs no slumber, when man must sleep or drop...
>
> -Erewhon
> (Samual Butler)

§8.1. Introduction

In this chapter, we finally turn to the details of the e-CO_2 calculations we have performed and the results thereby obtained. The background for the discussions herein has been laid in Chapter 2 - 7, and we shall assume familiarity with this material.

Because of the rather large amount of material to be presented here, this chapter is divided into two main sections. Following this brief introduction, we begin in section 8.2 with a detailed analysis of the technical aspects of the computations.

This part will hopefully serve as a guide to carrying out electron-molecule calculations in the theoretical framework heretofore outlined and focuses primarily on numerical procedures and facets of the calculation which were not addressed in earlier chapters, especially the question of convergence. [See especially sections 3.6, 3.7, 4.5, 6.6, 6.7, and 8.2 for details.] Of course, e-CO_2 is used as an example throughout. In section 8.3, we present our final converged cross sections and related quantities for the e-CO_2 problem. It is here that we address various physical questions associated with the collision and try to see what can be learned from all this work. Thus, §8.2 is recommended to readers gearing up to perform their own calculations and §8.3 to those interested in physics.

It is impossible to present all the numbers we obtained throughout various stages of the calculations; the convergence tests alone would fill a small library. We have chosen to supply a large selection of results in the "physics section" 8.3 and to try to give enough detail in section 8.2 to justify our assertions and conclusions.

We shall be looking at several types of cross sections (see Chapter 7) in the course of this chapter. In addition to the total and momentum transfer cross sections, σ_{tot} and σ_{mom}, respectively, we shall focus on $\sigma_\eta^{(m)}$, where η = g or u for gerade or ungerade symmetry respectively. These cross sections are defined for a particular symmetry (c.f., section 6.2) such as Σ_g (m = 0,

$\eta = g)$, Π_u ($m = 1$, $\eta = u$) etc. At one level more basic, we may have occassion to comment on particular partial wave contributions to the cross section, $\sigma_{\ell\ell'}^{(m)}$. These quantitues are related to T-matrix elements by

$$\sigma_{\ell\ell'}^{(m)} = \frac{\pi}{k^2} |T_{\ell\ell'}^{m}|^2 .$$

Finally, we shall look at eigenphases and their sums for particular symmetries (see section 7.1). Although a certain amount of physical insight can be derived from cautious use of these quantities, their primary usefulness (in our opinion) is in convergence studies of the sort discussed in the next section.

The numbers here reported were obtained in the body frame of reference in Chapter 6. We initially began our studies in the lab frame, and a few numbers and conclusions from this early work appear in Appendix 2 along with a derivation or two. However, as we studied the problem it became apparent that the nature of the interaction potential necessitated partial waves with very large values of ℓ in the interior region. In the lab frame, this means an enormous number of channels, because each additional rotational state introduces only a few channels. In the body frame, the number of partial waves is equal to the number of channels. Since about the same number of partial waves are required in the two frames, it follows that the convergence problems are less severe in the body frame. Finally, one should keep in mind that owing to the very small spacing of the rotational energy levels in CO_2 (see Chapter 2), there are on the

order of 100 open rotational channels in the lab frame at a scattering energy of only 0.01 Ryd. [Of course, not all of these (by any means) are required for convergence. See reference (1).]

§8.2. Low-energy Electron-Molecule Scattering: Technical Aspects.

The computer program used to carry out these calculations exists in both lab- and body-frame versions. In both cases, we made very extensive tests of the program using e-H_2 scattering as our "benchmark" case. These included:

(1). lab-frame tests at scattering energies from 0.03 Ryd. to 1.5 Ryd with and without polarization for comparison with the results of Lane and Geltman;[2]

(2). body-frame tests in the same energy range for comparison with the results of Tully and Berry;[3]

(3). body-frame tests including exchange as described in Chapter 4 for comparison with cross sections of Hara[4] and with results of Henry and Lane.[5]

In all cases, agreement was excellent.

This code has provisions for variable step size in the integration mesh. It is necessary to have a fairly tight mesh in the region of strong potential, especially near r = 0 and near the nuclear singularities. The final integration mesh used in these calculations (including long-range interactions) is (in units of a_o)

0.0	to	0.02	in steps of 0.001
0.02	to	3.00	in steps of 0.01
3.00	to	27.0	in steps of 0.1
27.0	to	90.0	in steps of 0.2
90.0	to	130.0	in steps of 0.5

The choice of $r = 130\ a_o$ as a final integration point was determined by examining T-matrix elements, eigenphases, and cross sections at integration points r_i and r_{i+1} and letting i increase until our convergence criterion was met. Convergence will be discussed in detail below; for now let us remark that unless otherwise stated all cross sections we present will be converged to better than 1%.

At the outset, we calculated cross sections for several values of m, choosing to concentrate on two scattering energies, 0.005 Ryd. and 0.05 Ryd. It fast became apparent that the contribution to the total cross section due to values of $m > 1$ was negligible at the scattering energies of interest. For example, at 0.005 Ryd. the converged total cross section in the static-exchange approximation ($\alpha_0 = \alpha_2 = 0$) including Σ and Π symmetries is 50.9941 a_o^2, while the contribution from $m = 2$ is 0.9426 a_o^2, and that from $m = 3$ is 0.3002 a_o^2. Similar results obtain at other energies and with the inclusion of polarization (see Chapter 5). Therefore we shall focus on Σ_g, Σ_u, Π_g, Π_u symmetries.

We can easily understand the relative importance of low-m

symmetries from elementary effective potential arguments such as those of section 3.7. For m greater than 2, the effective potential is essentially pure barrier, so the electron in a high-ℓ partial wave is unable to "feel" the strong short-range potential directly (see Figure 3.9). Of course, the long-range forces still have some effect on the scattering wavefunction, but in the final analysis this is less important than that of the short-range forces.

The initial convergence studies were carried out in an artificial potential obtained by using the static e-CO_2 potential of Chapter 3 without the r^{-3} quadrupole tail. Since we were primarily interested at this stage in acquiring a feel for the problem, this potential seemed desirable, primarily because it is necessary to integrate only to 15 a_0 to converge the cross sections in r. The procedure we adopted was to freeze N_λ, the number of expansion coefficients in the expansion of the static potential, Eq. (3.39), and study convergence in N_{cc}, the number of coupled channels (= the number of partial waves) included in the calculation. The resultant behavior is seen in Table 8.1, which shows cross sections at 0.05 Ryd. with λ = 0, 2, 4, and 6 included, indicating that convergence is smooth but that cases with far too few states give results which are off by as much as 50%. It is not satisfactory, in other words, to merely freeze N_{cc} and do the calculation; convergence tests are mandatory.

Of course, the problem solved in this table is not e-CO_2

Symm. \ N_{cc}	2	3	4	5	6	7	8	9
Σ_g	5.2278	86.7671	76.1237	69.8322	68.7291	68.4519	68.3818	68.3717
Σ_u	0.0776	0.0111	0.0006	0.0008	0.0018	0.0022	0.0028	0.0030
Π_g	3.2(-4)	4.5(-4)	0.0020	0.0329	1.1554	0.1119	0.0846	0.0812
Π_u	20.9103	59.8970	20.6928	5.8042	3.7624	3.3697	3.3027	3.2929
Δ_g	1.1(-4)	1.1(-4)	1.1(-4)	1.2(-4)	1.2(-4)	1.2(-4)	1.2(-4)	1.2(-4)
Δ_u	1.0(-8)	1.0(-8)	1.0(-8)	1.1(-8)	1.1(-8)	1.1(-8)	1.1(-8)	1.1(-8)
Total	26.2162	146.6760	96.8193	75.6703	73.6490	71.9359	71.7716	71.7784

TABLE 8.1

Cross Sections $\sigma^{(m)}$ and σ_{tot} in the static approximation with q = 0 in units of a_o^2 . The scattering energy is 0.05 Rydbergs. N_{cc} is the number of channels. The final converged cross section for this case is 71.7449 a_o^2. Included are coefficients for λ = 0, 2, 4, and 6.

scattering even in the extreme static-no-quadrupole approximation; it is some artificial problem defined by a potential with only four expansion coefficients in the potential energy. The results do illustrate the large number of channels required for even this simple case. When one recalls (from Chapter 3) that the final converged potential energy required up to $\lambda_{el} = 28$ and $\lambda_{nuc} = 80$, this comment begins to acquire some perspective.

To study convergence as we approach the true e-CO_2 potential in this model, we increased N_λ, converging the cross sections in N_{cc} at each stage in the calculation. In Table 8.2, we show cross sections for N_λ up to 10; again, the purpose here is to illustrate the convergence behavior of the problem. It is worth noting from these two tables that, as expected, large-m contributions to the cross sections are small and converge most rapidly. Moreover, we find that for a particular value of m, the "bonding symmetries" (Σ_g, Π_u, Δ_g, etc.) converge more slowly than do the "non-bonding symmetries". This is readily understood; for example, Σ_g symmetry corresponds to m = 0, ℓ = 0, 2, 4,..., while Σ_u corresponds to m = 0, ℓ = 1, 3, 5,... Clearly, the symmetry with the s-wave contributor will be most affected by the short-range potential. Alas, it is true that the most important contributors to the total cross sections are invariably those which converge most slowly. In point of fact, the cross sections of Table 8.2 certainly are NOT converged.

In the course of obtaining these results, we first encountered

Symm. \ λ_{max}	2	4	6	8	10	12	14	16	18
Σ_g	48.8966	94.1177	68.3702	59.6961	54.7470	51.6689	49.7088	48.4416	47.6084
Σ_u	0.3159	0.0520	0.0030	0.1045	0.4805	2.0771	25.8069	20.4357	3.2939
Π_g	0.07387	9.5032	0.0867	0.3476	0.0689	0.0102	0.0045	0.0029	0.0022
Π_u	7.3529	4.6366	3.2916	4.0311	7.7086	17.6299	40.9668	89.5212	174.3648
Δ_g	7.4(-5)	1.4(-4)	1.2(-4)	1.2(-4)	1.2(-4)	1.1(-4)	1.1(-4)	1.1(-4)	1.1(-4)
Δ_u	8.4(-7)	8.5(-8)	1.1(-8)	1.0(-8)	1.0(-8)	1.0(-8)	1.0(-8)	1.0(-8)	1.0(-8)
Total	56.6392	108.3100	71.7449	64.1796	63.0052	71.3862	116.4872	158.4016	225.2694
N_{cc}	6	9	11	13	15	17	18	20	20

TABLE 8.2

Cross sections in a_o^2 at 0.05 Ryd. for $\lambda = 0, 2, \ldots, \lambda_{max}$ using $v_\lambda(r)$ for e-CO_2 scattering. Only short-range static interactions are included, and all cross sections are converged in number of partial waves to better than 1%, and the final row shows the number of channels required for this criterion.

the need for the transformation-truncation procedure of section 6.5. For values of λ_{max} up to and including 8, the transformation procedure made only very small changes, and those in the smaller contributions of $\sigma_{\ell\ell'}^{(m)}$ to the final cross sections. For calculations including more coefficients in the potential energy, the procedure is necessary. The clue to its importance comes from an examination of the inverse of $\underset{\sim}{I}^2$ at r_{max}. We recall from section 6.5 that this quantity is required for calculation of the K-matrix a la Eq. (6,75). We found that for large N_λ, the product of this matrix and its inverse, which should be the unit matrix, had huge off-diagonal elements, typically of the order 10^3 to 10^5; i.e., the inversion was not proceeding as it should. Fortunately, it is invariably elements corresponding to high-ℓ partial waves that are most affected.

A very important question in implementing this procedure is where (and how frequently) one must transform. We initially tried transformation at only one point and found that if we waited "too long" to transform (i.e., choose too large an r_{trans}), the results were incorrect. For example, Table 8.3 shows an 11-channel short-range-only case with six terms in the potential expansion. For this potential, we found that within the range $r_{trans} = 0.1\ a_o$ to $r_{trans} = 1.0\ a_o$, cross sections are independent of where we carry out the transformation. Also shown in the table are some multiple-transformation runs. In general, it is mandatory to do multiple transformations for strong and highly anisotropic potentials

Symm. \ r_{trans}	0.1[a]	1.0	1.5	1.7	2.0	4.0	5.0	6.0	7.0	11.0
Σ_u	0.4789	0.4789	0.4789	0.4795	0.2721	0.8230	0.3534	0.6790	0.3888	0.6353
Π_u	7.7711	7.7711	7.7711	7.7757	14.8702	0.4930	0.4238	0.3345	0.4984	28.6388
Total	8.2500	8.2500	8.2500	8.2362	15.1424	1.3161	0.7772	1.0135	0.8872	29.2741

Symm. \ r_{trans}	1.0(5.0)[b]	2.0(2.0)[b]	9.0(2.0)[b]	(3,6)[b]	300(300)[c]
Σ_u	0.4789	0.2721	0.2665	0.4789	0.2176
Π_u	7.7711	14.8702	0.5877	7.7711	0.4689
Total	8.2500	15.1424	0.8542	8.2500	0.6865

TABLE 8.3

Cross sections in a_o^2 for $N_c = 11$, $\lambda_{max} = 10$, $q = 0$, ungerade symmetry at $k^2 = 0.05$ Ryd. illustrating results of transformation procedure. In the top rows, we transform only once, at $r = r_{trans}$.

(a). Results at 0.1, 0.2, 0.30, 0.5, 0.7, 0.9, 1.0, and 1.5 are identical.
(b). Transform every 5.0 a_o beginning at 1.0, etc.
(c). Stabilize every 3 points inside the barrier and every 6 outside.

in electron-molecule scattering; the reasons for this were discussed in Chapter 6. However, if one waits too long to do the first transformation, all is lost - the I^2-matrix will not be invertible regardless of what one does. Finally, it is interesting to observe from the table that in this example, where we include only six $v_\lambda(r)$ coefficients, it is possible to achieve the same results by frequent stabilizations. For more realistic potentials, this is not the case, and, in fact, when long-range terms are included one must both stabilize and transform to avoid numerical instability.

The final version of the transformation procedure simply incorporates an input variable, N_{trans}, which tells the code to transform every N_{trans} points in the integration (quadrature). Similar parameters define the frequency of stabilization within and beyond the limit of the centrifugal barrier.

The truncation procedure is easier to implement and quite reasonable physically, since, as we suggested in Chapter 6, one can reliably use the effective potential as grounds for such truncation. We simply introduce a truncation radius, r_{trunc}, and, at this point in the integration, throw away all channels in the physical wavefunction with $\ell \geq \ell_{max}$, the latter being a second parameter of input. Several examples can be found in Table 8.4 for the same case used to illustrate the transformation in Table 8.3.

As we saw in Chapter 3 (section 3.7), the effective potential is different for different symmetries. This must be kept in mind in determining the two truncation parameters. For example, in the

ℓ_{trunc} \ r_{trunc}	2.0	4.0	10.0	∞(a)
9	0.0727(Σ) 77.8271(Π)	0.4789(Σ) 7.7712(Π)	0.4789(Σ) 7.7711(Π)	0.4789(Σ) 7.7711(Π)
3		0.4754(Σ) 7.7727(Π)		
7		0.4788(Σ) 7.7717(Π)		
13		0.4789(Σ) 7.7711(Π)		

TABLE 8.4

The truncation approximation illustrated for N_{cc} = 11, λ_{max} = 10, ungerade symmetry at k^2 = 0.05 Ryd. Short-range static interactions only are included. All channels with $\ell \geq \ell_{trunc}$ are removed at $r = r_{trunc}$.
(a). No truncation.

full static-exchange-with-polarization calculations, to be discussed below, we found $\ell_{trunc} = 10$ to be satisfactory for Σ_g, Σ_u, and Π_u symmetries, but $\ell_{trunc} = 16$ was required for Π_g symmetry over the energy range of interest. Throughout we choose $r_{trunc} = 4.0\ a_o$, although sensitivity checks suggest that values as small as $3.0\ a_o$ are satisfactory for some symmetries and energies.

When we include the long-range quadrupole interaction in our calculation, it becomes necessary to integrate to a considerable distance to achieve stable cross sections. We use $r_{max} = 130\ a_o$, which provides our usual better-than-1% convergence for the total cross sections. In this case, it is necessary to both transform and stabilize. This manifests itself in two ways:

(1). contributions $\sigma^{(m)}_{\ell\ell'}$ corresponding to large values of ℓ and ℓ' are unreasonably large;

(2). the T-matrix is not symmetric.

In part, these features reflect the fact that we must integrate over a much larger mesh when long-range interactions are incorporated in the calculation. Consequently there is greater opportunity for linear dependence to creep into the homogeneous solution being developed.

In such cases we still truncate at $4.0\ a_o$. Moreover, it is not necessary to transform at r values beyond r_{trunc}, since the truncation radius is well beyond the location of the nuclear singularities and the strong coupling, which mixes very small high-ℓ

components with very large low-ℓ components, won't be present.

Naturally, all of these conclusions are potential-dependent and must be checked as we include more and more expansion coefficients in the potential energy, or as we introduce different kinds of interactions (e.g., exchange). We shall not reproduce here all the convergence tests we carried out; suffice it to say that the parameters given when we do quote results correspond to the aforementioned convergence criterion.

In studies of polar molecule scattering (in particular, e-LiF collisions) in a laboratory frame, it has been found[16] that including long-range interactions improves convergence of the total cross sections in N_λ, allowing convergence by $\lambda_{max} = 8$ at low energies. This is not the case for e-CO_2 collisions, as attested by Table 8.5, which presents cross sections in a model potential defined by augmenting $v_2(r)$ with a q/r^3 interaction with $q = -3.85981$ au and $r_c^q = 1.4\ a_o$, $p = 6$. Two energies a decade apart are studied.

Notice that here we actually converged one symmetry, Π_g, at 0.005 Ryd. In fact, cross sections corresponding to $m > 1$ are converged in this model by $\lambda_{max} = 14$ but contribute very little to the total cross section. It is clear from Table 8.5 that we are nowhere near a truly converged realistic e-CO_2 interaction potential.

A careful study of our particular short-range static expansion coefficients led to the separation of each coefficient into electronic and nuclear contributions (as discussed at length in section 3.6)

E = 0.05 Ryd

symm \ λ_{max}	14	16	18	20
Σ_g	9.8107	15.5461	22.9074	31.4859
Σ_u	52.6655	71.1432	93.2714	118.5601
Π_g	0.2091	10.3407	0.9419	0.6589
Π_u	9.7451	13.3127	18.1534	24.2224
Total	73.8456	111.7578	136.6891	176.3423
N_{cc}	16	17	18	19

E = 0.005 Ryd

symm \ λ_{max}	14	16	18	20	22	24	26
Σ_g	9.2877	17.1737	27.5739	40.1108	54.6637	71.1237	89.5775
Σ_u	11.5434	12.2994	13.0034	13.7248	14.4646	15.2167	15.9846
Π_g	0.3615	0.3835	0.3798	0.3792	0.3789	0.3788	0.3789
Π_u	4.4684	4.9165	5.6182	6.7965	8.9211	13.3933	25.2019
Total	26.9509	36.1380	47.9401	62.3761	79.7930	101.4772	132.5076
N_{cc}	16	17	18	19	20	21	22

Table 8.5

Cross sections in a_o^2 at two energies showing convergence behavior in λ_{max} in a model potential incorporating a $1/r^3$ long-range interaction. Total cross sections include m = 2,3,4, and 5 contributions. [N_{trans} = 7, r_{trunc} = 7, r_{trunc} = 4.0, ℓ_{trunc} = 10, r_{max} = 130 a_o, N_{stab} = (3,6); r_c^q = 1.4, p = 6].

and consequently to the convergence of the potential. This is illustrated in Table 8.6, which shows cross sections at 0.05 Ryd. in our old short-range (q = 0) model potential and in the q = 3.85981 model. Clearly, convergence is at hand. In fact, one can obtain cross sections converged to within 5% with a maximum electronic λ of 22 and nuclear λ of 60. For our 1% criterion, we choose maximum values of 28 and 80, respectively. We have found in all cases that this is adequate. The behavior of the cross sections at our lower test energy of 0.005 Ryd. were similar to those shown in Table 8.6. This step was one of the key advances in performing the calculation, and without it converged cross sections would not have been attained.

Using the above facts and techniques, we were able to calculate cross sections in the true static e-CO_2 potential. These results will be presented and discussed in the next section.

Before turning to a look at exchange, perhaps a word about eigenphases is in order. Thus far we have not presented any of these here, although we did calculate them in our program. For studies such as those of this section, the eigenphases are moderately useful as indicators that convergence in the cross sections is near. However, they converge sooner than do the cross sections of physical interest. Thus a 1% difference between two eigenphases (or eigenphase sums) in a convergence study may signify a 10% - 20% discrepency in the cross sections. This is particularly acute at low energies. Nevertheless, eigenphases have their usefulness, and we shall present

λ_{nuc} / symm	q = 0				q = 3.85981				
	40	50	60	70	40	50	60	70	80
Σ_g	45.7125 (45.6877)	45.6472	—	—	139.9995	173.2146	187.6373	191.8965	193.0149
Σ_u	0.1847	0.1520	0.1400	0.1367 (0.1338)	—	—	—	192.3641	190.9954
Π_g	0.0013 (0.0013)	—	—	—	0.5026	0.4971	0.4961	0.4959	--
Π_u	456.8214	429.9505	424.1398	423.2734 (423.1910)	—	—	—	109.9524	110.0790

Table 8.6

Cross sections in two model potentials (with and without long-range interaction) at 0.05 Ryd using N_{cc} = 24 and a maximum electronic λ of 28. In this table, λ_{nuc} is the maximum λ for which nuclear contributions were included in $V(\vec{r})$. (Other parameters are the same as for Table 8.5). The numbers in parentheses show corresponding calculations for $\lambda^{e\ell}_{max}$ = 26.

some in the sequel.

Incorporating exchange via a local potential as outlined in Chapter 4 has a considerable effect on the cross sections, as we shall see in the next section. Of concern at present is the effect on convergence of said cross sections in number of channels. Since on the whole the exchange contribution deepens the potential (i.e., makes it more attractive) we expect to need more channels. Sure enough, this is precisely what happens, and we encounter as a result a whole host of new numerical problems, most of which were dealt with in section 6.7.

The AAFEGE potential, which was dropped on theoretical grounds (see section 4.4) is the stronger of the two local exchange potentials we considered and hence the most difficult to converge. This is suggested by the results of Table 8.7. [It is worth reminding ourselves how important stabilization can be. To this end, we show in parentheses in this table a couple of results for 25 channels without stabilization.] Having chosen not to study the AAFEGE potential further, we proceeded to try to converge the HFEGE potential case.

This suddenly brought up the exploding Neumann functions previously introduced in section 6.7D. To suggest the regions of r where this becomes a problem, we show in Table 8.8 that value of r at which the Ricatti-Neumann function exceeds 10^{300} for two values of k and for several values of N_{cc} and ℓ_{max}. This led us to introduce the Neumann cutoff procedure described in Chapter 6.

Sym \ λ_{max}	24	26	28
Σ_g	44.8814 (221.0895)	50.5032	60.4535
Σ_u	7.3655 (7.4865)	7.3017	—
Π_g	0.3304 (0.3304)	0.3303	0.3302
Π_u	3.9433 (3.3535)	3.9437	—
Δ_g	1.1019	—	—
Δ_u	0.0447	—	—

TABLE 8.7

Static-exchange cross sections in a_o^2 using the AAPTAE: a convergence study. The energy is 0.05 Ryd., $q = 3.89981$ a.u. with $r_c^q = 4.0\ a_o$ and $p = 6$. Included are short-range expansion coefficients up to $\lambda_{eff} = 28$ and $\lambda_{nuc} = 80$. [$N_{trunc} = 7$, $r_{trunc} = 4.0$, $\lambda_{trunc} = 10$, $N_{stab} = (3,6)$, $r_{max} = 130\ a_o$]. Numbers in parentheses for $N = 25$ show results without stabilization.

N_{cc}	ℓ_{max}	r_{cut} $k^2 = .005$	r_{cut} $k^2 = .05$
29	56	0.001	—
30	58	0.002	—
31	60	0.003	0.001
32	62	0.004	0.001
33	64	0.006	0.002
34	66	0.009	0.003
35	68	0.013	0.004

TABLE 8.8

Radii r_{cut} at which the Ricatti-Neumann function exceeds 10^{312} for two energies. N_{cc} is the number of channels which would be included in a calculation corresponding to the values of ℓ_{max} and r_{cut} shown.

Our first thought was to simply use the largest available number, 10^{312}, as a cutoff constant. However, curiosity regarding the procedure led us to try to determine just how low we could set this constant. The results were rather suprising, to say the least. As Table 8.9 reveals, a very small cutoff constant, say, 10^{130}, must be reached before the results deteriorate. Even more suprising is the observation that reducing this constant can resolve numerical difficulties which would otherwise produce divergent cross sections in Σ_g symmetry as N_{cc} is increased. This is a result of some importance, since this contribution to the various cross sections of interest to us is by far the largest at low energies. Thus, in Table 8.10 we see that a cutoff exponent of 240 gets us much closer to convergence than does 312.

A couple of ancillary points should be mentioned at this juncture. First, the divergence seen in Table 8.9 is potential dependent. To demonstrate this, we returned to the static approximation at 0.005 Ryd., where we had converged Σ_g cross sections in the static approximation by $N_{cc} = 27$ and where none of the difficulties here under discussion were present. Using a cutoff of 10^{312}, we pushed N_{cc} up to 32 without obtaining peculiar behavior. Second, the symmetry of the T-matrix improved as we decreased the cutoff constant (provided that we did not go to the ridiculous extreme of, say, 10^{100}, which is simply too small). [Stabilization improves the symmetry of the T-matrix to the point that such lack of perfect symmetry as remains does not affect the cross sections.

	N_{cc} = 28		N_{cc} = 29	
n_c(exp)	σ^o	δ^o_{sum}	σ^o	δ^o_{sum}
No cutoff	42.6438	-0.1439	—	—
312	—	—	45.6207	-0.1485
308	42.6438	-0.1439	45.6188	-0.1485
300	42.6438	-0.1439	45.6064	-0.1484
290	42.5913	-0.1438	45.8203	-0.1488
280	42.5910	-0.1438	41.6021	-0.1422
260	42.5910	-0.1438	41.7236	-0.1424
240	42.5910	-0.1438	41.7237	-0.1424
200	42.5910	-0.1438	41.7237	-0.1424
150	42.5910	-0.1438	41.7237	-0.1424
130	42.5932	-0.1438	42.5931	-0.1438
100	51.3421	-0.1570	51.3421	-0.1570

TABLE 8.9

Cross sections and eigenphase sums for Σ_g symmetry at 0.005 Ryd. in the e-CO_2 static-exchange problem using the HFEGE. N_{cc} is the number of channels. Other parameters are the same as in Table 8.7. (Only the power of 10 for the Neumann cutoff parameter is shown in the leftmost column.)

n_c (exp) \ N_{cc}	28	29	30	31	32
312	42.6438	45.6207	50.5259	—	—
240	42.5910 (-0.1438)	41.7237 (-0.1424)	40.9753 (-0.1412)	40.3354 (-0.1402)	57.7477 (-0.1658)

TABLE 8.10

Convergence studies for two Neumann cutoffs in static-exchange (HFEGE) e-CO_2 scattering at 0.005 Ryd. Parameters are as in Table 8.9. The numbers in parentheses are eigenphase sums. Only Σ_g symmetry is included here.

One can live comfortably with asymmetry in, say, the third or fourth decimal places.] Third, sensitivity to the cutoff constant is greater for larger N_{cc}, as reflected in Table 8.9.

One must be careful to distinguish the divergent behavior of certain cross sections from the Neumann overflow. As we saw in the 28 channel case, it was in a sense coincidental that the two effects appeared simultaneously. Had we been working on a smaller computer, the Neumann overflow would have been discovered far sooner.

These results all suggest that we can converge our Σ_g cross sections (and other symmetries) via judicious choice of the cutoff constant. But what is the cause of the divergent behavior which we are trying to get rid of? Well, it too is tied up in the inversion of the I^2-matrix.

Recall that we first tackled this problem by means of the transformation procedure. To see that the inversion difficulty is back again, we showed that one can achieve the same result by transforming very fequently as he achieves by reducing the cutoff constant. Thus, if we set the constnat equal to 10^{312} (so the computer can caluculate all the numbers it requires) and sets $N_{trans} = 2$, we obtain precisely the same results (for several cases studied, i.e., the two in Table 8.9, for example) as with a constant of 10^{150} and $N_{trans} = 10$. Clearly, it is preferable from a monetary point of view to reduce the constant and keep the frequency of transformation as large as possible, since each additional transformation entails

inversion of a large matrix.

However pleasant it may be to just decrease the cutoff constant and watch ones cross sections converge, a word of caution is in order. We must repeatedly verify our choice of the cutoff constant, since this parameter is dependent on the potential, on the scattering energy, and on the number of channels. Fortunately, the range of valid choices for the constant for a particular calculation is quite large, so this problem is diminished considerably in actual practice.

There is still another way to address the problem directly, and that is to carry out the matrix manipulations (addition, multiplication, inversion, etc.) in double precision. This is perhaps the world's worst way to treat this situation, since on some machines (e.g., a CDC machine) double precision is a software rather than a hardware feature, and, as such, it is unbelievably time consuming. Nevertheless, we did verify that this produces the same results as the Neumann cutoff procedure in one case, $N_{cc} = 28$. [The run in question took on the order of 9 times as much computer time as did the corresponding single-precision calculation. Clearly, this isn't a feasible way to proceed in practice for production runs.]

In retrospect, the whole problem could have been avoided by scaling the Green's functions at small r. One could scale $\underset{\sim}{G}^1(r)$ up and $\underset{\sim}{G}^2(r)$ down or, alternately, simply calculate the product

$\underset{\sim}{G}^1(r) \cdot \underset{\sim}{G}^2(r)$, which is all that is needed until we reach the asymptotic region, where we must extract $\underset{\sim}{I}^2(r_{max})$ for inversion and calculation of the K-matrix. This poses no problem, though, since it is only at small r that this heinous problem arises.

Although induced polarization (see Chapter 5) has a considerable effect on the cross sections for electron-CO_2 scattering, it does not significantly alter the convergence behavior in N_{cc} discussed thus far. Essentially, this is because only $v_0(r)$ and $v_2(r)$ are affected by this interaction, and these are not greatly altered. Moreover, $v_2(r)$ already has taken into account a stronger long-range potential, the r^{-3} quadrupole interaction in the static potential.

This, however, brings us to one last important technical detail. There is in our definition of the contribution to the total potential energy due to induced polarization interactions a cutoff radius, which we call r_c^P. There is no ab-initio way to determine this parameter if one proposes to use the analytic form we have selected for the long-range potential energy. Of course, we could have arbitrarily declared there to be a particular region of space within which the static potential was to be some prechosen percentage of the full potential and adjusted r_c^P accordingly.

We chose instead to take advantage of the well-established 3.8 eV resonance in the Π_u symmetry. This so-called shape resonance corresponds to a quasi-bound state (crudely visualized, an electron trapped between the hump in the potential energy and the

origin) rather than to a negative energy state. We can adjust the position of this resonance by varying the polarization cutoff radius and thereby changing the term $v_2(r)P_2(\cos\theta)$. The polarization interaction, which is clearly treated semi-empirically in this formulation, has the net effect of making the electron-molecule interaction potential surface more attractive. This, in turn, causes the resonance to move down.

It turns out that the resonance is quite sensitive to the choice of polarization cutoff. This is illustrated in Figure 8.1 and the accompanying Table 8.11, which show the variation in the resonance energy and the cross section for selected values of r_c^p. We see from the table that the choice $r_c^p = 2.59\ a_o$ leads to a resonance energy of 3.8 eV, the experimentally determined value. For contrast, we also present in this table part of our studies at a slightly different resonance energy, 3.4 eV; we shall use this extra case to illustrate sensitivity of cross sections to the potential in the next section.

Notice that in a sense we scale only the Π_u symmetry, the potential thereby obtained being used for all symmetries over a wide range of energies with no further adjustment. This is especially important since, as we shall see, different symmetries dominate in different energy regimes. The symmetry here adjusted is dominant only in the vicinity of the resonance.

E_{res} = 3.8 eV

r_c^p	2.50	2.55	2.56	2.57	2.58	2.59	2.60	2.65
σ_u^1	16.9404	49.6280	61.5421	74.1833	84.8322	89.9101	87.4401	38.0579
δ_{sum}^1	-0.4790	-0.8717	-1.0093	-1.1748	-1.3661	-1.5736	1.3605	0.6625

E_{res} = 3.4 eV

r_c^p	2.40	2.50	2.60
σ_u^1	8.4286	98.0350	16.9069
δ_{sum}^1	-0.3078	-1.4328	0.3958

TABLE 8.11

Tuning of the Π_u resonance: cross sections and eigenphase sums for e-CO_2 scattering in the SEWP approximation using the HFEGE, with α_o = 17.9, α_2 = 9.19, q= -3.85981, r_c^q = 4.0, p = 6, N_{trans} = 7, r_{trunc_2} = 4.0, ℓ_{trunc} = 10, r_{max} = 130 a_o, and N_{cc} = 23. The cutoff radius is in a_o and cross sections in a_o^2. Eigenphase sums are in radians.

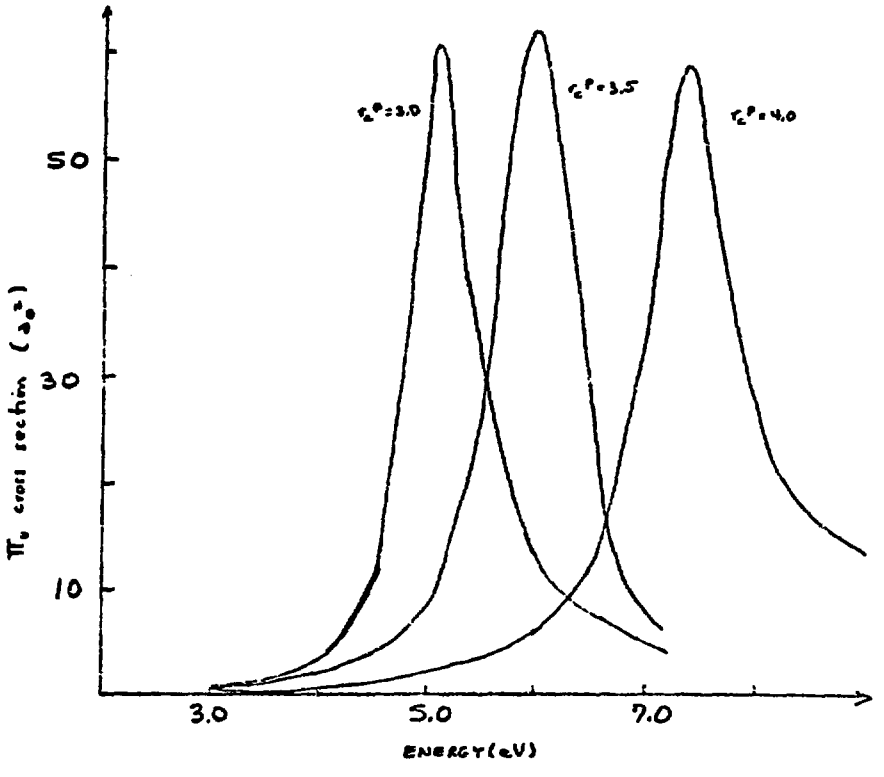

Figure 8.1

Cross Sections for e-CO_2 (Π_u symmetry) in the SEWP approximation showing the sensitivity of the behavior near resonance to the polarization cutoff parameter.

§8.3. The Final Converged Results for e-CO_2 Scattering

Having traversed in the last section the labarynthine paths of the computations we carried out, we can at last look at some final cross sections. Without further ado, we present in Table 8.12 converged cross sections for e-CO_2 scattering in all m = 0 and m = 1 symmetries for energies from 0.07 eV to 10.0 eV. There is a resonance at 3.8 eV in Π_u symmetry, as required. We shall refer to this as CASE 1 to distinguish it from the comparison calculations with E_{res} = 3.4 eV, which will cleverly be dubbed CASE 2. These cross sections are converged to less than 1% in Σ_u, Π_g, and Π_u symmetries and to better than 3% in Σ_g symmetry. The parameters for this (and subsequent) results are (once and for all)

α_0 = 17.9 au

α_2 = 9.19 au

q = -3.85981 au

$r_c^q = 4.0\ a_o$

$r_c^p = 2.59\ a_o$ (CASE 1) or $2.5\ a_o$ (CASE 2)

N_{cc} = 32 (Σ_g), 23 (Π_u), 14 (Σ_u, Π_g)

λ_{el}^{max} = 28

λ_{nuc}^{max} = 80

$r_{max} = 130\ a_o$

N_{trans} = 7

$n_c = 10^{250}$ (Neumann cutoff)

Symm \ E(eV)	0.07	0.1	0.5	1.0	2.0	3.0	3.5
Σ_g	226.7339	179.4213	37.9246	15.1480	6.8633	5.1104	4.6909
Σ_u	3.7153	3.4513	3.8029	6.0101	10.5967	13.9785	15.1616
Π_g	0.2106	—	0.1148	—	0.1136	—	0.0948
Π_u	9.3535	10.6070	12.6696	9.3535	4.6191	6.7117	30.5329

Symm \ E(eV)	4.0	5.1	5.9	8.0	10.0
Σ_g	4.3939	3.9877	3.8261	3.8702	5.3371
Σ_u	16.0546	17.1792	17.4502	16.8578	15.4439
Π_g	0.1332	0.3106	0.5096	1.2089	1.9802
Π_u	45.3868	4.7014	3.7754	4.6436	5.8722

TABLE 8.12

Converged cross sections (in a_o^2) for e-CO_2 scattering (Case 1). We use the parameters defined in the text.

$r_{trunc} = 4.0\ a_o$

$\ell_{trunc} = 10$

$N_{stab} = 6$

Exchange Potential = HFEGE potential

The corresponding eigenphase sums are presented (for completeness) in Table 8.13.

In Figure 8.2, we show graphs of these cross sections for Σ_g, Σ_u, and Π_u symmetries. The Π_g symmetry yields very small contributions, and is a special case which we shall take up below.

Before turning to a discussion of each symmetry in turn, it is worth glancing at Table 8.14 and comparing the results therein with those in Table 8.12. The former table presents cross sections at selected energies calculated in the Born Approximation. The related theory was presented in section 7.5. Clearly, the BA is quite unsuccessful for total cross sections. In contrast, it is true that one can reliably predict particular T-matrix elements in the Born Approximation. For example, for $|\Delta\ell| = 2$ and ℓ and ℓ' large, say, greater than 5, the T-matrix elements obtained at low energies agree with the coupled-channel results to four decimal places. (These are, however, less important by far than other elements, which is why the results of Tables 8.12 and 8.14 don't agree too well.) This suggests the possiblity of using the Born Approximation for certain channels and a more accurate procedure for others. A procedure like this has been used in electron-polar

symm \ E(ev)	0.07	0.1	0.5	1.0	2.0	3.0	3.5
Σ_g	0.2927	0.3120	0.2982	0.2279	0.1050	-0.0092	-0.0637
Σ_u	-0.0444	-0.0523	-0.1203	--0.2043	-0.3695	-0.5155	-0.5802
Π_g	-0.0068	--	-0.0096	--	-0.0013	--	-0.0198
Π_u	0.0377	0.0479	0.1225	0.1518	0.1546	0.2291	0.5641

symm \ E(ev)	4.0	5.1	5.9	8.0	10.0
Σ_g	-0.1157	-0.2170	-0.2754	-0.3405	-0.2509
Σ_u	-0.6400	-0.7552	-0.8269	-0.9781	-1.0905
Π_g	-0.0315	-0.0566	-0.0775	-0.1318	-0.1763
Π_u	-0.8611	-0.3377	-0.3356	-0.4236	-0.5236

Table 8.13

Eigenphase sums corresponding to the cross sections of Table 8.12 (Case 1). (Radians are used.)

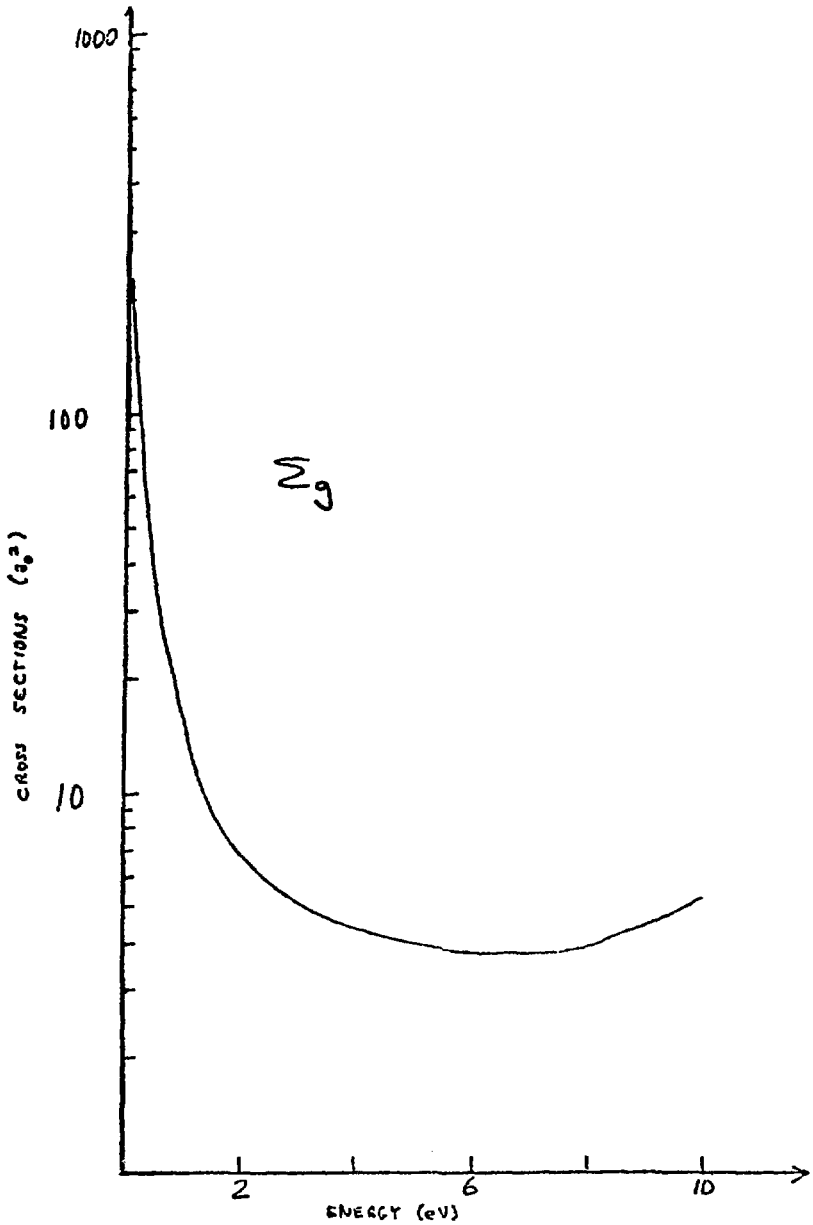

Figure 8.2

Cross sections for e-CO_2 in the SEWP approximation for Σ_g, Σ_u, and Π_u symmetries. The parameters for this calculation are defined in the text.

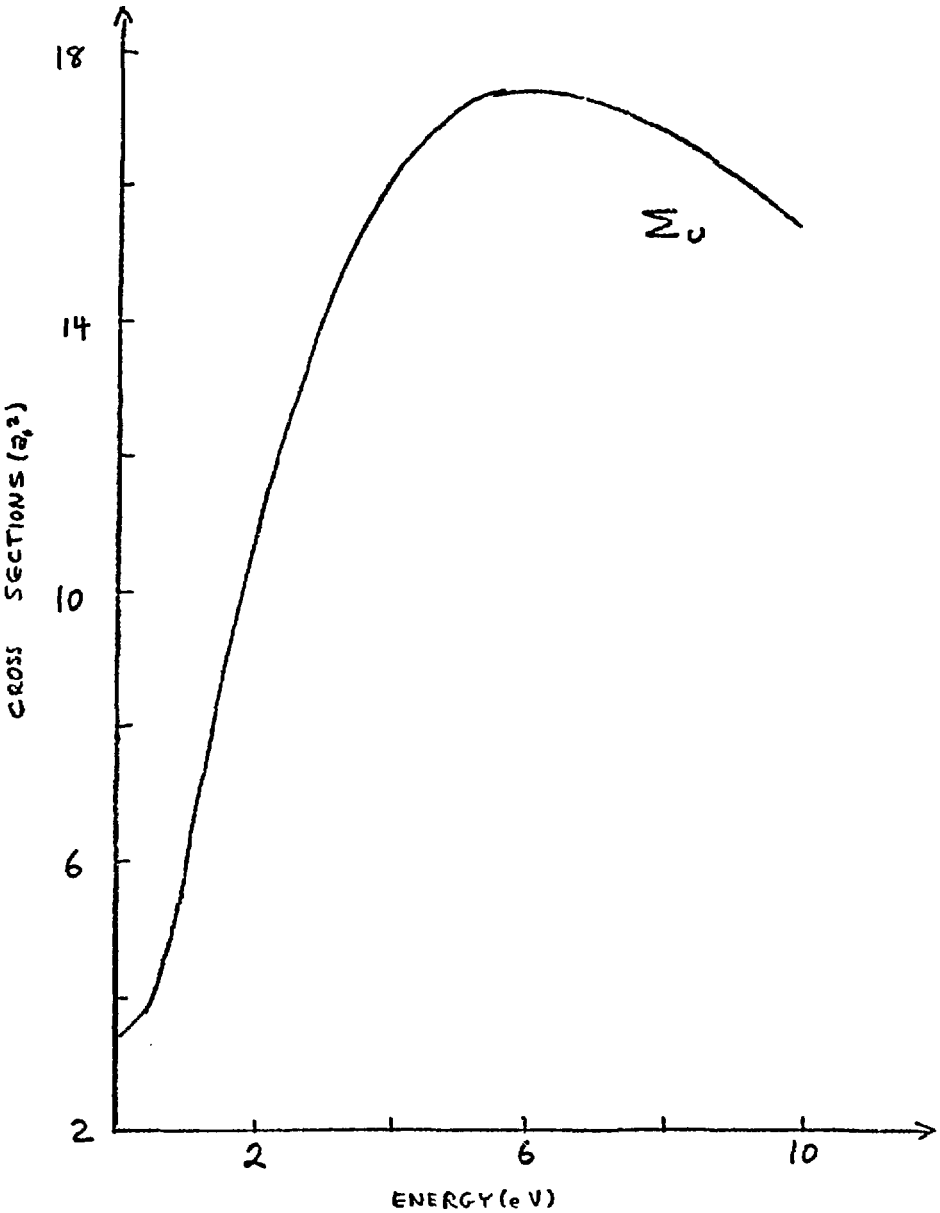
18
14
10
6
2
CROSS SECTIONS (a_0^2)
Σ_v
2
6
10
ENERGY (e V)

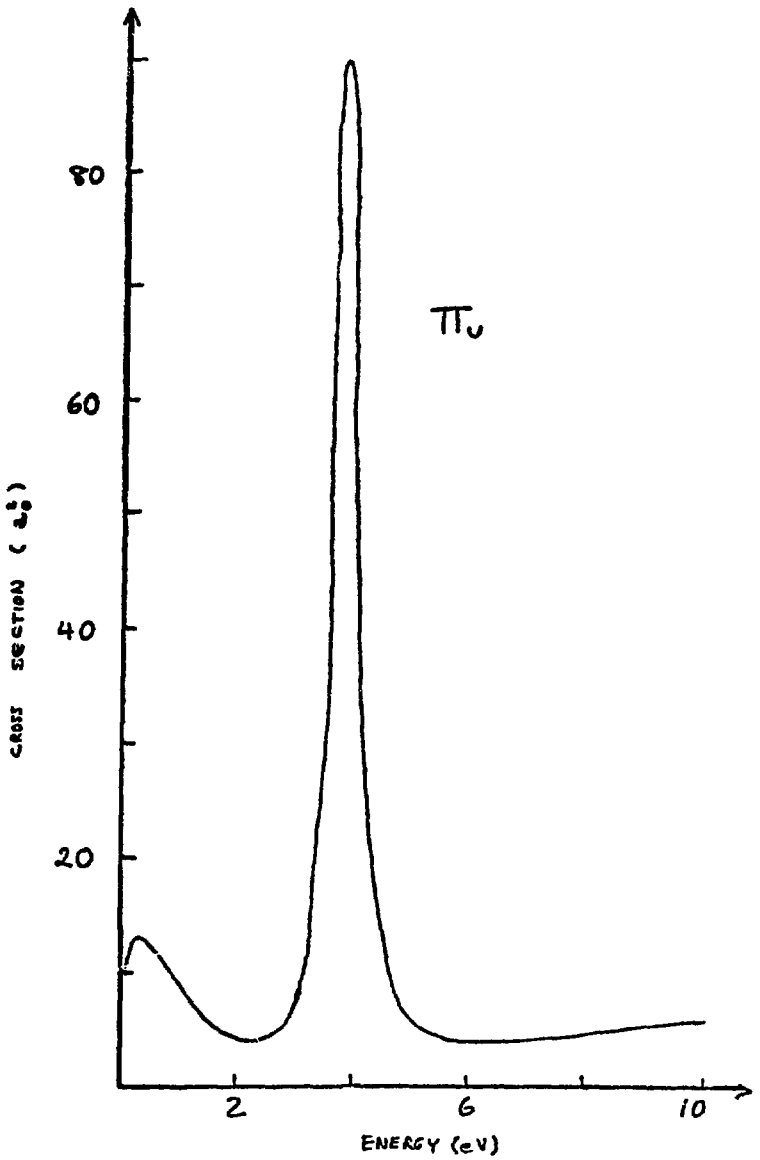
80
60
40
20
CROSS SECTION (a_0^2)
Π_u
2
6
10
ENERGY (eV)

symm \ E(ev)	0.07	0.1	0.5	1.0	2.0	3.0
Σ_u	2.7785 (3.7153)	2.1083 (3.4513)	0.3050 (3.8029)	2.6969 (6.0101)	10.3103 (10.5967)	16.3992 (13.9785)
Π_g	0.1987 (0.2106)	0.1760 --	0.1134 (0.1148)	0.1922 --	0.4868 (0.1136)	0.8550 --
Π_u	10.2075 (9.5901)	11.7177 (10.6070)	25.9399 (12.6696)	37.8507 (9.3535)	50.0600 (4.6191)	52.5170 (6.7117)

Table 8.14

Test of the Born Approximation for e-CO_2 scattering: cross sections in a_o^2 taking into account only long-range interactions (quadrupole and induced polarization). Numbers in parentheses are coupled-channel results from Table 8.12.

molecule scattering[8], but its extension to our problem is not transparent due to the overwhelmingly important partial wave coupling.

Before leaving the subject of the Born Approximation, it is worth pointing out that even the shape of the individual-symmetry cross sections vs. energy is wrong for most symmetries. There doubtless exists an energy low enough that the Born Approximation is valid for this problem, but it clearly is not 0.07 eV.

Certain features of the scattering fair leap out from the tables and graphs presented thus far. At low energies, below, say, 0.1 eV, the Σ_g symmetry is overwhelmingly dominant. In point of fact, it is scattering in this symmetry, largely due to short-range forces, which gives rise to the enormous low-energy cross sections observed in the experiments discussed in Chapter 2 (see the results for total and momentum transfer cross sections below). Convergence, as we saw in section 8.2, is slow but sure in this symmetry. The eigenphase sums are dominated by s-wave at the low energies, which is precisely the partial wave most affected by the short-range potential. At slightly higher energies (say, 0.1 eV to 1.0 eV) d-waves begin to contribute, and above a few eV, even g-waves are important.

Of considerable interest is the other "bonding symmetry", Π_u, for it is the resonant symmetry. Figure 8.3 shows the eigenphase sums for this symmetry in CASE 1 (the solid line) in a fashion which clearly shows the resonant behavior. Examination of the individual eigenphases and associated eigenvectors reveal that

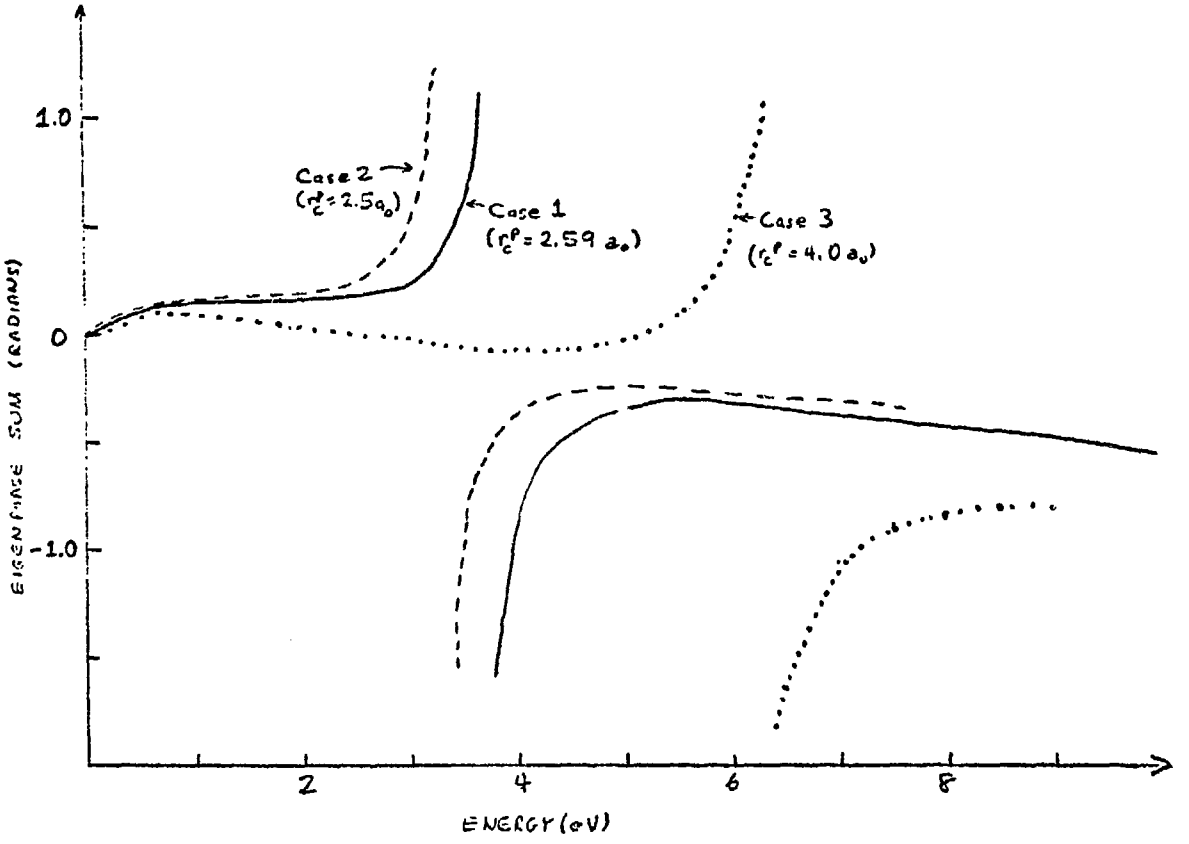

Figure 8.3

Eigenphase sums for e-CO_2 scattering in Π_u symmetry showing the sensitivity to the choice of polarization cutoff parameter. The SEWP approximation is used with parameters as defined in the text.

is a p-f resonance, about 60% p and 40% f.

The behavior of the eigenphase sum as energy decreases reflects the influence of the long-range forces, which begin to dominate as k^2 approaches 0. We see the sum increase from zero initially (all these results are modulo π), which is due to the repulsive r^{-3} quadrupole interaction. This is, in fact, predicted by the Born Approximation [see Eq. (7.55)]. As energy further increases away from zero, the attractive r^{-4} induced polarization interaction begins to take effect and pulls the sum down again. Eventually, it grows enormously as we approach the resonance energy, where it plumets through an integral multiple of π and, in the figure, goes negative. The behavior here elucidated is reflected in the cross sections of Figure 8.2c.

It is important to understand the sensitivity of such features as those we have been discussing to the potential and, in particular, to the one "arbitrary" feature of our efforts, the polarization cutoff radius. Such a comparison can be made with the aid of Table 8.15, which shows cross sections and eigenphase sums in CASE 2 for certain selected symmetries and energies which are displayed for CASE 1 in Table 8.12. (See also Table 8.13.) We should emphasize that the change in the potential between the two cases is very slight; we merely move the cutoff radius a mere 0.09 a_o closer to the origin. The effect is quite interesting.

There clearly are differences in the quantitative results.

	0.07	0.1	0.5	1.0	2.0	3.0	4.0
Σ_g	329.1171	259.3198	56.4800	23.2204	9.6117	6.1743	--
	(0.3589)	(0.3828)	(0.3797)	(0.3122)	(0.1932)	(0.0827)	--
Σ_u	--	3.4243	3.6920	5.8008	10.2579	13.5954	15.6793
	--	(-0.0521)	(-0.1185)	(-0.2009)	(-0.3633)	(-0.5074)	(-0.6304)
Π_g	--	0.1817	0.1101	0.1373	0.1283	0.0868	0.1078
	--	(-0.0081)	(-0.0067)	(-0.0035)	(-0.0015)	(-0.0058)	(-0.0222)
Π_u	9.6972	10.7700	13.4541	10.5369	6.5195	23.5981	9.3905
	(0.0380)	(0.0483)	(0.1267)	(0.1622)	(0.1868)	(0.4601)	(-0.3730)

Table 8.15

Cross sections in a_o^2 and eigenphase sums (in parentheses) in radians for e-CO_2 scattering in Case 2 (E_{res} = 3.4 eV and r_c^p = 2.5 a_o).

However, the important qualitative features remain unchanged, e.g., dominance of Σ_g at low energies and, as the dotted line in Figure 8.3 attests, the nature of the resonance.

These results suggest considerable sensitivity to the polarization cutoff, so it is worth trying one further case (called CASE 3). We choose here the rather extreme value of $r_c^p = r_c^q$, which, recall, was 4.0 a_o. This produces a rather considerable reduction in the polarization potential. We have chosen to examine only the resonant symmetry for this case, cross sections for which can be found in Table 8.16. The resonance is considerably broadened and moves up in energy to $\sim$6.0 eV (see the dotted curve in Figure 8.3).

A different sort of sensitivity study can be performed which addresses the energy dependence of the HFEGE potential [recall Eq. (4.39)]. Although calculation of this contribution is certainly not a major part of the total effort required to obtain cross sections at any one energy, it would be nice if we could ignore the energy dependence of the exchange potential and simply compute it once and for all. To study this possibility, we freeze E_i, the scattering energy in the definition of the exchange potential at 0.005 and calculate Π_u cross sections at a number of energies. The results, labelled CASE 4 in Table 8.16, are discouraging, and indicate that this is a poor way to proceed, except at the very lowest energies. In the work reported here the HFEGE potential is recalculated at each scattering energy.

E(eV)	0.07	2.0	3.0	3.5	4.0	5.0	6.0	6.5
Case 3	8.8997 (0.0358)	0.5995 (0.0391)	0.6862 (-0.0270)	1.3659 (-0.0527)	2.3314 (-0.0684)	5.9186 (-0.0310)	32.8714 (0.4817)	54.5505 (-1.6398)
Case 4	8.8997 (0.0358)	0.7560 (0.0492)	0.5716 (-0.0060)	1.1471 (-0.0228)	2.2205 (-0.1791	19.4999 (0.3290)	12.4425 (-0.6600)	-- --

Table 8.16

Cross sections in a_o^2 for two special cases chosen to reveal the sensitivity of e-CO_2 scattering to the potential. Case 3 corresponds to $r_c^p = 4.0\ a_o$. Case 4 is the same as 3 except that the HFEGE potential is held constant at $k^2 = 0.005$. The symmetry is Π_u.

We remarked above that Π_g symmetry was rather special. The first point to note is that the cross sections for this symmetry are the smallest of those under consideration; this is clear from Table 8.15. The cross section in CASE 2 appears in Figure 8.4, from which it is evident that these cross sections wiggle about more than the typical electron-molecule results. The reason for this behavior is that long-range interactions are more important for this symmetry than for the other three we have studied. It is also significant that more partial waves contribute equally (or nearly so) to scattering in this symmetry than in the others examined.

Further insight into this case can be gained by a study of the eigenphases. In contrast to the other three important symmetries, in Π_g scattering, there is no single dominant eigenphase in the sum. The two largest eigenphases together with the sum are shown in Figure 8.5, which clearly reveals considerable cancellation.

A second manifestation of this sensitivity to comparatively high-ℓ partial waves and to long-range forces is the need for a larger value of the truncation order than in other symmetries. For example, at 0.1 eV, the eigenphase sum is 0.0004, -0.1336, and -0.0035 for ℓ_{trunc} = 10, 12, and 16, respectively. The change in the cross section is not quite so great; we find cross sections of 0.1326 a_o^2, 0.1352 a_o^2, and 0.1373 a_o^2 for these three cases.

If one is satisfied with a less stringent convergence criterion than we here employ, these problems can be swept under the rug. As

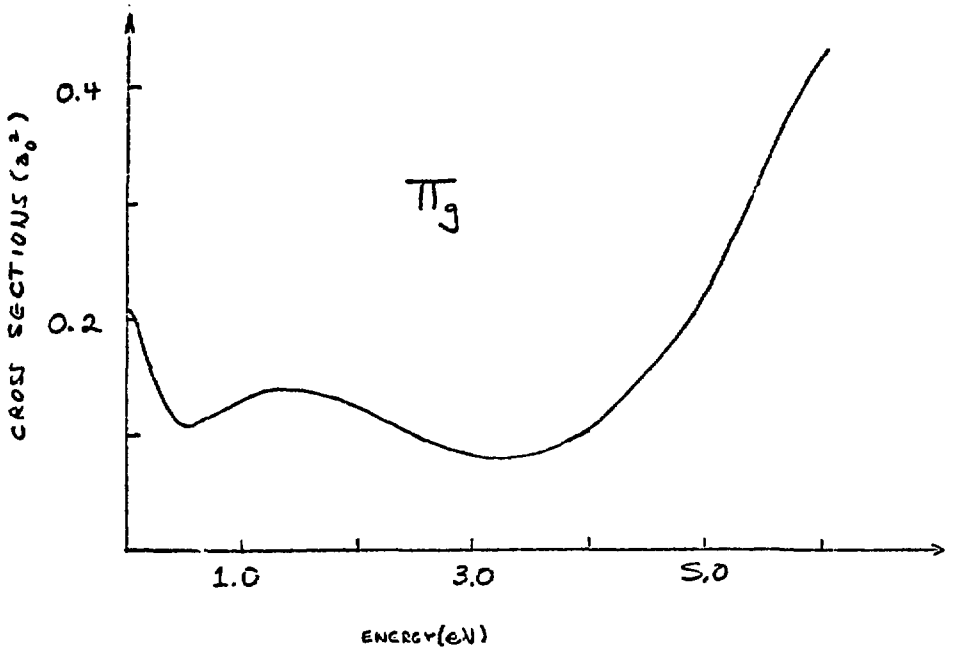

Figure 8.4

Cross sections in the SEWP approximation for e-CO_2 scattering (Π_g symmetry) using a cutoff parameter of $2.5a_o$ (CASE 2).

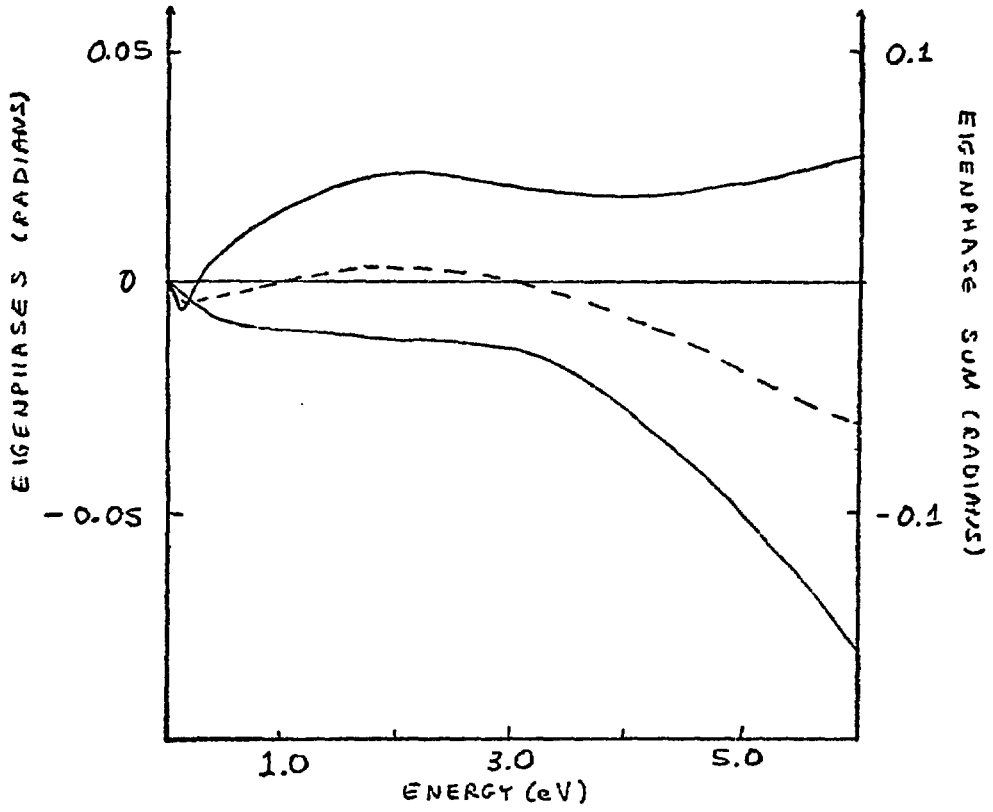

Figure 8.5

The two largest eigenphases (solid curve) and the sigenphase sum (dashed curve) for e-CO_2 scattering in the Π_g symmetry using the SEWP approximation (CASE 2).

we shall see below, the effect of ignoring this symmetry on the total, momentum transfer, and even differential cross sections is not great.

Computed total and momentum transfer cross sections in both atomic units and square angstroms for CASE 1 are presented in Table 8.17, where the latter are compared with the experimental results of Phelps et. al.[9] As the table reveals, agreement is quite good. We see that at low energies (around 0.1 eV), the total and momentum transfer cross sections are approximately equal, reflecting the unimportance of forward scattering at these energies.

The reasons for the behavior of the total cross sections as a function of energy are clear from the discussion of the cross sections for the individual symmetries as given above. In order to obtain a deeper understanding of these results, we studied the changes induced in the total and momentum transfer cross sections when selected symmetries were deleted. The results for CASE 1 appear in Table 8.18 for selected (hopefully) illustrative energies. We find that Π_g is essentially unnecessary, while the other "non-bonding" symmetry, Σ_u must be included. Notice that at 0.07 eV scattering in the Σ_g symmetry contributes almost 95% of the total and momentum transfer cross sections, while at 2.0 eV, Σ_u is clearly the principal contributor.

Lastly, we should look at differential cross sections. These are calculated according to the formulae and procedures of section 7.3 and are shown in Figure 8.6 for CASE 1 at several energies. The first thing one notices about these results is that they are

E(eV)	0.07	0.1	0.5	1.0	2.0	3.0	3.5	4.0
$\sigma_{tot}(T)$	237.9836 (66.6354)	194.6609 (54.5050)	54.5459 (15.2728)	30.5319 (8.5489)	22.1906 (6.2134)	25.8061 (7.2257)	50.4730 (14.1324)	68.6035 (19.2090)
$\sigma_{mom}(T)$	216.8731 (60.7245)	173.5418 (48.5917)	45.9881 (12.8767)	30.7730 (8.6164)	26.4095 (7.3947)	28.4128 (7.9556)	50.1233 (14.0345)	18.4336 (19.3452)
$\sigma_{mom}(E)$	228.57 (64.00)	—	38.57 (10.8)	—	18.75 (5.25)	—	—	—

E(eV)	5.1	5.9	8.0	10.0
$\sigma_{tot}(T)$	26.1767 (7.3295)	25.5627 (7.1575)	21.6867 (6.0723)	28.6318 (8.0169)
$\sigma_{mom}(T)$	24.9316 (6.9808)	22.5867 (6.3243)	7.1040 (6.5856)	24.4773 (6.8454)
$\sigma_{mom}(E)$	—	—	—	43.21 (12.10)

TABLE 8.17

Total and momentum transfer cross sections in a_o^2 and $\mathring{A}^2$ (in parentheses) for e-CO_2 scattering (Case 1). Experimental momentum transfer cross sections obtain from reference (9).

E(eV)	0.07	0.5	1.0	2.0	10.0
All Symm	237.9836 (216.8731)	54.5459 (45.9881)	—	22.1906 (26.4095)	28.6318 (24.4477)
No Π_g	237.7749 (216.8952)	54.4334 (46.0746)	30.5319 (30.7730)	22.0788 (26.3807)	26.6528 (26.1586)
No Π_g, Σ_u	234.0947 (194.8713)	50.6279 (33.9738)	24.5178 (17.5151)	11.4822 (9.8750)	11.2091 (11.6896)
No Π_u	228.4839 (246.3389)	41.8679 (50.1311)	21.1722 (28.4159)	17.5715 (23.7431)	22.7597 (19.2171)
Σ_g only	224.5950 (224.5950)	37.9499 (37.9499)	6.8632 (6.8632)	5.3370 (5.3370)	15.1581 (15.1581)

TABLE 8.18

Study of total and momemtum transfer (in parenthesis) cross sections as certain symmetries are deleted. Case 1 is considered. All results are in atomic units.

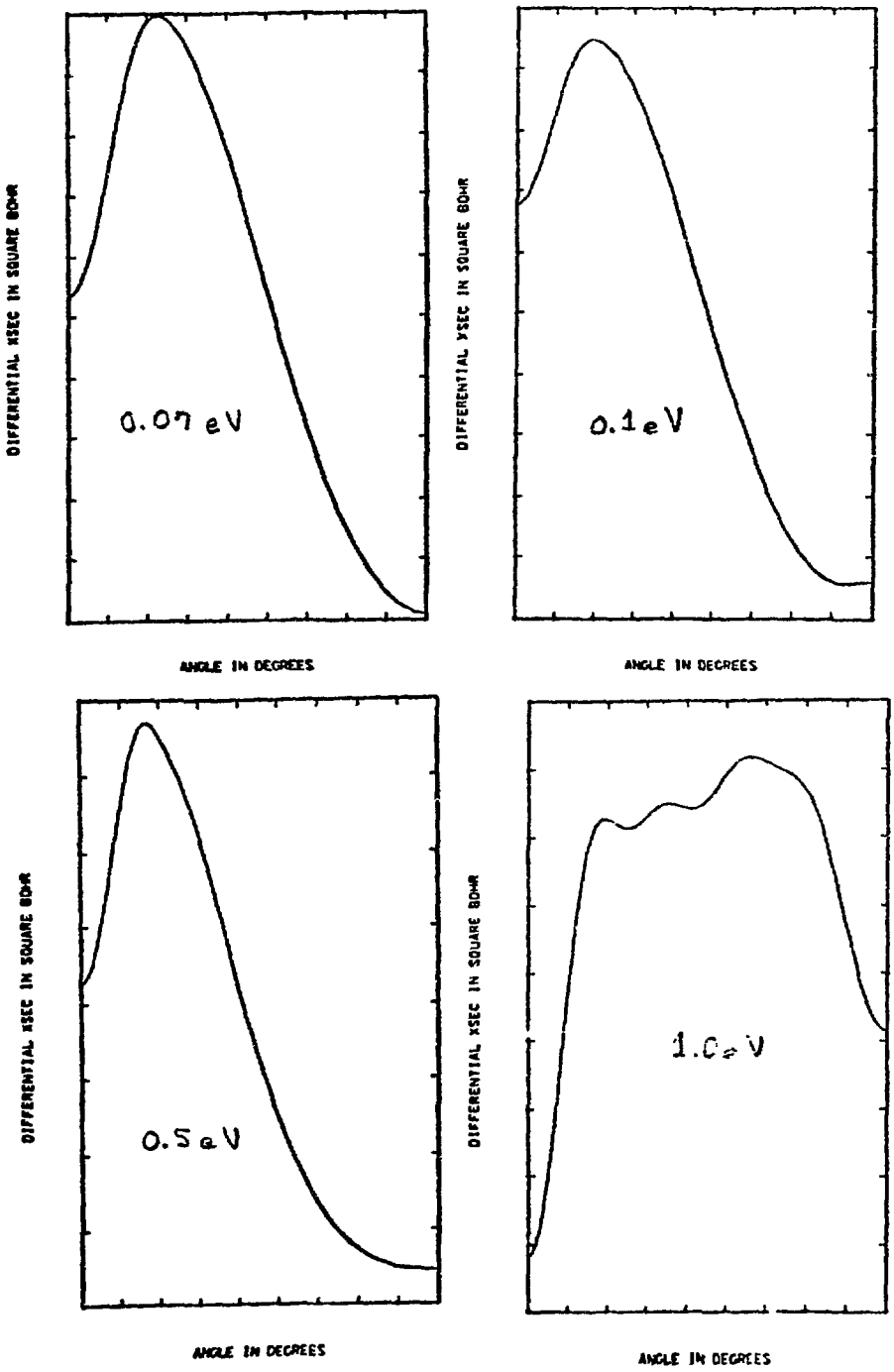

Figure 8.6

Differential cross sections for e-CO_2 scattering in the SEWP approximation at several energies (CASE 1).

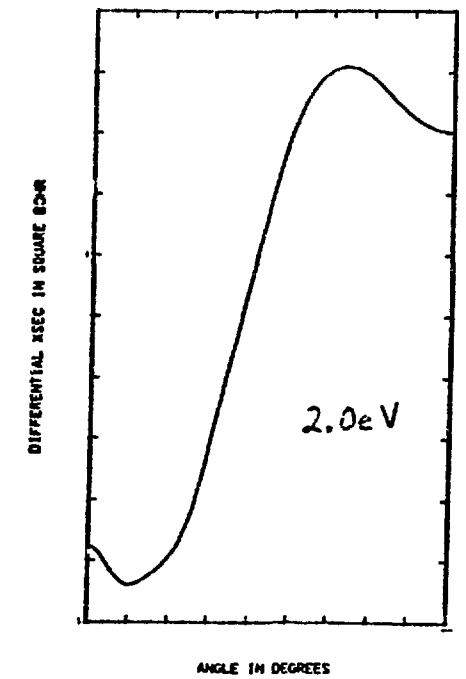
DIFFERENTIAL XSEC IN SQUARE BOHR
2.0eV
ANGLE IN DEGREES

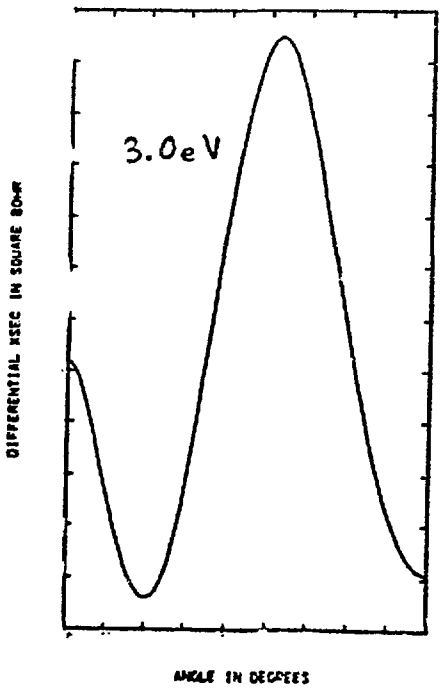
DIFFERENTIAL XSEC IN SQUARE BOHR
3.0eV
ANGLE IN DEGREES

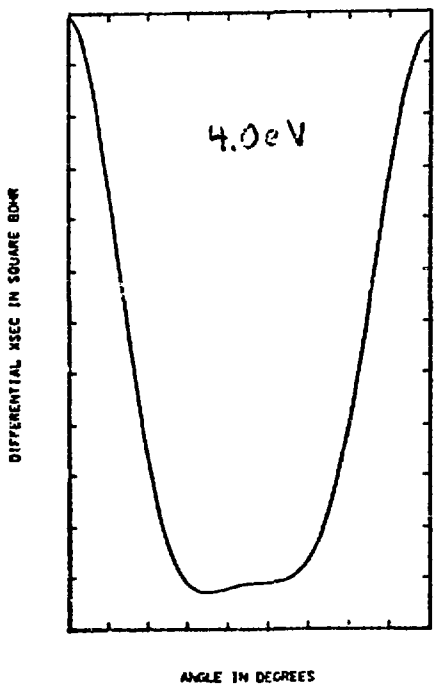
DIFFERENTIAL XSEC IN SQUARE BOHR
4.0eV
ANGLE IN DEGREES

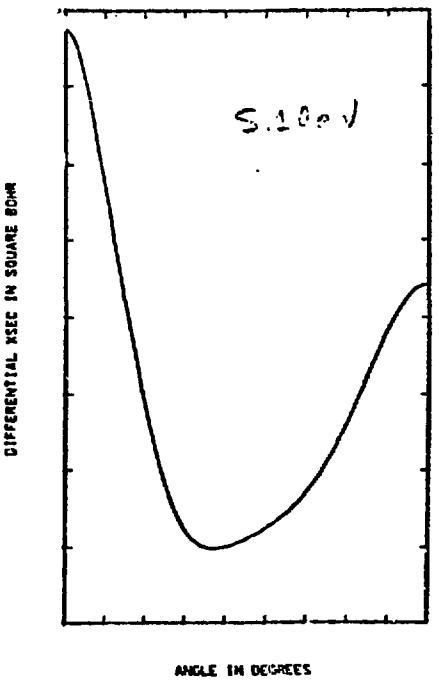
DIFFERENTIAL XSEC IN SQUARE BOHR
5.10eV
ANGLE IN DEGREES

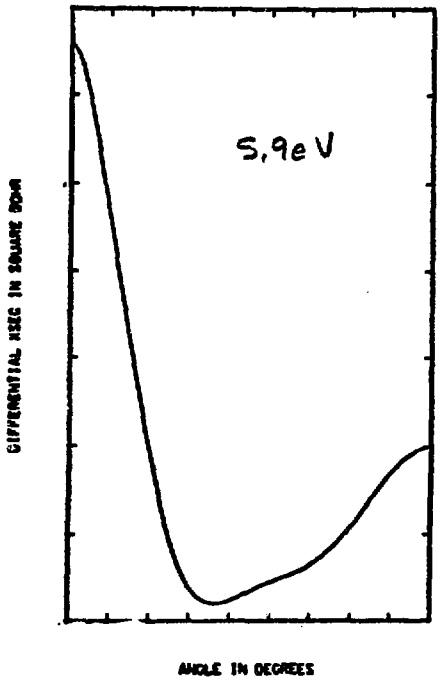
5.9eV
DIFFERENTIAL XSEC IN SQUARE BOHR
ANGLE IN DEGREES

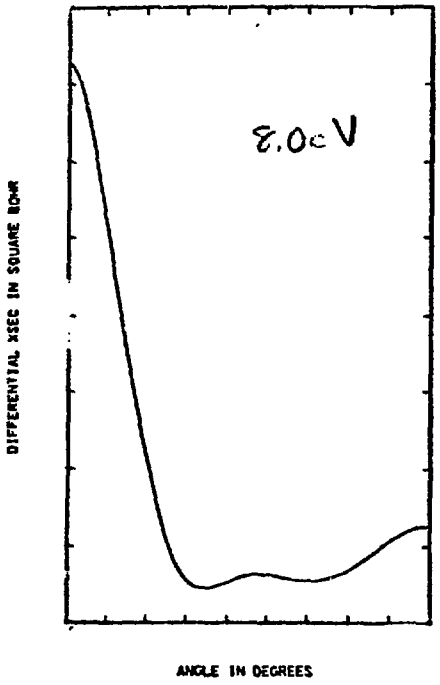
8.0eV
DIFFERENTIAL XSEC IN SQUARE BOHR
ANGLE IN DEGREES

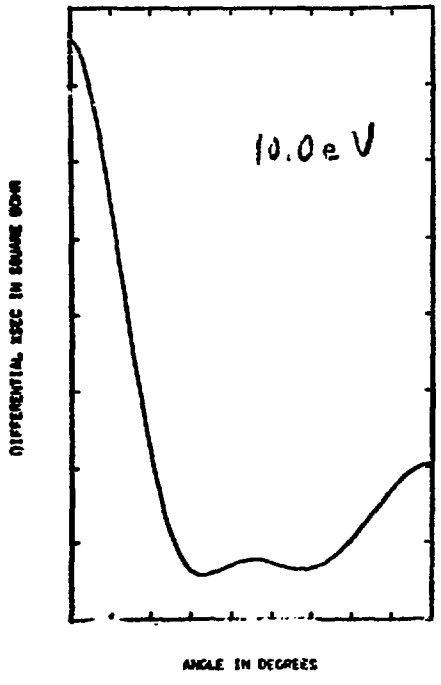
10.0eV
DIFFERENTIAL XSEC IN SQUARE BOHR
ANGLE IN DEGREES

rather strange.

Actually, the low- ($\leq$ 0.5 eV) and high- ($\geq$ 3.5 eV) energy differential cross sections are not all that unreasonable. For example, the 4.0 eV result clearly shows the p + f character of the nearby resonance. But what are we to make of the graphs for 1.0 eV - 3.0 eV? The shape of these plots is certainly atypical.

By way of diagnosis, we studied the sensitivity of the differential cross sections to the potential in CASE 1 and in CASE 2. In Figure 8.7 we compare these results at two energies, 0.1 eV and 1.0 eV. Clearly, the behavior at the higher energy is quite unusual, suggesting an extreme sensitivity in the T-matrix. One should keep in mind the important fact that differential cross sections are notoriously hard to predict theoretically with confidence (they are also quite difficult to measure experimentally, particularly at small angles). This obtains because these cross sections sample the T-matrix quite extensively and also take into account interference effects (recall Chapter 7).

To further study the behavior of the differential cross section, we tried several selective deletions of the sort discussed in conjunction with Table 8.18 at a wide range of energies. Three typical cases are presented in Figure 8.8. At the low and high energies, the following observations can be made:

(1). deletion of Π_g T-matrix elements does not alter the shape of $d\sigma/d\theta$.

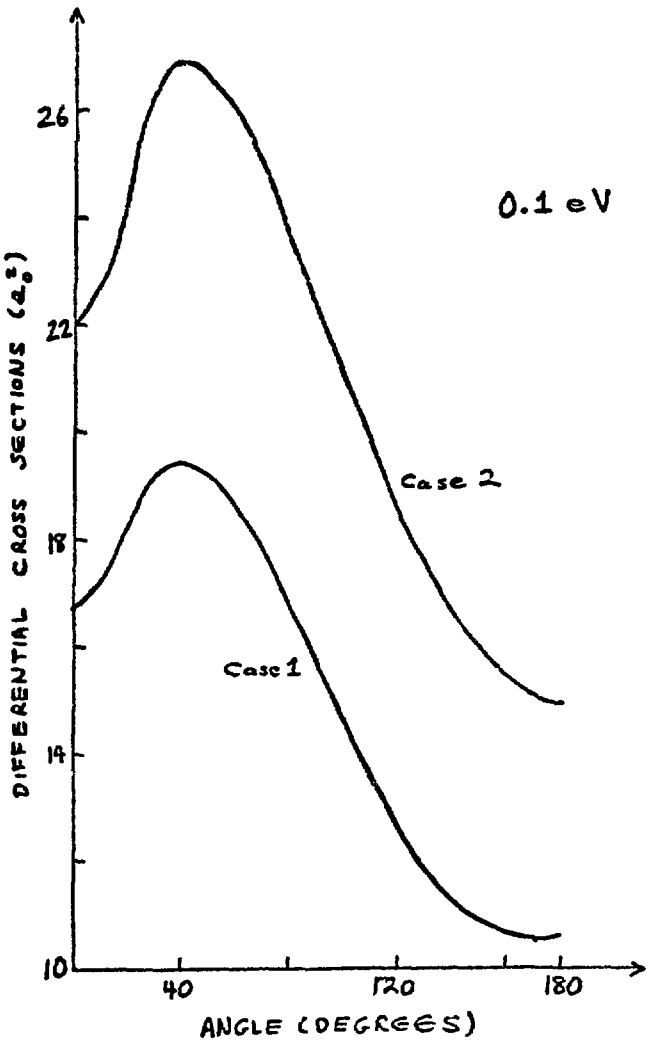

Figure 8.7

Illustration of the dependence of the differential cross sections for $e-CO_2$ scattering on the potential (polarization contribution) at two energies, 0.1 eV and 1.0 eV.

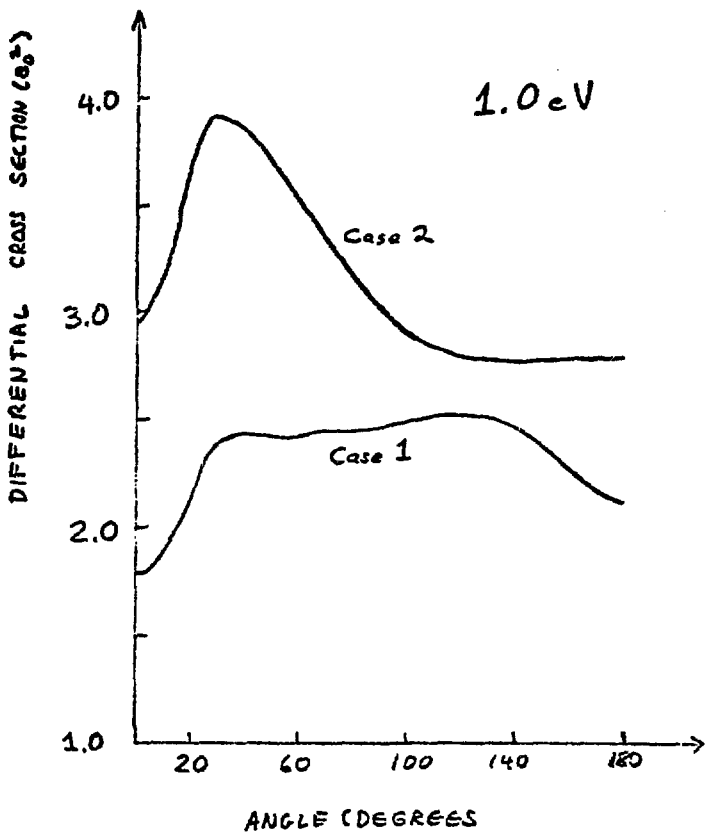
DIFFERENTIAL CROSS SECTION (a_0^2)
4.0
3.0
2.0
1.0
1.0 eV
Case 2
Case 1
20
60
100
140
180
ANGLE (DEGREES

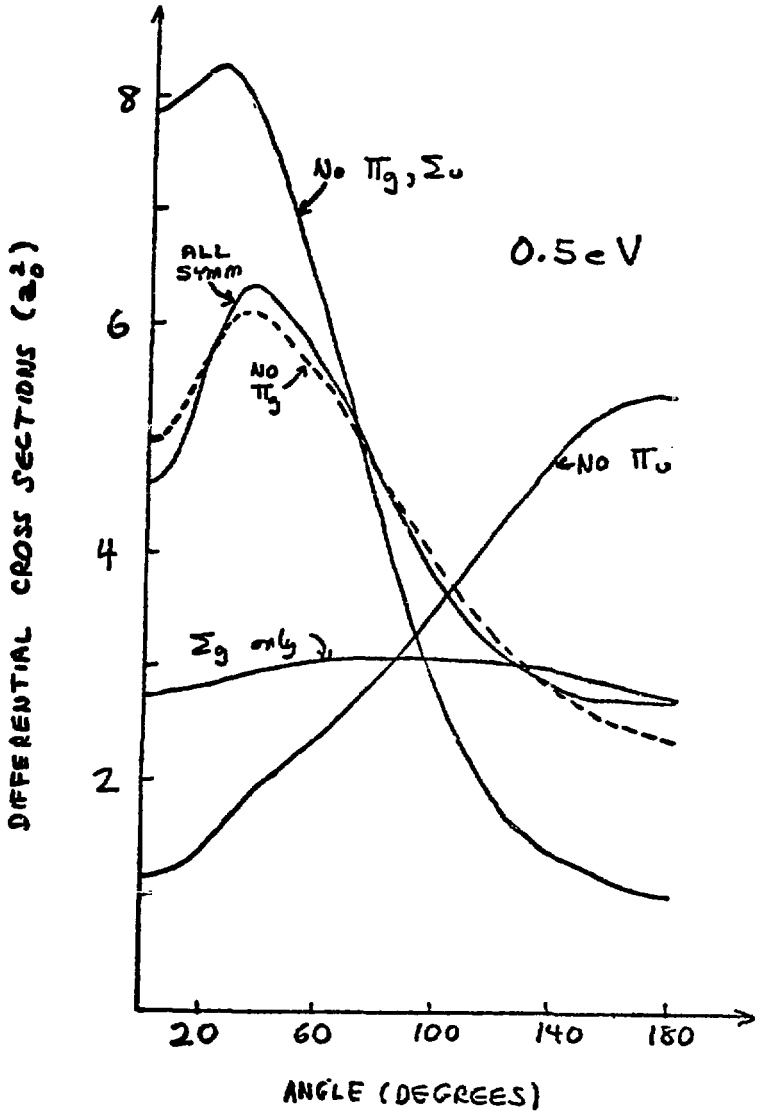

Figure 8.8

Differential cross sections for e-CO_2 scattering at several energies showing selective deletions of certain symmetries.

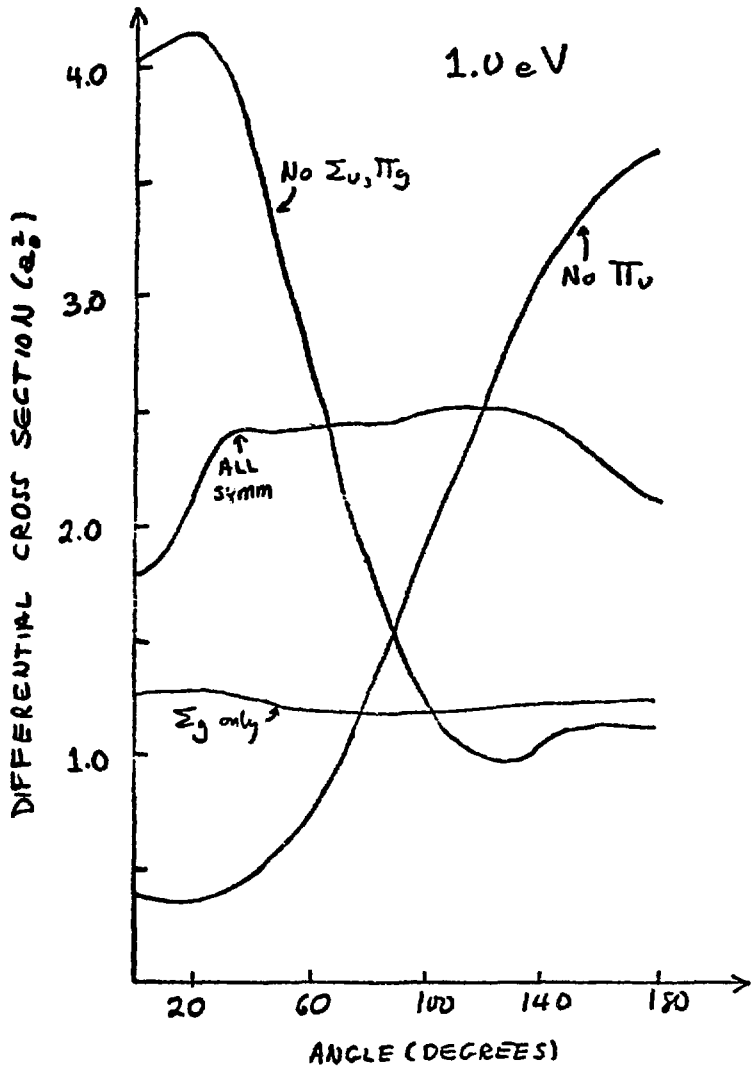
1.0 eV
4.0
3.0
2.0
1.0
DIFFERENTIAL CROSS SECTION (a_0^2)
No Σ_u, Π_g
No Π_u
ALL Symm
Σ_g only
20
60
100
140
180
ANGLE (DEGREES)

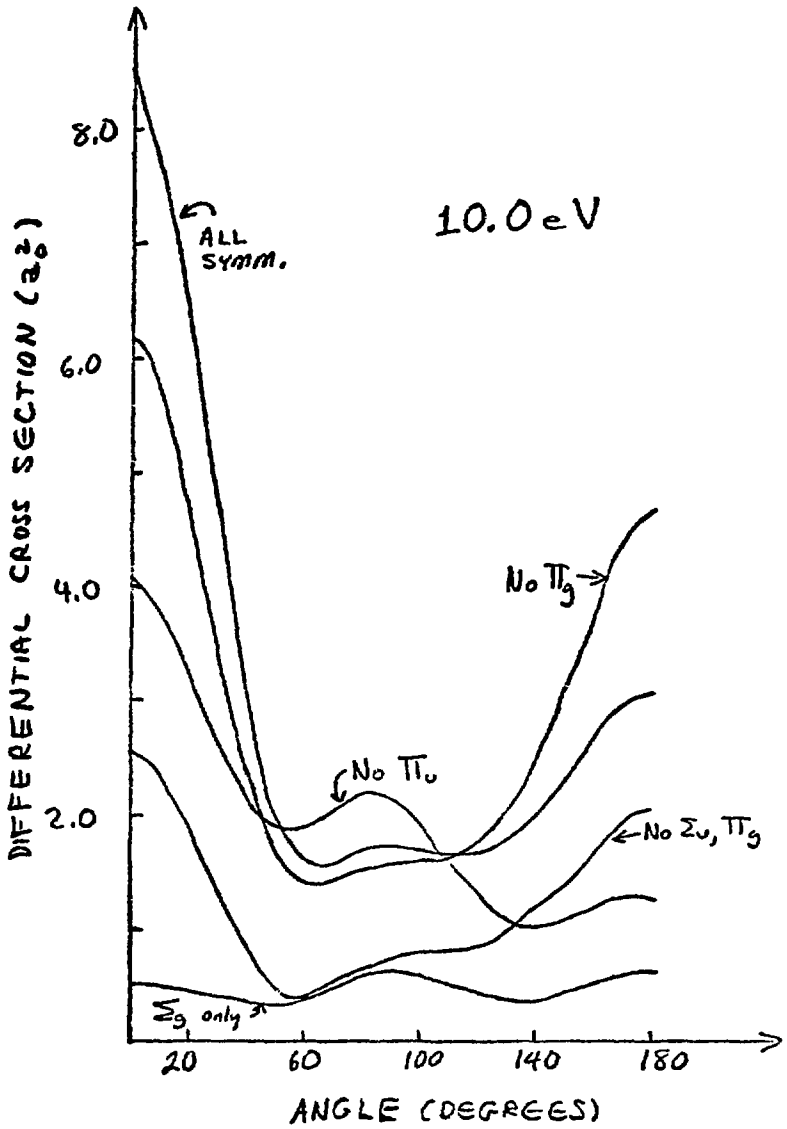
10.0 eV
ALL SYMM.
No Π_g
No Π_u
No Σ_u, Π_g
Σ_g only
8.0
6.0
4.0
2.0
20
60
100
140
180
DIFFERENTIAL CROSS SECTION (a_0^2)
ANGLE (DEGREES)

(2). deletion of both "non-bonding symmetries" has no major qualitative effect on the shape in angle;

(3). deletion of the Π_u symmetry completely alters the shape;

(4). deletion of all but Σ_g symmetry yields differential cross sections which only vaguely approximate the full result.

The figure shows that the 1.0 eV case is anomalous with respect to observations (2) - (4). This was also found to be true at 2.0 eV and 3.0 eV but in all the other cases examined (0.07, 0.1, 0.5, 3.5, 4.0, 5.1, 5.9, 8.0, 10.0 eV) the behavior found was consonant with the above observations.

In addition to the physical insight one gains from studies like these, they clearly suggest that the 1.0 - 3.0 eV cases are somehow special. This was further suggested by a series of studies we carried out in which only the largest N T-matrix elements of each contributing symmetry were retained in the calculation of the differential cross section. We found typically that by N = 2, the cross sections would be converged for angles greater than about 60^o, while by N = 4, they were converged from 0^o to 180^o. However, at 1.0 eV, the results for N = 1 through N = 5 oscillated about something resembling the shape shown in Figure 8.6, never clearly converging.

The final clue to this mystery is provided by the asymptotic decoupling approximation of section 7.6. We present in Figure 8.9

comparison for the differential cross sections in the full calculation and the ADA at several energies. The disparity between the behavior in the ADA of these cross sections from 1.0 eV to 3.0 eV and the results at other energies is quite evident.

Using these clues and a very detailed analysis of which T-matrix elements go into the differential cross section at selected energies, we have concluded that our calculated results for $d\sigma/d\theta$ in the energy range roughly defined by 1.0 eV to 3.0 eV are too sensitive to be reliable. We find that at these energies, the interference of various channels and symmetries is most important, and the differential cross sections depend precariously on the T-matrix being accurate to more than four significant figures, that is to a greater degree of accuracy than even our rather rigid criteria provide.

Of course, such a level of accuracy is not required to determine the total or momentum transfer cross sections of Table 8.12, and we have considerable confidence in these results. Moreover, we have no reason to doubt our differential cross sections for scattering energies outside this energy range. However, one should always keep in mind the aforementioned sensitivity of these cross sections to the T-matrix. It is unfortunate that there are no extensive sets of reliable differential cross sections for e-CO_2 scattering in the literature at present, as these would provide an interesting comparison for these calculations.

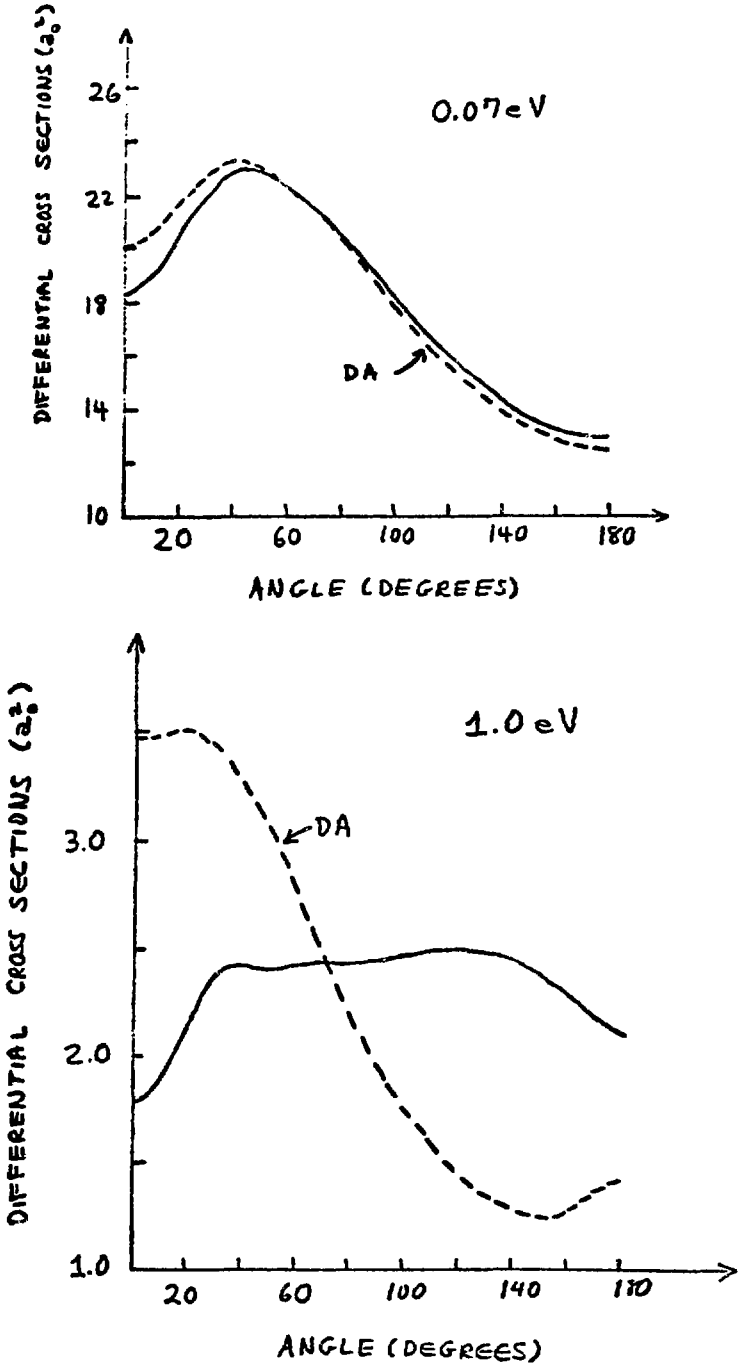

Figure 8.9

Differential cross sections for e-CO_2 scattering in the coupled channel calculation compared with results obtained in the asymptotic decoupling approximation defined in the text.

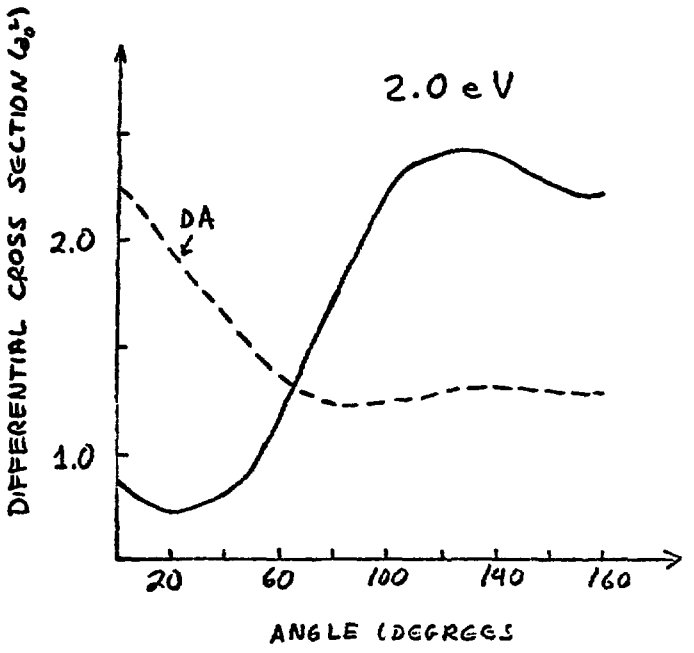
2.0 eV
DA
2.0
1.0
20
60
100
140
160
ANGLE (DEGREES

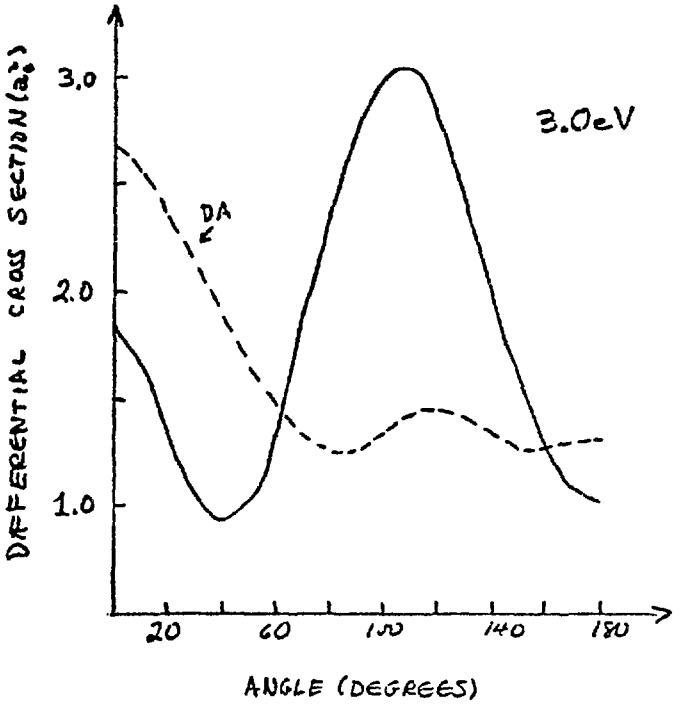
3.0eV
DA
3.0
2.0
1.0
20
60
100
140
180
ANGLE (DEGREES)

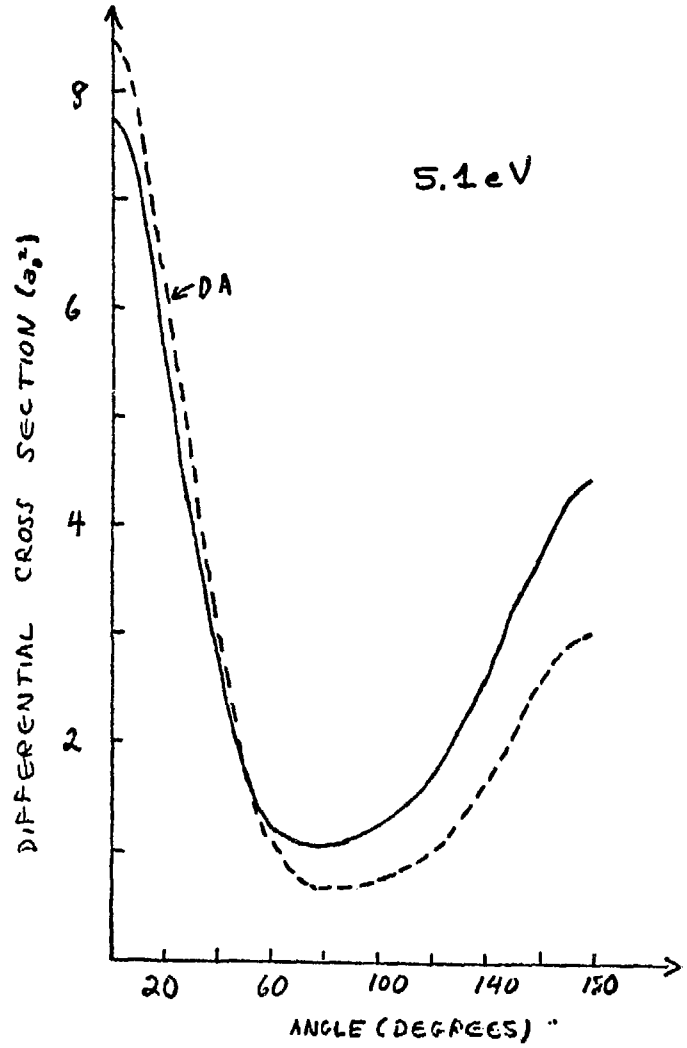
5.1eV
DA
DIFFERENTIAL CROSS SECTION (a_0^2)
8
6
4
2
20
60
100
140
180
ANGLE (DEGREES)

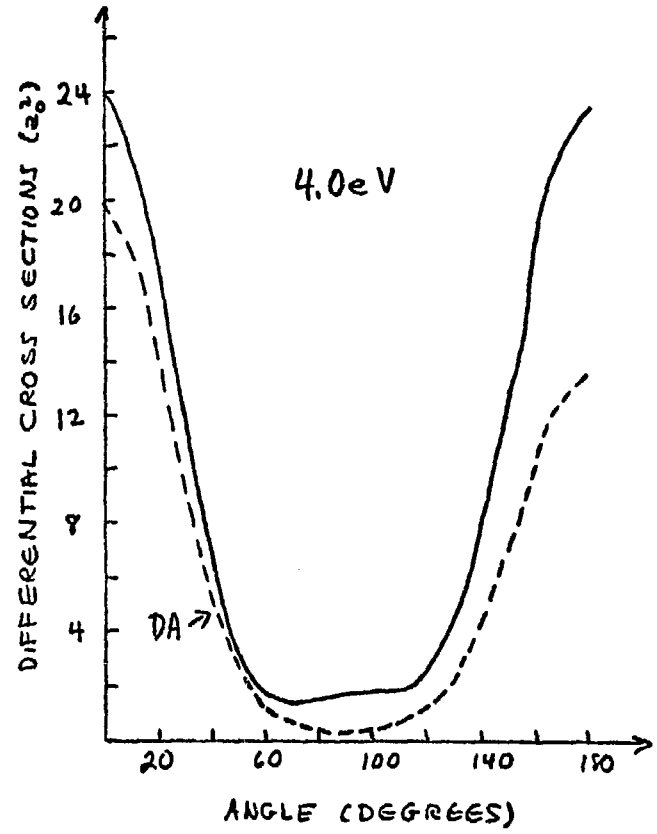
4.0eV
DA
DIFFERENTIAL CROSS SECTIONS (a_0^2)
24
20
16
12
8
4
20
60
100
140
180
ANGLE (DEGREES)

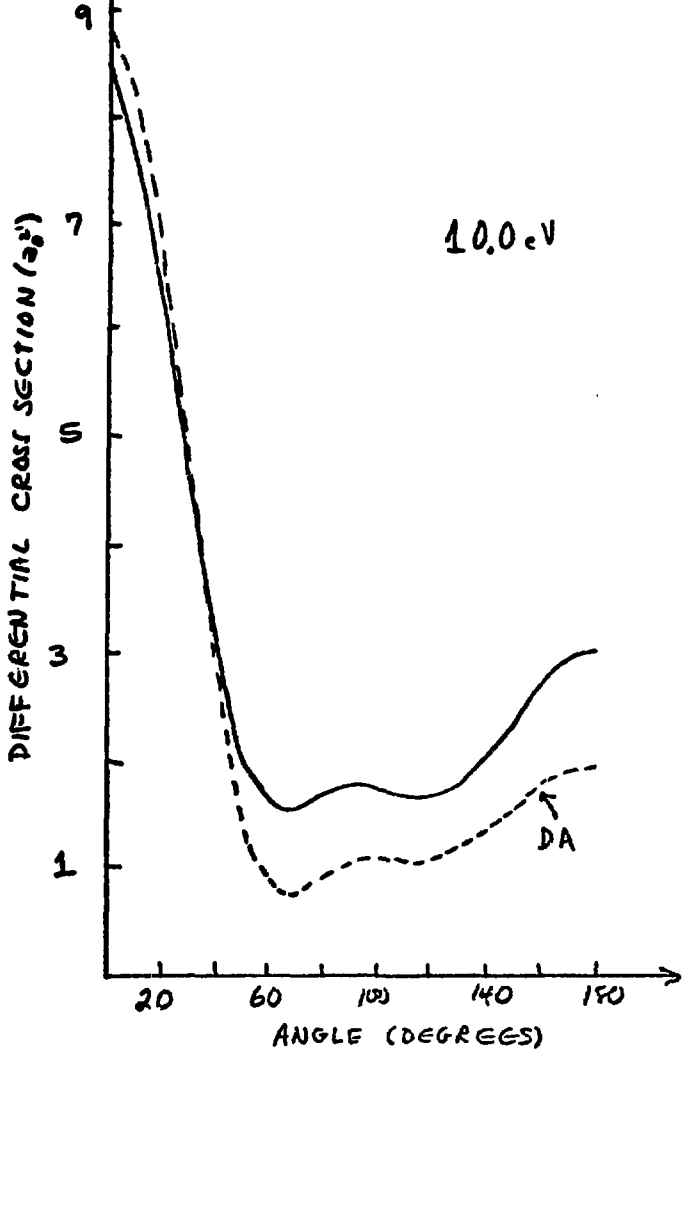
10.0 eV
DIFFERENTIAL CROSS SECTION (a₀²)
9
7
5
3
1
DA
20
60
100
140
180
ANGLE (DEGREES)

§8.4. Conclusion

The manner in which we used the graphs of Figure 8.9 obtained in the asymptotic decoupling approximation might suggest that this (or its near equivalent, the low-ℓ spoiling approximation) is a valid way to proceed in studying this problem. This is not, in general true, unless one seeks merely qualitative information or order-of-magnitude results. To illustrate this assertion, we show in Table 8.19 total and momentum transfer cross sections obtained in the full theoretical analysis and in the ADA. Clearly, it is only at the lowest energies that the latter is reliable.

Another perfectly reasonable question to pose is: does one have to take into account both exchange and polarization? Our sensitivity checks reported above suggest that the answer is "yes", particularly if one has interest in quantitative results. But suppose we are interested only in the qualitative behavior of the scattering. Can we get an understanding of the physics of the collision without all this effort?

The answer is, rather emphatically, "no". This is revealed by Figure 8.10, which compares cross sections in three approximations;

SEWP	static-exchange-with-polarization
SE	static-exchange
S	static

The SEWP approximation is the one employed for the calculations reported in the last section and our best model of the true e-CO_2 interaction. The point of Figure 8.10 is not so much that the

E(eV)		0.07	0.1	0.5	1.0	2.0	3.0	3.5
σ_{tot}	(T)	237.9836	194.6609	54.5459	30.5319	22.1906	25.8061	50.4730
	(ADA)	235.6109	192.4727	51.7659	26.8862	17.2550	18.6227	30.9515
σ_{mom}	(T)	216.8731	173.5418	45.9881	30.7730	26.4095	28.4128	50.1233
	(ADA)	211.3744	167.9891	38.8486	21.6921	16.2462	17.1868	28.5661

E(eV)		4.0	5.1	5.9	8.0	10.0
σ_{tot}	(T)	65.9660	26.1767	25.5627	26.5789	28.6318
	(ADA)	41.4058	21.3116	21.3184	21.8441	21.5499
σ_{mom}	(T)	68.6035	24.9316	22.5867	21.6867	24.4773
	(ADA)	37.1253	16.7296	16.0825	16.0699	15.8613

TABLE 8.19

Cross sections in a_o^2 for e-CO_2 scattering in the SEWP approximation (labeled T) and the asymptotic decoupling approximation (labeled ADA).

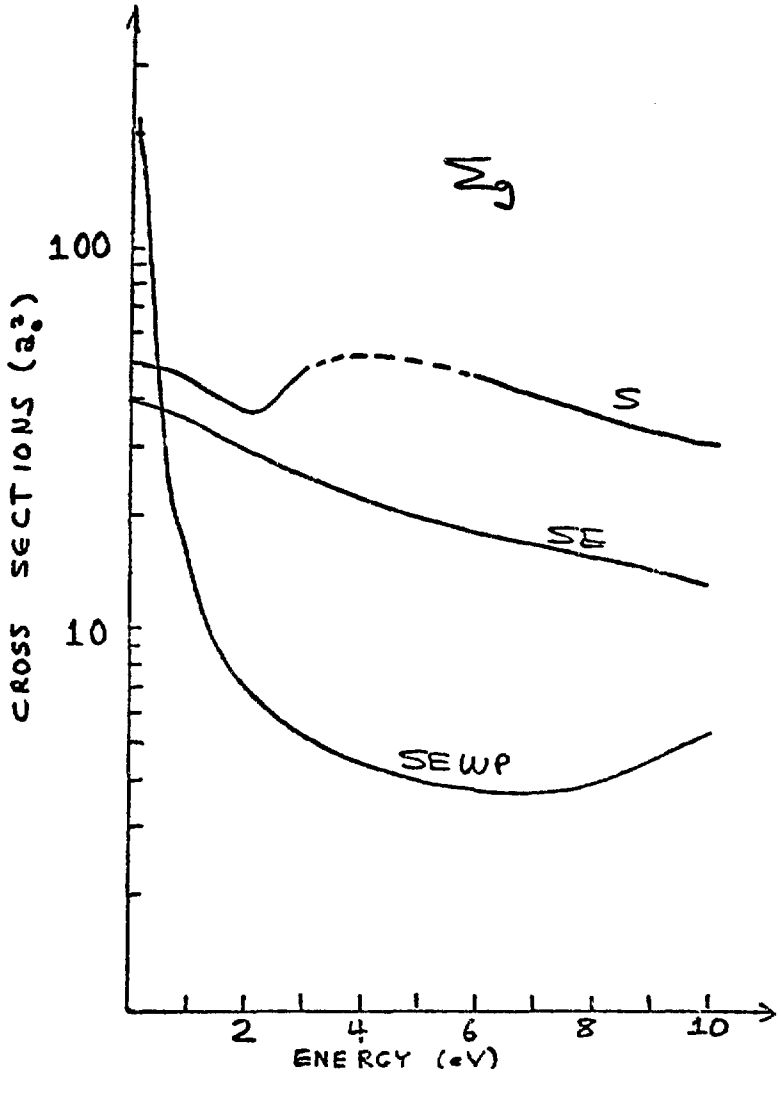

Figure 8.10

Comparison of cross sections in several symmetries for e-CO_2 collisions calculated using the static (S), static-exchange (SE) and static-exchange-with-polarization (SEWP) approximations as defined in the text.

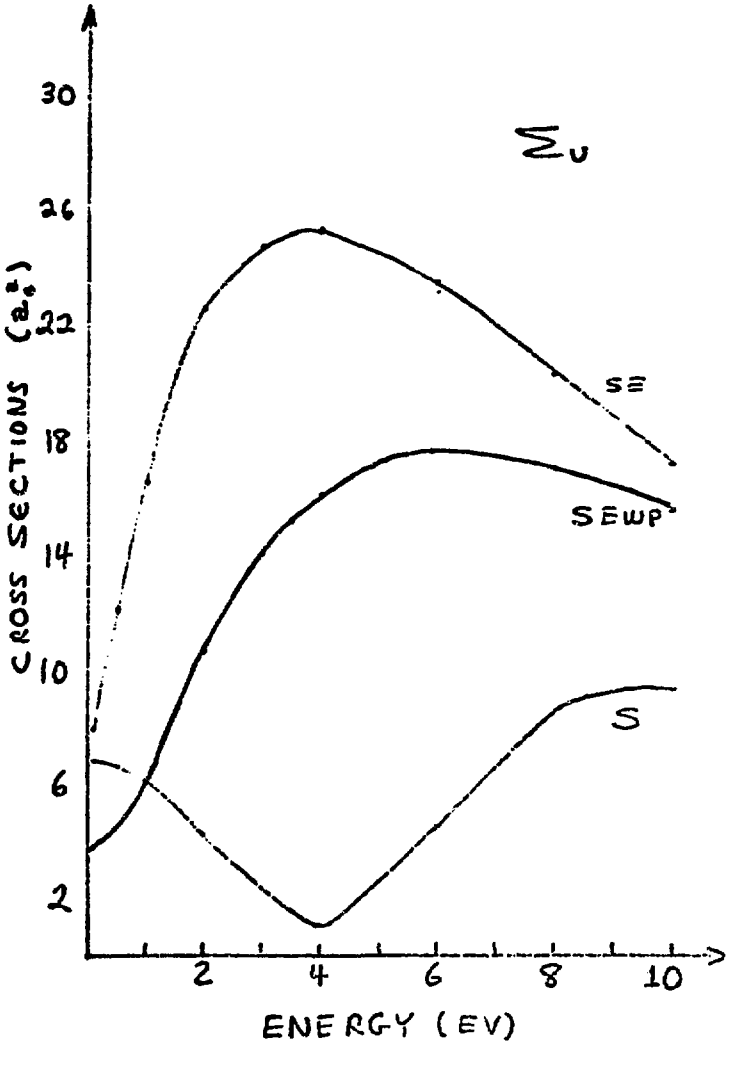
Σ_v
CROSS SECTIONS (a_0^2)
30
26
22
18
14
10
6
2
SΞ
SEWP
S
2
4
6
8
10
ENERGY (EV)

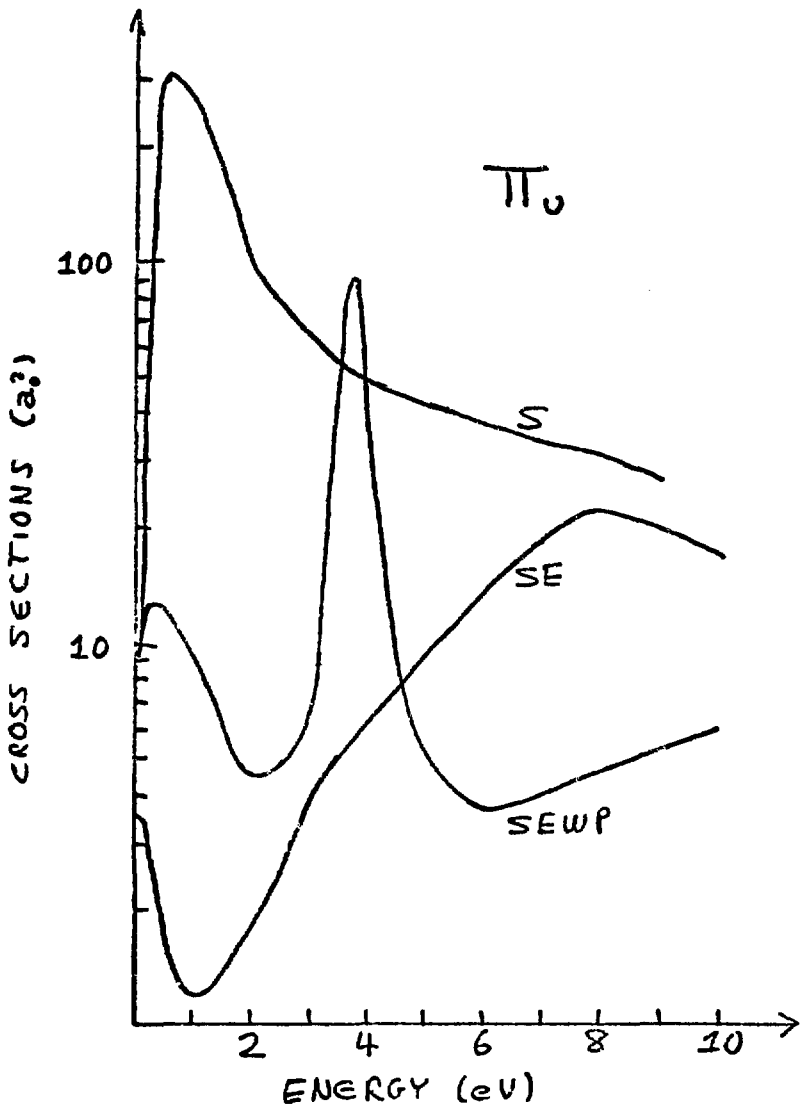
π_u
100
10
CROSS SECTIONS (a_0^2)
S
SE
SEWP
2
4
6
8
10
ENERGY (eV)

numerical values of the cross sections differ in the various approximations but that the physics one predicts theoretically is not correct if either exchange or polarization is neglected. This is further illustrated by the momentum transfer cross sections of Figure 8.11. (We did not calculate enough points in the static approximation to determine the precise behavior of σ_{mom} between 0.1 and 2.0 eV, so this part of the curve is dashed. The three points we did calculate in this energy range are indicated on the dashed portion of the S curve.) Notice in particular how poor the static-exchange approximation is in this case. This is a little suprising. It is remotely possible that this in part reflects the admittedly approximate way we have included exchange. And it is possible that the results of a true Hartree-Fock static-exchange calculation would do a little better. However, it seems unlikely that the fundamental physics reflected in these results would be changed.

In conclusion, it is worth remarking on the similarities between the behavior we have observed in this problem and that characteristic of electron scattering from rare gases (e.g., Ar, Kr, Xe). Total cross sections for e-Ar scattering have been determined by Thompson[10] in the three approximations we have considered and are reproduced in Figure 8.12. (Of course, the details of the inclusion of different interactions are not the same as in our studies.) While we certainly don't wish to make too much of the analogy, it is interesting that spurious peaks appear in the static

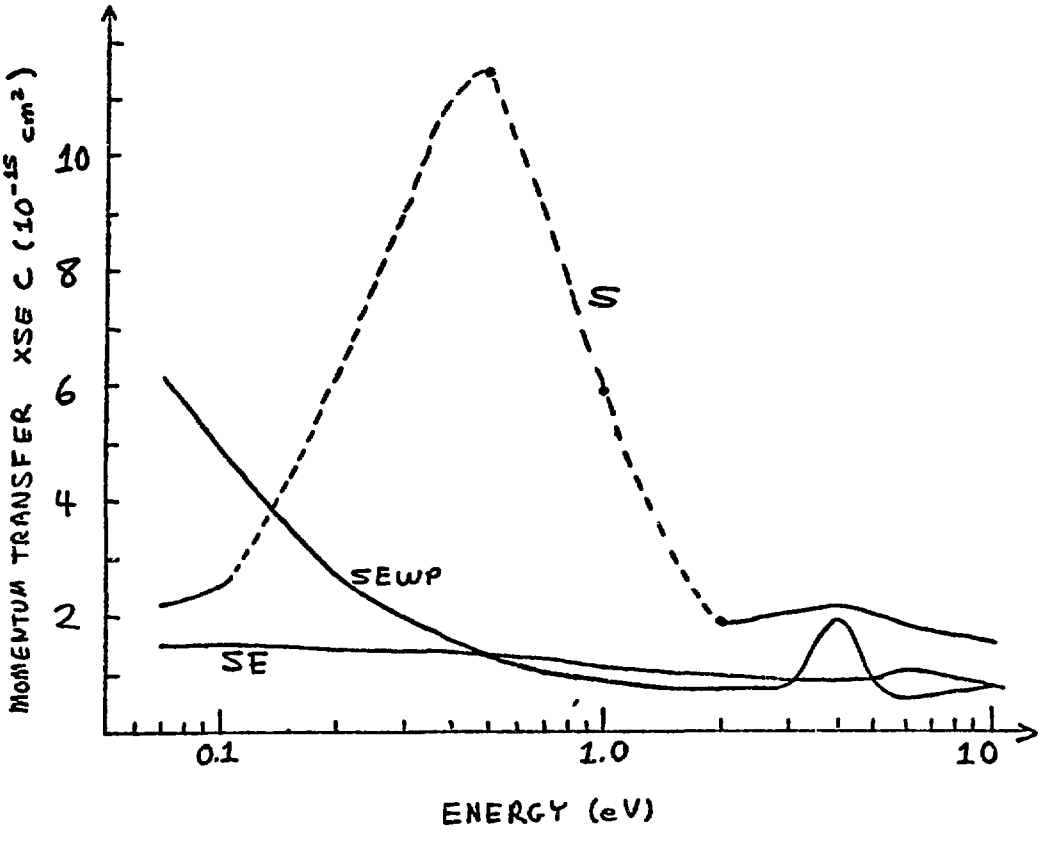

Figure 8.11

Momentum transfer cross sections for e-CO_2 collisions in the three approximations of Figure 8.10.

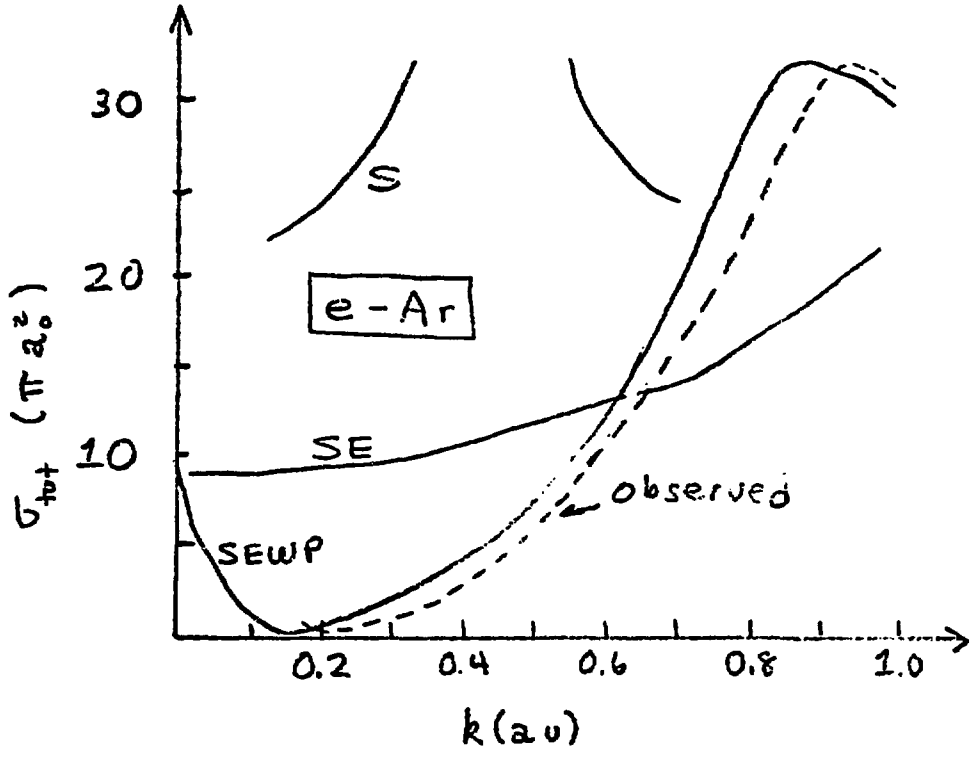

Figure 8.12

Cross sections for e-Ar scattering in static (S), static-exchange (SE), and static-exchange-with-polarization (SEWP) approximations. [Source: D. G. Thompson, Proc. Roy. Soc. (London) A 294, 160 (1966)]

approximation, that the static-exchange results are less strongly energy dependent than are the true cross sections, and that the static-exchange-with-polarization cross sections rise at low energies. All these features are also evident in our e-CO_2 results. Of course, in the rare gases, what we are seeing is a Ramsauer-Townsend minimum, which is simply[11] a deep minimum in the cross section caused by the phase shift passing through a multiple of π at the energy of the minimum. Physically, the effect reflects the fact that at this energy the scattering wave-function has been shifted by exactly one wavelength, so that the "effective phase shift" is zero. The minimum is seen in rare gases because they are closed shell systems whose potential energies consequently fall off quite rapidly beyond a certain radius, leaving something which looks a bit like a potential hole. Enormous low-energy cross sections can be caused by a nearly bound (or "virtual") state with zero angular momentum. This manifests itself as a zero of the S-matrix on the positive imaginary k-axis, as opposed to a true bound state, which shows up as a zero on the negative imaginary k-axis.[12]

While it would clearly be a gross oversimplification to assert that one can safely think about CO_2 as a rare gas in the context of electron scattering, the similarities are provocative, particularly in so far as they comment on the importance of various interactions to the physics of the collision event.

Chapter 9. By Way of Conclusion

> I walk among the fragments
> of the future, that future which I
> contemplate. All my thoughts and
> striving is to compass and gather
> into one thing what is a figment
> and a riddle and a dismal accident.
> And how could I bear to be a man
> if man was not a poet and a solver
> of riddles and a savior of accidents.
>
> -Friedrich Nietzsche
> Thus Spake Zarathustra

Taking a broad perspective on this research, we could assert that the point of it all is that one actually can cope theoretically to a fairly high degree of accuracy with electron-molecule problems involving very large and very aspherical targets. We see no reason why the techniques and procedures here described cannot be applied to homonuclear and heteronuclear molecules at least as large as CO_2. We have seen that considerable care must be exercised (a) in certain numerical aspects of the problem and (b) in calculation of the potential energy. At least in the e-CO_2 problem, the results are strongly dependent on $V(\vec{r})$. This explains, by the way, why the observed e-N_2O cross sections are quite different from those for e-CO_2 collisions (recall that N_2O is isoelectronic with CO_2). For one thing, N_2O is an asymmetric linear molecule. Its charge distribution

is different from that of CO_2 and hence there is no reason to expect an analogy between the two systems in electron scattering. Additionally, because of its symmetry, N_2O has a dipole moment, which leads to an r^{-2} interaction term in the potential energy which is not present in e-CO_2 interactions.

We consider significant the fact that a number of interesting physical features of the e-CO_2 collision are explained by our calculations: e.g., the 3.8 eV shape resonance, the anomalous low-energy momentum transfer cross sections, and the dominance of certain symmetries in particular energy regimes.

It should be noted that we have not taken into account short-range electron correlation or vibrational channels. The latter are probably more serious since, as we recall from Chapter 2, our scattering energies are well above the threshold for excitation of the various vibrational modes. We believe that the dominant effect of including vibrational excitation in these calculations would be to broaden and lower (slightly) the resonance peak which we find at 3.8 eV.

It would be possible to use the theory here developed to describe vibrational excitation, either through the adiabatic fixed-nuclei approximation or in a distorted-wave framework. Such an investigation could prove to be worthwhile, especially in light of the intense interest among experimentalists in the 000→001 transition in the CO_2 laser.

A minor refinement in the present study might entail a more accurate treatment of exchange. Quite frankly, the success

of the HFEGE approximate exchange potential came as something of a suprise, for, comparatively speaking, this is a very easy way to handle exchange. Its theoretical underpinnings suggest that perhaps it is somewhat reasonable but in no way led us to expect it to perform as well as it did. To some extent, we may be partially correcting the inadequacies of the HFEGE potential by adjusting our induced polarization potential via the cutoff parameter discussed in Cbapter 5. Although not at all unreasonable, a cutoff of 2.59 a_o is a bit smaller than one would intuitively expect. And it is true that, if anything, the HFEGE potential is a little weak. An extremely interesting study could be carried out by supplementing the local potential energy we used with an orthogonalization procedure; this possibility was discussed at length in Chapter 4.

The present techniques will handle a wide range of molecular targets in collisions with electrons having incident kinetic energies in the range from several hundredths of an eV to a few tens of eVs. It is not clear that the numerical procedures we employed (as discussed in Chapter 6) can be pushed too much farther to handle, say, electron-benzene collisions, or e-H_2CO, or other such problems. All the computational difficulties we encountered will be exacerbated for systems with even stronger and/or more anisotropic interaction potentials.

One way to handle such systems is via a pseudopotential or model potential. One seemingly promising way to approach the generation of such a potential is to model the true potential

seen by the scattering electron inside a certain radius r from any of the target nuclei by a constant. This idea is based on the fact that while in a static calculation the scattering wavefunction is very sensitive to the inner part of the attractive well, when exchange is taken into account a strong orthogonalization constraint "grabs onto" the wavefunction, making it less sensitive to the detailed nature of the short-range attractive well. A variety of other ways of approaching this idea can be conjoured up, and now that we have fairly accurate results for a single electron-big molecule collision for comparison purposes, this seems a most promising avenue of investigation.

As the scattering energy increases, the theoretical and practical limitations on the coupled-channel method become progressively more accute. In fact, one of the major problems currently facing electron-molecule theorists is that of excitation of <u>electronic states</u> of the target. It is here that the more well established conventional methods encounter considerable difficulty, not the least of which is due to the huge number of important open channels in the problem.

In response to this challenge, researchers have recently proposed a variety of interesting and novel approaches to this problem. We have developed the Pseudo-Bound-State (PBS) procedure, which builds on the idea that a positive-energy variational wavefunction for a molecular ion (e.g., H_2^-) is identical to the system wavefunction for electron scattering for the neutral target (e.g., H_2) at an incident kinetic energy equal to the variational

energy. The theoretical background of PBS and its application to low-energy e-H_2 collisions (s-wave) have been discussed by the author in a recent publication, which can be found in Appendix 1.

This method works well when coupling of partial waves is negligible beyond the value of r at which the quality of the continuum variational function deteriorates owing to the finite size of the basis. It is especially successful for scattering in partial waves of a symmetry which corresponds to that of one of the target (core) orbitals, for then orthogonalization of these functions diminishes the sensitivity of the scattering function to the detailed short-range nature of the static potential.

We are in the process of investigating a multi-channel extension of the PBS procedure which is based on the Generalized Pseudopotential Method of Tully[1] and Zarlingo et. al,[2] A study of the application of this new procedure to e-He and e-H_2 collisions is well under way but is ancillary to the subject matter of this report.

Both of these methods are closely allied theoretically to the R-matrix method. This approach was borrowed from nuclear physics and applied to electron-atom scattering by Burke and others [3] and has recently been successfully applied to electron-molecule scattering by Schneider.[4] We have begun research in this area, applying the method to elastic and electronically inelastic e-N_2 scattering.

These and other related techniques, most of which are

based on the use of L^2-variational wavefunctions, are very likely to break open the problem of electronically inelastic scattering. Further, it is not overly optomistic to speculate that a blend of old and new electron-molecule collision theories together with some sort of model potential ideas may render soluble the problem of electron collisions with very large targets.

We shall not cease from exploration
And the end of all our exploring
Will be to arrive where we started
And know the place for the first time.

-T. S. Eliot
"Little Gidding" from
Four Quartets

APPENDICES

Appendix 1

Pseudo-bound-state study of low-energy electron-molecule collisions: Elastic e-H_2 scattering

Phys. Rev. A 12, 2361 (1975)

Michael A. Morrison and Neal F. Lane

Pseudo-bound-state study of low-energy electron-molecule collisions: Elastic e-H_2 scattering*

Michael A. Morrison† and Neal F. Lane
Physics Department, Rice University, Houston, Texas 77001
(Received 6 January 1975; revised manuscript received 23 June 1975)

A study of the low-energy elastic e-H_2 scattering information contained in multiconfiguration variational wave functions for a low-lying (positive) energy of the H_2^- system is described. The wave function is calculated using standard bound-state techniques, employing the modified valence-bond method with a basis set of Slater-type orbitals, and from it are obtained starting values at moderate electron-molecule separations for a simple single-channel scattering calculation, which is carried out beyond the region where exchange and coupling of partial waves are thought to be important. Results are presented for s_σ elastic scattering for incident-electron energies $\lesssim 10$ eV in the static-exchange approximation with polarization included by means of an adiabatic polarization potential. The study shows that the standard H_2^- variational function does indeed provide a good approximation to the elastic scattering wave function in the region close to the molecule, but that care must be taken in choosing the basis set. Comparisons are made with other more traditional calculations.

I. INTRODUCTION

The theoretical treatment of electron–diatomic-molecule scattering is complicated mainly by the two-center nature of the potential energy.[1] Methods which utilize one-center expansions[2] will inevitably encounter convergence difficulties at higher energies or for large-Z molecules. Approaches which do not involve the one-center expansion have been developed in the fixed-nuclei approximation, and appear to have considerable promise.[3–5] These methods describe the electronic state in the body frame and focus on the complicated region close to the target molecule where the potential energy is least isotropic and where exchange effects are most important. Similarly, one may expect certain types of electronic-excitation processes and temporary negative-ion formation to be powerfully dealt with using these approaches. While the body frame is appropriate when the electron is close to the molecule, the scattering process is actually defined in the laboratory system, and a frame transformation is required.[6] This is particularly simple when the "adiabatic-nuclei approximation" ("impulse approximation") is valid,[1,7,8] for in that case solution of the equations in the lab frame is not required.

In the case of electron-H_2 scattering, static-exchange calculations have been carried out both in the body[4,5,9–11] and laboratory[2] frames. In the latter case, rotational excitation is treated via a close-coupling expansion, where sufficient terms are included to guarantee convergence. Polarization of H_2 by the incident electron is important for low-energy collisions, and has been included via an adiabatic polarization potential[12,13] in both body-frame[11] and lab-frame[2] treatments. The adiabatic-nuclei approximation has been successfully applied to calculate rotational-excitation cross sections using fixed-nuclei phase shifts.[7,14] Application has also been made to vibrational-excitation, where interpretation of the results is less clear.[15–18]

In the work reported here, we also concentrate on obtaining a suitable description of the system wave function when the electron is close to the H_2 target. What we describe is in some ways more a model study than the development of a method. Our study was stimulated by the one-dimensional model calculations of Taylor, Hazi, and Fels.[19] In short, they found that positive-energy wave functions constructed from square-integrable (L^2) basis functions provide scattering information for both resonant and nonresonant states, under certain conditions. We have examined this approach for a rather complex three-dimensional problem: low-energy e-H_2 scattering. The point of view has been adopted that except for the asymptotic scattering boundary conditions, the electronic features of the e-H_2 collision physically resemble a molecular structure problem of the H_2^- ion. Since this negative ion has no bound states for separations near the H_2 equilibrium value,[20] eigenfunctions corresponding to the lowest variational roots should approximate the true continuum wave function corresponding to low incident-electron energies, at least in the vicinity of the target. If so, then an approximate scattering orbital can be projected out and simple potential scattering techniques used to continue the function into the asymptotic region. For moderate electron-molecule separations, the interaction potential can be simply and accurately represented, while near the target

exchange, correlation, and coupling of partial waves complicate the problem. A somewhat similar point of view has been taken with regard to e-H collisions by Zarlingo, Ishihara, and Poe.[21]

In order to carry out this investigation, a computational technique was employed which uses a standard linear variational method (modified valence bond) to obtain low-lying positive-energy variational H_2^- wave functions from which body-frame phase shifts are obtained via a simple numerical solution of the potential scattering problem in the outer region. This procedure has been used to calculate elastic s_σ e-H_2 cross sections for energies below 10 eV and yields results which are in good agreement with more elaborate scattering calculations.[2,9] The H_2 molecule was chosen for the present study because of its relative simplicity in comparison with other molecules and because fairly accurate experimental and theoretical results are available for comparison. At low incident energies ($\lesssim$1 eV) the total cross section is dominated by elastic scattering, primarily s_σ, and the asymptotic coupling between different partial waves is known to be weak.[2,22]

In Sec. II the computational technique alluded to earlier is described. Elastic s_σ phase shifts and cross sections are presented and discussed in Sec. III, where they are compared with the results of other calculations and where the sensitivity of the results to various features of the basis set is analyzed. Finally, in Sec. IV, we comment on limitations and possible extensions of this work. Throughout this paper, the H_2 internuclear separation is fixed at $1.4a_0$ and atomic units are employed.

II. PSEUDO-BOUND-STATE TECHNIQUE

Our approach to the study of e-H_2 collisions can be viewed as consisting of a structure calculation, which yields low-energy variational H_2^- wave functions, followed by a simple potential scattering calculation, which yields phase shifts and cross sections for elastic s-wave scattering. The necessary structure calculations were carried out using a modification of a general diatomic-molecule program which was originally developed by the Molecular Physics Group at the University of Texas.[23] This program performs multiconfiguration variational calculations[24] using modified valence-bond wave functions. Each wave function is composed of Slater-type orbitals (STO's), and allowance is made for varying linear and nonlinear parameters. The scattering calculations involve extraction of the desired partial wave from the variational H_2^- function and a simple single-channel numerical integration.

A. Structure problem

The first step is generation of a core H_2 function. We construct a simple two-center single-configuration function for the ground state ($X^1\Sigma_g^+$) of the Wang form,[25] viz.,

$$\psi_{X^1\Sigma_g^+}(\vec{r}_1,\vec{r}_2) = |1s^a\bar{1}s^b| + |1s^b\bar{1}s^a|, \tag{1}$$

where the overbar denotes spin "down" and the basis functions $1s^a$ and $1s^b$ are STO's corresponding to s orbitals on nuclei a and b, respectively, e.g.,

$$\bar{1}s^a(\vec{r}_{1a}) = N_1 e^{-\alpha r_{1a}} Y_0^0(\vec{r}_{1a})\beta(1), \tag{2}$$

where $\beta(1)$ is the "spin-down" eigenfunction. The nonlinear parameter α is taken to be the same for like orbitals on different centers and is allowed to vary in this step until a minimum H_2 energy is obtained for a given internuclear separation.

The next step entails calculation of H_2^- functions of the appropriate symmetry, e.g., $^2\Sigma_g^+$ functions for s_σ scattering. This is a multiconfiguration calculation; each configuration is a properly symmetrized linear combination of products of the core H_2 function [Eq. (1)] and an additional STO. Thus the core is "frozen." This corresponds to the static-exchange approximation and does not take correlation into account. (Long-range polarization effects are incorporated into the scattering calculation in a manner described in Sec. III B) A typical two-center configuration for the $^2\Sigma_g^+$ state of H_2^- is

$$\Phi_i(\vec{r}_1,\vec{r}_2,\vec{r}_3) = |1s^a\bar{1}s^b\varphi_i^a| - |\bar{1}s^a 1s^b\varphi_i^a| \pm |1s^b\bar{1}s^a\varphi_i^b| \mp |\bar{1}s^b 1s^a\varphi_i^b|, \tag{3}$$

where φ_i^a is an arbitrary STO centered on nucleus a and the upper (lower) signs correspond to φ_i^a of even (odd) parity. Notice that for $^2\Sigma_g^+$ wave functions, ns, np_0, and nd_0, ... STO's may be used for φ_i^a or φ_i^b. The full N-configuration $^2\Sigma_g^+$ wave function is then

$$\psi_{^2\Sigma_g^+}(\vec{r}_1,\vec{r}_2,\vec{r}_3) = \sum_{i=1}^{N} c_i \Phi_i(\vec{r}_1,\vec{r}_2,\vec{r}_3). \tag{4}$$

The nonlinear parameters in φ_i^a and φ_i^b were not allowed to vary in this step.

B. Scattering problem

One way to examine the relationship between the $^2\Sigma_g^+$ variational H_2^- wave function and the actual scattering function is to compare s_σ phase shifts derived from the two. In the case of the variational function, four steps are required[26]: (i) projection of the approximate continuum orbital φ from the $^2\Sigma_g^+$ variati nal function; (ii) orthogonal-

ization of the orbital φ to the $1\sigma_g$ core orbital; (iii) one-center expansion of φ; and (iv) numerical integration of the appropriate radial scattering equation, starting with the s_σ radial function in the one-center expansion.

In the first step, we extract the approximate continuum orbital φ by selecting from $\psi_{^1\Sigma_g^+}(\vec{r}_1, \vec{r}_2, \vec{r}_3)$ the linear combination of $\varphi_i^a + \varphi_i^b$ which multiplies the frozen-core $^1\Sigma_g^+$ target wave function. Thus, in keeping with the frozen-core approximation, we write

$$\psi_{^1\Sigma_g^+}(\vec{r}_1, \vec{r}_2, \vec{r}_3) = \mathcal{A}\,\psi_{^1\Sigma_g^+}(\vec{r}_1, \vec{r}_2)\varphi(\vec{r}_3), \tag{5}$$

where $\mathcal{A}$ enforces antisymmetrization, and where

$$\varphi(\vec{r}_3) = \sum_{i=1}^{N} c_i\left[\varphi_i^a(\vec{r}_3) + \varphi_i^b(\vec{r}_3)\right]. \tag{6}$$

The approximate continuum orbital φ is then orthogonalized to the $1\sigma_g$ H_2 core orbital, i.e.,

$$\varphi' = \varphi - \langle 1\sigma_g | \varphi \rangle 1\sigma_g. \tag{7}$$

For approximate orbitals φ of other symmetries, e.g., σ_u, π_g, etc., this step is, of course, not required. In one version[27] of the pseudopotential approach to electron-molecule scattering, the orthogonalization in Eq. (7) is applied as a constraint to the solution of the scattering equations for φ. To facilitate examination of particular partial-wave phase shifts, we convert $\varphi(\vec{r}_3)$ to a one-center representation (the origin of coordinates being the midpoint of the internuclear axis) by expanding it in spherical harmonics, the radial coefficients being designated by $u_{lm}(r_3)$.

Our central assumption is that the variational function is an accurate representation of the scattering function at least in the region near the target, where exchange effects are particularly important. Outside this "exchange region," we expect the effects of exchange and the coupling of partial waves to be negligible for low-energy e-H_2 collisions. Therefore we use the value of the radial wave function and its slope at the boundary of the exchange region, $r = r_{ex}$, to initialize the solution of the single-channel (body-frame[6]) scattering equation

$$\left(\frac{d^2}{dr_3^2} - \frac{l(l+1)}{r_3^2} + k^2 - 2V(r_3)\right)u_{lm}(r_3) = 0, \tag{8}$$

which is integrated into the asymptotic region. In Eq. (8) k^2 is the incident-electron energy (in Ry) and $V(r_3)$ is the diagonal matrix element of the effective static potential energy augmented to include long-range polarization and quadrupole interactions. The effective potential energy contains short-range terms due to the static Coulomb electron-molecule interactions of the form given by Lane and Geltman[22] and the long-range quadrupole and adiabatic polarization terms given by Henry and Lane.[2] The choice of initialization point r_{ex} will be discussed below. In the calculations reported in Sec. III the Numerov algorithm[28] was used to integrate Eq. (8).

III. RESULTS AND DISCUSSION

A. Basis sets

Variation of the nonlinear parameter α in the single-configuration H_2 wave function of Eq. (1) produced a root corresponding to an electronic energy of -1.139 hartrees for $\alpha = 1.169$ as compared to the much more accurate multiterm theoretical value of -1.1745 hartrees obtained by Kolos and Wolniewicz.[29] Using this as the core function, multiconfiguration continuum H_2^- functions were calculated. Initially, the nonlinear parameters in these functions were chosen somewhat arbitrarily, but in such a way as to create a basis set ("type I") consisting of functions which together span the region of space close to the target ($r \lesssim 3a_0$). Using this approach to choose the nonlinear parameters, it was necessary to use 25 basis functions to obtain reasonably good phase shifts. The STO parameters for $N = 25$ and the resulting coefficients c_i of Eq. (4) for the lowest root ($E = 0.0688$ eV) are shown in Table I. The s_σ projection of this 25-configuration radial function, orthogonalized to the core orbital, is shown in Fig. 1 and compared to a body-frame close-coupling function[30] at the same energy, 0.0688 eV. Notice that there is a node in the variational function at $r_{node} \simeq 2.15a_0$.

A second type of basis set ("type II"), found to be more satisfactory, is constructed in a systematic manner. For s_σ scattering, we form an N-configuration basis set by employing s-wave STO's centered on the two nuclei with a fixed value of the nonlinear parameter α in all basis functions and $n_i = 1, 2, \ldots, N$. (This type of H_2^- function was also used by Winter and Lane[5] in their Fredholm-determinant study of e-H_2 collisions.) As will be seen below, this systematic basis gives better results with fewer configurations.

B. Phase shifts and cross sections

In order to examine phase shifts and cross sections extracted from these H_2^- variational functions, it is necessary to select a value of r_{ex} at which the numerical integration of Eq. (8) is to be initialized. It was found to be convenient to choose $r_{ex} = r_{node}$. Then the second initialization parameter [the slope or, equivalently, the value of

$u_{s_g}(r_3)$ at a nearby point] merely scales the wave function and does not affect the phase shifts. It will be shown, however, that there is nothing really special about the node, and that any value of r_{ex} within a certain range is equally satisfactory.

Starting at $r_{node} = 2.15a_0$, corresponding to the node of the lowest root obtained with a basis set of type I with $N=25$, we obtain the s_g elastic phase shifts shown in the column labeled 25 in Table II. The corresponding cross sections are shown by the solid curve labeled 25 configurations in Fig. 2. The dashed curve in this figure shows the close-coupling results[2] obtained by using the same wave function for H_2. (The node in this function occurs[30] at $\sim 2.18a_0$.) Since the variational wave function used to start the integration corresponds to an energy of 0.0688 eV, it is perhaps surprising that agreement is good over a range of energies from 0.05 to 10.0 eV. This behavior, which was also observed when other basis sets of type II were used (see below), reflects the fact that at low energies the inner part of the s_g scattering function does not vary substantially with energy because the s_g "potential energy" is strongly attractive. This general observation is confirmed by careful examination of the energy insensitivity of nodes in low-energy close-coupling functions.[30] Hence calculation of low-energy phase shifts using an L^2 variational function need not be tied to the energy of the variational root. (In preliminary results[31] for higher partial waves, where the effective potential near $r=0$ is weaker, we see somewhat greater sensitivity to energy.)

TABLE I. STO parameters [see Eq. (2)] and variational coefficients [see Eq. (4)] for the lowest-energy root (0.0688 eV) for the $N=25$ variational $H_2^-\ ^2\Sigma_g^+$ calculation (basis set type I).

	n_i	l_i	α_i	c_i
1	1	0	4.0	−0.433 953 (−1)
2	1	0	7.5	0.177 696 (−1)
3	1	0	15.0	−0.369 676 (−3)
4	2	0	5.0	0.332 551 (−1)
5	2	1	4.0	−0.121 819 (−3)
6	3	0	5.0	−0.653 321 (−2)
7	3	1	4.5	0.711 701 (−4)
8	3	2	3.5	0.524 209 (−4)
9	4	0	3.5	0.415 405 (−2)
10	4	1	3.0	−0.104 272 (−2)
11	4	2	2.5	−0.581 696 (−3)
12	4	3	2.0	−0.178 686 (−3)
13	5	0	1.0	0.364 248 (+1)
14	6	0	1.0	−0.449 717
15	7	0	1.0	0.490 023 (+1)
16	6	0	0.5	−0.132 906 (+2)
17	7	0	0.7	0.141 986 (+2)
18	4	0	1.5	0.915 007 (−1)
19	4	1	1.0	0.221 578 (−2)
20	4	0	0.5	−0.159 820 (+2)
21	4	1	0.35	−0.304 966 (−1)
22	5	1	1.5	−0.350 348 (−2)
23	7	0	0.5	0.108 070 (+2)
24	8	0	0.41	−0.237 406 (+1)
25	8	0	0.35	0.125 031 (+1)

I. Table II we present phase shifts for several energies for type-II basis sets with $N=11$, 12, 13, and 14 together with the energy of the lowest variational root and the location of the corresponding node, which was used to initialize integration of Eq. (8). In Table III, results are given in the *static-exchange approximation* [polarization terms in $V(r_3)$ set to zero] so that (i) comparison can be made with other existing theoretical calculations, and (ii) convergence can be examined without the possible masking effect of the long-range polarization potential. (Increasing N was found to lower the energy of the lowest root and spread the other roots in energy.) As N increases, the phase shifts for $E \lesssim 1$ eV appear to converge to values in good agreement with other theoretical results,[2,9] which are also shown in these tables.

It is important to note that r_{ex}, the boundary of the exchange region, is not uniquely defined. In the calculations reported above, we chose $r_{ex} = r_{node}$ for convenience. In Fig. 3 we present a graph of s_g elastic cross sections at 0.05 eV for the case $N=14$ and $\alpha=0.75$ vs the starting radius at which integration of Eq. (8) was initialized. Clearly,

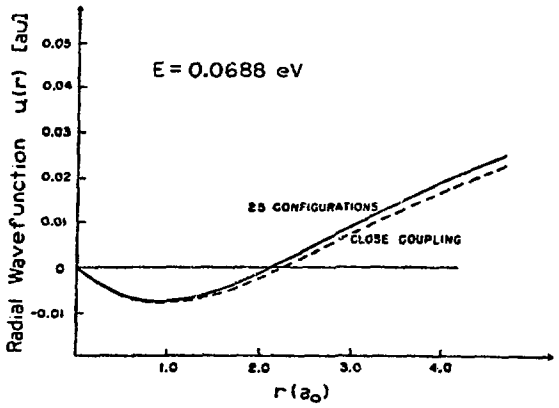

FIG. 1. Comparison of 25-configuration type-I variational s_g radial scattering function at 0.0688 eV (lowest root) with the $J=0$ close-coupling wave function of Henry and Lane (Ref. 2) at this energy (dashed curve). The node (first zero) in the variational function is at $\sim 2.15a_0$. The node in the close-coupling function is at $\sim 2.18a_0$ (Ref. 23).

TABLE II. Phase shifts (in radians) for elastic s_g e-H_2 scattering obtained from variational wave functions calculated using various basis sets: type I (N = 25) and type II (N = 11, 12, 13, 14), where N is the number of configurations. The N = 25 basis set is shown in Table I. For the type-II basis sets, α = 0.75. Energies are in eV. Also shown is the energy of the lowest variational root and the nodal location for each case. The column labeled cc shows close-coupling eigenphase shifts of Henry and Lane (Refs. 2 and 30). All results include polarization via an adiabatic polarization potential as described in the text.

N / E	Type I	Type II				
	25	11	12	13	14	cc
0.05	3.049	3.047	3.058	3.053	3.054	3.0536
0.07	3.030	3.028	3.041	3.035	3.036	3.0351
0.1	3.004	3.002	3.018	3.010	3.012	3.0111
0.2	2.938	2.935	2.956	2.946	2.948	2.9475
0.3	2.885	2.881	2.906	2.894	2.896	2.8968
0.5	2.797	2.792	2.825	2.810	2.812	2.8143
1.0	2.631	2.625	2.669	2.648	2.652	2.6604
2.0	2.391	2.382	2.441	2.413	2.418	2.4458
3.0	2.204	2.193	2.236	2.231	2.236	2.2883
4.0	2.045	2.033	2.113	2.076	2.082	2.1623
6.0	1.779	1.765	1.860	1.816	1.823	1.9667
10.0	1.357	1.339	1.459	1.403	1.412	1.4459
r_{node} ($\times a_0$)	2.15	2.17	2.04	2.10	2.09	
E_{var}	0.0688	0.1359	0.1171	0.1020	0.0928	

r_{node} is a reasonable choice for r_{cc}, but it is not essential that the integration start there. Indeed, for p_σ-wave scattering, there is no node close to the origin; nevertheless the integration could be carried out using the value of $u_{p_\sigma}(r_3)$ and its slope at some reasonable value of r_{cc}. Figure 3 also shows that within a certain region, from ~$1.6a_0$ to ~$2.4a_0$ in this case, it does not matter where the long-range adiabatic polarization potential is introduced.

We have examined the sensitivity of the s_σ phase shifts to α, the nonlinear parameter in the STO basis functions. Table IV contains the s_σ phase shifts (with polarization) for N = 14 and α = 0.5, 0.75, and 1.0. (Increasing α was found to increase the lowest variational root and spread the energies.) In the cases shown in Tables II–IV, a "flat region" in the graphs of cross section vs r_{start} analogous to that in Fig. 3 is evident. However, as N is decreased, the width of the region decreases, centering on r_{node}. Similarly, for too large or too small a value of α (e.g., α<0.5 or $\alpha \geq$1.0), the region disappears completely. This behavior suggests that some care must be exercised in choosing optimum values of N and α.[32]

In Fig. 2, s_σ cross sections corresponding to the N= 14 case are also shown. For the latter case, integration was initialized at $r_{cc} = r_{node} = 2.09a_0$, corresponding to a 14-configuration variational root at an energy of 0.0928 eV. This calculation is, of course, considerably less expensive than the 25-configuration calculation, and appears to yield results in better agreement with those of close-coupling calculations. Fitting the 14-configuration s_σ cross section at 0.05 eV to the s-wave modified-effective-range-theory (MERT) equation,[31] we obtain a scattering length of $A = 1.20a_0$. With this value, the simple MERT equations yield cross sections in excellent agreement with close-coup-

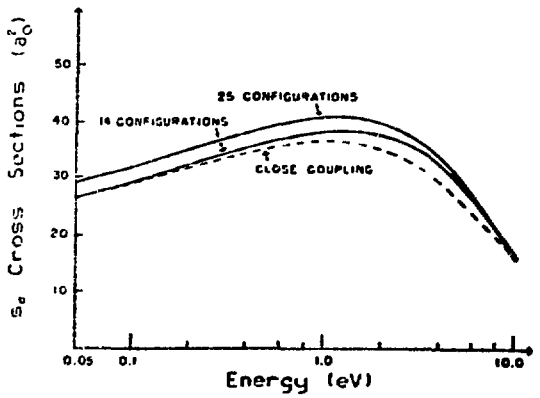

FIG. 2. Elastic s_σ e-H_2 cross sections obtained from pseudo-bound-state procedure using variational H_2^- functions constructed from a type-I N = 25 basis set and a type-II N = 14 basis set (solid lines). Polarization is included via an adiabatic polarization potential outside the exchange region. Close-coupling (J = 0) results of Henry and Lane (Ref. 2) (static-exchange approximation) using the same polarization potential are also shown (dashed curve).

TABLE III. Phase shifts (in radians) for elastic s-, e-H_2 scattering obtained from variational wave functions calculated using various basis sets: type I (N = 25) and type II (N = 11, 12, 13, 14) where N is the number of configurations. The N = 25 basis set is shown in Table I. For the type-II basis sets, α = 0.75. Energies are in eV. The column labeled cc shows close-coupling phase shifts of Henry and Lane (Ref. 2). The column labeled se shows static-exchange results of Tully and Berry (Ref. 9). No polarization is included.

E \ N	Type I	Type II					
	25	11	12	13	14	cc	se
0.034	...	3.034	3.040	3.037	3.038		3.0394
0.05	3.012	3.091	3.019	3.015	3.016	3.0134	
0.07	2.989	2.987	2.996	2.992	2.993	2.9900	
0.1	2.959	2.956	2.9[illegible]	2.963	2.963	2.9605	
0.136	...	2.926	2.939	2.933	2.934		2.939
0.2	2.882	2.880	2.896	2.888	2.890	2.8959	
0.3	2.824	2.821	2.841	2.832	2.833	2.8290	
0.5	2.731	2.727	2.753	2.741	2.743	2.7394	
0.544	2.713	2.710	2.736	2.724	2.726		2.737
1.0	2.561	2.556	2.592	2.575	2.578	2.5780	
1.224	...	2.494	2.534	2.515	2.518		2.541
2.0	2.321	2.313	2.364	2.341	2.345	2.3593	
2.177	2.295	2.278	2.331	2.306	2.310		2.352
3.0	2.136	2.127	2.189	2.160	2.165	...	
3.401	2.071	2.061	2.128	2.097	2.102		2.174
4.0	1.981	1.969	2.042	2.009	2.014	2.0754	
4.899	1.856	1.844	1.925	1.888	1.894		2.006
6.0	1.719	1.705	1.794	1.753	1.760	...	
10.0	1.404	1.397	1.400	1.348	1.357	1.6092	

ling cross sections for energies up to 10 eV. A scattering length of $1.32a_0$ is obtained from the cross sections extracted from the 25-configuration wave function, and $1.19a_0$ is obtained from the close-coupling cross sections. Chang[21] has performed a fit of the MERT equation to the results of electron drift and diffusion measurements[22] and finds a scattering length of $1.26a_0$. This value yields cross sections larger than those of Henry and Lane,[2] suggesting that the latter may be some-

TABLE IV. Phase shifts (in radians) for elastic s_α scattering obtained from variational calculations (basis set II with N = 14 and various values of α). Energies are in eV. Also shown are the energies of the lowest variational root and the node for each case.

E \ α	0.5	0.75	1.0
0.05	3.058	3.054	3.063
0.07	3.041	3.036	3.047
0.1	3.018	3.017	3.025
0.2	2.956	2.948	2.966
0.3	2.906	2.896	2.919
0.5	2.825	2.812	2.840
1.0	2.669	2.652	2.689
2.0	2.441	2.416	2.469
3.0	2.263	2.236	2.297
4.0	2.113	2.082	2.151
6.0	1.860	1.823	1.905
10.0	1.565	1.412	1.515
r_{node} (a_0)	2.04	2.09	1.98
ε_{var}	0.0411	0.0928	0.1586

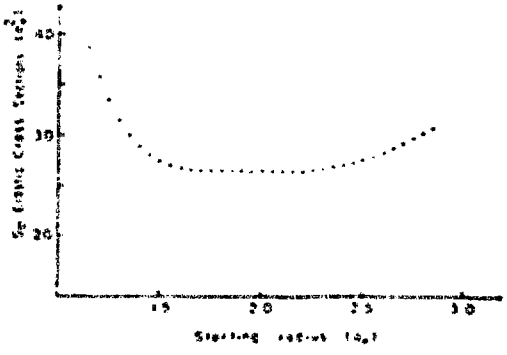

FIG. 3. Cross sections for s_α elastic e-H_2 scattering at 0.05 eV obtained using a type-II N = 14 variational wave function with α = 0.75 and an adiabatic polarization potential. The horizontal axis shows the value of r at which the single-channel integration of Eq. (8) for $u_{s_\alpha}(r)$ was initiated using the values of the s_α projection of the variational radial wave function and its derivative at r.

what too small. This would be the case, for example, if their adiabatic polarization potential is too strong owing to neglect of the nonadiabatic distortion potential.[36]

IV. CONCLUSIONS

The results discussed above suggest that there is valid electron-molecule scattering information, for some cases over a fairly wide range of energies, contained in low-energy variational wave functions for the corresponding negative ion. In cases where the coupling of partial waves is weak beyond a certain radius and the potential energy is strongly attractive near the origin, phase shifts can be obtained by the procedure outlined in Sec. II. This procedure may be applicable to larger homonuclear molecules, where the short-range potential energy is stronger than in H_2. However, for energies large enough so that the nondiagonal S-matrix elements become large, the procedure must be modified. A sufficient number of linearly independent solutions must be obtained so that the multichannel asymptotic boundary conditions can be enforced. One procedure for doing this is that suggested by Zarlingo, Ishihara, and Poe,[37] based on the work of Tully.[38] The same qualifying remarks also apply to the extension of the present work to inelastic scattering. However, in cases where the adiabatic-nuclei approximation is valid,[1,7,8,39] the body-frame calculation is strictly elastic.

The quality of the variational H_2^- wave function can be improved by including more basis functions. A comparison of results obtained with the 25-configuration and 14-configuration functions suggest that further investigation of systematic basis sets would be fruitful. Unfortunately, very large compact basis sets introduce numerical problems (linear dependence) in the multiconfiguration calculation. Thus it becomes necessary either to project certain troublesome eigenfunctions or go to greater machine precision—perhaps both. Finally, correlation effects could be studied by the expedient of "unfreezing" the core H_2 wave function.

ACKNOWLEDGMENTS

We are grateful to R. J. W. Henry, A. U. Hazi, D. J. Schneider, and T. G. Winter for useful discussions. We are especially indebted to Dr. Henry for sending us the close-coupling wave functions and cross sections. We also acknowledge the technical assistance of J. Black and J. A. Hayward, who participated in various stages of this research, and of W. Reets, who assisted with the molecular-structure code used in these calculations.

---

*Research supported in part by the U. S. Energy Research and Development Administration and the Robert A. Welch Foundation.

†Fannie and John Hertz Foundation Fellow.

[1] D. E. Golden, N. F. Lane, A. Temkin, and E. Gerjuoy, Rev. Mod. Phys. 43, 642 (1971); K. Takayanagi and Y. Itikawa, Adv. At. Mol. Phys. 6, 105 (1970).

[2] R. J. W. Henry and N. F. Lane, Phys. Rev. 183, 221 (1969).

[3] P. G. Burke, Comput. Phys. Commun. 6, 288 (1974).

[4] T. N. Rescigno, C. W. McCurdy, Jr., and V. McKoy, Phys. Rev. A 11, 825 (1975), and references therein; B. I. Schneider, Bull. Am. Phys. Soc. 19, 1230 (1974), and private communication.

[5] T. G. Winter and N. F. Lane, Chem. Phys. Lett. 30, 363 (1975).

[6] E. S. Chang and U. Fano, Phys. Rev. A 6, 173 (1972).

[7] E. S. Chang and A. Temkin, Phys. Rev. Lett. 23, 399 (1969).

[8] C. Bottcher, Chem. Phys. Lett. 4, 329 (1969).

[9] J. C. Tully and R. S. Berry, J. Chem. Phys. 51, 2024 (1969).

[10] R. L. Wilkins and H. S. Taylor, J. Chem. Phys. 42, 3572 (1967). See footnote 29 of Ref. 1.

[11] S. Hara, J. Phys. Soc. Jpn. 27, 1009 (1969).

[12] N. F. Lane and R. J. W. Henry, Phys. Rev. 173, 183 (1968).

[13] S. Hara, J. Phys. Soc. Jpn. 27, 1592 (1969).

[14] S. Hara, J. Phys. Soc. Jpn. 27, 1592 (1969).

[15] H. A. Abram and A. Herzenberg, Chem. Phys. Lett. 1, 197 (1969).

[16] F. H. M. Faisal and A. Temkin, Phys. Rev. Lett. 28, 203 (1972).

[17] A. Temkin and F. C. Sullivan, Phys. Rev. Lett. 23, 1037 (1974).

[18] R. J. W. Henry and E. S. Chang, Phys. Rev. A 5, 276 (1972).

[19] H. S. Taylor and A. U. Hazi, Phys. Rev. A 1, 1109 (1970); A. U. Hazi and H. S. Taylor, Chem. Phys. Lett. 8, 582 (1971). See also A. Hazi, Chem. Phys. Lett. 20, 251 (1973).

[20] H. S. Taylor and F. E. Harris, J. Chem. Phys. 39, 1012 (1963); H. S. Taylor and J. Hershbach, J. Chem. Phys. 49, 344 (1968).

[21] D. G. Zarlingo, T. Ishihara, and R. T. Poe, Phys. Rev. Lett. 35, 1053 (1975).

[22] N. F. Lane and S. Geltman, Phys. Rev. 160, 53 (1967).

[23] J. C. Browne, Ph.D. thesis (University of Texas, 1971) (unpublished).

[24] H. F. Schaefer, III, *The Electronic Structure of Atoms and Molecules* (Addison-Wesley, Reading, Mass., 1972).

[25] S. C. Wang, Phys. Rev. 31, 579 (1928).

[26] M. A. Morrison and N. F. Lane, Bull. Am. Phys. Soc.

19, 1539 (1979); M. A. Morrison, M.A. thesis (Rice University, 1974) (unpublished).
[27]Cf. P. G. Burke and N. Chandra, J. Phys. B 5, 1696 (1972).
[28]D. R. Hartree, *The Calculation of Atomic Structures* (Wiley, New York, 1957).
[29]W. Kolos and L. Wolniewicz, J. Chem. Phys. 43, 2429 (1965).
[30]R. J. W. Henry (private communication).
[31]M. A. Morrison, J. A. Hazgard, and N. F. Lane, Bull. Am. Phys. Soc. 19, 1196 (1974).
[32]See comments on choices of basis functions by A. L. Sinfailam and R. K. Nesbet, Phys. Rev. A 6, 2118 (1972).
[33]T. F. O'Malley, L. Spruch, and L. Rosenberg, J. Math. Phys. 2, 491 (1961).
[34]E. S. Chang, Phys. Rev. A 9, 1644 (1974).
[35]R. W. Crompton, D. K. Gibson, and A. I. McIntosh, Aust. J. Phys. 22, 715 (1969).
[36]J. Callaway, R. W. LaBahn, T. J. Pu, and W. M. Duxler, Phys. Rev. 168, 12 (1968).
[37]J. C. Tully, Phys. Rev. 181, 7 (1969).
[38]M. Shugard and A. U. Hazi (private communication).

Appendix 2. Electron-Molecule Scattering in the Lab Frame

In the body of this work we formulated the electron-molecule scattering problem in a body-fixed reference frame corresponding to the polar axis frozen along the internuclear axis. Early formulations of the problem (e.g., reference (3) of Chapter 3) used a space-fixed or laboratory reference frame. The author has discussed the relation between the two frames and how to transform the scattering function between the frames in Chapter 7 and elsewhere (see reference (2) of Chapter 3). Here we would like to review the lab-frame analysis and present a few numbers for e-CO_2 scattering in this picture.

We begin (as usual) with the Schroedinger Equation for the electron-molecule system,

$$(\mathcal{H} - E_{k\Gamma})\Psi_{k\Gamma}(\vec{r}_i, \vec{R}_\alpha, \vec{r}) = 0. \qquad (1)$$

where Γ denotes the set of quantum numbers needed to uniquely label a state of the target and where k is the incident wavenumber. Applying the Born-Oppenheimer Approximation to the target, we can write the target molecular wavefunction as

$$\psi_\Gamma(\vec{r}_i, \vec{R}_\alpha) = \Phi_{n\alpha}(\vec{r}_i, \vec{R}_\alpha)\, \textcircled{H}_{jm_j\alpha}(\hat{R}_\alpha), \qquad (2)$$

where $\Phi_{n\alpha}$ is an electronic wavefunction and $\Theta_{jm_j\alpha}$ is a rotational wavefunction. We neglect vibrational states. The subscript α thus denotes any other quantum number(s) needed to fully specify the molecular state. For a Σ state of a linear molecule, we have

$$\Theta_{jm_j\alpha}(\hat{R}_\alpha) = Y_j^{m_j}(\hat{R}), \tag{3}$$

where $\hat{R}$ is the orientation of the internuclear axis in the space-fixed laboratory reference frame.

Now, to proceed we couple the angular momentum of the target molecule, $\vec{j}$, to the orbital angular momentum of the incident electron, $\vec{\ell}$ to form the total angular momentum vector,

$$\vec{J} = \vec{j} + \vec{\ell}. \tag{4}$$

The projection of $\vec{J}$ on our space-fixed z-axis is related to m_j and m_ℓ by

$$M_J = m_j + m_\ell \tag{5}$$

and to the quantum number J by the familiar relation

$$M_J = -J, -J+1, \ldots, J-1, J. \tag{6}$$

The total angular momentum $\vec{J}$ is a constant of the motion of the system (electron + molecule), so we can find eigenfunctions of the Hamiltonian which are also eigenfunctions of J^2 and J_z. Suppose we let $(j\ell)$ denote the initial state of the system. Then the coupled angular functions are defined by

$$\mathcal{Y}_{j\ell}^{JM_J}(\hat{r},\hat{R}) = \sum_{m_j m_\ell} C(j\ell J; m_j m_\ell M_J) Y_\ell^{m_\ell}(\hat{r}) Y_j^{m_j}(\hat{R}), \qquad (7)$$

and we can expand the syste wavefunction as

$$\Psi_{j\ell n}^{JM_J}(\vec{r}_i,\vec{R},r) = \sum_{j'\ell'} \frac{1}{r} u_{j'\ell'}^{(njl)} \mathcal{Y}_{j'\ell'}^{JM_J}(\hat{r},\hat{R}), \qquad (8)$$

where we have introduced an additional subscript n to connote the electronic state of the target.

The summation in Eq. (7) is restricted by the usual conditions on the Clebsch-Gordan coefficients. The summation in Eq. (8) contains a finite number of angular terms. Here we shall limit ourselves to the sigma target states and, in particular, to the ground state.

If we now substitute these expansions into the Schroedinger Equation and carry out the usual algebraic manipulations, we obtain a set of coupled equations of the form

$$\left[\frac{d^2}{dr^2} - \frac{\ell'(\ell'+1)}{r^2} + k_{jj'}^2\right] u_{j'\ell'}^{Jj\ell}(r) = \sum_{j''\ell''} \langle j'\ell' | \bar{V} | j''\ell'' \rangle u_{j''\ell''}^{Jj\ell}(r) \qquad (9)$$

where exchange has been neglected (see reference (3) of Chapter 4 for the details of inclusion of exchange). The channel wavenumber appearing in Eq. (9) is defined by

$$k_{jj'}^2 + \epsilon_{j'} = k_{jj}^2 + \epsilon_j \ , \tag{10}$$

where ϵ_j is the energy of the target molecule in rotational state j. The matrix element appearing in (9) is simply

$$\langle j'\ell'|\bar{V}|j''\ell''\rangle = \int \mathcal{Y}_{j'\ell'}^{JM_J *} \bar{V} \, \mathcal{Y}_{j''\ell''}^{JM_J} \, d\hat{r} \, d\hat{R} \ , \tag{11}$$

where $\bar{V}$ is the usual averaged static potential energy for the ground state (see the elaborate discussions of Chapter 3).

We saw in the text discussion of this material that the matrix element $\bar{V}$ is easily expanded in Legendre polynomials, viz.,

$$\bar{V}(\vec{r}) = \sum_{\lambda=0}^{\infty}{}' v_\lambda(r) P_\lambda(\cos\theta) \ , \tag{12}$$

with $v_\lambda(r)$ given by Eq. (3.40). Then the full matrix elements appearing in Eq. (9) is given by

$$V^J_{j'\ell',j''\ell''}(r) = \sum_{\lambda=0}^{\infty}{}' f_\lambda(j'\ell' j''\ell''; J) v_\lambda(r) \ , \tag{13}$$

where the coefficients f_λ (called Percival-Seaton coefficients) are

given by

$$f_\lambda(j'\ell'j''\ell'';J) = (-1)^{j''-j+J}(2\lambda+1)^{-1}[(2j'+1)$$
$$\otimes(2j''+1)(2\ell'+1)(2\ell''+1)]^{\frac{1}{2}}C(\ell'\ell''\lambda;00)C(j'j''\lambda;00) \qquad (14)$$
$$\otimes W(j'\ell'j''\ell'';J\lambda)$$

with W(j' ℓ' j" ℓ"; J λ) the familiar (sic) Racah coefficient.

As we mentioned in Chapter 9, our initial e-CO_2 studies were carried out in the laboratory frame. Convergence difficulties due to the enormous number of partial waves required to converge the cross sections forced us to shift to the body-frame as described in Chapter 6. Typical behavior of the individual cross sections as the numer of rotational states is increased is shown in Table 1, which pertains to an incident energy of 0.01 Ryd. with λ = 0,2,4, and 6 included in the expansion of Eq. (12). Only short-range interactions are taken into account in these calculations. We should point out that for $\lambda_{max} \gtrsim 8$, the transformation procedure described in section 6.6 must be used to overcome numerical difficulties analogous to those encountered in the body-frame analysis.

j' \ N	4	5	6	7
0	102.4356	88.0599	85.7441	85.1582
2	0.0098	0.0058	0.0051	0.0050
4	1.6(-8)	1.2(-8)	1.2(-8)	1.1(-8)

TABLE 1

Cross sections in a_0^2 for e-CO_2 scattering in the laboratory frame at 0.01 Ryd. Only J=0 is shown. Short-range static interactions for λ = 0, 2, 4, 6 are included. N is the number of states and j' is the final rotational state. Excitation is from an initial state j = 0 to final state j'.

REFERENCES AND NOTES

References and Notes, Chapter 1

(1). M. A. Morrison, "Electron-Molecule Scattering Scudies Using Bound-State Variational Methods: Application to SSCP Scattering and s-wave Elastic e-H_2 Collisions," M.S. Thesis, Rice University, 1974 (unpublished).

(2). M. A. Morrison and N. F. Lane, Phys. Rev. A 12, 2361 (1975). See also Bull. Amer. Phys. Soc. 18, 1530 (1973) and (with J. A. Haggard) Bull. Amer. Phys. Soc. 19, 1186 (1974).

(3). N. N. Sobolev and V. V. Sobovikov, Invited Papers Fifth ICPEAC Leningrad, L. Branscom (ed.), p. 49 (1967).

(4). A preliminary account of this research has been reported. See M. A. Morrison, L. A. Collins, and N. F. Lane, Bull. Amer. Phys. Soc. 20, 1470 (1975).

References and Notes, Chapter 2

(1). Much of the factual information here presented obtains from G. Herzberg, Molecular Spectra and Molecular Structure II Infrared and Raman Spectra of Polyatomic Molecules; New York: Van Nostrand Reinhold, 1945.

(2). M. Tinkham, Group Theory and Quantum Mechanics; New York: McGraw Hill, 1964, see Chapter 2 and 3.

(3). M. A. Morrison, T. L. Estle, and N. F. Lane, Quantum States of Atoms, Molecules, and Solids; Englewood Cliffs, New Jersey: Prentice-Hall. See Chapter 14, especially Figure 14.5 and ensuing discussion.

(4). See chapter 17 of reference (3).

(5). See E. B. Wilson, J. C. Decius, and P. L. Cross, Molecular Vibrations: The Theory of Infrared and Raman Vibrational Spectra; New York: McGraw-Hill, 1955, especially Chapters 2 and 3.

(6). M. Vucelić, Y. Öhrn, and J. R. Sabin, J. Chem. Phys. 59, 3003 (1973).

(7). L. A. Gribov and V. N. Smirnov, Soviet Phys. Uspekhi, 4, 919 (1962).

(8). G. Amat and M. Pimbert, J. Molec. Spect. 16, 278 (1965).

(9). R. S. Mullikan, J. Chem. Phys. 3, 720 (1935); Rev. Mod. Phys. 14, 204 (1942).

(10). W. Moffitt, Proc. Roy. Soc. (London) A 196, 524 (1949).

(11). J. F. Mulligan, J. Chem. Phys. 19, 347 (1951).

(12). A. D. McLean, J. Chem. Phys. 32, 1595 (1960); 38, 1347 (1963).

(13). A. D. McLean, B. J. Ransil, and R. S. Mullikan, J. Chem. Phys. 32, 1873 (1960).

(14). J. A. Pople and G. A. Segal, J. Chem. Phys. 44, 3289 (1966).

(15). H. Satz, C. L. Tang, and G. F. Koster, J. Appl. Phys. 37, 4278 (1966). Vibrational wavefunctions.

(16). S. D. Peyerimhoff, R. J. Buenker, and J. L. Whitten, J. Chem. Phys. 46, 1707 (1967). Gaussian basis set.

(17). J. A. Pople, D. L. Beveridge, and P. A. Dobosh, J. Chem. Phys. 47, 2026 (1967).

(18). M. D. Newton, W. A. Latham, W. J. Hehre, and J. A. Pople, J. Chem. Phys. 52, 4064 (1970).

(19). N. W. Winter and C. F. Bender, Chem. Phys. Lett. 20, 489 (1973).

(20). C. R. Claydon, G. A. Segal, and H. S. Taylor, J. Chem. Phys. 52, 3387 (1970). Semi-empirical approximation to the Hartree-Fock SCF procedure. See also reference (26) for comment on this work.

(21). L. W. Larkin and B. J. Hasted, Chem. Phys. Lett., 5, 325 (1970).

(22). J. N. Eardsley, J. Chem. Phys. 51, 3384 (1969).

(23). J. Pacansky, V. Wahlgren, and P. S. Bagus, J. Chem. Phys. 62, 2740 (1975).

(24). I. Cadez, M. Tronc, and R. I. Hall, J. Phys. B. 7, L132 (1974).

(25). M.J.W. Boness, J. B. Hasted, and J. W. Larkin, Proc. Roy. Soc. A 305, 493 (1968).

(26). M. Krauss and D. Neumann, Chem. Phys. Lett. 14, 26 (1972).

(27). K. O. Hartman and J. C. Hisatsune, J. Chem. Phys. 44, 1913 (1966).

(28). M. E. Jacox and D. E. Milligan, Chem. Phys. Lett. 28, 163 (1974).

(29). C. Ramsauer and R. Kollath, Ann. Phys. Lpz. 4, 91 (1930).

(30). L. G. Christophoru, G. S. Hurst, and A. Hadjiantoniou, J. Chem. Phys. 44, 3506 (1966).

(31). J. L. Pack, R. E. Voshall, and A. V. Phelps, Phys. Rev. 127, 2084 (1962). Drift velocity measurements.

(32). R. D. Hake and A. V. Phelps, Phys. Rev. 158, 70 (1967).

(33). F. C. Fehsenfeld, J. Chem. Phys. 39, 1653 (1963).

(34). C. K. Rhodes, M. J. Kelly, and A. Javan, J. Chem. Phys. 48, 5730 (1968).

(35). A. Skerbele, M. A. Dillon, and E. N. Lassettre, J. Chem. Phys. 49, 5042 (1968).

(36). C.J.S.M. Simpson, K. B. Bridgman, and T.R.D. Chandler, J. Chem. Phys. 49, 513 (1968).

(37). M.J.W. Boness and G. J. Schultz, Phys. Rev. Lett. 21, 1031 (1968).

(38). E. N. Lassettre, A. Skerbele, and M. A. Dillon, J. Chem. Phys. 50, 1829 (1969).

(39). A. Andrick, D. Danner, and H. Ehrhardt, Phys. Lett. 29A, 346 (1969).

(40). A. Stamatovic and G. J. Schultz, Phys. Rev. 188, 213 (1969).

(41). W. L. Nighan, Phys. Rev. A. 2, 1989 (1970).

(42). M. Krauss, S. R. Mielczarek, D. Neumann, and C. E. Kuyatt, J. Geophys. Res. 76, 3733 (1971).

(43). Y. Itikawa, Planet. Space Sci. 19, 993 (1971).

(44). D. Spence, J. L. Mauer, and G. J. Schultz, J. Chem. Phys. 57, 5516 (1972).

(45). P. D. Burrow and L. Sanche, Phys. Rev. Lett. 28, 333 (1972).

(46). L. Sanche and G. J. Schultz, J. Chem. Phys. 58, 479 (1973).

(47). R. I. Hall, A. Chutjian, and S. Trajmar, J. Phys. B 6, L264 (1973).

(48). A. Stamatovic and G. J. Schultz, Phys. Rev. A 7, 589 (1973).

(49). J. J. Lowke, A. V. Phelps, and B. W. Irwin, J. Appl. Phys. 44, 4664 (1973).

(50). M.J.W. Boness and G. J. Schultz, Phys. Rev. A 9, 1969 (1974).

(51). R. Tice and D. Kivelson, J. Chem. Phys. 46, 4743 (1967); 4748 (1967).

(52). M. A. Morrison and N. F. Lane, Bull. Amer. Phys. Soc. 20, 240 (1975). See also H. T. Davis and L. D. Schmidt, Chem. Phys. Lett. 16, 260 (1972).

(53). Y. Itikawa, At. Data and Nucl. Data Tables, 14, 1 (1974).

(54). M. Morrison, M. S. thesis, Rice University, 1974 (unpublished).

(55). D. G. Thompson, Proc. Roy. Soc. (London) A 294, 160 (1966).

(56). See F. Reif, Fundamentals of Statistical and Thermal Physics; New York: McGraw-Hill, 1965.

(57). C. J. Elliott, O. P. Judd, A. M. Lockett, and S. D. Rockwood, LASL Informal Report, LA-5562-MS; 1974.

(58). D. C. Tyte, Advan. Quant. Elec. I; New York: Academic Press, 1970, p. 129 ff.

(59). B. A. Lengyel, Lasers, New York: Wiley-Interscience, 1971 (Second Edition), p. 343 ff.

(60). P. K. Cheo, J. Appl. Phys. 38, 3563 (1967).

References and Notes, Chapter 3

(1). M. A. Morrison, T. L. Estle, and N. F. Lane, Quantum Status of Atoms, Molecules, and Solids; Englewood Cliffs, New Jersey: Prentice-Hall Inc., 1976. See Chapter 11, especially section 11.2.

(2). M. A. Morrison, "Electron-Molecule Scattering Studies Using Bound-State Variational Methods: Application to SSCP Scattering and s-wave Elastic e-H_2 Collisions," M.S. Thesis Rice University, 1974 (unpublished).

(3). A. M. Arthurs and A. Dalgarno, Proc. Roy. Soc. A 256, 540 (1960). For application to electron-H_2 collisions, see N. F. Lane and S. Geltman, Phys. Rev. 160, 53 (1967) and R.J.W. Henry and N. F. Lane, Phys. Rev. 183, 221 (1969). A review of this theory can be found in D. E. Golden, N. F. Lane, A. Temkin, and E. Gerjuoy, Rev. Mod. Phys. 43, 642 (1971), section 3.

(4). Henry F. Schaeffer, The Electronic Structure of Atoms and Molecules: A Survey of Rigorous Quantum Mechanical Results; Reading Mass.: Addison-Wesley Publishing Co., 1972. This text is extremely useful for the reader who knows something about molecular structure theory and wants a broad (and critical) sketch of what has been done circa 1972 in the field. It has lots of references and is cheap, too.

(5). M. Yoshimine and A. D. McLean, Int. J. Quant. Chem. IS, 313 (1967); A. D. McLean and M. Yoshimine, IBM J. Res. Dev. 12, 206 (1968).

(6). A. D. McLean and M. Yoshimine, "Tables of Linear Molecule Wave Functions," IBM J. Res. Dev. Supp., November, 1967. This fantastically useful and easy to use set of tables treats many homonuclear and heteronuclear diatomics and a few triatomics. Some molecules are studied in more than one configuration (e.g., various internuclear spacings).

(7). C.C.J. Roothaan, Rev. Mod. Phys. 23, 69 (1951); 32, 179 (1960).

(8). See the review by R. K. Nesbet, Advan. Chem. Phys. 9, 321 (1965) and references therein. At a more "text-bookish" level try D. B. Cook, Ab initio Valence Calculations in Chemistry; New York: John Wiley and Sons, 1974. Although unbelievably expensive and devoid of an index, this book contains some useful discussions.

(9). See Chapter 15 of reference (1) for an introduction to molecular orbital theory. Buy this book.

(10). E. Clementi, "Tables of Atomic Functions," IBM J. Res. Dev. Supp. 9, 2 (1965). See also E. Clementi, J. Chem. Phys. 40. 1944 (1964).

(11). See Chapter 12 of reference (1) for a fairly thorough introductory treatment of the Born-Oppenheimer approximation.

(12). S. Huzinaga and C. Arnau, J. Chem. Phys. 53, 451 (1970); E. Clementi, R. Matcha, and A. Veillard, J. Chem. Phys. 47, 1865 (1967).

(13). See Chapter 3 of A. G. Turner, Methods in Molecular Orbital Theory; Englewood Cliffs, New Jersey: Prentice-Hall, Inc., 1974. Also useful is F. A. Cotton, Chemical Applications of Group Theory; New York: Wiley-Interscience, 1971 (Second Edition).

(14). See Chapter 9 of reference (1). Single-configuration molecular (electronic) wavefunctions are discussed in Chapter 16.

(15). A. D. McLean, J. Chem. Phys. 39, 2653 (1963). See also the very significant work by T. Dunning, J. Chem. Phys. 53, 2823 (1970) and elsewhere on polarization orbitals.

(16). See Chapters 5 and 6 of R. McWeeny and B. T. Sutcliffe, Methods of Molecular Quantum Mechanics; New York: Academic Press, 1969 for an introduction to CI calculations. Copious references to the literature may be found in W. G. Richards, T.E.H. Walker, and R. K. Hinkley, A Bibliography of Ab Initio Molecular Wavefunctions. Supplement for 1970-1973; London: Clarendon Press, 1974. At the time of writing, no CI calculations for CO_2 are in the literature.

(17). A. D. McLean and M. Yoshimine, J. Chem. Phys. 45, 3467 (1966).

(18). See Chapters 13 and 14 of the ever-popular reference (1).

(19). G. Herzberg, Molecular Spectra and Molecular Structure III. Electronic Spectra and Electronic Structure of Polyatomic Molecules; New York: Van Nostrand Reinhold, 1966.

(20). L. C. Snyder and H. Basch, Molecular Wavefunctions and Properties: Tabulated from SCF Calculations in a Gaussian Basis Set; New York: John Wiley and Sons, 1972. This book, along with the tables of reference 6, should be part of every computer-minded quantum mechanic's arsenal.

(21). W. W. Bell, Special Functions for Scientists and Engineers; London: D. Van Nostrand Co. Ltd, 1968. Chapter 3 deals with Legendre polynomials and establishes the definitions used in this work. For enormous quantities of useful formulae and tables, see M. Abramowitz and I. A. Stegun, Handbook of Mathematical Functions; Washington: NBS, 1964, Chapter 8.

(22). F. S. Acton, Numerical Methods that (Usually) Work; New York: Harper and Row, 1970, Chapter 4. This is surely the most delightful book on this subject ever written and very valuable besides. Also useful is W. E. Grove, Brief Numerical Methods; Englewood Cliffs, New Jersey: Prentice-Hall, Inc., 1966, Chapter 6.

(23). H. A. Bethe and E. E. Salpeter, Quantum Mechanics of One- and Two-Electron Atoms; Heidelberg: Springer-Verlag, 1957.

(24). M. E. Rose, Elementary Theory of Angular Momentum; New York: John Wiley and Sons, 1957, p. 241.

(25). See p. 60 of reference (24).

(26). See the Appendix of reference (23).

(27). See p. 62 of reference (24) or p. 230 of reference (1).

(28). A. R. Edmonds, Angular Momentum in Quantum Mechanics; Princeton, New Jersey: Princeton University Press, 1960. Other standard references on this subject are D. M. Brink and G. R. Satchler, Angular Momentum; London: Clarendon Press, 1968 (Second Edition) and B. R. Judd, Angular Momentum Theory for Diatomic Molecules; New York: Academic Press, 1975. The last named text uses an elegant, beautiful, and often confusing tensor notation throughout.

(29). See sections 10 and 11 of reference 24.

(30). See A. Ralston and H. S. Wilf, Mathematical Methods for Digital Computers, Volume I; New York: John Wiley and Sons, 1967, Chapter 22.

(31). See A. Ralston and H. S. Wilf, Mathematical Methods for Digital Computers, Volume II; New York: John Wiley and Sons, 1967, Chapter 8.

(32). U. Fano, Comm. At. Mol. Phys. 1, 140 (1970).

(33). J. Tully and R. S. Berry, J. Chem. Phys. 51, 2056 (1969). The jargon "low-ℓ spoiling" was coined by V. McKoy et al. in an as-yet-unpublished paper. We applied this idea to e-H_2 collisions in the so-called pseudo-bound-state method; see reference (2) and M. A. Morrison and N. F. Lane, Phys. Rev. A, 12, 2361 (1975) for an account of this work.

(34). D. E. Stogryn and A. P. Stogryn, Mol. Phys. 11, 371 (1966).

(35). A. D. McLean, J. Chem. Phys. 38, 1347 (1963).

(36). M. Vucelić, Y. Öhrn, and J. R. Sabin, J. Chem. Phys. 59, 3003 (1973).

(37). A. D. Buckingham, Quart. Rev. Chem. Soc. (London) 13, 183 (1959).

(38). A. D. Buckingham, R. L. Disch, and D. A. Dunmur, J. Am. Chem. Soc. 90, 3104 (1968).

(39). F.H.M. Faisal, J. Phys. B: Atom Molec. Phys. 3, 636 (1970).

(40). N. Chandra, Phys. Rev. A 12, 2361 (1975).

References and Notes, Chapter 4

(1). For a general introduction to exchange effects see M. A. Morrison, T. L. Estle, and N. F. Lane, Quantum States of Atoms, Molecules, and Solids; Englewood Cliffs, New Jersey: Prentice-Hall, Inc., 1976, Chapter 8.

(2). See Chapter 10 of reference (1).

(3). See R.W.B. Ardill and W. D. Davison, Proc. Roy. Soc. A 340, 465 (1968) for details of incorporation of exchange in the coupled equations technique and R.J.W. Henry and N. F. Lane, Phys. Rev. 183, 221 (1969) for applications to e-H_2 collisions. A more detailed discourse on all this can be found in Chapter 4 of M. Morrison, M.S. thesis, Rice University, 1974 (unpublished).

(4). See J. C. Slater, Quantum Theory of Atomic Structure, Volume II; New York: McGraw-Hill, 1960, Chapter 17 for a very detailed analysis of this problem.

(5). N. F. Lane and S. Geltman, Phys. Rev. 160, 53 (1967).

(6). See any standard treatment of partial waves in electron-molecule scattering such as those of reference (4).

(7). See, for example, reference (24). See also J. C. Tully and R. S. Berry, J. Chem. Phys. 51, 2056 (1969). Our application appears in M. A. Morrison and N. F. Lane, Phys. Rev. A 12, 2361 (1975).

(8). S. Hara, J. Phys. Soc. Japan 22, 710 (1967). A couple of errors appear in this paper: on the first line of Eq. (4), 1/3 should be replaced by 1/2. In Eq. (21), k_m should be replaced by k_{max}, the right hand side should be preceded by a minus sign, and in the line following π should be replaced by π^2. In the footnote at the bottom of p. (714), "Eq. (22-16)" should be replaced by "Eq. (A22-16)".

(9). J. C. Slater, Phys. Rev. 81, 385 (1951).

(10). See, for example, J. C. Slater and H. M. Krutter, Phys. Rev. 47, 559 (1935) and P.A.M. Dirac, Proc. Cambridge Phil. Soc. 26, 376 (1930) for introductory material on this model.

(11). F. Reif, Fundamentals of Statistical and Thermal Physics, New York: McGraw Hill, 1965 contains plenty of background on Fermi-Dirac (and other) statistics.

(12). See Chapter 21 and, more generally, Part Three of reference (1).

(13). Appendix 22 of reference (4).

(14). J. C. Slater, Phys. Rev. 82, 538 (1951), and references (9) and (13).

(15). J. C. Slater, Quantum Theory of Matter; New York: McGraw-Hill, 1968 (Second Edition).

(16). See Chapter 22 and especially Eq. (22.10) of reference (1).

(17). D. A. Liberman, Phys. Rev. 171, 1 (1968). Note that Liberman's definition of $F(\eta)$ on p. 1 differs from that of Slater in, say, reference (13) by a factor of 2.

(18). See, for example, R. B. Leighton, Principles of Modern Physics: New York: McGraw-Hill, 1959.

(19). For an interesting application of an extension of the Thomas-Fermi theory, see K. Yonei, J. Phys. Soc. Japan 22, 1127 (1967).

(20). The importance to electron-molecule collisions was first clearly indicated by H.S.W. Massey and R. O. Ridley, Proc. Phys. Soc. (London) A 69, 659 (1956). For the electron-atom problem, see M. J. Seaton, Phil. Trans. Roy. Soc. A 245, 469 (1953) and Proc. Roy. Soc. (London) A 241, 522 (1957). Also try P. M. Morse and W. P. Allis, Phys. Rev. 44, 269 (1933).

(21). M. E. Riley and D. G. Truhlar, J. Chem. Phys. 63, 2182 (1975). Two errors in this paper should be noted: in Eq. (14), the exponent should be 1/3 not 1/2 while in Eq. (15) it should be 1/2 not 1/3.

(22). Lee A. Collins (private communication).

(23). No work on scattering theory would be complete without at least one reference to the classic work N. F. Mott and H.S.W. Massey, The Theory of Atomic Collisions; London: Oxford University Press, 1965 (Third Edition). Go look at p. 33 ff.

(24). P. G. Burke and A. L. Sinfailam, J. Phys. B: Atom. Molec. Phys. 3, 641 (1970).

(25). See J.E.G. Farina, Quantum Theory of Scattering Processes, Oxford: Pergammon Press, 1973, section 1.5.

(26). P. G. Burke and N. Chandra, J. Phys. B: Atom Molec. Phys. 5, 1696 (1972). Corrections: V_p in Eq. (5) is not the same as V_p in Eq. (3). In Eq. (10), ^pv should be replaced with V. In Eq. (12), $2\ell'-1$ should be replaced with $2\ell'+1$. In Eq. (18), λ should be replaced with π twice. In Eq. (26), $|\ |$ should be squared. Whew!

(27). For a general review of pseudopotential theory, see J. D. Weeks, A. Hazi, and S. A. Rice, Adv. Chem. Phys. 16, 283 (1969).

(28). K. Simon, Mechanics; Reading, Mass.: Addison-Wesley, 1971.

(29). P. G. Burke, N. Chandra, and F. A. Gianturo, J. Phys. B: Atom. Molec. Phys. 5, 2212 (1972).

(30). N. Chandra and P. G. Burke, J. Phys. B: Atom. Molec. Phys. 6, 2355 (1973).

(31). N. Chandra, Comp. Phys. Commun. 5, 417 (1973).

(32). P. G. Burke, N. Chandra, and F. A. Gianturo, Mol. Phys. 27, 1121 (1974). In Eq. (9), C should be replaced with ρ. Effectively, this entire paper can be dismissed since the expansion coefficients $v_\lambda(r)$ for e-CO were incorrect. A correction appears in N. Chandra, Phys. Rev. A 12, 2361 (1975).

(33). See D. E. Golden, N. F. Lane, A. Temkin, and E. Gerjuoy, Rev. Mod. Phys. 43, 642 (1971) and H.S.W. Massey, Electron and Ionic Impact Phenomena, Vol. II: Electron Collisions with Molecules and Photoionization; London: Oxford University Press, 1969.

(34). See, for example, J. D. Craggs and H.S.W. Massey, "The Collisions of Electrons with Molecules," Handbuch der Physik, Vol. 37, Part I, edited by S. Flugge; Berlin: Springer-Verlag, 1959; p. 334 ff.

(35). A detailed analysis appears in Henry and Lane and in Morrison as indicated in reference (4).

References and Notes, Chapter 5

(1). The adiabatic theory as applied to electron-atom collisions is discussed in V. M. Martin, M. J. Seaton, and J. B. G. Wallace, Proc. Phys. Soc. (London) 72, 701 (1958).

(2). See section 4.7 of M. A. Morrison, T. L. Estle, and N. F. Lane, Quantum States of Atoms, Molecules, and Solids; Englewood Cliffs, New Jersey: Prentice-Hall, Inc., 1976.

(3). B. H. Bransden, A. Dalgarno, T. L. John, and M. J. Seaton, Proc. Phys. Soc. (London) 71, 887 (1958). In Eq. (23) of this paper, V_{n0} should be a function of r not just r and ψ_o under the integrand is a function of $\vec{r}'$ not of $\vec{r}$. In Eq. (46) w should be replaced by W.

(4). See chapter 4 of reference (2).

(5). See N. F. Mott and J. N. Sneddon, Wave Mechanics and Its Applications; Oxford: Clarendon Press, 1948.

(6). See Table I of reference (3).

(7). For a useful review of the calculation of polarizabilities, refer to J. O. Hirschfelder, C. F. Curtis, and R. B. Bird, Molecular Theory of Gases and Liquids; New York: John Wiley and Sons, 1954, p. 937 ff.

(8). L. Castillejo, I. C. Percival, and M. J. Seaton, Proc. Roy. Soc. (London) A 254, 259 (1960). The relevant sections are 1 and 5. Correction: In Eq. (84), the integral is over $d\tau_1$.

(9). M. A. Morrison, M. S. Thesis; Rice University (1974) (unpublished).

(10). Cutoff functions are endlessly popular in collision physics. See, for example, A. Dalgarno and N. Lynn, Proc. Phys. Soc. (London) A 70, 223 (1957); J. W. Cooper and J. B. Martin, Phys. Rev. 126, 1482 (1962); M. M. Klein and K. A. Brueckner, Phys. Rev. 111, 1115 (1958), and D. R. Bates and H. S. W. Massey, Phil. Trans. Roy. Soc. (London) A 239, 269 (1943).

(11). See N. F. Lane and S. Geltman, Phys. Rev. 160, 53 (1967). Correction: In Eq. (14), sin and cos should be interchanged.

(12). A. D. Buckingham, Advan. Chem. Phys. 12, 107 (1967).

(13). See N. F. Lane and R. J. W. Henry, Phys. Rev. 173, 183 (1968); R. J. W. Henry and N. F. Lane, Phys. Rev. 183 221 (1969). In Eq. (7) of this work, $J_i\ell$ should be replaced by $Jj\ell$. See also Chapter 6 of reference (9).

(14) See Table 13.2-3 of reference (7), p. 950.

References and Notes, Chapter 6

(1). M. A. Morrison, M. S. Thesis, Rice University, 1974 (unpublished). See Chapter 4 and references therein.

(2). W. N. Sams and D. J. Kouri, J. Chem. Phys. 51, 4809 (1969).

(3). W. N. Sams and D. J. Kouri, J. Chem. Phys. 51, 4815 (1969).

(4). W. N. Sams and D. J. Kouri, J. Chem. Phys. 52, 4144 (1970); 53, 496 (1970). See also R. G. Newton, J. Chem. Phys. 53, 1298 (1970) for historical comments on the work in these papers.

(5). E. F. Hayes and D. J. Kouri, J. Chem. Phys. 54, 878 (1971); E. F. Hayes, C. A. Wells, and D. J. Kouri, Phys. Rev. A 4, 1017 (1971).

(6). An application to reactive scattering appears in E. F. Hayes and D. J. Kouri, Chem. Phys. Lett. 11, 233 (1971). See also J. T. Adams, R. L. Smith, and E. F. Hayes, J. Chem. Phys. 61, 2193 (1974).

(7). D. L. Knirk, E. F. Hayes, and D. J. Kouri, J. Chem. Phys. 57, 4770 (1972); D. L. Knirk, J. Chem. Phys. 57, 4782 (1972).

(8). E. R. Smith and R. J. W. Henry, Phys. Rev. A 7, 1585 (1973); 8, 572 (1973).

(9). A. Temkin and K. V. Vasavada, Phys. Rev. 160, 109 (1967); A. Temkin, K. V. Vasavada, E. S. Chang, and A. Silver, Phys. Rev. 186, 57 (1969). See also section 4 of D. E. Golden, N. F. Lane, A. Temkin, and E. Gerjuoy, Rev. Mod. Phys. 43, 642 (1971). The present author has discussed this theory and conditions for its validity in Chapters 2 and 4 of reference (1) above.

(10). D. M. Chase, Phys. Rev. 104, 838 (1956); E. S. Chang and A. Temkin, Phys. Rev. Lett. 23, 399 (1969); ---, J. Phys. Soc. Japan 29, 172 (1970); A. Temkin and F. H. M. Faisal, Phys. Rev. A 3, 520 (1971); A. Temkin and E. C. Sullivan, Phys. Rev. Lett. 33, 1057 (1974).

(11). See chapter 14 of M. A. Morrison, T. L. Estle, and N. F. Lane, Quantum States of Atoms, Molecules, and Solids; Englewood Cliffs New Jersey: Prentice-Hall, Inc., 1976.

(12). See Chapter 3 of reference (1) above or K. Smith, The Calculation of Atomic Collision Processes; New York: John Wiley and Sons, 1971.

(13). See, for example, G. Forsythe and C. B. Moler, Computer Solution of Linear Albegraic Systems; Englewood Cliffs, New Jersey: Prentice-Hall, Inc., 1967 or R. Courant and D. Hilbert, Methods of Mathematical Physics; New York: Interscience Publishers, Inc., 1937, 1953.

(14). See references listed under reference (3) of Chapter 3.

(15). E. S. Chang and U. Fano, Phys. Rev. A 6, 173(1973). See also U. Fano, Comm. At. Mol. Phys. 2, 47 (1970) for an interesting discussion of the physical content of this theory.

(16). D. R. Hartree, The Calculation of Atomic Structures; New York: John Wiley & Sons, 1975. See also N. F. Lane and S. Geltman, Phys. Rev. 160, 53 (1967).

(17). L. A. Collins, "Rotational Excitation in Slow Collisions of Helium with Diatomic Hydrides: HF, DF, HCl, and DCl," PhD Thesis, Rice University, 1975 (unpublished). See chapter 4.

(18). See Part I of S. Geltman, Topics in Atomic Collision Theory; New York: Academic Press, 1969.

(19). E. Rainville and P. Bedient, Elementary Differential Equations; New York: Macmillan, 1969.

(20). See section 4.11 of W. W. Bell, Special Functions for Scientists and Engineers; London: D. Van Nostrand, Co. Ltd., 1968 and Chapter 10 of M. Abramowitz and I. A. Stegun, Handbook of Mathematical Functions; Washington: NBS, 1964.

(21). J. R. Taylor, Scattering Theory; New York: John Wiley and Sons, 1972.

(22). See Chapter 9 of Jon Mathews and R. L. Walker, Mathematical Methods of Physics; New York: W. A. Benjamin, 1970 (Second Edition),

(23). See Chapter 4 of L. S. Rodberg and R. M. Thaler, Introduction to the Quantum Theory of Scattering; New York: Academic Press, 1967.

(24). A. Messiah, Quantum Mechanics, Vol. I; Amsterdam: North-Holland, 1965. Appendix.

(25). F. S. Hildebrand, Methods of Applied Mathematics; Englewood Cliffs, New Jersey: Prentice-Hall, Inc., 1965 (Second Edition). See chapter 3. See also reference (22) above.

(26). C. Green, Integral Equations Methods; London: Nelson, 1969. See also H. Hochstadt, Integral Equations; New York: Wiley, 1973.

(27). See Abramowitz and Stegun [reference (20) above] for tables of quadrature points. General discussions on various quadrature schemes and background information may be sought in references (22) and (30) of Chapter 3.

(28). F. J. Corbato and J. L. Uretsky, J. Assoc. Comp. Mach. 6, 366 (1956)

(29). See pp. 452 - 453 of Abramowitz and Stegun [reference (20) above].

(30). See p. 959 of I. S. Gradshteyn and I. M. Ryzhik, Tables of Integrals, Series, and Products; New York: Academic Press, 1965.

(31). See Chapter 10 of reference (29) above and the awesome Tables of the Bessel Functions of the First Kind, Harvard University Press, 1960. These fourteen (!) volumes include orders from 0 to 135.

(32). See Chapter 3 of M. E. Rose, Elementary Theory of Angular Momentum; New York: John Wiley and Sons, 1957.

(33). R. S. Caswell and L. C. Maximon, "Fortran Program for the Calculation of Wigner 3j, 6j, and 9j Coefficients for Angular Moments $\leq$ 80," NBS Technical Note 409; Washington, D. C.: Government Printing Office, 1966.

(34). See K. Schulten and R. G. Gordon, J. Math. Phys. 16, 1961 (1975); 16, 1971 (1975).

(35). See Appendix C of reference (17) above and references therein.

(36). See, for example, Chapter 1 of reference (25).

References and Notes, Chapter 7

(1). M. S. Child, Molecular Collision Theory; New York: Academic Press, 1975. See pp. 96, 130.

(2). See, for example, P. G. Burke and A. L. Sinfailam, J. Phys. B 3, 641 (1970).

(3). M. A. Morrison, M.S. Thesis; Rice University, 1974 (unpublished) See Chapter 4.

(4). We use the conventions of M. E. Rose, Elementary Theory of Angular Momentum; New York: John Wiley and Sons, 1957. See Chapter IV for the properties and definitions of the D-matrices.

(5). L. S. Rodberg and R. M. Thaler, Introduction to the Quantum Theory of Scattering; New York: Academic Press, 1967.

(6). Cf Chapter 3 of W. W. Bell, Special Functions for Scientists and Engineers; London: D. Van Nostrand Co., 1968.

(7). B. I. Schneider, Phys. Rev. A 11, 1957 (1975). We are grateful to Dr. Schneider for providing us with numerical tables of differential cross sections for comparison.

(8). See references (11) and (13) of Chapter 5. See also Chapter 7 of reference (3) above.

(9). P. G. Burke and N. Chandra, J. Phys. B 5, 1696 (1972). See also reference (1) above.

(10). T. F. Jordan, Linear Operators for Quantum Mechanics; New York: John Wiley and Sons, 1970.

(11). A. M. Arthurs and A. Dalgarno, Proc. Roy. Soc. (London) A 256, 540 (1960).

(12). E. Merzbacher, Quantum Mechanics; New York: John Wiley and Sons, 1970 (Second Edition). See Chapter 16.

(13). J. R. Taylor, Scattering Theory: The Quantum Theory of Nonrelativistic Collisions; New York: John Wiley & Sons, 1972. See especially section 11-j and Chapter 9.

(14). E. Gerjuoy and S. Stein, Phys. Rev. 97, 1671 (1955); 98, 1848 (1955).

(15). I. S. Gradshteyn and I. M. Ryzhik, Tables of Integrals, Series, and Products; New York: Academic Press, 1965 (Fourth Edition)

(16). See Chapter 7 of reference (6) above.

(17). L. C. Biedenharn, J. Math. Phys. (N.Y.) 2, 433 (1961)

References and Notes, Chapter 8

(1). W. R. Garrett, Phys. Rev. A 11, 1297 (1975).

(2). N. F. Lane and S. Geltman, Phys. Rev. 160, 53(1967). Detailed tabulations of the results of this work were provided by Dr. N. Lane.

(3). J. Tully and R. S. Berry, J. Chem. Phys. 51, 2056 (1969).

(4). S. Hara, J. Phys. Soc. Japan 22, 710 (1967). See reference (7) of Chapter 4 for some corrections to this paper.

(5). R. J. W. Henry and N. F. Lane, Phys. Rev. 183, 221 (1969).

(6). Lee A. Collins (private communication).

(7). M. J. W. Boness and G. J. Schultz, Phys. Rev. A 9, 1969 (1974).

(8). O. H. Crawford and A. Dalgarno, J. Phys. B 4, 494 (1971). See also A. C. Allison, J. Phys. B 8, 325 (1975).

(9). J. J. Lowke, A. V. Phelps, and B. W. Irwin, J. Appl. Phys. 44, 4664 (1973).

(10). D. G. Thompson, Proc. Roy. Soc. (London) A 294, 160 (1966).

(11). See N. F. Mott and H. S. W. Massey, The Theory of Atomic Collisions; London: Oxford University Press, 1965 (Third Edition).

(12). K. Smith, The Calculation of Atomic Collision Processes; New York: John Wiley & Sons, 1971.

References and Notes, Chapter 9

(1). J. C. Tully, Phys Rev. 181, 7(1969)

(2). D. G. Zarlingo, T. Ishihara, and R. T. Poe, Phys. Rev. Lett., 28, 1093 (1972).

(3). P. G. Burke and W. D. Robb, Advan. At. Mol. Phys. 11, 143 (1975). See also references herein.

(4). B. I. Schneider, Phys. Rev. A 11, 1957 (1975).

ACKNOWLEDGMENTS

I wish to express my gratitude to Neal F. Lane, my research director, and to Lee A. Collins, who collaborated with me on part of this research. I would also like to acknowledge the members of the Atomic and Molecular Theory Group at Rice University, especially Thomas Winter, Peter Hickman, Walter Streets, Larry Carlson, Alan Haggard, and Robert Garbs. At LASL, I would like to thank Group T-6, especially Dale Henderson, David Cartwright, Barry Schneider, James Cohen, Richard Preston, and Greg Parker. Finally, I am grateful to the Fannie and John Hertz Foundation for its financial support over the last three years, and to the Associated Western Universities and LASL for making possible my stay at LASL.

☆ US GOVERNMENT PRINTING OFFICE: 1976—677-343/181